TRANSCRIPTIONAL REGULATION OF SLC6A19 ALONG THE CRYPT–VILLUS AXIS

EMRAH TÜMER

A THESIS SUBMITTED FOR THE DEGREE OF

DOCTOR OF PHILOSOPHY

OF THE AUSTRALIAN NATIONAL UNIVERSITY

February 2016

Statement of Originality

The research presented in this thesis was performed in the Research School of Biology, The Australian National University under supervision of Professor Stefan Bröer. The data is the result of original research, has not previously been submitted for a degree, and my own work, with all contributions from others explicitly stated.

Abstract

Digestion of proteins takes place mainly in the small intestine followed by the absorption of amino acids and peptides by enterocytes. The absorption surface area in the intestine is drastically increased by finger-like protrusions along the small intestinal lumen (called villi) and invaginations (called crypts). Enterocytes develop from stem cells in the crypt and differentiate into mature enterocytes while moving along the crypt–villus axis. The *Slc6a19* mRNA and its resulting B^0AT1 protein show a striking increase of expression towards the tip of the villi and are virtually absent in the crypts.

In my PhD research, I investigated transcription factors and epigenetic modulators that regulate *Slc6a19* expression. The *Slc6a19* gene encodes the neutral amino acid transporter B^0AT1, which provides the main mechanism of neutral amino acid absorption in the intestine. My experiments demonstrate that epigenetic modifications and transcription factor distribution orchestrate B^0AT1 expression along the crypt–villus axis.

Acknowledgements

Firstly, I would like to thank my supervisor **Professor Stefan Bröer** for his support and guidance through my PhD research and thesis editing. This thesis would have not been possible without him.

I would like to thank **Angelika Bröer** for sharing her knowledge and techniques on this project, and delicious pastry she made during my time here.

I would also to thank **Dr. Torsten Jülich**, for his patience, friendship and encouragement.

Further, I would like to thank to my advisory member **Dr. Juleen Cavanaugh** for her help in these years.

Most importantly I would like to thank my **family** for their unconditional love and support of my endeavours.

My utmost gratitude goes to **Allah** for everything that I am blessed with.

Dedication

To My Parents & Elif

Publication and presentations arising from this study

Peer-reviewed Journal:

- **Tümer E**, Jüelich T, Bröer A, S Balkrishna, Bröer S (2013) Enterocyte-specific regulation of the apical nutrient transporter SLC6A19 (B^0AT1) by transcriptional and epigenetic networks. **Journal of Biological Chemistry** 288 (47), 33813-33823.

Conference Presentations:

- Transcriptional regulation of B^0AT1 (*Slc6a19*) gene, the gene mutated in Hartnup disorder. The 2011 Gage Ion Channels and Transporters Conference, 18^{th}-20^{th} April 2011, Canberra, Australia
- A new model for the regulation of the amino acid transporter B^0AT1 in the intestine. International Congress of Human Genetics 2011, 11-15 October 2011, Montreal, Canada.
- Does DNA methylation play a role in B^0AT1 transcriptional regulation along crypt-villus axis? International Union of Physiological Sciences Congress 2013, 21-26 July 2013, Birmingham, UK.
- Does DNA methylation play a role in B^0AT1 transcriptional regulation along crypt-villus axis? CHARM Canberra Health Annual Research Meeting 2013, 20-23 August 2013, Canberra, Australia.
- The role of DNA methylation in B^0AT1 transcriptional regulation along crypt-villus axis. The American Society of Human Genetics 2013, 22-26 October 2013, Boston, USA.

Table of Contents

List of Figures

List of Tables

Abbreviations

ACE2	Angiotensin-converting enzyme 2
Caco-2	Colon adenocarcinoma cell lines
cDNA	Complementary DNA
ChIP	Chromatin immunoprecipitation
CpG	Cytosine-guanine dinucleotides
C/EBP	CCAAT/enhancer-binding protein
DMEM	Dulbecco's Modified Eagle's Medium
DNA	Deoxyribonucleic Acid
dNTP	Dinucleotide triphosphate
DNMT	DNA methyltransferase
DTT	Dithiothreitol
EDTA	Ethylenediaminetetraacetic acid
E. coli	*Escherichia coli*
ENCODE	Encyclopedia of DNA Elements
FBS	Foetal bovine serum
FOXA2	Fork-head box A2
GAPDH	Glyceraldehyde-3-phosphate dehydrogenase
h	Hours
H3K27ac	Acetylated histone H3 tail at lysine 27
H3K4me3	Tri-methylated histone H3 at lysine 4
HEK293	Human Embryonic Kidney 293
HDAC	Histone deacetylase
HNF	Hepatocyte nuclear factor
HMT	Histone methylase
KEGG	Kyoto Encyclopaedia of Gene and Genomes
LB	Luria-Bertani broth for bacteria culture
Lgr5	Leucine-rich repeat containing G-protein coupled receptor 5
MBD	Methyl-CpG-binding domain
PBS	Phosphate Buffered Saline

PCR	Polymerase Chain Reaction
RNA	Ribonucleic Acid
HAT	Histone acetyl transferases
HEPES	hydroxyethylpiperazineethanesulfonic acid
kb	Kilo bases
min	Minutes
MeCP2	Methyl-CpG-binding-protein
MODY	Maturity onset diabetes of the young
mRNA	Messenger ribonucleic acid
PPAR	Peroxisome proliferator-activated receptors
qRT-PCR	Quantitative real-time RT-PCR
RPMI	Roswell park memorial institute
sec	Seconds
SD	Standard deviation
SDS	Sodium dodecylsulfate
TAE	Tris-acetate-EDTA
TF	Transcription factor
T_m	Melting temperature
TSS	Transcription start site
UCSC	University of California, Santa Cruz
V	Volt
Mnase	Micrococcal nuclease
qPCR	Quantitative PCR

Chapter 1 Introduction

1.1 Amino acid transport systems

Proteins are an essential part of nutrition and are required for normal functioning and maintenance of the human body. Once ingested, various gastrointestinal digestive enzymes break down the proteins into amino acids and peptides. Amino acids and peptides are then absorbed by epithelial cells (enterocytes) lining the small intestine. Amino acid absorption into enterocytes is mediated by many different amino acid transport systems (Silk et al., 1985).

After absorption, amino acids are delivered to all the organs and to the kidneys by the circulatory system. To prevent their loss into the urine, they are reabsorbed in proximal tubules by amino acid transporters after filtration by the kidney glomerulus. Different types of amino acid transport systems function to absorb amino acids and peptides across the enterocyte cell membrane, and in the proximal tubule including parts of the renal glomerulus. Renal amino acid transport systems are similar to the intestinal transporters (Young and Freedman, 1971).

The pioneering amino acid transport studies conducted in the 1960s (Oxender and Christensen, 1963) established that distinct amino acid transport systems accept different groups of amino acids, and that these systems may exhibit overlapping substrate specificities. Distinct transport systems for neutral, cationic and anionic amino acids were subsequently identified (Oxender and Christensen, 1963). Later, intestinal transporters for neutral amino acids, cationic amino acids, anionic amino acids, glycine, proline and hydroxyproline were described and characterised in the 1980s (Munck, 1980, Stevens and Wright, 1987).

Several amino acid transport systems have been characterised in epithelial cells. System $b^{0,+}$ transports cationic and neutral amino acids. It is Na^+-independent (Chillarón et al., 2001). A heterodimer formed by SLC3A1 and SLC7A9 was identified as the molecular correlate of this system (Feliubadaló et al., 1999). System B^0 is a Na^+-dependent transporter that carries all neutral amino acids, but has limited activity for glycine or proline (Stevens et al., 1982). The molecular correlate of the system B^0 is B^0AT1 (SLC6A19) which is the major neutral amino acid transporter (Bröer et al., 2004). The Na^+-dependent IMINO system preferentially transports glycine and proline (Stevens and Wright, 1987). The molecular correlate of this system is apical transporter SLC6A20

(Kowalczuk et al., 2005). Anionic amino acids are taken up by system $X^-_{AG.}$ It is a Na^+-dependent aspartate/glutamate transporter. It has been showed that EAAT3 the molecular correlate of this transporter (Kanai and Hediger, 2003). Proline and glycine are transported by the IMINO system (Stevens and Wright, 1985). The molecular correlate of this system has been identified as the proton amino acid transporter PAT1 (Anderson, 2003).

1.2 The small intestine

The gastrointestinal tract originates from three embryonic germ layers: the endoderm, mesoderm and ectoderm. Anatomically, the gut has been divided into two parts: the small intestine and the large intestine. The small intestine comprises the duodenum, the jejunum, and the ileum (Barker et al., 2008). Histologically, the wall of the small intestine consists of the following layers: mucosa, submucosa, muscularis propria, and serosa. The mucosal layer contains cuboidal epithelial cells, the connective tissue, and the muscular layers. The submucosa layer contains the connective tissue that supports the mucosa and the muscular layer; the latter is responsible for peristaltic movements throughout the gastrointestinal tract (Sancho et al., 2004).

1.2.1 Crypt–villus functional unit

Proteins are digested mainly in the small intestine, and the resultant protein-derived nutrients are absorbed by epithelial cells (van der Flier and Clevers, 2009). The intestinal absorptive surface area is highly expanded by finger-like microscopic protrusions into the small intestinal lumen, called villi, and by invaginations, called crypts (Heath, 2010). The bottom of an intestinal crypt houses five or six stem cells; these cells divide every 24 h (Barker et al., 2007). Such a high growth rate is necessary to replace the epithelial cells which slough off at the tip of a villus every 24 h (Sato et al., 2009). In addition to progenitor cells, there are 25-42 clonogenic stem cells which can regenerate progenitor cells if necessary (Booth and Potten 2000). The newly generated cells differentiate into four different cell types: enterocytes, goblet cells, enteroendocrine cells, and Paneth cells (Huet et al., 1987). Enterocytes (in this thesis the term enterocytes refers to the absorptive cells of the differentiated epithelium, not including goblet, enteroendocrine or Paneth cells) are the most numerous cell type of the mature intestinal epithelium and they absorb

most nutrients from the lumen. Enterocytes are crucial for the final step of protein digestion. Peptides of 2-10 residues length, are generated by the action of gastric and pancreatic proteases. These are further digested into individual amino acids, di- and tripeptides by brush-border peptidases located on enterocytes (Erickson and Kim, 1990). Goblet cells secrete the intestinal mucus into the lumen for lubrication and protection of the epithelium. The enteroendocrine cells secrete hormones which regulate gastrointestinal functions and communicate with the rest of the body. The Paneth cells secrete lysozymes, antimicrobials, and defensins all of which have important functions in antibacterial protection and innate immunity. The first three cell types migrate towards the villus tip; the Paneth and stem cells are the only cells that reside at the crypt bottom (**Figure 1.1**) (Clatworthy and Subramanian, 2001).

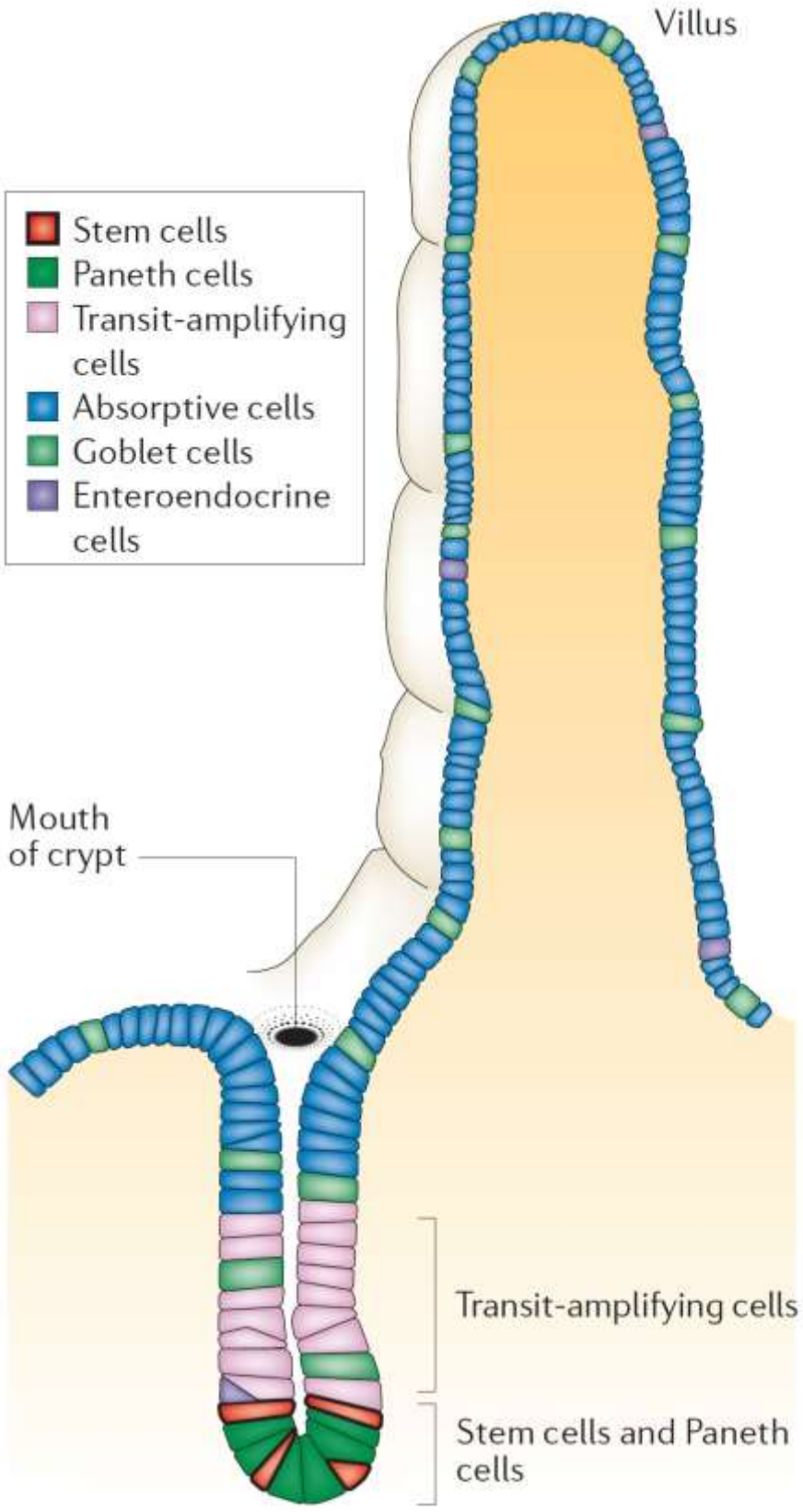

Figure 1.1: The intestinal crypt–villus structure

The stem cells residing in the crypt renew the epithelial cells on the villus. Arrows indicate migration of the differentiated cells along the crypt–villus axis. Epithelial cells migrate towards the villus tip, where they slough off into the intestinal lumen. The Paneth cells and stem cells reside within the crypt niche. From (Crosnier et al., 2006).

1.3 Homeostatic regulation of intestinal development

Different mechanisms regulate maturation of the intestinal cells from the progenitor cells in the crypt to mature cells in the villus. Here, I briefly describe the important signalling pathways and the transcription factors that are involved in intestinal development.

1.3.1 The Wnt signalling is involved in intestinal development

Wnt signalling is involved in many aspects of development, including proliferation and differentiation of the intestinal epithelium (van de Wetering et al., 2002). Proteins involved in Wnt signalling are conserved in animals (Cadigan and Nusse, 1997). Wnt signalling is conveyed through three different intracellular signalling cascades: the first is the canonical Wnt pathway (Wnt/β-catenin signalling) which controls β-catenin stability. β-Catenin has an important function in cell adhesion. The second is the Wnt/Ca^{2+} pathway (non-canonical Wnt pathway) that activates the calcium/calmodulin-dependent protein-kinase complex in the cytoplasm. Lastly, another non-canonical Wnt pathway (the planar cell-polarity pathway) interacts with the Rho family of GTPases, ultimately controlling cytoskeletal dynamics. These pathways are initiated by the Wnt protein, which is produced by mesenchymal cells underlying the epithelial cell layer and surrounding the intestinal crypt. The Wnt protein binds to the Frizzled cell-surface receptor (Lewis, 2007).

When Wnt signalling is inactive, the cytoplasmic β-catenin is captured by a destruction complex which is composed of at least four proteins: the scaffolding protein axin, the tumour suppressor adenomatous polyposis coli (APC), casein kinase I, and glycogen synthase kinase 3 (GSK3). This complex phosphorylates cytoplasmic β-catenin which is then ubiquitinated and degraded in the proteasome (**Figure 1.2**) (Scoville et al., 2008, Lewis, 2007, Sokol, 2007).

In the presence of Wnt, activated cell's surface Frizzled receptor inhibits the destruction complex, causing β-catenin translocation from the cytoplasm into the nucleus. In the nucleus, β-catenin interacts with the T-cell-factor (TCF) to activate transcription of Wnt target genes (**Figure 1.2**) (Logan and Nusse, 2004).

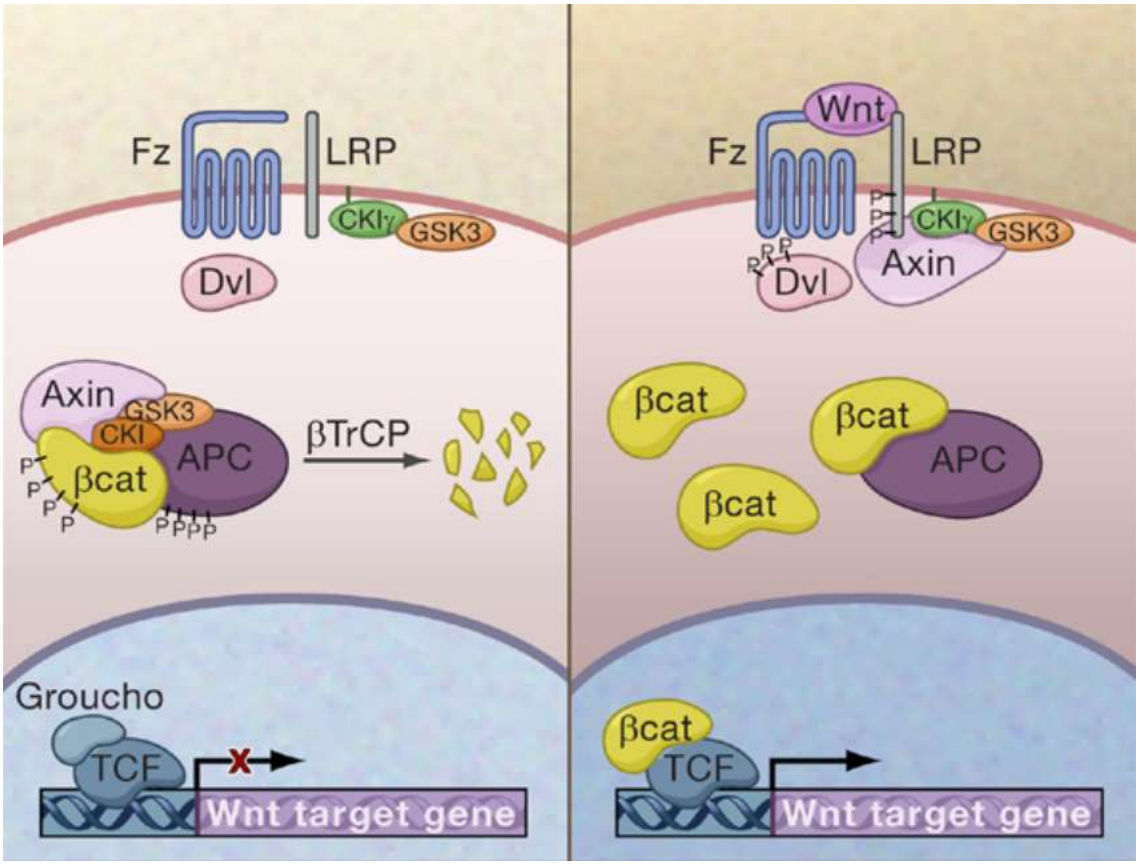

Figure 1.2: The canonical Wnt pathway

(**Left panel**) In the absence of Wnt stimulation, the β-catenin is degraded by the destruction complex, which includes adenomatosis polyposis coli (APC), axin, glycogen synthase kinase 3 (GSK3), and casein kinase I (CKI). (**Right panel**) The binding of Wnt ligand to its receptor Frizzled (Fz) and the LRP co-receptor, inactivates the destruction complex in the cytoplasm. Non-phosphorylated β-catenin translocates to the nucleus and binds the T-cell factor (TCF) to activate the transcription of target genes. From (Clevers, 2006).

1.3.1.1 Wnt/β-catenin signalling in the intestine

The Wnt signalling pathway is important in the intestinal homeostasis, by regulating stem cell populations (Clevers, 2006).

Mutations of various members of this tightly regulated pathway lead to serious intestinal pathologies. For example, deletion of the mouse intestinal *Tcf4* gene causes loss of progenitor cells in the proliferative niche of the intestine (Korinek et al., 1998). Thus, the Wnt pathway is fundamental to the maintenance of the proliferative cells. In agreement with this notion, mutations of *Apc*, (a tumour suppressor gene which negatively regulates the Wnt pathway), causes crypt enlargement and interruption of cell migration from the crypt to the villus (Sansom et al., 2004). *Apc* mutations were also

found to be associated with intestinal cancers in humans (Morin et al., 1997). In addition, the Wnt pathway stimulates maturation of the Paneth cells in the intestinal crypt (van Es et al., 2005).

1.3.2 Transcription factors (TFs) involved in intestinal development

Many transcription factors have been implicated in enterocyte maturation. Here, the most important candidates are introduced.

1.3.2.1 SOX9

The SOX (Sry-related HMG box) family of transcription factors contain the HMG (high-mobility group) DNA-binding domain. SOX and Sry (sex determining region Y) proteins share ~50% identity in their HMG domain. SOX factors are well-conserved proteins amongst vertebrates (Dong et al., 2004). At least 20 different human and murine SOX proteins exist, and these are subdivided into eight subgroups (Bowles et al., 2000). SOX proteins are mainly involved in organ development and tissue maturation, but mutated SOX proteins are also associated with malignancies (Kiefer, 2007).

SOX9 is an important SOX protein involved in crypt–villus development (Kormish et al., 2010). The main function of SOX9 in the intestine is enterocyte maturation and crypt formation (Bastide et al., 2007). SOX9 is also essential for the development of male gonads, the neural crest, and cartilages (Morais da Silva et al., 1996, Zhao et al., 1997, Cheung and Briscoe, 2003). In the mouse, SOX9 is expressed in many different organs; *Sox9* mRNA and protein can be detected in the lower third of the intestinal crypts, in colon crypts, the Paneth cells (Blache et al., 2004), and in the epithelium of pancreatic and biliary ducts (**Figure 1.3**) (Furuyama et al., 2011). TCF proteins, which function in Wnt-targeted gene regulation, also have the same DNA-binding domain as SOX does (van Beest et al., 2000).

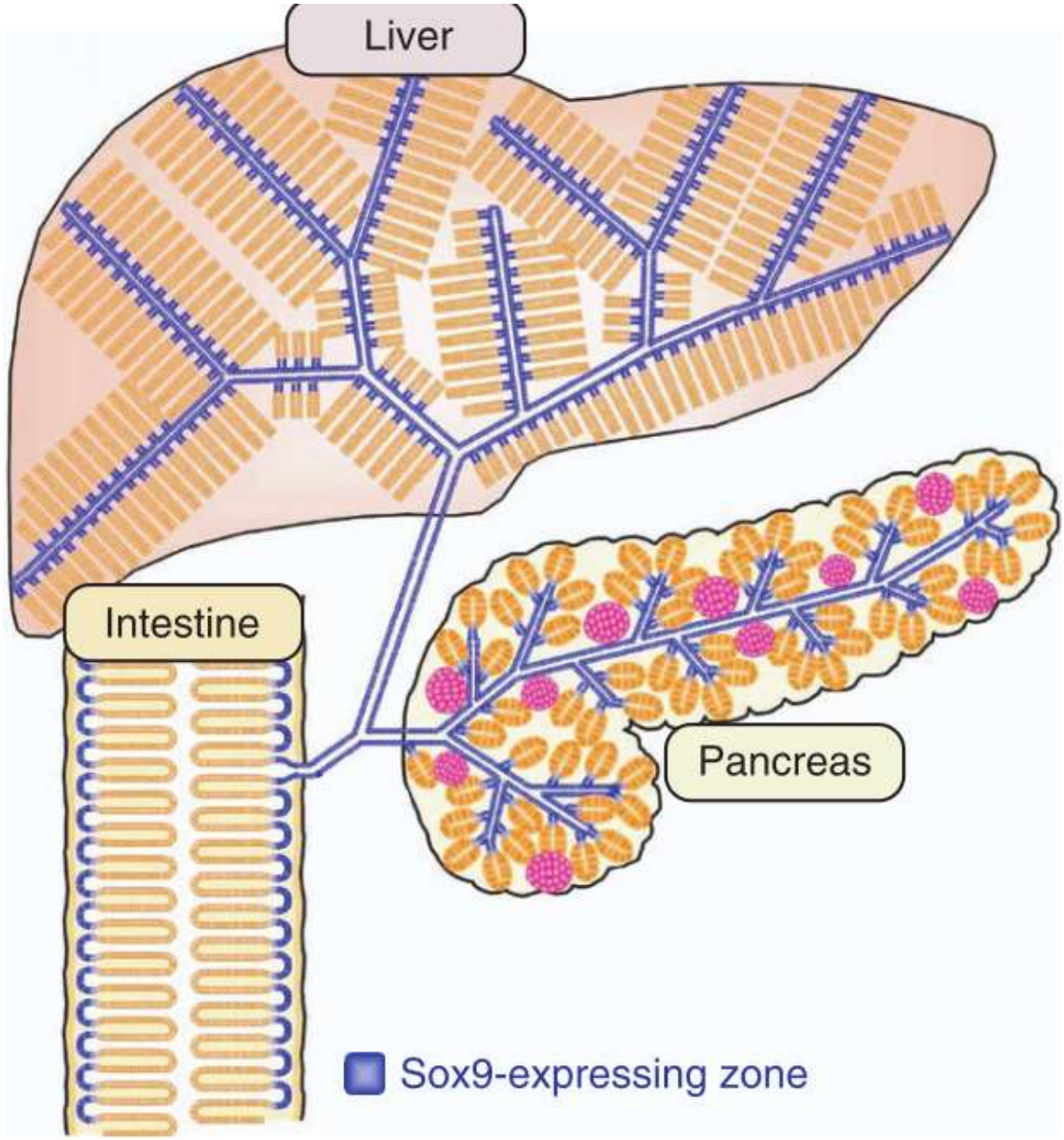

Figure 1.3: The SOX9 expression profile in the gastrointestinal system

SOX9 is significantly expressed in the extrahepatic biliary tract, pancreatic duct cells and intestinal crypts. From (Furuyama et al., 2011).

1.3.2.2 Interaction between SOX9 and Wnt/β-catenin

The Wnt pathway and SOX expression are important in the development of different organs. The interaction between SOX9 and β-catenin has been shown to be essential for cartilage development. β-catenin deletion, and inversely, SOX9 overexpression can interrupt chondrocyte differentiation (Akiyama et al., 2004). In the female gonad, activated SOX9 can repress Wnt/β-catenin pathway, and this leads to a male sex determination during development (Bernard et al., 2008). In the intestines, Wnt

signalling orchestrates crypt formation and promotes stem cell proliferation. SOX9, by contrast, inhibits the Wnt pathway and promotes differentiation of the stem cells into mature intestinal cell types. Therefore, interaction between SOX9 and Wnt is essential for the cell proliferation–maturation balance (Kormish et al., 2010).

SOX9 mutations have been shown to cause loss of the Paneth cells in the crypts (Bastide et al., 2007, Mori-Akiyama et al., 2007). Cdx2 and Muc2 proteins are highly expressed in the mature enterocytes in the villi and known as differentiation markers; however, in the crypts, they are transcriptionally repressed by SOX9 (Blache et al., 2004). As a result, SOX9 is thought to be a key transcription factor to repress the proliferation programs in the progenitor cells in the crypts.

In summary, these studies indicate that SOX9 down-regulates the Wnt pathway, and that, together with the Wnt/β-catenin pathway, it plays an important role in the homeostasis of intestinal development.

1.3.2.3 HNF1a

Hepatocyte nuclear factors (HNFs) encode a family of transcription factors. These were first identified as transcription factors that regulate hepatocyte specific genes. This family includes five transcription factors; HNF1, HNF4, HNF6, C/EBP (CCAAT/enhancer binding protein), and FOXA2 (fork-head box A2) (Costa et al., 2003).

Studies in mice revealed that Hepatocyte nuclear factor 1 alpha (HNF1a) is expressed in kidney, pancreas, intestine and stomach (Blumenfeld et al., 1991). In the kidney, it is exclusively expressed in the proximal tubules but not throughout the entire nephron (Pontoglio et al., 1996). HNF1a-deficient mice die around weaning time due to hepatomegaly. Also, these mice show signs of aminoaciduria (Lee et al., 1998, Pontoglio et al., 1996). The HNF4a-knockout mice show the renal Fanconi syndrome because of dysfunction of the proximal renal tubules. The renal Fanconi syndrome is characterised by diabetes, glycosuria, and aminoaciduria, indicating loss of renal and pancreatic functions (Pontoglio et al., 1996). It has been shown that HNF1a-knockout mice excrete three times more of the neutral amino acid proline in urine than wildtype mice (Bonzo et al., 2010).

Within the gastrointestinal system, HNF1a mRNA can be detected from the stomach down to the colon, and the gene is expressed along the crypt–villus axis in the intestine (Boudreau et al., 2002, Serfas and Tyner, 1993). A study showed that in the intestine of HNF1a-null mice, epithelial barrier function, Paneth cell differentiation, and crypt cell proliferation were disrupted (Lussier et al., 2010). HNF1a is also essential for pancreatic islets development (Pontoglio et al., 1996, Shih et al., 2001, Tronche et al., 1997). Mutations in the HNF1a gene are the most common reason for maturity onset diabetes of the young (MODY) (Yamagata et al., 1996b).

1.3.2.4 HNF4a

HNF4a (hepatocyte nuclear factor 4 alpha) is a member of the nuclear receptor super family (Sladek et al., 1990), and is highly conserved in vertebrates (Ryffel, 2001). In mice, the HNF4a gene is located on chromosome 2 and it consists of 11 exons. The tissue expression profile of HNF4a is similar to that of HNF1a, and it was initially identified as a transcriptional regulator of hepatic genes such as the fibrinogen, albumin, and α1-antitrypsin (Cereghini et al., 1987). HNF4a is expressed in differentiated adult cells located in the liver, pancreas, stomach, intestine, skin and kidney (Taraviras et al., 1994). HNF4a is highly expressed in blastocysts at day 4.5 and in the visceral endoderm at day 5.5. It is also expressed in the embryonic liver and gut (Duncan et al., 1994). The HNF4a knockout is embryonically lethal, demonstrating its crucial role as a transcription factor in early development (Duncan et al., 1994). Certain HNF4a gene mutations cause maturity onset diabetes of the young (Yamagata et al., 1996a). Additional studies demonstrated that HNF4a is a key regulator of crypt formation and goblet-cell maturation (Garrison et al., 2006).

Interestingly, not only do HNF4a and HNF1a share similar expression patterns, but they also appear to be regulating each other's transcription, being linked through a transcriptional feedback loop (Shih et al., 2001).

1.3.2.5 Other TFs

A variety of TFs are involved in intestinal cell differentiation. The transcription factor CDX2 is necessary for intestinal development (Lorentz et al., 1997) and together with HNF1a, regulates sucrose-isomaltase and lactase-phlorizin hydrolase gene

expression along the crypt-villus axis (Mitchelmore et al., 2000). GATA4 is another crucial TF which is required for activation of intestinal genes involved in nutrient absorption (Bosse et al., 2007). CDX2 and GATA4 appear to be sufficient to activate many of the enterocyte-specific genes in the mammals (Benoit et al., 2010). SPDEF and FOXA2 TFs are exclusively expressed in cells residing in crypts (Besnard et al., 2004). SPDEF is required for maturation of intestinal Paneth and goblet cells (Gregorieff et al., 2009), while FOXA2 regulates goblet cell differentiation via activation of Muc2, which induces expression of mucin secreted by the goblet cells (Ye and Kaestner, 2009).

1.4 B^0AT1 protein

System B^0 is a Na^+-dependent, low-affinity transport system that takes up neutral amino acids. It was initially described as neutral brush border system (NBB) by a study of rabbit intestinal brush border membrane vesicles (Stevens et al., 1982) and afterwards, it was renamed as system B^0, to designate broad neutral amino acids (Maenz and Patience, 1992).

In 2004, the molecular correlate of this transport system was identified in mouse and named B^0AT1 (B^0-like amino acid transporter 1). B^0AT1 was found to be highly expressed on the apical membrane of intestinal brush borders and kidney proximal tubules (Bröer et al., 2004). It is a member of the solute carrier (SLC) family 6, also known as the neurotransmitter transporter family. Unlike other members of the solute carrier (SLC) family 6, the B^0AT1 transport function is Cl^--independent (Bohmer et al., 2005).

1.4.1 Structure of B^0AT1 protein

Structure of the SLC6 transporters is similar to the crystal structure of the bacterial leucine transporter (LeuT). The LeuT transporter of the bacterium *Aquifex aeolicus* is a structural homolog of the mammalian B^0AT1 protein (Yamashita et al., 2005). LeuT has 12 transmembrane α-helices. Particularly, the first and sixth helix of both proteins show high similarity, containing residues that are important for substrate and ion binding. Both proteins mediate Na^+-dependent, Cl^--independent transport of a broad range of neutral amino acids (Broer, 2006).

According to the LeuT-based homology model, the B^0AT1 structure is characterized by 12 transmembrane helices and intracellular N- and C- termini. Helices 1 and 6 are crucial for substrate translocation in the protein. Additionally, helix 8 has a role in substrate binding (**Figure 1.4**) (Broer, 2006).

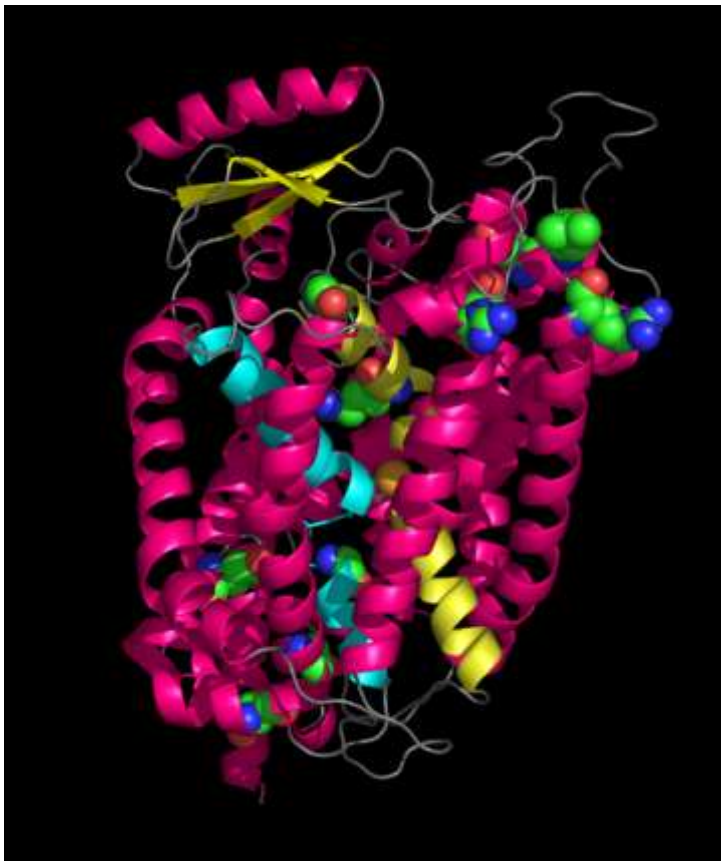

Figure 1.4: Homology model of B^0AT1 based on the structure of LeuT

The B^0AT1 model was generated based on the crystal structure of the bacterial leucine transporter, LeuT. Helix 1 (yellow) and helix 6 (blue) are indicated among other helices (pink). From (Broer, 2008).

1.4.2 Tissue distribution and cellular localization of B^0AT1

The B^0AT1 protein is mainly present in the kidney and the intestine. In the kidney, B^0AT1 is highly expressed in the cells of the S1 and S2 segments of the proximal tubule (Romeo et al., 2006). Here, B^0AT1 protein expression is limited to the brush border membrane of the proximal tubules (Kleta et al., 2004). B^0AT1 expression in the digestive system is evident predominantly in the duodenum, the jejunum and the ileum (Terada et al., 2005). In the intestine, B^0AT1 is highly expressed in the villus tip, but not at the crypt bottom (Bröer et al., 2004). B^0AT1 is also expressed, to some extent, in the colon, pancreas, and prostate (Kleta et al., 2004).

1.4.3 Interaction of B^0AT1 with other proteins

Intracellular trafficking of B^0AT1 to the cell membrane is an important step required for its proper functioning. To date, two trafficking proteins have been found in the kidney and the intestine, namely collectrin (TMEM27) and angiotensin-converting enzyme 2 (ACE2), respectively.

Collectrin was named according to its presumed location in the cells of the renal collecting ducts. Collectrin expression was later confirmed in the pancreas, stomach, jejunum, ileum, heart, lung, spleen, and liver (Akpinar et al., 2005, Danilczyk et al., 2006). In 2006, Danilczyk and colleagues showed that in collectrin-deficient mice, neutral amino acids were excreted into the urine. Further analysis revealed that expression of collectrin was similar to B^0AT1 expression in the kidney tubules (Danilczyk et al., 2006, Malakauskas et al., 2007). B^0AT1 cell surface expression in the proximal tubule was significantly reduced in collectrin-null mice.

However, collectrin is not expressed in the intestinal brush border where B^0AT1 is highly expressed (Kowalczuk et al., 2008). In the intestine, B^0AT1 requires a different cofactor to transport it to the enterocyte apical membrane. Studies in *Xenopus laevis* oocytes showed that co-expression of the brush-border peptidase ACE2, which shows homology with the transmembrane domain of collectrin (Zhang et al., 2001), and B^0AT1 increased the uptake of neutral amino acids due to increased B^0AT1 surface expression (Kowalczuk et al., 2008, Camargo et al., 2009). ACE2 also has an important regulatory role in the renin-angiotensin system, which is crucial for renal and cardiovascular functions (Burrell et al., 2004). ACE2 is associated with diseases of the cardiovascular system (Crackower et al., 2002)

In collectrin-deficient mice, B^0AT1 was almost absent in the luminal membrane of the renal proximal tubules, thereby causing neutral aminoaciduria (Danilczyk et al., 2006). By contrast, amino acid composition in the urine of ACE2-deficient mice was not affected (Camargo et al., 2009). The B^0AT1 (*Slc6a19*)-null mice show aminoaciduria similar to collectrin-null mice but in addition have reduced body size and body weight and also show weak insulin responses in the pancreas (Broer et al., 2011).

1.4.3.1 Hartnup disorder

Hartnup disorder is an autosomal recessive inherited disorder which is characterized by aminoaciduria, and a photosensitive pellagra-like skin rash. Occasionally cerebellar ataxia, nystagmus and tremor are observed. It was first described in 1956 (Baron et al., 1956). Intestinal absorption and renal absorption of most neutral amino acids were reduced in this disorder. Nowadays, protein-rich diets appear to compensate for deficient neutral amino acid uptake; therefore, in developed countries, Hartnup patients are usually asymptomatic (Broer, 2009). Newborn screening programs in Australia and North America showed an incidence of about 1 case per 30,000 newborns (Levy 2001).

Neutral aminoaciduria is the diagnostic hallmark of Hartnup disorder. Aminoaciduria is caused by the renal defect, whereas other symptoms are likely caused by the lack of intestinal neutral amino acid uptake. The pellagra-like symptoms may result from a lack of tryptophan. Pellagra is typically caused by Niacin deficiency, the vitamin involved in NAD(P)H biosynthesis. However, the body can, to some extent, produce NAD(P)H, using the essential neutral amino acid tryptophan, the uptake of which is reduced in Hartnup disorder. NADPH among other roles is necessary for fatty acid biosynthesis and glutathione reduction. Typical manifestations of Pellagra are bilateral, symmetric and photosensitive dermatitis, dementia, and diarrhoea (Broer, 2009).

Homozygosity mapping performed by a Japanese group established that Hartnup disorder is linked to chromosome band 5p15 (Nozaki et al., 2001). Subsequently, Kleta et al. (Kleta et al., 2004) and Seow et al., (Seow et al., 2004) found that *SLC6A19* gene mutations cause Hartnup Disorder. So far, 21 different mutations associated with Hartnup disorder have been identified, including missense and nonsense deletions, splicing and small deletions (Broer, 2009). Functionally, all of these mutations cause loss of neutral amino acid transportation (Broer and Palacin, 2011). Among these mutations, the most frequent in caucasians is 517 G→A causing a D173N replacement in the protein (Azmanov et al., 2008). While many mutations were not informative with regard to protein function, B^0AT1(R240Q) results in loss of transport function only when auxiliary proteins are co-expressed with B^0AT1. No defect was observed when it is expressed without auxiliary proteins (Kowalczuk et al., 2008). Subsequently, it was demonstrated that the collectrin binding site is in close proximity to residue R240 (Fairweather et al., 2015).

1.5 *SLC6A19* gene structure

The *SLC6A19* gene encodes for B^0AT1. *SLC6A19* is located on the chromosomal region 5p15.33 in humans; in the mouse, it is located on chromosome 13 and maps to region 13C1. The gene has 12 exons and encodes a protein of 634 amino acids in both species (**Figure 1.5**) (Broer, 2006).

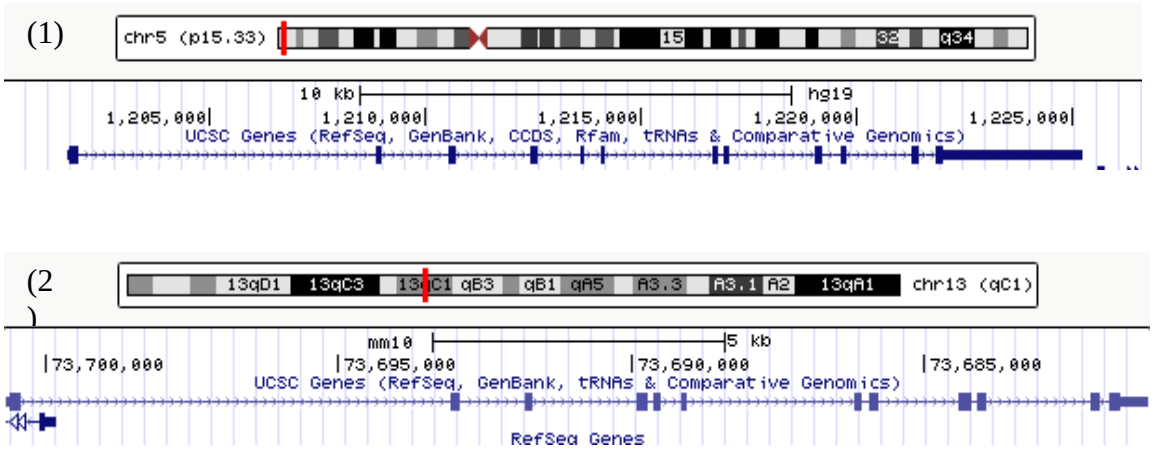

Figure 1.5: Chromosomal locations of Slc6a19 in human and mouse

Location of human and mouse *Slc6a19* genes using the UCSC Genome Browser (http://genome.ucsc.edu). 1) The human *Slc6a19* is located at chr5p15. 2) The mouse *Slc6a19* is located at chr13qC1.

1.6 Transcriptional regulation

Almost every cell has an identical copy of the entire genomic material, yet each cell type expresses its unique complement of proteins (Russell, 2002). Activation of specific network of genes during differentiation and development is the basis of existence of many different cell types. Gene expression can be regulated at multiple points (**Figure 1.6**), the most important of which occurs at the initiation of transcription (Alberts, 2004).

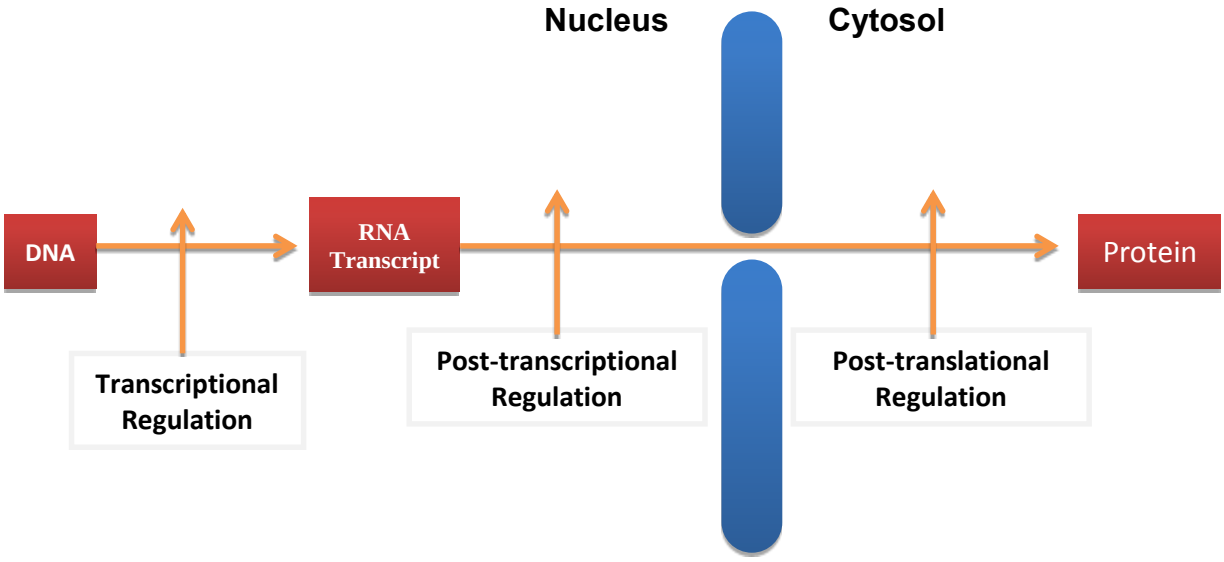

Figure 1.6: The central dogma of gene regulation

The control points during gene expression and protein synthesis are shown. Control of transcription and translation occurs at three major checkpoints: transcriptional, post-transcriptional, and post-translational regulation.

Well-orchestrated interactions between DNA regulatory elements (which include promoter-binding elements), RNA polymerase enzymes, and histones ensure timely and well-coordinated transcription of different genes. Accessibility of transcription factors to DNA is regulated by chromatin modifications, thereby constituting an additional level of transcriptional regulation.

1.6.1 Promoter recognition

To initiate the transcriptional process, RNA polymerases must be positioned upstream of the first exon of the target gene in the promoter region. Formation of a transcription preinitiation complex, which incorporates a polymerase and several general transcription factors, is necessary for RNA polymerase to bind to its correct site with correct orientation (Wolpert, 2007).

1.6.1.1 Promoter elements

In eukaryotes, different promoter elements are defined according to their positions. These elements are the core promoter elements, proximal promoter elements, and distal promoter elements (enhancers).

1.6.1.1.1 Core promoter elements

A core promoter element is the minimum DNA sequence required to initiate proper transcription by the transcription initiation complex. This region spans ~40 base pairs (bp) upstream of the transcription start site (TSS). The main core promoter elements identified across a wide range of promoters are BRE (TFIIB recognition element), TATA (TATA box), Inr (initiator element), and DPE (downstream promoter element). Importantly, it is not necessary for all these elements to be found in each promoter region. Rather, they appear in different combinations, usually depending on the particular regulatory requirements of a specific gene (**Figure 1.7**) (Latchman, 2008).

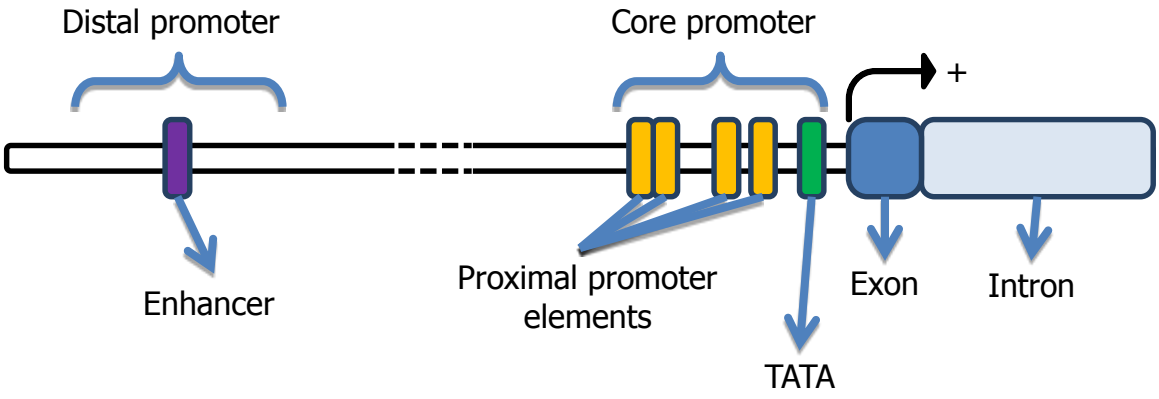

Figure 1.7: An eukaryotic promoter region and its regulatory elements

Graph shows specific DNA regulatory components and regions, including the TATA box, proximal (core) promoter elements, and the enhancer. From (Lodish, 2003).

In most TATA box-containing eukaryotic promoters, the core promoter element is located 25–35 bp upstream of the TSS. This sequence is recognized by the TATA-binding protein to initiate transcription. Except for housekeeping genes, most genes require this sequence in their promoter regions for activating transcription.

1.6.1.1.2 Proximal promoter elements

Proximal promoter elements are located ~50–200 bp upstream of the TSS. Two frequently identified elements within this region are the GC box and CCAAT box. These DNA sequences can be recognized by transcription factor Sp1 and CCAAT-binding transcription factor (CTF), respectively (Lodish, 2003).

1.6.1.2 Enhancers

Enhancers are position-independent, positive regulatory elements that are present in eukaryotic cells, but usually absent in prokaryotic cells. The activity of enhancers does not depend on their exact location or distance from the promoter. They can be found thousands of base pairs away from the TSS, either downstream or upstream of its target gene promoter (Lodish, 2003).

1.6.1.3 Other elements

Silencers are regulatory DNA elements that have an opposite function to enhancers, i.e. they act to decrease gene transcription. There are two types: position-dependent and position-independent silencers. Their position is variable in mammalian genomes. Another regulatory element is the insulators (boundary elements) which are located up to 3 kb from TSS and mainly prevent the interactions between the enhancers and the promoters (Lodish, 2003).

1.6.2 Transcription factors

Transcription factors are regulatory proteins that non-covalently interact with specific DNA sequences via relevant DNA-binding domains. TFs can positively or negatively control the rate of gene expression. This regulation is often tissue-specific or elicited by appropriate signals. The human genome contains ~2000 transcription factor genes, amounting to roughly 10% of the genome (Wolpert, 2007).

The activity of TFs is based on two major domains. These domains are the DNA-binding domain and the activation domain. The DNA-binding domain recognises specific DNA sequences within regulatory regions of genes, whereas the activation domain

interacts with other protein complexes comprising the transcriptional machinery (Lewin, 2004).

In eukaryotes, many different types of DNA-binding motifs have been identified. The most commonly observed motifs are helix-turn-helix, zinc-finger, leucine zipper, and helix-loop-helix motifs. The most studied motif is the helix-turn-helix motif, which is found in the homeodomain family, for instance, HNF1a. This motif has two helices that are linked to each other by a short turn. The C-terminal helix of this motif fits into the major groove of the DNA helix and binds a specific DNA sequence. It is, therefore, called the recognition helix. The N-terminus helps to position the C-terminal helix (Strachan and Read, 2004).

Another DNA-binding domain is the zinc finger. This domain includes a zinc molecule inside the helical structure of the recognition helix. HNF4a contains an example of this group. Some TFs have more than one zinc-finger domain.

In leucine zipper TFs, the α-helix has regular leucine repeats, which are necessary for dimerization. This motif contains two α-helical proteins forming homodimers or heterodimers, which bind to a specific DNA region, with both helices (Watson, 2003).

The helix-loop-helix motif has a short and a longer α-helix, which are bound together by a loop. The dimer gains flexibility with the loop structure. Together with another helix-loop-helix protein, they can form a homodimeric or heterodimeric structure (Watson, 2003).

The second characteristic domain of TFs is the transcription activation domain (TAD), which is essential for transcription initiation via interaction with the transcription initiation complex. In contrast to DNA-binding domains, TADs do not interact with DNA structures. These domains mostly interact with general TFs to recruit the RNA polymerase II to the promoter (Tjian and Maniatis, 1994). General TFs such as TFIIB, TFIID, and TFIIF can interact with different activation domains (Blau et al., 1996). For instance, AF2 is the activation domain of the HNF4 protein, and it binds to TFIIB, and this interaction recruits the preinitiation complex (Malik and Karathanasis, 1996).

1.6.2.1 Regulation of TFs

Almost all cell types express a set of housekeeping genes, which are necessary for basic cell functions. In contrast, the tissue-specific genes are expressed in the specific cell types only. Therefore, regulation of TFs is an important mechanism underlying development and differentiation in organisms. This process is achieved by different steps in TF expression and activation.

TFs themselves are controlled by external signalling. Gene expression can be triggered by extracellular signals such as growth factors, hormones, chemokines, cytokines and apoptosis factors. Each of them shows its effects via different intracellular pathways and TFs. The STAT pathway, for instance, is activated by cytokines and growth factors. The activated cytokine receptor triggers STAT phosphorylation in the cytoplasm and promotes dimerization of phosphorylated STAT. The activated dimers can then enter the nucleus to start transcription of target genes (Lodish, 2003).

1.6.3 Epigenetics

Epigenetic factors can modify transcriptional regulation without affecting the DNA code. Intriguingly, these changes can be inherited through mitosis (Nussbaum et al., 2007). Epigenetics alter gene expression by modulating DNA methylation or histone modifications. Epigenetic modifications have been studied extensively over the last several decades (Razin and Riggs, 1980, Holliday, 1996).

1.6.4 Chromatin modifications

In eukaryotes, genetic information is compacted as chromatin. This compaction prevents TFs from binding to regulatory DNA regions (see **Section 1.6.1.1**). Therefore, chromatin unpacking is a prerequisite of transcriptional regulation. It is now established that chromatin not only plays a role in packaging the genomic material, but also plays a central role in transcriptional regulation (Turner, 2002).

Chromatin packing is regulated by histones, protein components of chromatin that compact the DNA (see **Section 1.6.4.1**). Inactive genes are in a highly condensed state, inaccessible to transcription factors. Chromatin remodelling and histone modifications

can reversibly unpack the compacted DNA to let activators access their corresponding binding sites (Fischle et al., 2003).

1.6.4.1 Histone modifications

Histones are positively charged proteins, which associate with DNA. Five different histone subtypes exist in eukaryotic cells, namely H1, H2A, H2B, H3, and H4. A histone octamer contains two H2A–H2B and two H3–H4 dimers. Approximately 150 bp of DNA wrap around each octamer of core histones to form a complex called the nucleosome (Kornberg and Lorch, 1999).

Histones N-terminal tails (**Figure 1.8**) bind DNA and stabilise the chromatin structure. Post-translational modifications in histone tails, such as methylation, acetylation, phosphorylation, and ubiquitination, regulate chromatin stability and, therefore, transcriptional regulation (Kouzarides, 2007).

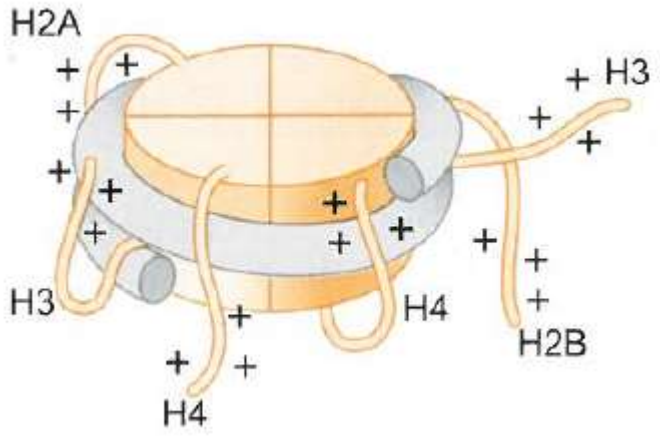

Figure 1.8: Structure of histone tails

The DNA double helix wraps around histone octamers containing the H2A, H2B, H3, and H4 subunits. N-terminal tails of each histone are chemically modified to regulate nucleosome DNA accessibility. From (Watson, 2003).

Histone acetyl transferases (HATs) catalyse addition of acetyl groups to lysine residues on the N-terminal tails of histones. This causes loss of their positive charges, which in turn weakens their binding to negatively charged DNA. As a result, DNA

becomes accessible, and the transcription initiation complex can bind the promoter region to start transcription. The acetylation reaction is reversible; histone deacetylases (HDAC) remove the acetyl groups from lysine residues and thereby reduce the accessibility to the nucleosomal DNA (Richards and Elgin, 2002).

Similarly, methylation of histone H3 tails by histone methyl transferases (HMTs) can control gene transcription. HMTs can transfer a methyl group onto lysine or arginine residue in a histone. Usually, methylation of amino acid residues of histones negatively regulates gene activation by blocking TF interaction with DNA (Berger, 2002, de la Cruz et al., 2005).

1.6.4.2 Chromatin remodelling

In some situations, histone modification is not sufficient for the TFs to bind the target promoter. Often, chromatin remodelling, an ATP-dependent process, is required to increase the accessibility of the target gene for transcription.

Activators bind to their specific DNA sequences and recruit a chromatin remodelling complex that alters the chromatin structure. Chromatin remodelling systems act together with histone-modifying enzymes to assist TF binding to their cognate sequences. Chromatin complexes can make this change via sliding, transferring, or restructuring a nucleosome on the DNA (**Figure 1.9**) (Strachan and Read, 2004).

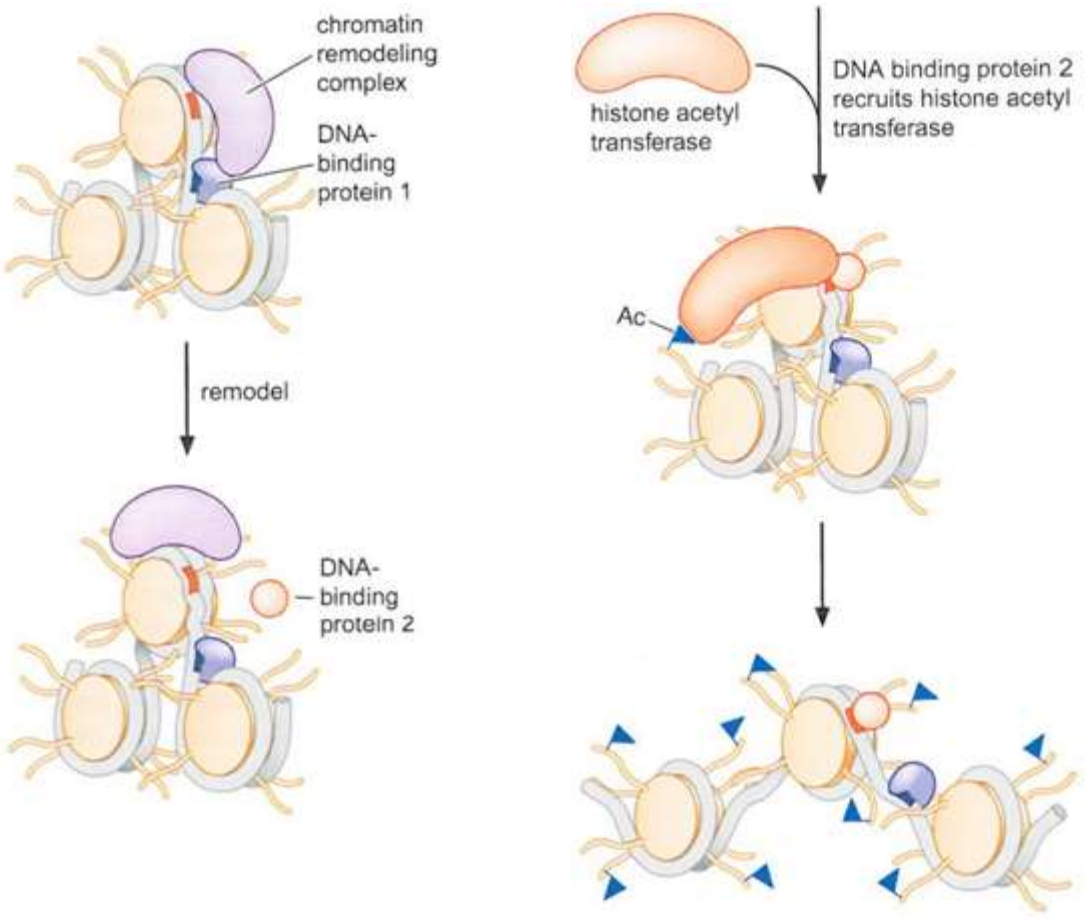

Figure 1.9: Chromatin remodelling and histone modifications are working together.

A chromatin remodelling complex is recruited by DNA-binding protein 1 to alter nucleosome accessibility. Action of the DNA-binding proteins stimulate formation of a more accessible chromatin structure by recruiting HATs to the target DNA region. From (Watson, 2003).

1.6.5 DNA methylation

DNA methylation can regulate transcription in eukaryotic cells, especially in mammals. Methylation of cytosine residues in cytosine–guanine dinucleotides (CpGs), which are located around the promoter region, can cause transcriptional inhibition. This modification disturbs the interaction of transcription factors with the promoter region. In general, DNA methylation correlates with an inactive gene status, but switching off a gene completely requires further modifications. This is achieved by a combination of DNA methylation and nucleosomal alterations (Cedar and Bergman, 2009).

Methylation patterns are heritable. During the replication process, methylated parental DNA strands are divided and passed onto daughter cells. Methylation of the

complementary new strand is completed by the maintenance methyltransferase which recognise the hemi-methylated pattern and methylates the CpG dinucleotide on the newly synthesized strand (**Figure 1.10**) (Alberts, 2004).

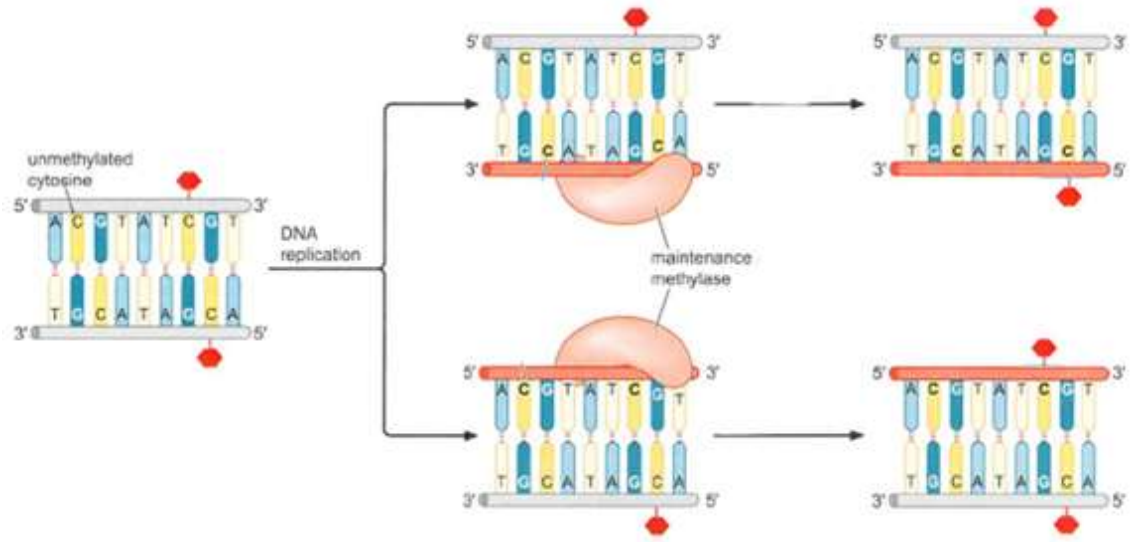

Figure 1.10: Maintenance methyltransferase

During DNA replication, the maintenance methyltransferase allows transfer of an existing DNA methylation pattern to a new DNA strand. From (Alberts, 2004).

1.6.5.1 CpG islands

In mammals, 70–80% of CpG dinucleotides are methylated across the whole genome, with the other non-methylated CpG dinucleotides concentrated in the gene promoter regions (Portela and Esteller, 2010). A region of 200 bp with at least 50% CpG content is considered a CpG island. CpG islands are commonly found as non-methylated regions in promoters of housekeeping genes and tissue-specific genes in differentiated cells.

1.6.6 DNA methylation and transcription

CpG methylation has a significant function in transcriptional control, chromosomal structure and organisation, and differentially expression of genes depending on their parent-of-origin, called genomic imprinting.(Robertson, 2002). Most promoter regions

have CpG-rich regulatory fragments, and some TF-binding sites contain CpG dinucleotides.

In the promoter of an inactive gene, a DNA methyltransferase (DNMT) adds a methyl group to position 5 of the cytidine generating 5-methylcytosine. Specific proteins, which recognise a methylated cytosine residue, can bind methylated sequences. These proteins can then switch off a gene completely through the action of HDACs and HMTs (**Figure 1.11**) (Watson, 2003).

DNA methylation in a promoter region can inhibit binding of the transcriptional initiation machinery or TFs in a number of ways. Firstly, methylation can inhibit TF binding (Tate and Bird, 1993). Secondly, some proteins specifically bind to methylated CpG residues and repress transcription by preventing TF binding to the target promoter region. For example, DNMTs can inhibit transcription via modifying histones. Studies have shown that DNMTs are associated with HDACs (Robertson, 2002).

Methylated CpGs can also be recognised by methyl-CpG-binding-protein (MeCP2) which recruits HDACs (Nan et al., 1998). Also, the DNA-methyl-binding domain (MBD) proteins interact with methylated DNA, in the same way as MeCP2, and can recruit proteins to suppress transcription.

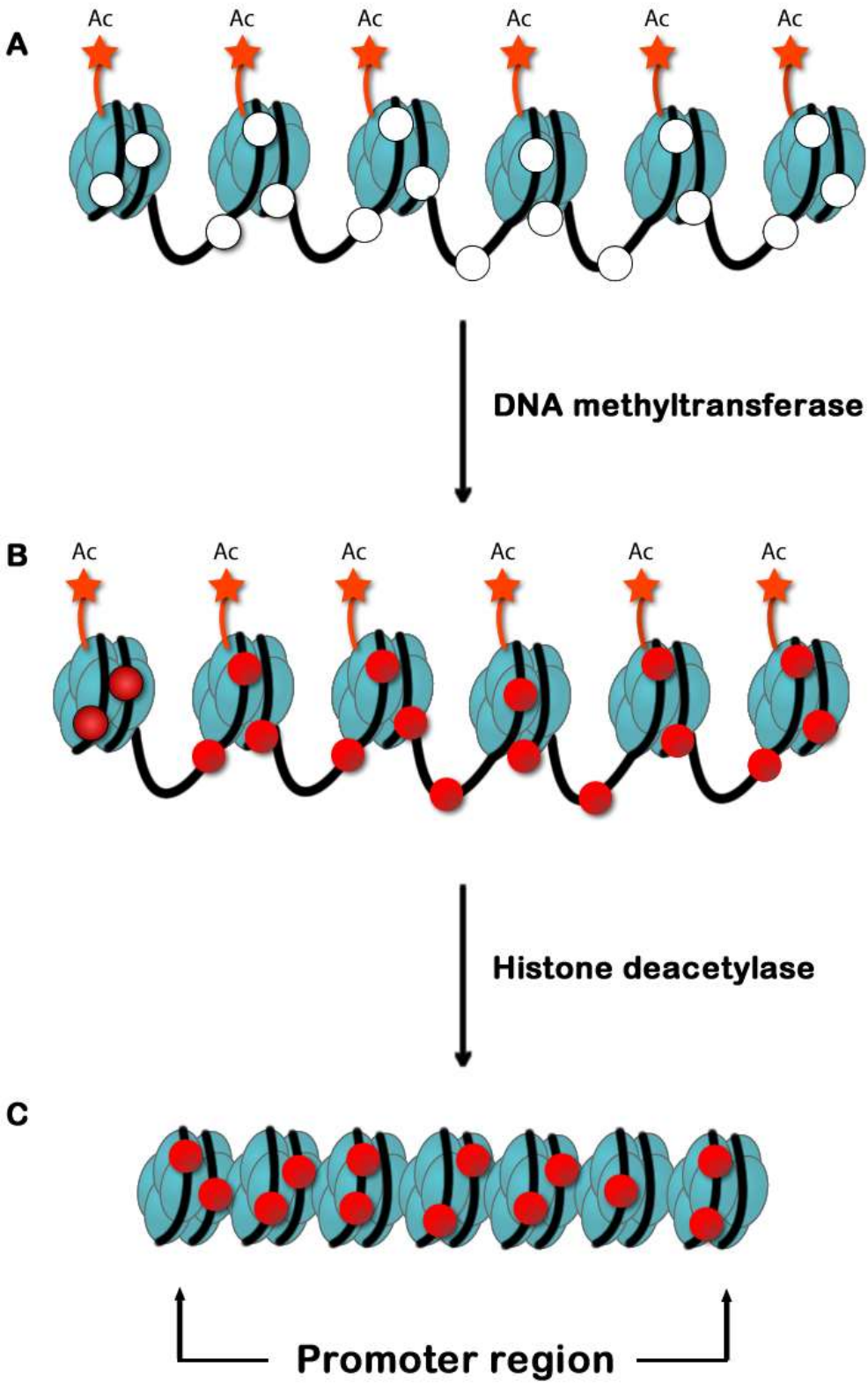

Figure 1.11: Collective effect of DNA methylation and histone modifications on the transcription

This figure illustrates the switching-off of an active gene by changing its DNA methylation and histone modification status. (**A**) DNMTs catalyse methylation on target DNA CpG dinucleotides. (**B**) This change triggers histone deacetylation. (**C**) Finally, DNA becomes more compact and this compaction leads to transcriptional silencing of a gene.

1.7 Project aims

The functional properties and physiological roles of B^0AT1 in different organs have been extensively studied (Bröer et al., 2004). However, not many studies have attempted to describe the regulatory elements of the *Slc6a19* gene. By bioinformatics analysis, Kikuchi et al. predicted a possible HNF1a-binding site on the *Slc6a19* promoter at position –126 to –110. Except this study no single study has been focused on the B^0AT1 regulation so far. The aim of this project was to investigate the transcriptional regulation of the neutral amino acid transporter B^0AT1 and to identify key control elements involved in its transcription.

1.8 Research questions

1. Does B^0AT1 mRNA expression mirrors its protein expression reported previously?
2. What are the regulatory elements in the promoter region of B^0AT1?
3. Why is B^0AT1 not expressed in intestinal crypt cells?
4. What transcription factors are involved in the positive regulation of B^0AT1 expression in cells located in the intestinal villi?
5. Does the nuclear chromatin status across the B^0AT1 promoter differ between the crypt and the villus?
6. Is DNA methylation involved in B^0AT1 transcriptional silencing outside the villus region (e.g. cells in the crypts or liver cells)?

Chapter 2 Material and Methods

2.1 Materials

2.1.1 Solutions

Table 2.1: Solutions used in this study

Luria-Bertani (LB) medium	**Luria-Bertani (LB) agar**
Tryptone 10 g	Tryptone 10 g
Yeast extract 5 g	Yeast extract 5 g
NaCl 10 g	NaCl 10 g
Add 1 L H_2O, pH = 7.0	Agar 15 g
Sterilized by autoclaving.	Add 1 L H_2O, pH = 7.0
	Sterilized by autoclaving.
Super optimal broth (SOB) medium	**Hanks Buffer**
Tryptone 20g	$CaCl_2$ 1.26 mM
Yeast extract 5g	KCl 5.4 mM
NaCl 8.5 mM	KH_2PO_4 0.44 mM
KCl 2.5 mM	$MgCl_2$ $6H_2O$ 0.5 mM
Add 1 L H_2O, pH = 7.0	$MgSO_4$ $7H_2O$ 0.4 mM
Sterilized by autoclaving, then add	NaCl 136.6 mM
$MgCl_2$ 10 mM	HEPES 10 mM
$MgSO_4$ 10 mM	Na_2HPO_4 2.7 mM
For SOC (also add glucose 20 mM)	pH 7.4
TB buffer	**Phosphate buffered saline (PBS, 10×)**
HEPES 10 mM, pH 6.7	NaCl 1.37 M
$CaCl_2$ 15 mM	KCl 26.8 mM
$MnCl_2$ 55 mM	Na_2HPO_4 80.6 mM
KCl 250 mM	KH_2PO_4 14.7 mM
Sterilized by filtration through a 0.22-μm filter	pH 7.4, sterilize by autoclaving

TAE buffer (50×)	**Cracking buffer (for rapid screening, 2×)**
Tris 2 M	Sucrose 0.2 g
Na_2EDTA 50 mM	SDS 50 µL of 10% (w/v) SDS
Glacial acetic acid 5.71 %	NaOH 40 µL 5M
pH 8.0	H2O top up to 1 ml
Tris buffered saline (TBS, 10×)	**Marker mix (for rapid screening)**
Tris-HCl 0.5 M, pH 7.5	KCl 4 M
NaCl 1.5 M	Bromophenol blue 0.4% (w/v)
Sterilized by autoclaving	

Tris-borate-EDTA buffer (TBE, 10×)
Tris 892 mM
Boric acid 890 mM
Na_2EDTA 20 mM
pH 8.0

2.1.2 Reagents and commercial kits

Opti-MEM®, DMEM/F-12, 0.25% trypsin–EDTA solution, 200 mM L-glutamine, Ultrapure™ 0.5 M EDTA, Ultrapure™ 10% SDS solution, heat inactivated foetal bovine serum (FBS) and 1× PBS buffer were purchased from Gibco® Life Technologies. Penicillin-streptomycin solution, DMEM, and oligonucleotides were obtained from Sigma-Aldrich®. RPMI 1640 medium with L-glutamine was purchased from PAA Laboratories. SimpleCHIP® Enzymatic Chromatin IP Kit was purchased from Cell Signaling Technology®. Power SYBR® Green PCR Master Mix, Supercoiled DNA ladder, SuperScript® III Reverse Transcriptase, T4 DNA ligase, Lipofectamine™ 2000 reagent, Lipofectamine® LTX, PureLink™ Quick Gel Extraction Kit, PureLink™ Quick Plasmid Miniprep Kit, Zero Blunt® TOPO® PCR Cloning Kit, and TOPO® XL PCR Cloning Kit were obtained from Life Technologies™. RNeasy Mini Kit, EpiTect® Bisulfite Kit, DNeasy® Blood & Tissue Kit, QIAquick® PCR Purification Kit, Rotor-Gene SYBR® green PCR Kit, and *Thermus aquaticus* (Taq) DNA polymerase were purchased from Qiagen. RNA 6000 Nano Labchip® Kit and QuikChange II Site-directed Mutagenesis Kit were purchased from Agilent. NucleoSpin® Plasmid purification Kit and NucleoBond Xtra Maxi EF were purchased from Macherey-Nagel. cOmplete, EDTA-free protease

inhibitor cocktail tablets were purchased from Roche. Phusion® high-fidelity DNA polymerase and T4 DNA Quick Ligation™ Kit were obtained from New England Biolabs® (NEB). Twenty-four-well cell culture plates were purchased from Iwaki. Dual-Luciferase® Reporter Assay System was purchased from Promega.

2.1.3 Antibodies

Antibodies used in chromatin immunoprecipitation assay (ChIP) are listed in **Table 2.2**.

Table 2.2: Antibodies used in this study

Antibody (anti-mouse)	**Source**	**Supplier (catalogue no)**
Histone H3 (acetyl K27)	Rabbit polyclonal antibody	Abcam (ab4729)
Histone H3 (tri-methyl K4)	Rabbit polyclonal antibody	Abcam (ab8580)
SOX9	Rabbit polyclonal	Abcam (ab3697)
TATA-binding protein	Mouse monoclonal	Abcam (ab51841)
HNF4a	Mouse monoclonal	Abcam (ab41898)
IgG	Rabbit polyclonal antibody	Cell signaling (2729)
Histone H3	Rabbit antibody	Cell signaling (4620)
HNF1a	Goat polyclonal	Santa Cruz (sc-6547X)

2.1.4 Vectors

The pcDNA 3.1 (+) vector was used for gene expression in mammalian cells (**see Section 2.6.4**). This vector contains a human cytomegalovirus (CMV) immediate–early promoter that achieves a high level of expression in a wide variety of cell lines. It contains the ampicillin- and neomycin resistance genes to facilitate selection in bacteria and cell lines, respectively.

pGL4.12[luc2CP] and pGL4.74[hRluc/TK] reporter vectors (Promega) were used in the dual luciferase assay (see **Section 2.6**). Promoter fragments were cloned into pGL4.12 vector to measure their activity. The pGL4.74 vector was used as an internal control in the dual luciferase assay. See **Table 2.3** for sources and comparison of these vectors. Detailed maps of the plasmids generated in this study are illustrated in the **Appendix 8.1.**

Table 2.3: Vectors used in this study

Vector	Features	Source
pcDNA3.1 (+)	• CMV promoter for optimal expression in a wide range of mammalian cells • SV40 polyadenylation site upstream of the CMV promoter • Neomycin- and ampicillin-resistance genes	Invitrogen
pGL4.12[luc2CP]	• Promoter-less • Firefly luciferase gene • Ampicillin-resistance gene	Promega
pGL4.74[hRluc/TK]	• Thymidine kinase promoter • Renilla luciferase gene • Ampicillin-resistance gene	Promega

2.1.5 Animals

Adult mice C57BL/6J (B6) mice were obtained from the Australian Phenomics Facility of The Australian National University (ANU) and housed under pathogen-free conditions. All experiments were approved by the ANU Animal Ethics and Experimentation Committee.

2.1.6 Antibiotics

Ampicillin: A stock solution of ampicillin sodium salt was dissolved in distilled water (50 mg/mL) and stored at –20 °C.

Penicillin-Streptomycin: This solution includes 10,000 IU of penicillin and 10 mg streptomycin per mL. The antibiotic aliquots were kept at 4 °C.

Kanamycin (ICN Biomedicals): A stock solution of kanamycin monosulphate was dissolved in distilled water (20 mg/mL) and aliquots were stored at –20 °C.

2.2 Bacterial experiments

2.2.1 Bacterial strains

Three strains of *Escherichia coli* (*E. coli*) were used as host bacteria for plasmid transformations (**Table 2.4**), namely the chemically competent DH5α, and electrocompetent XL-1 and strains. Aliquots of competent cells were stored at –80 °C.

Table 2.4: Bacterial strains were used in this study

Strain	Genotype	Source
E. coli DH5α	F–Φ80*lac*ZΔM15 Δ(*lac*ZYA-*arg*F) U169*rec*A1 *end*A1 *hsd*R17 (rk–, mk+) *pho*A *sup*E44 λ– *thi*-1 *gyr*A96 *rel*A1	Life Technologies
E. coli DH10B	F–*mcr*A Δ(*mrr*-*hsd*RMS-*mcr*BC) φ80*lac*ZΔM15 Δ*lac*X74 *rec*A1 *end*A1 *ara*D139 Δ (*ara, leu*)7697 *gal*U *gal*K λ- *rps*L *nup*G /*p*MON14272/*p*MON7124	NEB
E. coli XL-1 Blue	*rec*A1 *end*A1 *gyr*A96 *thi*-1 *hsd*R17 *sup*E44 *rel*A1 *lac* [F' *pro*AB l*ac*IqZ ΔM15 tn10 tet^r]	Stratagene

Strain	Genotype	Source
E. coli Top10	F–*mcr*A Δ(*mrr-hsd*RMS-*mcr*BC) Φ80*lac*ZΔM15 Δ*lac*X74 *rec*A1 *ara*D139 Δ(*ara leu*) 7697 *gal*U *gal*K *rps*L (StrR) *end*A1 *nup*G	Invitrogen

2.2.2 Transformation of electrocompetent bacteria

Plasmid DNA (2.5 µL) was added to electro-competent bacteria (*E. coli* XL-1 Blue) that were thawed on ice. The mixture was incubated on ice for 30 seconds and then transferred to a pre-chilled 0.2 cm electroporation cuvette (Astral). The cells were briefly exposed to a strong electrical field using a Bio-Rad Gene Pulser II (BioRad) set to 2.5 kV, 200 Ω and 25 µF. SOC medium (0.5–1 mL) was added to the cuvette immediately after the pulse and the mixture was transferred to a 15 mL Falcon tube. The cells were then allowed to recover from the electroporation for 60 min by shaking at 220 rpm at 37 °C.

The transformed cells were then plated onto LB-agar plates containing the appropriate antibiotic (100 µg/mL for ampicillin, 50 µg/mL for kanamycin) corresponding to the resistance gene present on the plasmid. The presence of the specific antibiotic in the medium ensured the growth of those cells that had taken up the plasmid. The plates were incubated overnight at 37 °C and visible colonies were further analysed (see **Section 2.4.1.3**).

2.2.3 Transformation of chemically competent bacteria

Aliquots (50 µL) of chemically competent bacteria (*E. coli* DH5α, DH10B or Top10) were thawed on ice and transferred into a pre-chilled 14 mL round bottom Falcon tube (BD Biosciences). One microliter of DNA was added to the bacteria. The tube was swirled and incubated on ice for 30 min. The transformation reaction was then placed in a 42 °C water bath for 45 seconds. The tube was immediately placed on ice for 2 min, after which 0.5 mL of SOC was added to the reaction. The bacteria were incubated at 37 °C for 60 min by shaking at 220 rpm. A volume of 150-250 µL of the reaction was plated onto an LB-agar plate containing the appropriate antibiotic to select transformed colonies. The plate was incubated overnight at 37 °C.

2.2.4 Bacterial growth

To culture transformed bacterial colonies, 10 mL of LB was placed in a 50 mL Falcon tube. The appropriate antibiotic was added to the LB at a final concentration of 100 μg/mL or 50 μg/mL for Ampicillin or Kanamycin, respectively. A sterile toothpick was used to pick a single transformed colony and was placed into the Falcon tube. The cultures were grown overnight in a rotatory shaker at 220 rpm at 37 °C.

2.3 Eukaryotic cell culture

2.3.1 Cell lines and cell culture

Cell lines used in this study were maintained in appropriate culture media (**Table 2.5**) at 37 °C in a humidified atmosphere of 5% CO_2 in an incubator. The cells were grown in 80-cm^2 tissue-culture flasks (Nunc) and cell density and morphology was examined on a daily basis by light microscopy. When cells reached 85–90% confluence, the medium was removed and the cells were detached from the surface of the flask by addition of 10 mL 0.25% trypsin–EDTA. After stopping trypsinization by adding media containing 10% FBS, the cells were transferred into a 50 mL falcon tube and collected by centrifugation at 1,500 rpm for 5 minutes. The pellet was resuspended with the relevant medium and centrifugation was repeated. After the supernatant was removed, the pellet was resuspended again in fresh medium and transferred into a new culture flask at a 1:20 ratio.

Table 2.5: Cell lines used in this study

Cell line	Description	Media
HeLa	Human cervix carcinoma cells	DMEM/F12 + 2 mM Q + 10% FBS
Caco-2	Human epithelial colorectal adenocarcinoma cells	DMEM/F12 +10% FBS +1% penicillin-streptomycin
FRTC	Rat thyroid cancer cells	DMEM/F12 + 5% FBS
HEK293	Human embryonic kidney cells	RPMI + 2 mM Q+ 5% FBS
HepG2	Human liver carcinoma cells	RPMI + 10% FBS

2.3.2 Counting of cell numbers

Cell suspensions were analysed and counted by using an automated cell counter (Scepter, Millipore).

2.4 Isolation and manipulation of DNA

2.4.1 DNA isolation

2.4.1.1 DNA extraction from mouse tissues

Isolation of DNA from C57BL/6J mice tissues was carried out using DNeasy Blood & Tissue Kit (Qiagen). The kidneys and intestine were used to isolate genomic DNA and its concentration was measured using a NanoDrop spectrophotometer (ThermoFisher Scientific).

2.4.1.2 Plasmid DNA isolation

Plasmids were isolated from overnight cultures using the NucleoSpin Plasmid Kit according to the manufacturer's protocol. Plasmid preparations for transient transfection of cell lines (see **Section 2.6.1**) were prepared using the NucleoBond Xtra Maxi Endotoxin-free Kit. The quality of the isolated plasmid DNA was checked using spectrophotometry (see **Section 2.8.2**) and agarose gel electrophoresis (see **Section 2.8.1**). The isolated plasmids were stored at –20 °C.

2.4.1.3 Rapid screening of transformed colonies

Following the transformation of the plasmid of interest, ~15 colonies were picked using a sterile toothpick or a pipet tip and re-streaked onto LB-agar plates containing appropriate antibiotic(s). After incubation at 37 °C overnight, a single colony was transferred to an Eppendorf tube using a toothpick. Forty µL of 10 mM EDTA (pH 8.0) was added to the tube and the bacteria were resuspended by vortex mixing. Fifty µL of freshly prepared 2× cracking buffer was added to lyse the bacteria and the mixture was mixed by a vortex and incubated for 5 minutes at 23 °C. After adding 10 µL of Marker mix, the tube was incubated on ice for 10 min. The samples were centrifuged at 4 °C for

3 min at 15,000×*g*. Of the supernatant, 20 µL was loaded onto a 1% agarose gel adjacent to a supercoiled DNA ladder (Invitrogen).

2.4.2 DNA experiments

2.4.2.1 Restriction enzyme digestion

Restriction digestion was used for cloning and linearization of plasmid DNA. Target DNA was typically digested for 2h by 10–20 U of a specific restriction enzyme in the recommended reaction buffer at the recommended temperature. The restriction enzymes were sourced from Invitrogen, NEB, or Takara Biotechnology.

2.4.2.2 Gel elution

Gel elution was used to clean PCR products, restriction enzyme digested DNA, and to separate the DNA fragments from unwanted vector impurities. Briefly, after electrophoresing the samples, the DNA fragment was cut out from the agarose gel using a scalpel and weighed. The DNA fragment was extracted from the isolated band using PureLink Quick Gel Extraction Kit. Spectrophotometry (see **Section 2.8.2**) was used to determine the concentration of the extracted DNA.

2.4.2.3 DNA ligation

To ligate DNA inserts into vectors, the T4 DNA Quick Ligation Kit was used. Ten µL 2× Quick Ligation Buffer and 1 µL of Quick T4 DNA ligase were added to a 1:3 molar ratio of vector to insert. The reaction mixture was incubated at 25 °C for 5 min after which the ligated DNA was precipitated by addition of 1 µL of yeast tRNA (5 µg/µL), 0.5 volumes of 7.5 M ammonium acetate, and 2.5 volumes of 100% ice-cold ethanol. The contents were mixed by a vortex and incubated for 10 min at 23 °C. The DNA was pelleted by centrifugation for 20 min at 16,000×*g* and the supernatant was discarded. A volume of 250 µL 70% ice-cold ethanol was added and the mixture was spun for a further 10 min at the same speed. The supernatant was discarded and the pellet was dried on the bench at 23 °C. The pellet was then dissolved in 5 µL of sterile water. A 2 µL aliquot of ligation product was later used to transform electro-component bacteria (see **Section 2.2.2**).

2.4.2.4 Polymerase chain reaction (PCR)

PCR reactions were performed using Taq DNA polymerase (Qiagen) according to the manufacturer's instructions. Each reaction contained 2 units of the polymerase enzyme, 1 μL of 10 mM deoxynucleotide triphosphate (dNTP) mix, 100 ng of DNA template, 5 μL of 10× PCR buffer, and 0.5 μM of the forward primer and 0.5 μM of the reverse primer in a final volume of 50 μL in distilled water. PCR reactions were run in a 96-well Veriti® thermal cycler (ABI) at the conditions shown in **Table 2.6**.

Table 2.6: Conditions of a PCR cycling

Process	**Temperature (°C)**	**Time (min:sec)**	**Number of repeats**
Denaturation	94	5:00	1
Denaturation	94	0:30	30
Annealing	50–58 (depending on the melting temperature (T_m) of primers)	0:30	
Extension	72	1:00	
Extension (Final)	72	10:00	1

In order to obtain proofread products, the PCR reactions were performed using *PfuUltra* high fidelity DNA polymerase (Agilent) or Phusion high-fidelity DNA polymerases according to the manufacturers' protocols. The products were separated on a 1% agarose gel (see **Section 2.8.1**). Thermal cycler conditions used in conjunction with *PfuUltra* and Phusion® high-fidelity DNA polymerases are listed in the **Appendix 8.2.**

2.4.2.5 Site-directed mutagenesis

QuikChange II Site Directed Mutagenesis Kit was used for this method. The entire plasmid was amplified by PCR using long primers (25–45 bp) with the desired mutation located in the centre of the primer (**Table 2.7**).

Table 2.7: Primer sequences used for site-directed mutagenesis

Red text indicates inserted mutations.

Mutation type	Sequence
HNF1a BS1(Mut1)	5′TGGAGGGGGTGGCTTAGCT**TCGG**AGGCTGGGTGCCTCTGCAG3′ 3′CTGCAGAGGCACCCAGCCT**CCGA**AGCTAAGCCACCCCCTCCA5′
HNF1a BS2(Mut2)	5′TGGGTGCCTCTGCAGATAAGGCA**GGCC**CAGTTCTGCAGGACGC3′ 3′GCGTCCTGCAGAACTG**GGCC**TGCCTTATCTGCAGAGGCACCCA5′
HNF1a mutation (R131W)	5′GCACAACATCCCCCAG**TGG**GAGGTGGTGGACACC3′ 3′GGTGTCCACCACCTC**CCA**CTGGGGGATGTTGTGC5′
HNF4a BS2(Mut2)	5′GGGTTGAGGTGC**TGAC**GGTTCTCTATAAAG3′ 3′CTTTATAGAGAACC**GTCA**GCACCTCAACCC5′
HNF4a BS4(Mut3)	5′GACAACAGAACACT**CCAC**GTCCTGTGAATTC3′ 3′GAATTCACAGGAC**GTGG**AGTGTTCTGTTGTC5′
HNF4a BS5(Mut4)	5′GTGAATTCTAG**TCAT**GTCACGTGTGCCAAG3′ 3′CTTGGCACACGTGAC**ATGA**CTAGAATTCAC5′
SOX9-BS1 Mut	5′CAGTGTGTTTGGT**TGAC**GGTCAGGCCCCTG3′ 3′CAGGGGCCTGACC**GTCA**ACCAAACACACTG5′
Sox9-Mut1	5′GCCTATGTCTGGG**CCTT**TGCAGGAGGAGGG3′ 3′CCCTCCTCCTGCA**AAGG**CCCAGACATAGGC5′
Sox9-Mut2	5′CAACCACTTGCCC**TGGG**TCTGCCGAGCTGCC3′ 3′GGCAGCTCGGCAGA**CCCA**GGGCAAGTGGTTG5′
SOX9 mutation (H65Y)	5′GCTGCGCGTGCAG**TAC**AAGAAAGACCACC3′ 3′GGTGGTCTTTCTT**GTA**CTGCACGCGCAGC5′
Spdef-mut	5′CAGGCCTTCAGCA**GGAT**CTCCTGTCCGTG3′ 3′CACGGACAGGAG**ATCC**TGCTGAAGGCCTG5′

Template DNA (50 ng) was mixed with 5 µL of the provided 10× reaction buffer, 125 ng of the sense primer, 125 ng of the antisense primer, and 1 µL of the dNTP mix. The final volume was adjusted to 50 µL using deionized water. One µL of *PfuUltra* high-

fidelity DNA polymerase (2.5 U/µL) was added to the reaction before performing PCR amplification (**Table 2.8**).

Table 2.8: PCR conditions for site-directed mutagenesis

Process	Temperature (°C)	Time (min:sec)	Number of repeats
Denaturation	95	0:30	1
Denaturation	95	0:30	16–18 cycles
Annealing	55	1:00/kb of plasmid	
Extension	68	4:00	1

The amplified DNA was digested for 3 hours with *Dpn*I (10 U/µL) at 37 °C to remove the template DNA. The DNA was then transformed into either chemically or electrocompetent *E. coli*.

2.5 Bioinformatics analysis

2.5.1 Alignment of promoter region

To identify the promoter regions conserved among different species, the promoter sequences were analysed using the University of California, Santa Cruz (UCSC) Genome Browser (http://genome.ucsc.edu). Using this method, regions of ~2.5 kb upstream of mouse *Slc6a19*, *Ace2*, and *Collectrin* transcription start sites were examined.

2.5.2 Prediction of transcription-factor-binding sites

The MatInspector program (http://genomatix.de) is a web-based bioinformatics tool which predicts transcription-factor-binding sites based on similarity of the input sequence to a library of known motifs (Quandt et al., 1995). A 2.5 kb fragment of *Slc6a19* promoter was analysed using this tool.

2.6 Reporter gene assay

The Dual-Luciferase® Reporter Assay system was used to identify effects of transcription factors on the mouse *Slc6a19* promoter. To this end plasmid

pGL4.12[luc2CP] containing the target promoter region, was expressed alone or was co-transfected with transcription factors of interest.

2.6.1 Principle of dual reporter assay

HEK293 cells were seeded out in 24 well plates at a density of 1×10^5 cells per well 24 hours before transfection. Transfections were performed using the Lipofectamine LTX (Invitrogen) reagent, according to the manufacturer's instructions.

Briefly, 500 ng of different *Slc6a19* promoter constructs in pGL4.12[luc2CP] vector (**Figure 2.1**), plus 100 ng of a transcription factor (TF) expressing vector (typically inserted into pcDNA3.1(+)), 5 ng of pGL4.74[hRluc/TK] control vector (**Figure 2.1**), and 2 µL of Lipofectamine LTX were added to 100 µL Opti-MEM®. The DNA solution was mixed and incubated for 30 min at 23 °C. After incubation, the mixture was added to HEK293 cells in a 24-well plate and incubated at 37 °C for 24 h.

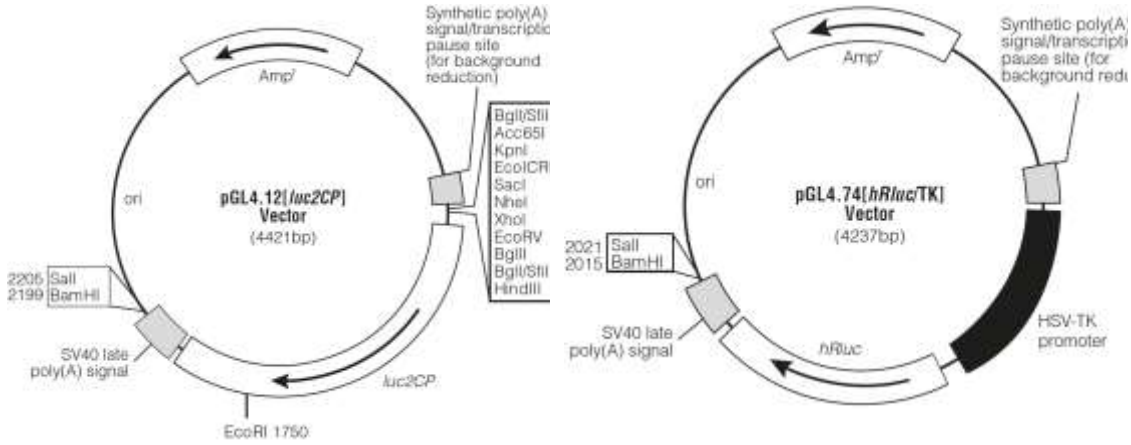

Figure 2.1: pGL4.12[luc2CP] plasmid and pGL4.74[hRluc/TK] plasmid were used as reporter plasmids in the Dual-Luciferase® Reporter Assay system.

pGL4.12 lacks a promoter sequence to start transcription of the *Firefly* Luciferase gene. Potential promoter sequences can be inserted upstream of the luciferase sequence. The *Renilla* luciferase, by contrast, is expressed constitutively from the *Herpes Simplex* thymidine kinase promoter (pGL4.74 vector). It serves as an internal control for the reporter gene assay system.

After 24 h of incubation, the cell medium was removed and, cells washed once with PBS (pH 7.4). Cell layers were lysed in 100 µL Passive Lysis Buffer (Promega) for 20 min at 23 °C using a shaker plate.

A 20 µL aliquot of the lysate was placed into a 1.5 mL Eppendorf tube containing 100 µL Luciferase Assay Reagent (LARII) and after 10 seconds, luminescence activity of the *Firefly* luciferase was measured using a Turner TD-20/20 illuminometer. Subsequently, 100 µL of Stop and Glo reagents was injected into the same tube to stop the Firefly luminescence and activate the *Renilla* luciferase. The relative luciferase activity was quantified by normalising the *Firefly* luciferase activity relative to the *Renilla* luciferase activity of the pGL4.74 control plasmid. Each transfection and measurement of luciferase activity was performed in triplicates.

2.6.2 Cloning of mouse *Slc6a19* promoter

Based on bioinformatic analysis, a 2.5 kb region upstream of the *Slc6a19* transcriptional start site was selected.

A 2551 bp fragment of the promoter spanning from position –2494 to +57, was generated using a two-step nested PCR amplification procedure. Initially, a 3013 bp section (–2639 to +374) of the promoter was amplified by PCR (**Table 2.9**). Two µL of the first PCR was used as a template for the second PCR targeting the 2551-bp promoter region. Primer Slc6a19(–2494) included a *Kpn*I restriction site and primer Slc6a19(+57) contained a *Bgl*II restriction site (**Table 2.9**). The final PCR product was purified and ligated (see **Section 2.4.2.3**) into a *Kpn*I/*Bgl*II digested pGL4.12 vector.

Table 2.9: Primers used for amplification of the *Slc6a19* promoter

Name	**Sequence**
Slc6a19(–2639)	5′ACCGGGTCATTTTTCTGCTCG3′
Slc6a19(+374)	3′TCCTGAGGAACATCCATCCAT5′
Slc6a19(–2494) *Kpn*I	5′ATGGTACCTTAGAGAGCTGCCTC3′
Slc6a19(+57) *Bgl*II	3′GAAGATCTCGCTGGGCTGGGCCGGGC5′

2.6.2.1 Preparing the truncated *Slc6a19* constructs

The truncated *Slc6a19* promoter constructs were generated using the full promoter construct in pGL4.12 using inverse PCR. Selection of the truncation points was based on sequence conservation. The resulting fragment sizes are listed in **Table 2.10**.

Table 2.10: Oligonucleotides used for the synthesis of B^0AT1 promoter deletion constructs

Promoter construct	Oligonucleotide	Insert size
pSlc6a19(–2494/+57)	5′ATGGTACCTTAGAGAGCTGCCTC3′	2551 bp
pSlc6a19(–1703/+57)	5′ATCTCTCTTGGTCTCTGTCCC3′	1760 bp
pSlc6a19(–1380/+57)	5′CTAGTTTCCCAGTGTGTTTGG3′	1437 bp
pSlc6a19(–972/+57)	5′GAGAAAGGGGATAGGGTAACA3′	1029 bp
pSlc6a19(–437/+57)	5′CTTCAGCCACCTTTAGGAATA3′	494 bp
pSlc6a19(–201/+57)	5′GTGCCCAGGCCTTCAGCAGG3′	258 bp
pSlc6a19(–136/+57)	5′GGTGCCTCTGCAGATAAGG3′	193 bp
pSlc6a19(–108/+57)	5′GTTCTGCAGGACGCGCCCT3′	165 bp
pSlc6a19(–37/+57)	5′GGTTCTCTATAAAGAGCCG3′	94 bp

2.6.3 Cloning of the *Ace2* and *Collectrin* promoter constructs

The mouse *Ace2* promoter sequence was amplified by nested PCR. Firstly, a fragment ranging from position –1602 to +254 was amplified. Subsequently, a shorter fragment from position –1509 to +170 was amplified by a nested PCR, using primers with incorporated *Xho*I and *Kpn*I restriction sites (**Table 2.11**). The final product was digested using *Xho*I and *Kpn*I, purified, and ligated into reporter vector pGL4.12.

The mouse *Collectrin* promoter DNA was generated by nested PCR. In the first PCR step, a fragment ranging from position –2125 to +266 was amplified (**Table 2.11**). In the second step, a smaller fragment (–1903 to +76) was generated using a primer set

that contained restriction sites for *Kpn*I and *Xho*I (**Table 2.11**). The final product was digested using *Kpn*I and *Xho*I, purified, and ligated into the reporter vector pGL4.12.

Table 2.11: Oligonucleotides used for the synthesis of *Ace2* and *Collectrin* promoter constructs

Promoter construct	Oligonucleotide
Ace2(–1602)F	5′CCGGGGTACTGCTTAGTTCA3′
Ace2(+254)R	3′ATTTTCCTCGGTGAGGGACT5′
Ace2 (–1509)*Xho*I	5′ATCTCGAGAGCTGACTGTGAGCATCCAC3′
Ace2 (+170)*Kpn*I	3′TAGGTACCGCCAAGATCCCATCCACTGA5′
Collectrin(–2125)F	5′CTCCTTGCGTACCTGCTTTC3′
Collectrin (+266)R	3′TTTCAAGCCACATGTCCAAA5′
Collectrin(–1903)*Kpn*I	5′ATGGTACCTGGTGGTGTTAGGTGTATT3′
Collectrin(+76)*Xho*I	3′TACTCGAGGCCGCAAACAGAAGACAAACT5′

2.6.4 Transcription factor constructs

Transcription factor complementary DNAs (cDNAs) used in this study were either cloned in our lab or obtained commercially.

The coding sequences of transcription factors HNF4a, SOX9, ATF4, PAX4, CREB3L3, GATA4, FOXA2 (HNF3b), NEUROG3, SMAD3, EGR1, and HNF1b were amplified on mouse intestinal cDNA by nested PCR. Initially, larger fragments were amplified using primers listed in **Table 2.12**. Subsequently, the coding sequence was amplified using the primers containing appropriate restriction sites. The final fragment was digested using the corresponding enzymes, purified, and ligated into mammalian expression vector pcDNA3.1(+). All transcription factor constructs were sequenced to confirm their identities (Biomolecular Resource Facility, John Curtin School of Medical Research (JCSMR), ANU).

The mouse HNF1a cDNA was purchased from Thermo Scientific (Clone ID:30471380). The mouse Cdx2 (BC103516) was purchased from Open Biosystems and cloned into the pcDNA3.1(+) (Invitrogen). The mouse GFP–STAT3 (embedded into pEGFP-C3) and the human Flag–STAT3 (embedded into pXJ40-FLAG) expression plasmids were kindly provided by Marie Bogoyevitch (Bio21 Institute, Melbourne).

Table 2.12: Primers used for cloning of TFs

Clone	Sequence	NCBI Ref. Seq.
HNF4a		NM_008261.2
mHNF4a-*BamH*I	5′TTGGATCCGGGAGAATGCGACTCTCTAAA3′	
mHNF4a-*EcoR*I	3′ATGAATTCAGCTTGCTAGATGGCTTCTTG5′	
SOX9		NM_011448.4
mSox9s	5′TTGGATCCATGAATCTCCTGGACCC3′	
mSox9a	3′ATGAATTCTCAGGGTCTGGTGAGCTG5′	
mSox9-*BamH*I	5′TTGGATCCATGAATCTCCTGGACCCCTT3′	
mSox9-*EcoR*I	3′ATGAATTCTCAGGGTCTGGTGAGCTGTGT5′	
ATF4		NM_009716.2
mAtf4-*BamH*I	5′TTGGATCCATGACCGAGATGAGCTTCCTG3′	
mAtf4-*EcoR*I	3′ATGAATTCTTACGGAACTCTCTTCTTCCC5′	
PAX4		NM_011038.1
mPax4s	5′GCTCTCCGTTTTCAGTTTGC3′	
mPax4a	3′GAGGCCTCTTATGGCCAGTT5′	
mPax4-*BamH*I	5′TTGGATCCATGCAGCAGGACGGACT3′	
mPax4-*EcoR*I	3′ATGAATTCTTATGGCCAGTTTGAGC5′	
CREB3L3		NM_145365.3
mCreb3l3s	5′AACATCCGGTGACGCTAGAC3′	
mCreb3l3a	3′GCCAGCCTGGTCTACAAGAG5′	
mCreb3l3-*Not*I	5′TTGCGGCCGCATGGATGGGGACATAGCG3′	
mCreb3l3-*Xba*I	3′ATTCTAGATCACAGCACCCCCAATGCA5′	
GATA4		NM_008092.3
mGata4-*EcoR*I	5′TTGGATCCATGTACCAAAGCCTGGCCAT3′	
mGata4-*BamH*I	3′ATGAATTCTTACGCGGTGATTATGTCC5′	
FOXA2 (HNF3b)		NM_010446.2
mHnf3bs	5′CCCGGGACTTAACTGTAACG3′	
mHnf3ba	3′GGTGAGACTGCTCCCTTGAG5′	
mHNF3-*EcoR*I	5′TTGGATCCATGCTGGGAGCCGTGAAG3′	
mHNF3-*BamH*I	3′ATGAATTCTTAGGATGAGTTCATAATAGG5′	
NEUROG3		BC104327.2
mNeurog3s	5′GGTGTGTGTGGGGGATACTC3′	
mNeurog3a	3′TGGAGCGAGAGTTTGATGTG5′	
mNeurog3-*Not*I	5′TTGCGGCCATGGCGCCTCATCCCTTGGA3′	
mNeurog3-*Xba*I	3′ATTCTAGATCACAAGAAGTCTGAGAACA5′	
SMAD3		NM_006754.6
mSmad3s	5′GCGGAGACCCAAACTTTCTA3′	
mSmad3a	3′GAAACAGGCTGGTGCCTTAG5′	
mSmad3-*EcoR*I	5′TTGGATCCATGTCGTCCATCCTGCCCTT3′	
mSmad3-*BamH*I	3′ATGAATTCCTAAGACACACTGGAACAGC5′	
EGR1		NM_007913.5
mEgr1s	5′CCACCCAACATCAGTTCTCC3′	
mEgr1a	3′GGCAGGGATGGTAAGTGAAA5′	
mEgr1-*EcoR*I	5′TTGGATCCATGGCAGCGGCCAAGGCCGA3′	
mEgr1-*BamH*I	3′ATGAATTCTTAGCAAATTTCAATTGTCCT5′	
HNF1b		NM_009330.2
mHNF1bs	5′CCCTCAACCCCTTCTTTTTC3′	

Clone	Sequence	NCBI Ref. Seq.
mHNF1ba	3′GGGTTTCTCCCTTCTCGTTG5′	
mHNF1b-*EcoR*I	5′TTGGATCCATGGTGTCCAAGCTCACGT3′	
mHNF1b-*BamH*I	3′ATGAATTCACCAGGCTTGCAGTGG5′	

2.7 RNA Studies

2.7.1 RNA extraction and quantitative PCR

2.7.1.1 Isolation of epithelial cells along the intestinal crypt–villus axis

Mouse intestinal tissue was isolated from an equal number of female and male mice (C57BL/6J (B6), 6 to 8 weeks old). To isolate cells populations from crypts and villi of mouse intestines, a fractionation method was used. This method used inversion of the intestinal lumen as described by Barnard et al. (1989) and optimized by Traber et al. (1991).

Briefly, the small intestine was cut after the duodenum and before the ileocaecal valve and perfused with ice-cold PBS, pH 7.4, containing 1mM dithiothretiol (DTT). Subsequently, a 6-cm-long section of mouse jejunum was inverted onto a plastic rod. The plastic rod was inserted into a purpose made hole in the cap of a 12–mL, plastic, round-bottom centrifuge tube, containing 10 mL citrate buffer (96 mM NaCl, 1.5 mM KCl, 27 mM sodium citrate, 8 mM KH_2PO4, and 5.6 mM Na_2HPO_4, pH 7.4). After sealing with Parafilm, the assembly was incubated on a rotatory shaker at 37 °C for 10 min. Subsequently, the citrate buffer was changed to 10 mL PBS (pH 7.4) containing 0.5 mM DTT, 1.5 mM EDTA, and 1 mg/mL bovine serum albumin at 37 °C. Rotary shaking was continued for 10–20 min until the solution turned opaque indicating detachment of cells from the intestinal lumen. The solution was removed and replaced by pre-warmed fresh solution until 5 to 7 fractions were collected. Cell viability was judged by Tryphan Blue exclusion (Strober, 2001).

2.7.1.2 RNA extraction and microarray studies

Total RNA was isolated using the RNeasy Mini Kit (Qiagen) according to the manufacturer's protocol. RNA quality was determined by using an RNA 6000 Nano LabChip® Kit on the Agilent Bioanalyzer 2100 (Agilent Technologies) platform

according to the manufacturer's protocol. RNA samples with and RNA integrity number (RIN) of ≥8 were used in subsequent microarray analyses (**Figure 2.2**).

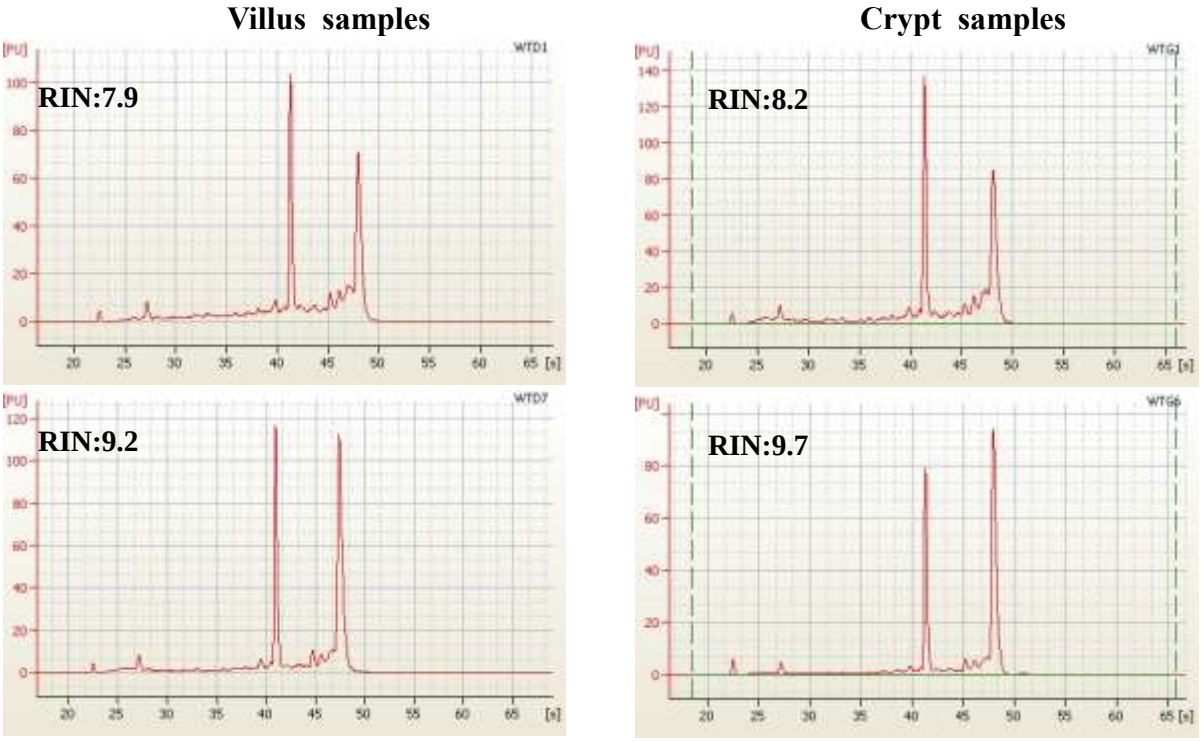

Figure 2.2: Quality analysis of microarray samples

The quality of the total RNA was examined using the Bionalyzer 2100 (Agilent). According to RIN values, the quality of the isolated cells from the crypt was slightly better than that from villus. In these electropherograms, the two peaks represent the 18s and 28s ribosomal RNA (rRNA).

Global gene expression was analysed using an Agilent SurePrint G3 Mouse Exon Microarray kit at the Ramaciotti Center, University of New South Wales, Sydney.

2.7.1.3 Complementary DNA synthesis

cDNA was generated from extracted RNA using the SuperScript™ III Reverse Transcriptase enzyme (Invtirogen). The reaction was prepared by adding 1 µL of oligo(dT) primer (Invitrogen), 0.5 mM of dNTPs, and 8 µL of total RNA (concentration, 250 ng/µL). The reaction was incubated at 65 °C for 5 min to denature RNA before being transferred onto ice for 1 minute. Subsequently, 4 µL of 5× First-Strand buffer, 1 µL of

0.5 mM DTT, 1 μL RNAseOut (Invitrogen), 0.5 μL SuperScript™ III, and 3.5 μL of sterile distilled water was added. The resulting mixture was incubated for 60 min at 50 °C. The reaction was stopped by heating at 85 °C for 5 min.

2.7.1.4 Quantitative real-time RT-PCR (qRT-PCR)

qRT-PCR was conducted using the Fast SYBR® Green master mix (Applied Biosystems) in conjunction with an Applied Biosystems 7900 instrument. The reaction mixture (10 μL) included 5 μL SYBR® Green master mix, 3 μL of sample cDNA (1:10 dilution) and 1 μL of each primer (final concentration, 200 nM). The samples were pipetted into a 394-well plate. The PCR cycling parameters were 50 °C for 2 min, followed by 40 cycles of denaturation at 95 °C for 15 s and 60 °C for 1 min. All samples were analysed in duplicates. Glyceraldehyde-3-phosphate dehydrogenase (GAPDH) cDNA served as an internal control. GAPDH previously used as a single reference gene to compare the gene expression in the crypt-villus axis (Anderle et al., 2005). Primers were designed using the Primer3 program (http://*frodo.wi.mit.edu/*) to amplify fragments of 170–250 bp. The primers used for qRT-PCR are listed in **Table 2.13**. To validate the quality of the mRNA for microarray analysis, mRNA expression of six selected genes was quantified by qRT-PCR.

Table 2.13: Primer sets used for RT-PCR and qRT-PCR amplifications

Name	Sequences
Lgr5	5′TAAAGACGACGGCAACAGTG3′ 3′GATTCGGATCAGCCAGCTAC5′
Slc6a19	5′CCGTCGTCTACGTGTATGGA3′ 3′ACCCAGTTGGGGTATGGAAT5′
Hnf1a	5′TCACAGACACCAACCTCAGC3′ 3′CCGTTGGAGTCGGAACTCT5′
Hnf4a	5′GCCAAGATTGACAACCTGCT3′ 3′ATTCAGATCCCGAGCCACTT5′
Gata4	5′TCAAACCAGAAAACGGAAGC3′ 3′GCCGGACACAGTACTGAATGT5′
Cdx2	5′GCAGTCCCTAGGAAGCCAAG3′ 3′CTGCGGTTCTGAAACCAAAT5′
GAPDH	5′AACTTTGGCATTGTGGAAGG3′ 3′CCCTGTTGCTGTAGCCGTAT5′
Sox9	5′TCAGATGCAGTGAGGAGCAC3′ 3′CCAGCCACAGCAGTGAGTAA5′

2.7.2 Microarray Analysis

2.7.2.1 Bioinformatics analyses of microarray data

Microarray data were analysed using the GeneSpring GX software (Agilent Technology). The GeneSpring software has tools for normalisation, statistical analyses, statistical interpretations, and quality control of gene expression data. Duplicate samples were prepared for each cell population. The normalisation step was performed as follows: individual probe sets were first filtered on expression between the 20^{th} and 100^{th} percentile in at least 2 out of 4 samples. After normalisation, the remaining probe sets were filtered for a more than three-fold change of expression. Unpaired *T*-tests, which were corrected with Bonferroni multiple testing, were applied on the differentially expressed genes. After normalisation and statistical analysis, 4464 probes were identified as differentially expressed genes.

2.7.2.2 Gene Ontology (GO) Analysis

Gene ontology (GO) is a bioinformatics tool designed to organise genes in different groups based on their attributes. To identify significantly enriched GO terms, differentially expressed genes from the microarray analysis were classified using GeneSpring GX software. GeneSpring GX program identified classes of genes based on $p < 0.01$. Each significant set of genes was grouped into different categories, based on biological processes, molecular function, and cellular components according to the GO consortium database (http://www.geneontology.org).

2.7.2.3 Pathway Analysis

The GeneSpring program was also used for pathway analysis of the 4464 differentially expressed genes. For a more selective pathway analysis a >10-fold change was set. The GeneSpring program uses the Kyoto Encyclopaedia of Gene and Genomes (KEGG) pathway database to identify significant pathways ($p < 0.05$).

2.8 Analysis of DNA and RNA

2.8.1 Agarose gel electrophoresis

DNA products were analysed using an agarose gel electrophoresis system. Briefly, the agarose gel (1%) was dissolved in the TAE buffer by boiling the mixture using microwave heating. After cooling the agarose to ~55 °C, it was poured into the electrophoresis apparatus containing a comb. Subsequently, the agarose was left to set and the gel was submersed in the TAE buffer, and the comb removed.

Approximately 20 μL of DNA products were mixed with the 6× loading buffer (Invitrogen) and loaded onto the gel wells. The presence of 60% glycerol in the loading buffer helped to sink the sample to the bottom of the well. This included bromophenol blue which assisted in the visualisation of DNA migration. Either a 1-kb or a 100-bp DNA ladder (NEB) was loaded as marker to determine the electrophoresed band sizes.

The electrophoresis tank (Bio-Rad) was run at 10 V/cm to separate DNA bands. The gel was stained with ethidium bromide solution (5 μL/mL) for 15 min before being photographed using a Gel-Doc UV system and an integrated imaging program (Vision-Capture).

2.8.2 Spectrophotometry

Both DNA and RNA samples were quantified using a NanoDrop Spectrophotometer (NanoDrop Technologies) at a wavelength of 260 and 280 nm using deionized water as a control.

2.8.3 DNA sequencing

DNA sequencing was performed by the Biomolecular Resource Facility (BRF) at JCSMR, ANU. Sequencing was performed using the Big Dye Terminator sequencing kit (ABI) and the Applied Biosystems 3730XL DNA analyser.

The sequencing reaction consisted of 2 μL of Big Dye Terminator (BDT), which included the polymerase enzyme and fluorescent nucleotides, 3 μL of a 5× BDT buffer (ABI), 3.2 pmol of the amplification primer (**Table 2.14**), 300 ng of template DNA, and

distilled water to adjust the final reaction volume to 20 µL. The contents of the reaction were mixed and placed in a 96 well Veriti thermal cycler (ABI). Cycling conditions are shown in **Table 2.15**.

Table 2.14: Primers used for sequencing

Name	Sequence
pcDNA3.1 Seq Antisense #10	3′CTGGCAACTAGAAGGCACAGT5′
pcDNA3.1 Seq Sense #6	5′GGCTAGCGTTTAAACTTAAGC3′
pcDNA3.1 Seq Antisense #7	3′TTAAACGGGCCCTCTAGACTC5′
pcDNA3.1 mHNF1a Seq Sense #8	5′GTCTACAACTGGTTTGCCAAC3′
pGL4.12 int100L #24	3′TGGTGGCTTTACCAACAGTA5′

Table 2.15: The Sequencing PCR conditions

Process	Temperature (°C)	Time (min:sec)	Number of repeats
Denaturation	94	5:00	1
Denaturation	94	0:10	30 cycles
Annealing	50	0:10	
Extension	60	4:00	
Extension (Final)	60	8:00	1

To purify the reaction, 2 µL of 3 M sodium acetate (pH 5.2) and 50 µL of ethanol (ice cold) were added to the 20 µL of the PCR reaction. After incubating the mixture at 23 °C for 15 min, it was spun at maximum speed for 20 min in a table top centrifuge. The supernatant was discarded, 250 µL of 70% ethanol was added, and the mixture spun for 5 min at maximum speed. After discarding the supernatant, the reaction was dried at 23 °C and delivered to the BRF for sequencing.

2.8.4 DNA bisulphite sequencing

Genomic DNA was isolated using DNeasy Blood & Tissue kit (Qiagen). Up to 200 µg of isolated genomic DNA was treated with an EpiTect Bisulfite Kit (Qiagen) according to the manufacturer's instructions. In this process, all unmethylated cytosine residues were converted to uracil nucleotides, whereas methylated cytosine residues (5-methylcytosine) remained intact during the treatment.

The promoter region was amplified by nested PCR from bisulphite-treated template DNA. In the first round, a 1639 bp fragment starting from position –1380 to +259 was amplified, followed by another amplification of a fragment ranging from position –1131 to +18. The PCR products were sequenced and analysed for the methylation status of all CpG dinucleotides in the selected region. Primers used to investigate CpG dinucleotides in the B^0AT1 promoter region are listed in **Table 2.16**. MethPrimer (http://www.urogene.org/methprimer/index1.html) was used for selecting and designing these methylation primers.

Table 2.16: Primers used in DNA methylation analysis

metB0AT1(–1380)	5′TTAGTTTTTTAGTGTGTTTG3′
metB0AT1(+259)	3′AAAAATACTATAACTTCCAC5′
metB0AT1(–1131)	5′GAGGAAAAAGATAATAGAAT3′
metB0AT1(+18)	3′AACACAAACCTCACCATAATAATC5′

The amplification was performed using the Taq polymerase (Qiagen) in a 50 µL reaction volume for 35 cycles under the following conditions: 94 °C for 5 min, 94 °C for 30 s, 50°C for 30 s, 72 °C for 1 min and a terminal extension at 72 °C for 5 min. A 50 µL aliquot of the amplification product was run on a 1% agarose gel, and gel elution was carried out using PureLink Quick Gel Extraction Kit (Invitrogen) according to the manufacturer's protocol (see S**ection 2.4.2.2**). The purified fragment of the correct product size was cloned using the Zero Blunt Topo XL cloning kit (Invitrogen). A small aliquot (2 µL) of the ligation reaction was transformed into chemically competent *E. coli* (TOP10 cells) (see **Section 2.2.3**). Ten colonies were grown overnight, plasmid was isolated and subjected to sequencing for confirmation of methylation status at the BRF. Methylation results were visualised by the BIQ Analyzer software (http://biq-analyzer.bioinf.mpi-inf.mpg.de/).

2.9 Protein-DNA interaction

2.9.1 Chromatin immunoprecipitation (ChIP)

Chromatin immunoprecipitation (ChIP) was performed using the SimpleChip Enzymatic Chromatin IP Kit #9003 (Cell Signaling Technology) according to the manufacturer's instructions. Freshly prepared tissue of mouse kidney cortex, liver, mucosa, or intestinal fractionations were used in the ChIP assay. Forty mg of each of the mouse tissues was cut into small pieces using a scalpel. The cut tissues were placed into the 15-mL falcon tubes with 1 mL ice cold PBS, pH 7.4, buffer containing the protease inhibitor cocktail (Cell Signaling Technology). Nuclear proteins were then cross-linked to the DNA by addition of freshly prepared formaldehyde (to a final concentration of 1.5%), and the tubes were incubated on a rotator for 20 min at 23 °C. The cross-linking was stopped by addition of glycine to a final concentration of 125 mM followed by further incubation on a rotator for 5 min at 23 °C. The tissues were centrifuged at 4 °C for 5 min at 1,500 rpm, and washed with 1 mL ice-cold PBS (pH 7.4) containing protease inhibitors. The centrifugation and washing steps were repeated seven times for seven fractions. The tissues were treated with 20–25 strokes in a Potter homogeniser, followed by centrifugation at 4 °C for 5 min at 1500 rpm. Chromatin was digested to 150–900-bp nucleosomal fragments using Micrococcal Nuclease (Mnase; Cell Signaling Technology) for 20 min at 37 °C. The reaction was stopped by adding EDTA. For further transcription factor studies, the nuclear membrane was fragmented by 25 strokes using a Potter homogeniser. For histone protein studies, the membrane was disrupted using a Misonix S-4000 sonicator at 15- s intervals for 2 min at 4 °C. The lysates then were centrifuged at 10000 rpm for 10 min at 4 °C to obtain the cross-linked chromatin in the supernatant.

The chromatin samples were immunoprecipitated with specific antibodies (listed in **Section 2.1.3**) at 4 °C with overnight rotation. After immunoprecipitation (IP) with the indicated antibodies, the IP mixture was incubated with ChIP Grade Protein G Magnetic Beads (#9006; Cell Signaling Technology) at 4 °C for 2 h with rotation. The magnetic beads were then washed with low-salt and high-salt ChIP buffer (Cell Signaling Technology). Subsequently, crosslinking was reversed in elution buffer and proteins were digested by adding proteinase K at 65 °C for 2 h. The DNA was purified using a spin column provided in the kit. Purified DNA fragments were analysed further by quantitative PCR (qPCR) and PCR amplifications using specific primers (**Table 2.17**).

Table 2.17: ChIP primer sets used for B^0AT1 promoter analysis

P1 (–139/+11)	5′CTGGGTGCCTCTGCAGATAA3′ 3′AAAGGGCAAGTGGTTGTGTC5′
P2 (–353/–136)	5′ATCAGTATCCTGCTGGTCTGT3′ 3′CCAGCCTAACCAGCTAAGCC5′
P3 (–495/–281)	5′CTGGAAGAACCCAAGCCATA3′ 3′GGAGGCATCTCCAGCAAATA5′
P4 (–501/–332)	5′CTGTGCCTGGAAGAACCCAA3′ 3′TACAGACCAGCAGGATACTGA5′
P5a (–858/–674)	5′CATGCCCCACCTAAGTCCT3′ 3′TACAGAGAAGCCAGCATGACA5′
P5 (–682/–502)	5′TGCTGGCTTCTCTGTATCTCCC3′ 3′GCTCCGTGCTCTAAGTGTCC5′
P6 (–984/–812)	5′GGAGGGGAATTTGAGAAAGG3′ 3′TGTTCGTTTCGTGCAAACAT5′
P7 (–1236/–976)	5′ATTTGGGCTTTAGGGGTGTT3′ 3′CCCCTACATCATGTCCTTGG5′
P8 (–1368/–1255)	5′TCTCAGGGTCCTTCTTCACC3′ 3′AACACCCCTAAAGCCCAAAT5′

2.10 Statistical analysis

All results are expressed as mean ± SD. $p < 0.05$ was considered to be statistically significant. For statistical comparison Student's t-test was used. All statistical studies were performed using GraphPad Prism v.6 (GraphPad Software).

Chapter 3 Comparison of differentially expressed genes along the crypt–villus axis

3.1 Introduction

Each villus can be separated anatomically into two regions, namely crypt and villus tip. Enterocytes are continually dividing and differentiating, starting in intestinal crypts, and migrating along a villus, until they eventually slough off at the villus tip (Cosentino et al., 1996). The B^0AT1 protein is expressed at the apical membrane of villus enterocytes but not in crypt cells. Previous studies also showed that B^0AT1 mRNA is highly expressed at the villus tips, while absent in intestinal crypts (Bröer et al., 2004). The comparison of these two regions should provide insight about transcriptional regulation of the *Slc6a19* gene on the intestinal surfaces.

Caco-2 cells are endowed with villi and have been used as a cellular model of intestinal enterocytes for transport and metabolic studies (Van Beers et al., 1995). Rodent IEC6 cells, by contrast, have been used as a model of crypt-like intestinal cells (Quaroni and Beaulieu, 1997, Quaroni and May, 1979, Trompette et al., 2004, Drago et al., 2006). Similarly, another progenitor-like cell model, the human intestinal epithelial cell line (HIEC), was used to study intestinal cell differentiation (Benoit et al., 2010, Escaffit et al., 2006).

As an alternative to cell lines, cell fractionation methods have been developed (Traber et al., 1991) and widely used to examine the function, proliferation or differentiation of intestinal epithelial cells along the crypt–villus axis. Alternatively, laser micro-dissection has been used to examine and characterise mouse or human intestinal epithelial cells (Anderle et al., 2005, Stappenbeck et al., 2003, Crosnier et al., 2006).

Initially, Olsen et al. (2004) established an online database of crypt–villus gene expression patterns in the mammalian intestine. The mammalian crypt–villus axis has also been studied by microarray analyses by a number of groups with different study objectives (Anderle et al., 2005, Mariadason et al., 2005, George et al., 2008). These studies have shown that genes associated with DNA synthesis are expressed in the crypt, whereas genes related to digestion and absorption of nutrients present in differentiated enterocytes of the villus.

3.2 Results

3.2.1 Validation of the crypt–villus cell fractionation

Using a rotatory shaking mechanism, cells were detached in different fractions (see **Section 2.7.1.1**). Initial fractions were enriched in enterocytes released from the tip, and later fractions were enriched in cells derived from the crypt.

Cell enrichment in fractions was assessed by qRT-PCR (see **Section 2.7.1.4**). For instance, fractions 1 and 2 contained high levels of *Slc6a19* mRNA, while it was barely detectable in fraction 7 (**Figure 3.1**). *Lgr5* (leucine-rich repeat containing G-protein coupled receptor 5), a crypt stem cell marker, showed an opposite trend and was highly enriched in fraction 7.

Accordingly, RNA from fraction 2 (villus) and 7 (crypt) were selected for microarray analyses. RNA samples were hybridised to Agilent arrays using 39,430 probe sets.

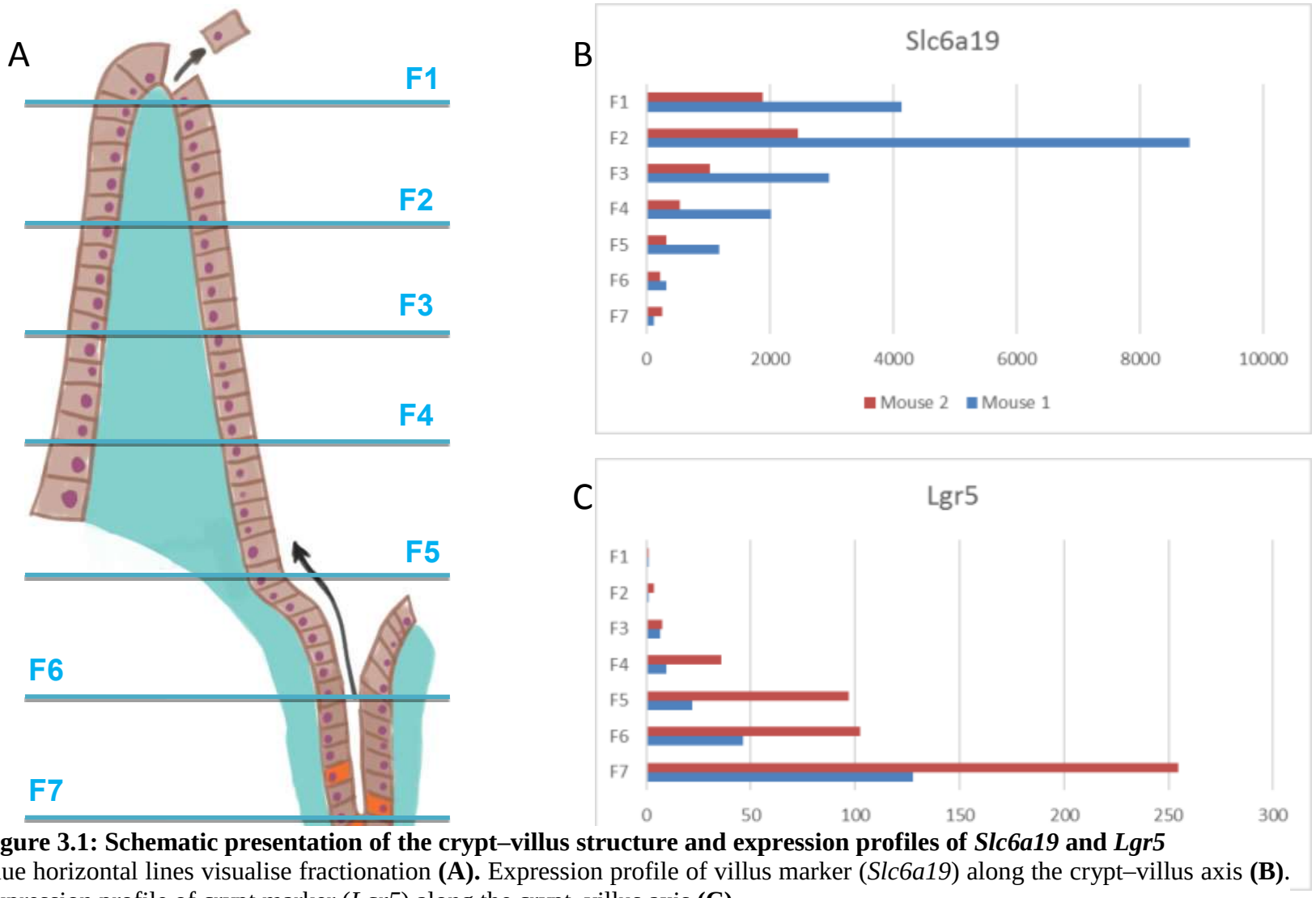

Figure 3.1: Schematic presentation of the crypt–villus structure and expression profiles of *Slc6a19* and *Lgr5*
Blue horizontal lines visualise fractionation **(A).** Expression profile of villus marker (*Slc6a19*) along the crypt–villus axis **(B).** Expression profile of crypt marker (*Lgr5*) along the crypt–villus axis **(C)**.

3.2.1.1 Validation of microarray data

The microarray data were validated through qRT-PCR of six selected genes (**Figure 3.2**). A high level of correlation was found between qRT-PCR and microarray results (R = 0.9146).

A

	Fold difference (Crypt vs Villus)	
Gene name	**Microarray**	**qRT-PCR**
Lgr5	+49.21	+115.69
Slc6a19	–18.36	–7.59
Hnf1a	+2.83	+4.11
Hnf4a	+3.42	+5.41
Gata4	+3.39	+4.98
Cdx2	+4.18	+3.23

B

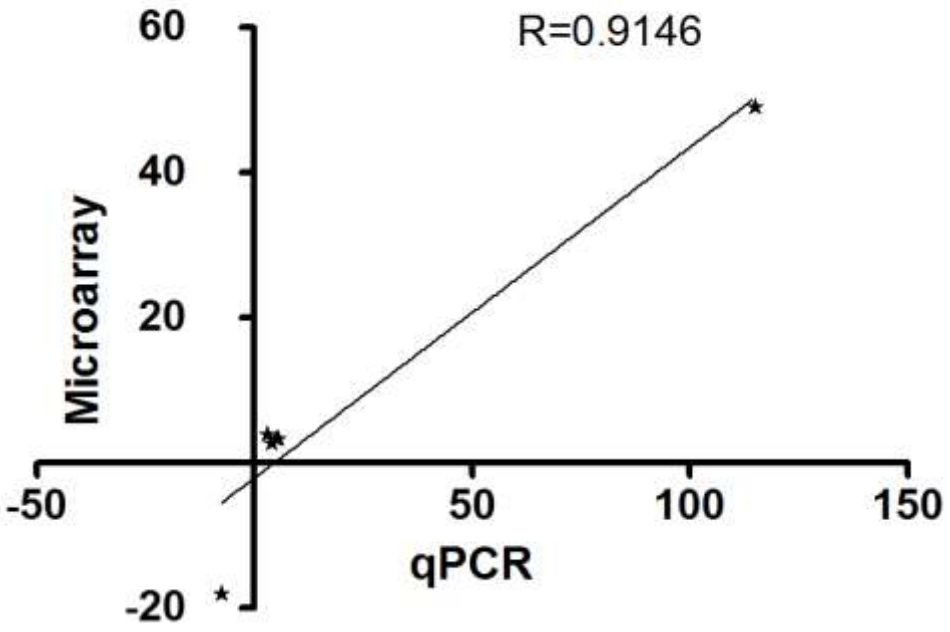

Figure 3.2: Confirmation of the microarray results by qRT-PCR

(**A**) Expression levels of selected genes as measured by microarray and qRT-PCR.
(B) Correlation between microarrays and qRT-PCR.

3.2.1.2 Gene ontology (GO) analysis

Gene ontology analysis was performed to identify genes that perform villus-specific or crypt-specific functions (see **Section 2.7.2.2**). More than 3000 differentially expressed genes were identified. Of these, 1,854 genes were up-regulated and 2,610 genes were down-regulated along crypt–villus axis.

Robustly expressed genes were categorised based on their involvement in biological processes, molecular functions, or cellular structures/organelles according to the GO consortium database (http://www.geneontology.org). In agreement with the roles of mature enterocytes in nutrient and ion absorption, transport-associated genes were highly enriched in the villus tip. A summary of the results is shown in Table 3.1. A detailed graph of gene ontology terms enriched in the villus is shown in **Appendix 8.3.**

Table 3.1: List of gene ontology (GO) categories significantly up-regulated in cells of the villus tip

"Total genes in GO class" stands for the number of genes included in a GO category. "Number of genes" stands for the actual number of genes that were up-regulated in the category. P <0.05 indicates statistical significance.

GO category	Total genes in GO class	Up-regulated genes	P-value
Biological process/organic substance transport	392	44	<0.01
Biological process/Na^+ transport	145	23	<0.01
Biological process/carboxylic acid transport	179	24	<0.01
Biological process/nitrogen compound transport	147	21	<0.01
Biological process/lipoprotein transport	12	5	<0.01
Cellular component/brush border	61	13	<0.01
Molecular function/symporter activity	114	20	<0.01
Molecular function/solute–sodium symporter activity	47	12	<0.01
Molecular function/cofactor transporter activity	11	5	<0.01
Molecular function/carboxylic acid transmembrane transporter activity	95	14	<0.01

Genes that were up-regulated in crypt cells were mostly associated with cell proliferation. This result is shown in Table 3.2. A more detailed graph showing gene ontology terms enriched in the crypt is shown in **Appendix 8.4.**

Table 3.2: List of gene ontology (GO) categories significantly up-regulated in crypt cells

"Total genes in GO class" stands for the number of genes included in a GO category. "Number of genes" stands for the actual number of genes that were up-regulated in the category. P <0.05 indicates statistical significance.

GO category	Total genes in GO class	Up-regulated genes	P-value
Biological process/M phase of mitotic cell cycle	216	63	<0.01
Biological process/cell cycle	787	115	<0.01
Biological process/chromosome segregation	105	30	<0.01
Biological process/DNA replication	152	25	<0.01
Biological process/DNA repair	291	33	<0.01
Cellular component/chromosome	498	61	<0.01
Cellular component/microtubules	627	68	<0.01
Cellular component/nuclear part	1745	120	<0.01
Molecular function/microtubule motor activity	44	10	<0.01

3.2.1.3 Pathway analysis

The GeneSpring program was used to categorize genes according to the Kyoto Encyclopaedia of Gene and Genomes (KEGG) (Kanehisa and Goto, 2000) (see **Section 2.7.2.3**).

In addition to genes involved in digestion and absorption, cell adhesion and cytoskeleton-associated pathways were significantly up-regulated in the villus compartment. This is consistent with a role of adherence and tight junctions between enterocytes functioning as an epithelial barrier (Champe et al., 2005). Furthermore, the brush border on the surface of differentiated enterocytes requires an elaborate cytoskeletal network to support the microvillus structure (Mooseker, 1985).

Digested dietary lipids, including cholesterol, free fatty acids, and monoacylglycerol, are absorbed by fully differentiated enterocytes and distributed to the body via chylomicrons (Shiau, 1987). Chylomicrons, which contain triacylglycerol, cholesterol, and phospholipids, are assembled in the endoplasmic reticulum of enterocytes and secreted into the lymphatic system which transports them to the blood (Champe et al., 2005). Accordingly, it is not surprising that expression of genes associated with lipid uptake and lipid biosynthesis was found to be up-regulated in villus cells. Also, genes associated with the peroxisome proliferator-activated receptors (PPAR) signalling pathway, which mediate chylomicron formation and lipid metabolism (Braissant et al., 1996), were highly expressed in the villus compartment.

Pathway analyses revealed that genes associated with immune functions, including T cell and B cell receptor signalling pathways, chemokine signalling pathways, interleukin signalling pathways, were highly enriched in villus. A summary of these pathways is shown in Table 3.3. In contrast to earlier studies, genes related to pathways associated with immune cell signalling were enriched in the villus. This is consistent with the fact that the differentiated epithelium harbors lymphocytes which are important for host defence against potential pathogens (Ferguson, 1977).

Table 3.3: Overrepresented KEGG pathways in the villus

"Pathway entities" refers to the number of genes corresponding to the KEGG pathways. "Matched entities" is the number of the significantly expressed genes in a pathway. The P-value indicates statistical significance.

Pathway	Pathway entities	Matched entities	P-Value
T cell receptor signalling pathway	133	62	<0.001
Regulation of actin cytoskeleton	151	54	<0.001
B cell receptor signalling pathway	156	54	<0.001
Chemokine signalling pathway	193	60	<0.001
PPAR signalling pathway	87	32	<0.001
Calcium regulation in the cardiac cell	150	48	<0.001
Integrin mediated cell adhesion	100	35	<0.001
Focal adhesion	191	53	<0.001
Insulin signalling	159	47	<0.001
Glycolysis and gluconeogenesis	48	21	<0.001
IL-2 signalling pathway	76	27	<0.001
IL-5 signalling pathway	69	24	<0.001
IL-4 signalling pathway	61	22	<0.001
Myometrial relaxation and contraction	157	43	<0.001
EGF1 signalling pathway	176	46	<0.001
Statin pathway	20	10	<0.001
Triacylglyceride synthesis	23	11	<0.001
G protein signalling pathways	91	27	<0.001
Kennedy pathway	14	8	<0.001
IL-6 signalling pathway	99	28	<0.001
Nuclear receptors in lipid metabolism	30	12	<0.001
Eicosanoid synthesis	19	9	<0.001
Selenium metabolism	31	10	<0.001
Adipogenesis	133	34	0.001
Purine metabolism	7	5	0.001
IL-3 signalling pathway	100	27	0.001

Similar to GO analysis, KEGG pathway analysis of crypt cells confirmed enrichment of mRNAs involved in cell proliferation, including those involved in DNA replication and cell cycle. A summary of the analysis is shown in Table 3.4.

As outlined in **Section 1.3.1.1**, Wnt signalling is important for regulation of stem cell populations in the crypt and maturation of Paneth cell. The microarray analysis confirmed that Wnt signalling pathway was up-regulated in the crypt tissue.

Table 3.4: KEGG pathways enriched in the crypt

"Pathway entities" refers to the number of genes corresponding to the KEGG pathways. "Matched entities" is the number of the significantly expressed genes in a pathway. The P-value indicates statistical significance.

Pathway	**Pathway entities**	**Matched entities**	**P-Value**
Ribosomal proteins	80	73	<0.001
DNA replication	41	34	<0.001
Cell cycle	88	49	<0.001
G1-to-S cell-cycle control	62	40	<0.001
Translation factors	51	26	<0.001
Purine metabolism	178	54	<0.001
mRNA processing	551	194	<0.001
miRNA regulation of DNA damage response	91	29	<0.001
Eukaryotic transcription initiation	41	21	<0.001
Homologous recombination	13	10	<0.001
TNFα NF-κB signalling	184	50	<0.001
Mismatch repair	9	8	<0.001
One carbon metabolism	29	13	<0.001
Nucleotide metabolism	19	9	<0.001
Mitochondrial gene expression	19	9	<0.001
TGF-β receptor signalling pathway	150	35	<0.001
Non-homologous end joining	8	5	0.001
Oestrogen signalling	74	19	0.003
Histone modifications	5	3	0.01
Wnt signalling pathway	109	22	0.03

3.2.1.4 Transcription factors

To determine which TFs could potentially regulate *Slc6a19* gene expression, microarray data for all TFs was separately analysed. TFs were classified into three groups, namely those that showed a more than 3-fold difference (up or down) between expression in the villus tip and crypts and those that were expressed with little change in expression. A total of 428 TFs showed significant expression along the crypt–villus axis. Among these, 73 TFs had higher expression in the tip and 68 TFs had higher expression in the crypts. Whilst 287 TFs were evenly expressed along the entire axis (**Figure 3.3**). A complete list of expressed TFs is presented in **Table 8.6**. A possible regulatory role of these TFs in transportation of nutrients along the crypt–villus axis was analysed further.

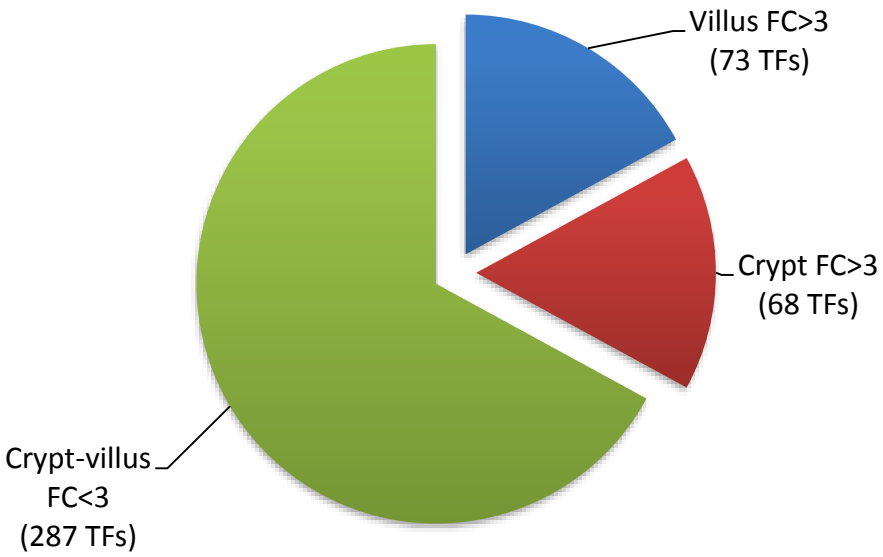

Figure 3.3: Proportion of TFs along the crypt–villus axis

Distribution of total 428 TF genes along the crypt–villus axis based on their expression profiles, each criteria $p < 0.05$.

3.3 Discussion

In this chapter, I investigated the genome-wide expression patterns of different genes using RNA derived from cells at the villus tip and cells from the crypts.

As shown in previous studies, B^0AT1 expression is higher at the villus tip than in the crypt region. To further analyse these two different regions, a modified version of a fractionation method developed by Traber et al. (Traber et al., 1991) was used. This method uses mechanical force (flushing of inverted intestine) to isolate intestinal epithelial cells from the crypts through villus tips. The method was employed successfully, as demonstrated by a significant enrichment of *Slc6a19* mRNA in villus tip fractions and of the well-known intestinal stem cell marker *Lgr5* in crypt fractions. Some limitations of the crypt–villus fractionation technique were observed. For instance, the technique appears to underrepresent cells derived from the very bottom of the crypt. Therefore, genes expressed in the crypt region may not be highly enriched in these fractions i.e. crypt genes such as *Cdx2* and *Tcf4* were found to be evenly expressed along the crypt–villus axis (**Table 8.6**).

3.3.1 Pathway and GO analysis

To gain insight into the biological processes underlying the expression of a specific set of genes at the villus tip, GO and KEGG pathway analyses were applied to the microarray data. These analyses confirmed that crypt and villus epithelial cells express entirely separate sets of genes.

In mature enterocytes at the villus tip, many genes were expressed that are involved in nutrient and ion absorption. Accordingly, GO categories associated with transporter-related genes were identified. This observation is consistent with earlier studies indicating that most genes associated with nutrient absorption were overrepresented in differentiated enterocytes (Mariadason, Nicholas et al. 2005, George, Wehkamp et al. 2008). A previous study also demonstrated that genes associated with lipid synthesis were up-regulated during crypt to villus differentiation (Stegmann, Hansen et al. 2006), which was confirmed by our microarray analyses.

In the crypt compartment, GO and KEGG analyses, identified genes that are involved in DNA replication. It has been reported that DNA synthesis quickly shuts down during crypt to villus transition (Stegmann et al., 2006). It has also been shown that genes

related to the Wnt signalling pathways were highly expressed in crypt cells (Stegmann, Hansen et al. 2006, Sabates-Bellver, Van der Flier et al. 2007). Our analysis confirms these previous reports.

3.4 Summary

In summary, these results showed significant alterations in expression of genes related to TFs and signalling pathways during the crypt–villus differentiation. More importantly, the analysis provides us with TF candidates that may control villus-specific regulation of the B^0AT1 transporter in mouse intestine. Our results further showed that the fractionation method successfully isolated crypt–villus cell populations.

Chapter 4 Transcriptional regulation of *Slc6a19* gene along the crypt–villus axis

4.1 Introduction

Finger-like protrusions, called villi, expand the intestinal epithelial surface area. Crypts are located at the base between villi. The crypt–villus axis is an important structural feature of the intestinal surface. Intestinal stem cells reside at the bottom of the crypts. Mature intestinal cells localise along the crypt–villus axis. Continuous division of stem cells generates new cells, which differentiate into absorptive enterocytes or secretory cells (see **Section 1.2.1**) while migrating up towards the villus tip. Intestinal secretory cells are categorised as enteroendocrine cells, goblet cells, Paneth cells and tuft cells (Barker and Clevers, 2007).

Previously, it was shown that B^0AT1 is highly expressed on the apical membrane of intestinal enterocytes (Bröer et al., 2004). While the functional properties of the protein have been extensively characterized and its physiological role in different organs has been elucidated, the transcriptional regulation underlying its localised expression has not been investigated. TFs play key roles in controlling cell differentiation along the crypt–villus axis (**Figure 4.1**). Some of the TFs that are involved in intestinal cell differentiation are summarised in the following paragraphs.

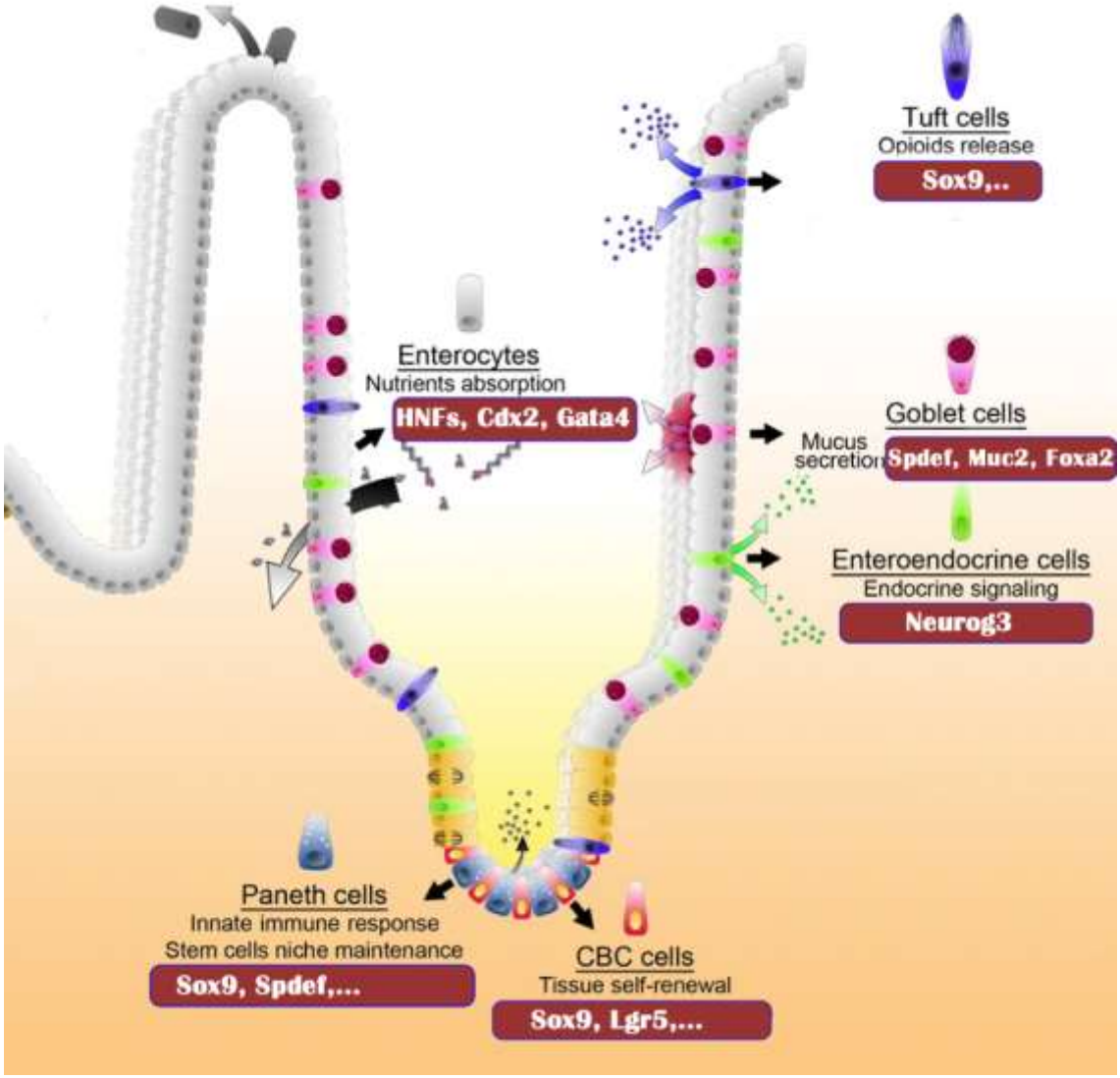

Figure 4.1: Distribution of differentiated intestinal cells along the crypt–villus axis

Transcription factors depicted in boxes control cell-type-specific gene expression required for cell differentiation; from (Gerbe et al., 2011).

4.1.1.1 Hepatocyte nuclear factors

The transcription factors HNF1a (see **Section 1.3.2.3**) and HNF4a (see **Section 1.3.2.4**) are necessary for hepatocyte development, but they are also expressed in the kidney, intestine and pancreas (Sladek et al., 1990, Pontoglio et al., 1996). In the kidney both TFs are exclusively expressed in the proximal tubules (Pontoglio et al., 1996). HNF1a and HNF4a are highly expressed in the crypts and villi, and are important for crypt formation (Sauvaget et al., 2002). HNF1a has a dimerization domain, a DNA-binding domain and a transactivation domain (Chouard et al., 1990). Another important

hepatocyte nuclear factor is HNF1b, which controls terminal cell differentiation of stems cells into mature enterocytes (D'Angelo et al., 2010).

4.1.1.2 SPDEF

SPDEF is a member of the Ets (E26 transformation-specific) family of TFs and is expressed in cells residing in crypts. SPDEF is particularly important for maturation of intestinal goblet and Paneth cells (**Figure 4.1**) (Gregorieff et al., 2009).

4.1.1.3 SOX9

In the intestine, SOX9 (see **Section 1.3.2.1**) is expressed in the progenitor cells located in the crypts. SOX9 is required for differentiation of stem cells into Paneth cells and goblet cells (**Figure 4.1**) (Bastide et al., 2007). As mentioned in **Section 1.3.2.2**, SOX9 is crucial for β-catenin/Wnt interaction, which is essential for crypt–villus formation (Sato et al., 2009). SOX9 is known to inhibit *Cdx2* and *Muc2* genes in the crypts; both proteins are expressed in the villus where SOX9 is not expressed (Blache et al., 2004).

4.1.1.4 NEUROG3

Neurogenin 3 (NEUROG3) is required for enteroendocrine cell development in the gastrointestinal tract and the pancreas (**Figure 4.1**) (Wang et al., 2006).

4.1.1.5 FOXA2

Forkhead box protein a2 (FOXA2) belongs to the forkhead class of DNA-binding proteins and is widely expressed in mouse intestinal crypts (Besnard et al., 2004). Foxa2 can activate *Muc2*, which encodes mucin secreted by the goblet cells. Foxa2 is important for regulation of goblet cell differentiation (Ye and Kaestner, 2009).

4.1.1.6 CDX2

CDX2 contains a homeobox domain that is required for the development and differentiation of the intestine (Lorentz et al., 1997). Sucrase–isomaltase (SI) was one of the first genes the expression of which along the crypt–villus axis was characterized in detail. These studies suggested that HNF1a and CDX2 are regulating gene activation (Traber, 1990). Similarly, HNF1a and CDX2 also regulate the lactase-phlorizin hydrolase (LPH) gene transcription in the intestine (Mitchelmore et al., 2000).

4.1.1.7 GATA4

GATA4 is a member of the zinc-finger family of TFs. GATA4 and HNF1a are necessary for expression of epithelial genes involved in nutrient absorption (Bosse et al., 2007). Together with CDX2, these TFs regulate many of the enterocyte-specific genes in the mammals (Benoit et al., 2010).

4.2 Results

4.2.1 Prediction of putative nuclear receptor response elements in the *Slc6a19* promoter

To identify relevant TFs and their binding sites on the *Slc6a19* (GenBank® accession number NM_028878) promoter, the UCSC Genome Browser (www.genome.ucsc.edu) was used (see **Section 2.5.1**). Fifteen different species were examined. Bioinformatic analysis revealed that a region located between –1960 and +57 of the TSS was conserved to some extent (**Figure 4.2**.**A**). Furthermore, another region close to the TSS was highly conserved (–228 to +57) among the different species (**Figure 4.2**.**B**). Therefore, in our studies, we targeted a 2.5 kb fragment of this region of the promoter sequence.

The proximal promoter of the mouse *Slc6a19* gene, as judged by conservation of the sequence across mammalian species, was relatively short, i.e. 228 bp. It is a typical class II promoter where the TSS is preceded by a TATA-binding motif (Weaver, 2012) at position –23 to –28 and a reasonably conserved transcription factor IIB recognition motif (position –39 to –46), comprising the binding sites for general TFs and for polymerase II (Weaver, 2012). The TSS CCACTT is similar to the mammalian consensus initiator sequence (Weaver, 2012).

A

B

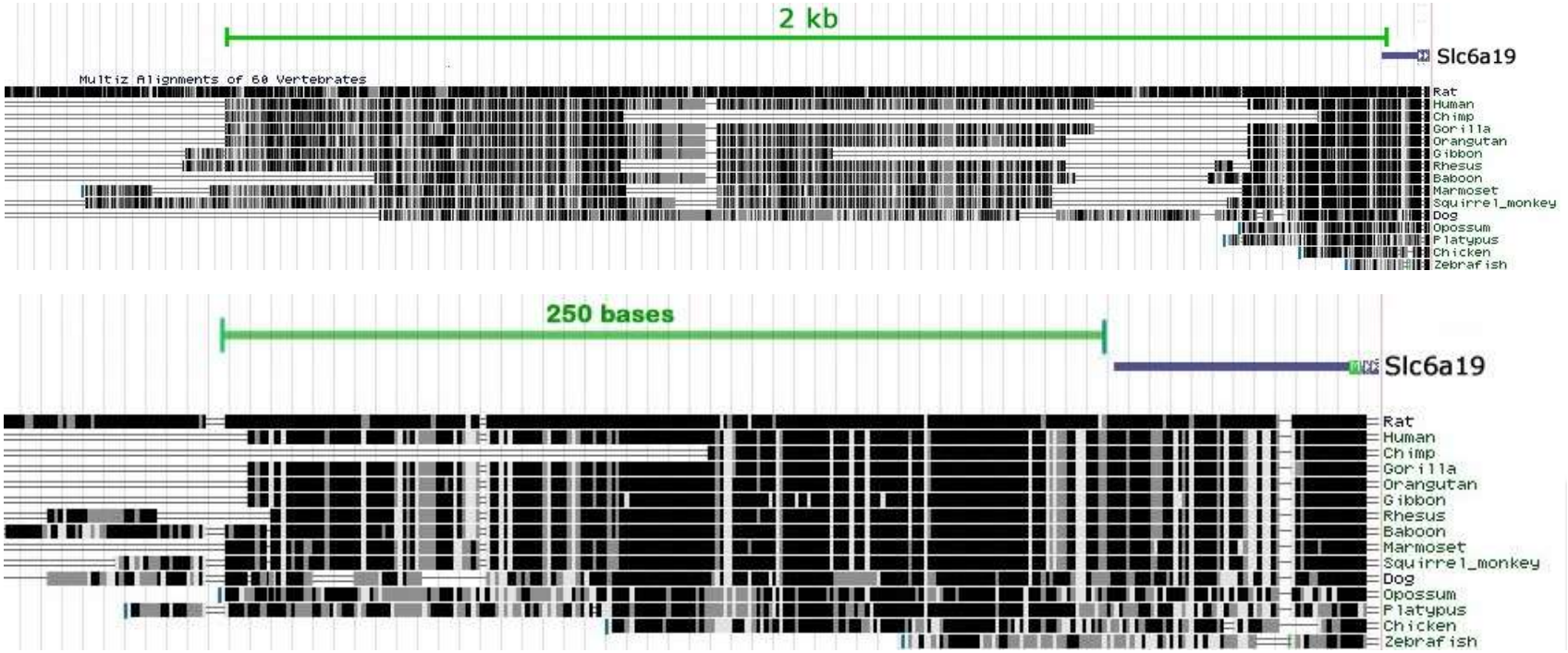

Figure 4.2: Promoter sequence alignment of *Slc6a19*

The UCSC Genome Browser was used for sequence alignment. The alignments include *Slc6a19* sequences from 15 species spanning position –2494 to +57 (**A**) and at higher resolution position –352 to +57 (**B**). Black domains indicate conserved regions when compared to the rat sequence.

Subsequently, the MatInspector program was used to identify TF candidates that potentially bind to this region. The MatInspector program found 227 different TF-binding sites in a 2.5 kb region upstream of the *Slc6a19* TSS. Candidates (see **Section 3.2.1.4**) with robust microarray expression along the crypt–villus axis (**Table 4.1**) were analysed further.

Table 4.1: Expression of candidate TFs in crypts or villi

TFs with robust expression in either crypts or villi are shown. GATA4, HNF1b and PAX4 are listed because they have been previously implicated in enterocyte maturation but do not have predicted promoter binding sites. A matrix number of 1.00 indicates an exact match with the TF consensus binding site, whereas 0.75 is considered a possible binding site for a TF. Revised location indicates results from mutagenesis data (shown below). The ratio of mRNA abundance along the crypt–villus axis was determined by microarray analysis. BS# was used to discriminate multiple binding sites.

TFs	Position	Strand	Matrix	Revised Location	Effect	Ratio Villus/Crypt (Microarray)
ATF4	–1212/–1204	–	0.99		0	0.90
CDX2	–36/–18	–	0.92		0	0.52
CDX2	–1212/–1194	–	0.87		0	0.52
CDX2	–1833/–1815	+	0.86		0	0.52
CREB3L3	–89/–69	+	0.95		0	8.80
EGR1	–167/–151	+	0.89		0	0.11
EGR1	–2112/–2096	+	0.86		0	0.11
FOXA2	–305/–289	–	0.99		0	0.32
FOXA2	–835/–819	–	0.99		0	0.32
GATA4	–	–	–		0	0.91
HNF1a–BS1	–126/–110	–	0.81	–126/–110	++	0.96
HNF1a–BS2	–153/–137	+	0.89		0	0.96
HNF1a–BS3	–1205/–1189	–	0.90		0	0.96
HNF1b	–	–	–	–	–	–
HNF4a–BS1	–239/–215	–	0.85	–41/–38	+++	1.10
HNF4a–BS2	–1368/–1344	+	0.93		0	1.10
HNF4a–BS3	–1701/–1677	+	0.88		0	1.10
NEUROG3	–2352/–2340	+	0.96		0	0.18
NEUROG3	–2474/–2462	+	0.98		0	0.18
PAX4	–	–	–		0	0.36
SMAD3	–228/–218	+	0.99		0	0.66
SMAD3	–2016/–2006	+	0.99		0	0.66
SOX9–BS1	–47/–23	+	0.77	–218/–215	0/– (on HNF activated promoter)	0.05
SOX9–BS2	–1150/–1126	+	0.967		0	0.05
SPDEF	–27/–7	+	0.86	–195/–192	++	0.71

TFs	Position	Strand	Matrix	Revised Location	Effect	Ratio Villus/Crypt (Microarray)
STAT3	–301/–283	+	0.77		0	10.6
STAT3	–303/–285	–	0.76		0	10.6
STAT3	–504/–486	–	0.97		0	10.6
STAT3	–718/–700	+	0.95		0	10.6
STAT3	–1044/–1026	–	0.959		0	10.6

4.2.2 Analysis of possible TF candidates

Twelve different TFs (**Table 4.1**) were identified as putative candidates regulating *Slc6a19* transcription. Their functional regulatory effects on the *Slc6a19* promoter activity were tested by luciferase reporter assays (see **Section 2.6**). GATA4, HNF1b and PAX4 were included because they have previously been identified as enterocyte differentiation regulators.

HEK293 cells were co-transfected with the full-length *Slc6a19* promoter pGL4(–2494/+57) (see **Section 2.6.2**) and each of the predicted TFs separately, namely ATF4, CDX2, CREB3L3, EGR1, FOXA2, GATA4, HNF1a, HNF1b, HNF4a, NEUROG3, PAX4, SMAD3, SOX9, SPDEF, or STAT3 (**Figure 4.3**).

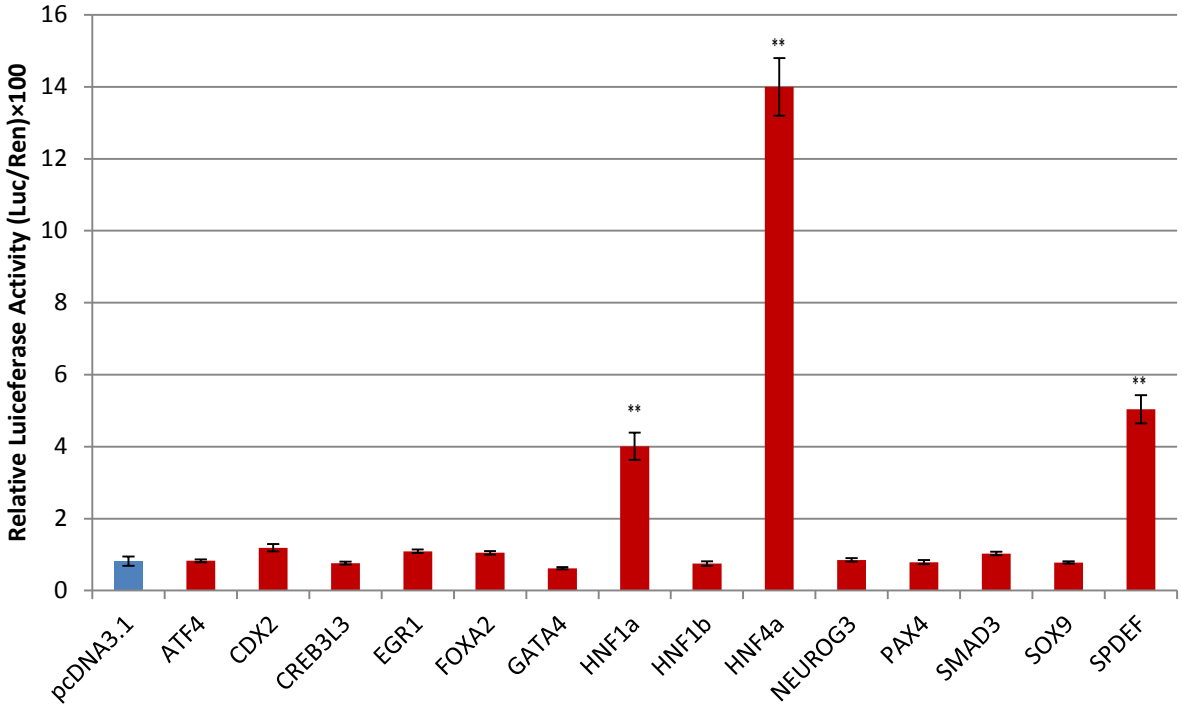

Figure 4.3: Effects of the different TFs on the *Slc6a19* promoter activity

HEK293 cells were co-transfected with three different plasmids. (i) *Firefly* luciferase inserted into pSlc6a19(–2494 to +57) (ii) *Renilla* luciferase in the control vector (iii) one of the following constructs: pcDNA3.1 carrier vector alone (blue bar), or pcDNA3.1 expressing ATF4, CDX2, CREB3l3, EGR1, FOXA2, GATA4, HNF1a, HNF1b, HNF4a, NEUROG3, PAX4, SMAD3, SOX9, or SPDEF. Twenty-four hours after transfection, luciferase activity was measured. Relative luciferase activity was determined by normalising the *Firefly* luciferase activity to the control *Renilla* luciferase activity. Transfections were repeated at least three times using triplicate samples. The data are means ± SD of triplicate experiments. (** $p < 0.01$).

STAT3 is unique it has to be activated after co-transfection. When not activated, STAT3 is located in the cytoplasm (Kishimoto, 1993); however, after phosphorylation, it translocates into the nucleus. STAT3 phosphorylation can be triggered by interleukin-6 (IL-6), a pro-inflammatory cytokine (Zhong et al., 1994). Two different constructs were used to express STAT3, namely, mouse STAT3–GFP and human STAT3, both inserted in a mammalian expression vector. Luciferase assays were hence performed after co-transfection of STAT3 and treatment with IL-6 (20 ng/mL).

Except for HNF1a, HNF4a, and SPDEF, none of the other candidates (**Table 4.1**) significantly activated the *Slc6a19* promoter (**Figure 4.3** and **Figure 4.4**).

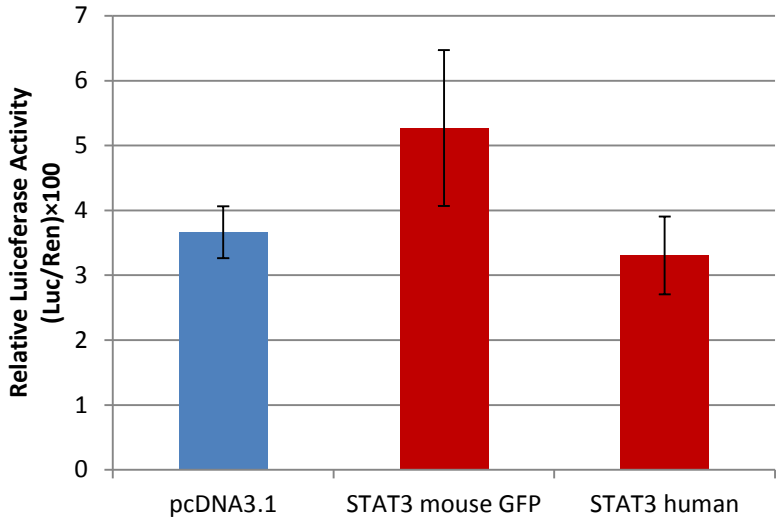

Figure 4.4: Characterization of STAT3-mediated transcriptional activation by reporter gene assays

HEK293 cells were co-transfected with three different plasmids. (i) *Firefly* luciferase inserted into pSlc6a19(–1703/+57) (ii) *Renilla* luciferase in the control vector (iii) one of the following constructs: mouse STAT3-GFP or human STAT3 empty pcDNA3.1 expression vector. Cells were treated with IL-6 to activate STAT3. Twenty-four hours after transfection, luciferase activity was measured. Relative luciferase activity was determined by normalising the *Firefly* luciferase activity to the control *Renilla* luciferase activity. Transfections were repeated at least three times using triplicate samples. The data are means ± SD of triplicate experiments.

4.2.3 HNF1a can activate the *Slc6a19* promoter

HNF1a is important for the differentiation of stem cells into epithelial cells in the intestine (D'Angelo et al., 2010). The MatInspector program predicted three different binding sites for HNF1a in the proximal region of the *Slc6a19* promoter (**Figure 4.5**). These putative binding sites were located at positions; –111 to –114 (HNF1-BS1), –144 to –147 (HNF1-BS2), and –1205 to –1189 (HNF1-BS3). To validate these binding sites, the *Slc6a19* promoter deletion constructs were co-transfected with HNF1a expression vectors into HEK293 cells. Seven different deletion constructs were used: pSlc6a19(–2494/+57), pSlc6a19(–1703/+57), pSlc6a19(–1380/+57), pSlc6a19(–972/+57), pSlc6a19(–437/+57), pSlc6a19(–136/+57), or pSlc6a19(–37/+57).

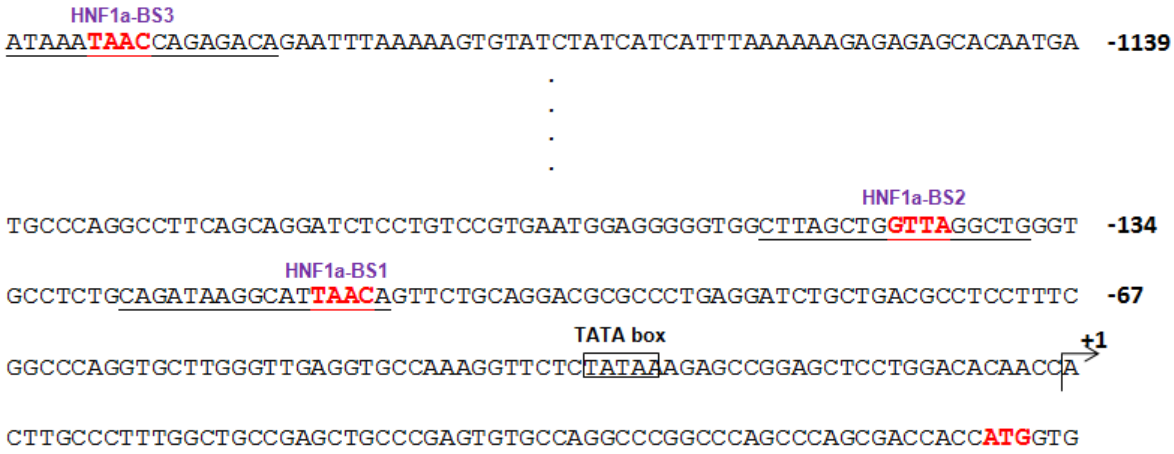

Figure 4.5: Locations of HNF1a-binding sites on the mouse *Slc6a19* promoter

Predicted HNF1a-binding sites are underlined and core binding sites indicated in red colour. The TATA box is marked by a box. The arrow indicates the TSS, designated as +1.

Figure 4.6 shows that except for the shortest construct pSlc6a19 (–37/+57), HNF1a coexpression caused a three to fivefold higher activity than the background activity measured in the absence of HNF1a. Even a construct comprising just 136 bp upstream of the TSS was fully active in the presence of HNF1a. This suggests that an HNF1a-binding site is located between positions –136 to –37 bp on the *Slc6a19* promoter.

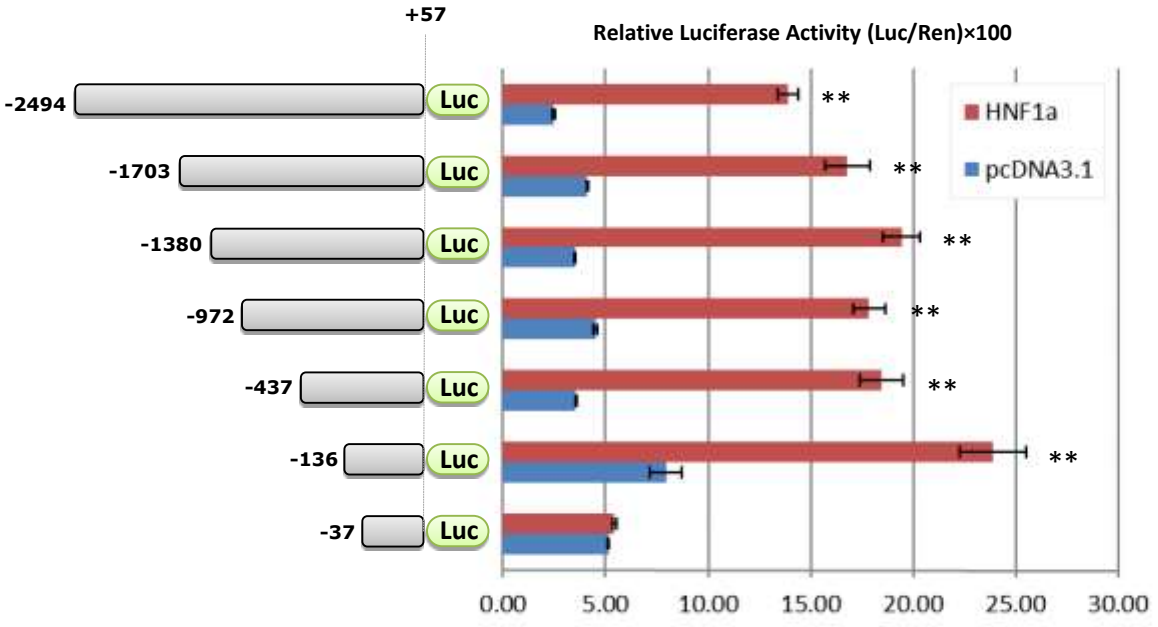

Figure 4.6: Identification of the *Slc6a19* promoter regions responsive to the HNF1a TF using luciferase reporter experiments *in vitro*

HEK293 cells were co-transfected with vectors expressing the *Firefly* luciferase downstream of the *Slc6a19* promoter deletion constructs and with the *Renilla* luciferase as control. HNF1a expression vector (red bars) or empty pcDNA3.1 expression vector (blue bars) was co-expressed to activate transcription or serve as control, respectively. The following promoter deletion constructs were used: pSlc6a19(–2494/+57), pSlc6a19(–1703/+57), pSlc6a19(–1380/+57), pSlc6a19(–972/+57), pSlc6a19(–437/+57), pSlc6a19(–136/+57), or pSlc6a19(–37/+57). Twenty-four hours after transfection, luciferase activity was measured. Relative luciferase activity was determined by normalising the *Firefly* luciferase activity to the control *Renilla* luciferase activity. P values indicate the significance derived from three experiments, each using triplicate transfections. The data are means ± SD of triplicate experiments. Significant increases of promoter activity due to co-transfection of HNF1a are indicated by asterisks (** $p < 0.01$).

To further examine the putative HNF1a-binding sites, we mutated the sites identified by the MatInspector program. Site-directed mutagenesis (see **Section 2.4.2.5**) was used to mutate two predicted HNF1a-binding sites in the pSlc6a19(–136/+57) and pSlc6a19(–437/+57) promoter constructs. Mutation of the HNF1a-BS1 at (–111/–114) (Hnf1a-Mut1) diminished activity compared with the activity of the corresponding wild-type promoter. The second mutation, HNF1-BS2 at (–144/–147) (HNF1a-Mut2), did not affect luciferase activity when co-transfected with HNF1a (**Figure 4.7**). The *in vitro* studies showed that the binding site at position –111 to –114 was responsible for expression of *Slc6a19* in the presence by HNF1a. No evidence was found for

MatInspector program predicted binding sites (**Table 4.1**) at positions–153 to –137 (HNF1-BS2) or –1205 to –1189 (HNF1a-BS3).

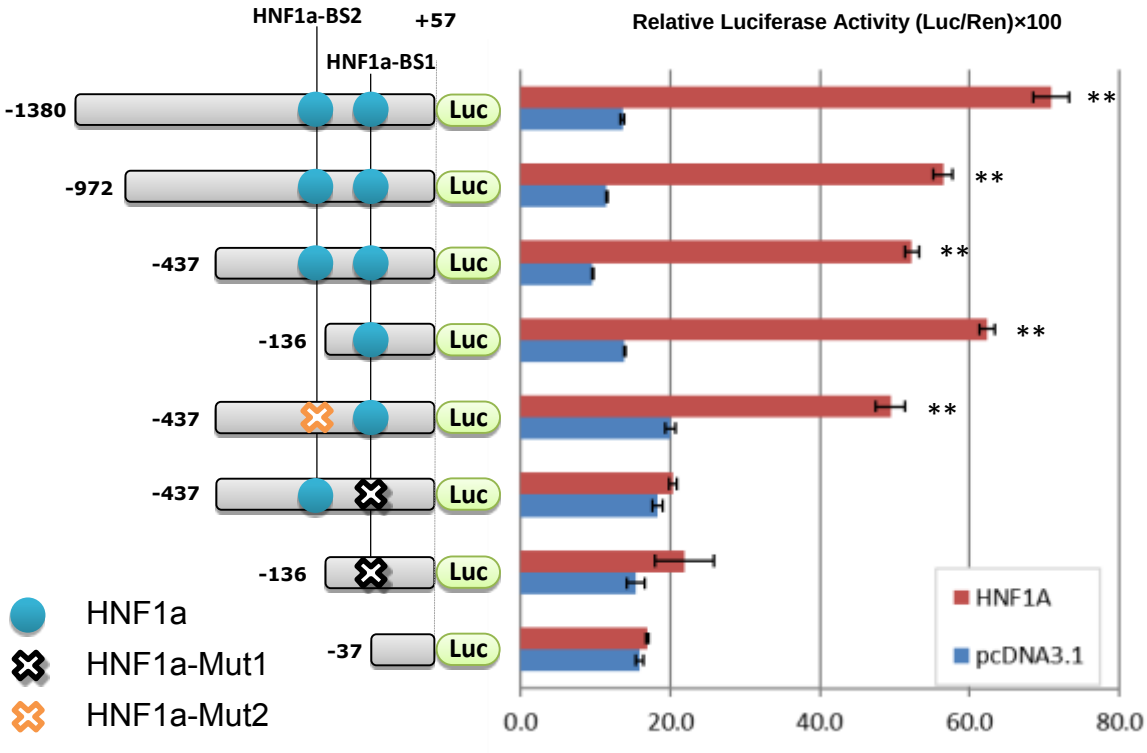

Figure 4.7: Detection of HNF1a-binding sites using mutated constructs

HEK293 cells were co-transfected with vectors expressing the *Firefly* luciferase downstream of the *Slc6a19* promoter constructs and with the *Renilla* luciferase as control. HNF1a expression vector (red bars) or empty pcDNA3.1 expression vector (blue bars) was co-expressed to activate transcription or serve as control, respectively. The following promoter constructs were used: pSlc6a19(–1380/+57), pSlc6a19(–972/+57), pSlc6a19(–437/+57), pSlc6a19(–136/+57), pSlc6a19(–437/+57)Mut2, pSlc6a19(–437/+57)Mut1, pSlc6a19(–136/+57)Mut1, or pSlc6a19(–37/+57). Twenty-four hours after transfection, luciferase activity was measured. Relative luciferase activity was determined by normalising the *Firefly* luciferase activity to the control *Renilla* luciferase activity. P values indicate the significance derived from three experiments, each using triplicate transfections. The data are means ± SD of triplicate experiments. Significant increases of promoter activity due to co-transfection of HNF1a are indicated by asterisks (* $p < 0.05$; ** $p < 0.01$).

To determine whether HNF1a could bind to the *Slc6a19* promoter within living cells, chromatin immunoprecipitation (ChIP) assay was used. The ChIP assay was performed using chromatin fragments isolated from intestinal enterocytes (see **Section 2.9.1**) and an antibody against HNF1a. Real-time PCR was subsequently performed to generate amplicons of 100-200 bp spanning the *Slc6a19* promoter from position –1368

to +11. ChIP analysis revealed that the promoter region from –139 to +11 could bind to HNF1a (**Figure 4.8**). This result was consistent with the luciferase assay, which indicated the presence of an HNF1a-binding site at position –111 to –114. An additional binding site for HNF1a was detected between –984 and –812; this site could not be observed by the reporter gene assays.

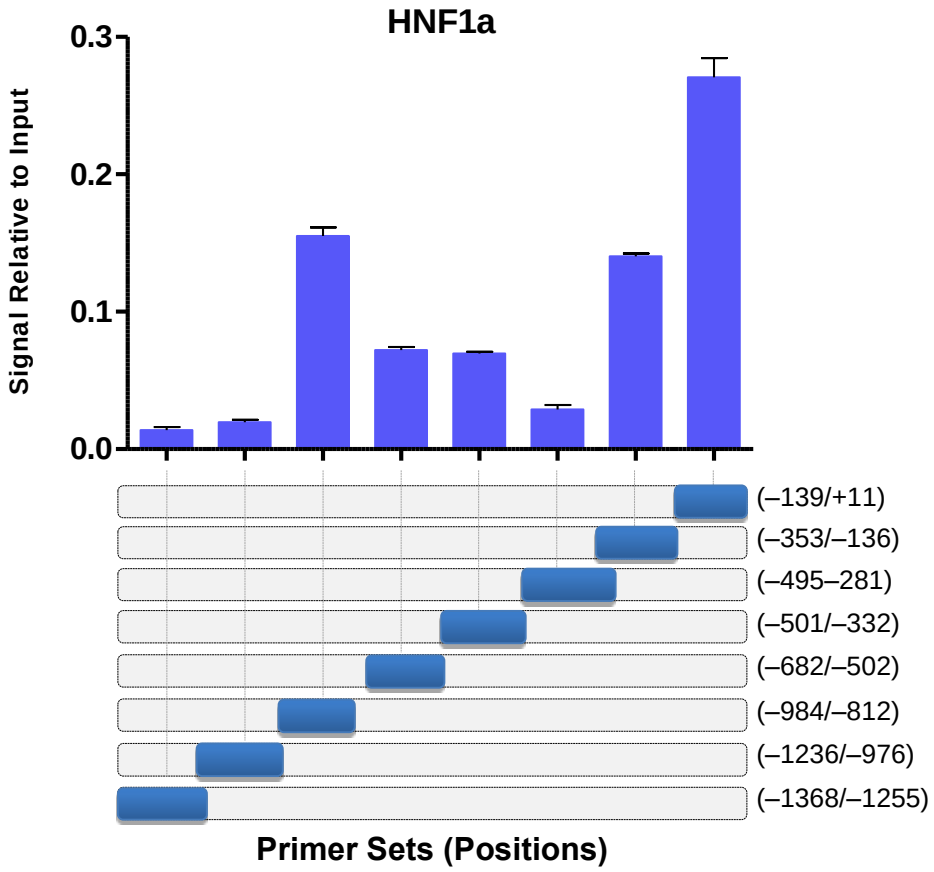

Figure 4.8: HNF1a directly binds to the *Slc6a19* promoter

ChIP assay was performed to identify proteins cross-linked to chromatin extracted from the mouse small intestinal epithelium. The chromatin was immunoprecipitated using an antibody against HNF1a. After DNA purification, the precipitated DNA was quantified by qPCR using primer sets specific for –139/+11, –353/–136, –495/–281, –501/–332, –682/–502, –984/–812, –1236/–976, or –1368/–1255 regions. The lower part of the graph shows the location of primer pairs used in the real-time PCR. The upper part of the graph indicates that ChIP signals relative to the input signal.

4.2.4 HNF4a activates the *Slc6a19* promoter

Our initial promoter experiment indicated that HNF4a is another activator of the *Slc6a19* promoter (**Figure 4.3**). HNF4a was highly expressed along the crypt–villus axis

(**Figure 4.18**). Three HNF4a-binding sites were predicted using the MatInspector program at positions –239 to –215 (HNF4a-BS1), –1368 to –1344 (HNF4a-BS2), and –1701 to –1677 (HNF4a-BS3). According to HNF4a consensus binding site (CAAAGT) (Wallerman et al., 2009), three additional binding sites were predicted by visual inspection at locations –1108 to –1105 (HNF4a-BS4), –1088 to –1085 (HNF4a-BS5), and –38 to –41 (HNF4a-BS6) (**Figure 4.9**). To confirm the possible binding sites *in vitro*, HNF4a was co-expressed with truncated *Slc6a19* promoter constructs: pSlc6a19(–2494/+57), pSlc6a19(–1703/+57), pSlc6a19(–1380/+57), pSlc6a19(–972/+57), pSlc6a19(–437/+57), pSlc6a19(–136/+57), or pSlc6a19(–37/+57).

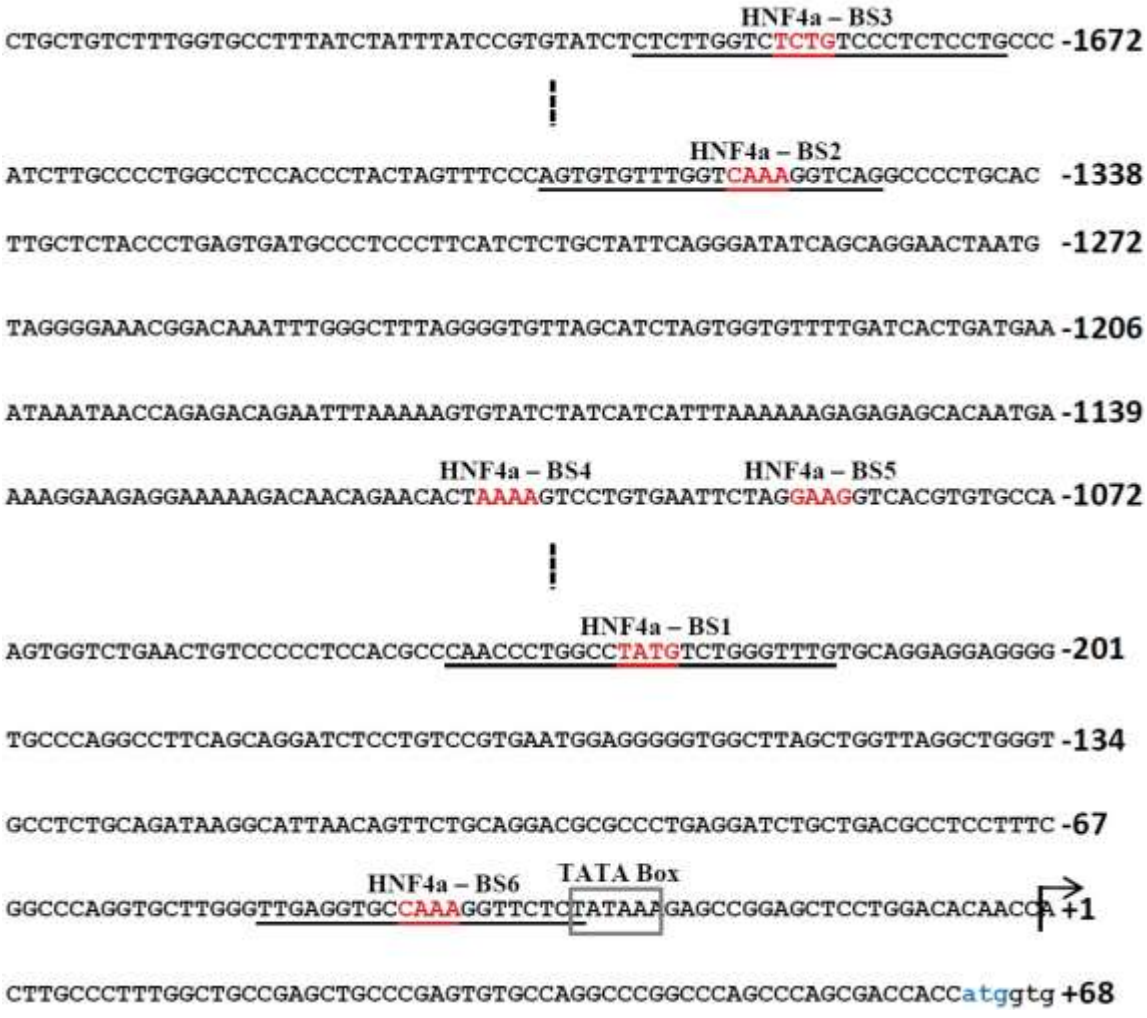

Figure 4.9: Location of putative HNF4a-binding sites on the *Slc6a19* promoter

Predicted binding sites for HNF4a are indicated on the *Slc6a19* promoter sequence. The TATA box is highlighted by a box. The arrow indicates the TSS designated as +1.

Co-expression of HNF4a activated the promoter about 20-fold in the longest construct pSlc6a19(–2494/+57) (**Figure 4.10**). This activation dropped to fourfold in construct pSlc6a19(–972/+57). The smallest construct did not show any significant promoter activity. These results suggested the presence of at least two HNF4a-binding sites.

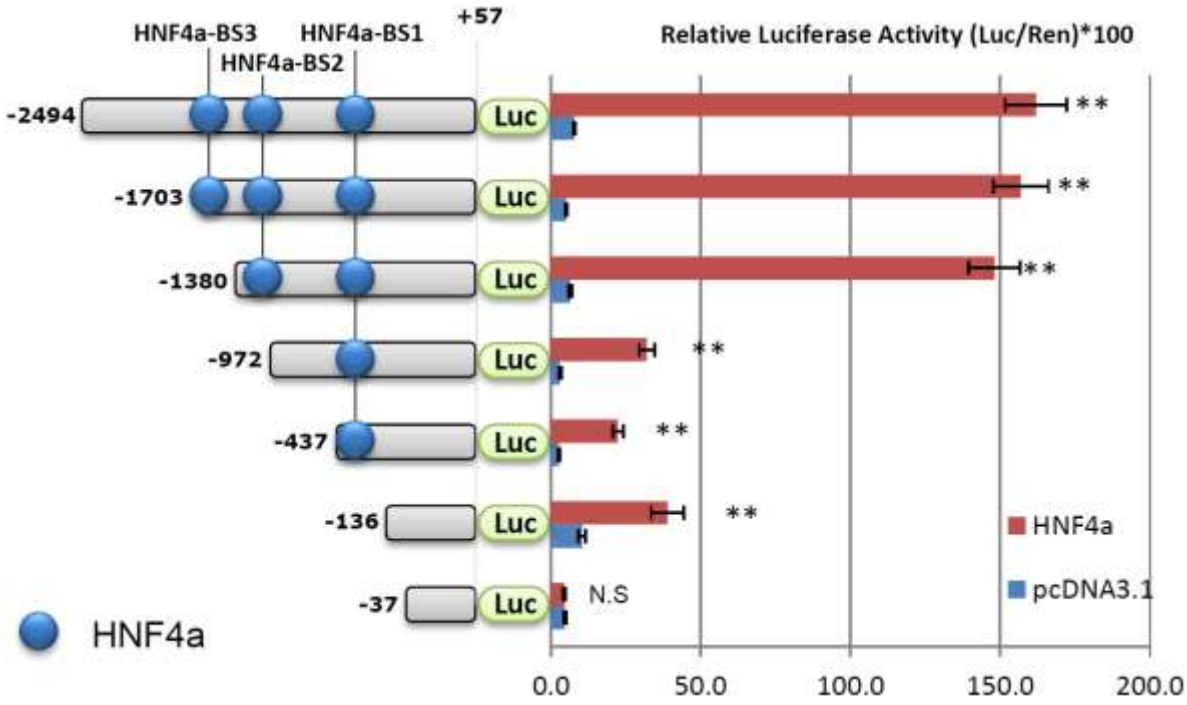

Figure 4.10: HNF4a induces luciferase expression driven by the *Slc6a19* promoter *in vitro*

HEK293 cells were co-transfected with vectors expressing the *Firefly* luciferase downstream of the *Slc6a19* promoter constructs and with the *Renilla* luciferase as control. HNF4a expression vector (red bars) or empty pcDNA3.1 expression vector (blue bars) was co-transfected to activate transcription or serve as control, respectively. The following promoter constructs were used: pSlc6a19(–2494/+57), pSlc6a19(–1703/+57), pSlc6a19(–1380/+57), pSlc6a19(–972/+57), pSlc6a19(–437/+57), pSlc6a19(–136/+57), or pSlc6a19(–37/+57). Twenty-four hours after transfection, luciferase activity was measured. Relative luciferase activity was determined by normalising the *Firefly* luciferase activity to the control *Renilla* luciferase activity. P values indicate the significance derived from three experiments, each using triplicate transfections. The data are means ± SD of triplicate experiments. Significant increases of the promoter activity due to co-transfection with HNF4a are indicated by asterisks (* $p < 0.05$; ** $p < 0.01$). N.S designates non-significant results.

Functional expression analysis did not show a significant activity difference between the pSlc6a19(–1703/+57) and the pSlc6a19(–1380/+57) deletion constructs. Similarly, luciferase activity did not show any significant decrease when we deleted the

region spanning –437 to –136. Therefore, we concluded that the predicted HNF4a-BS3 and HNF4a-BS1 sites were inactive in the *in vitro* assay system. Consequently, HNF4a-BS2 is most likely the actual binding site of HNF4a. In addition, the results suggested that there should be another binding site located between –136 and –37, which was not identified by the MatInspector program.

To determine the potential HNF4a-binding regions, we mutated their corresponding binding sites in the pSlc6a19(–1380/+57) and the pSlc6a19(–972/+57) reporter constructs (**Figure 4.11**). This included the atypical HNF4a-binding site between –136 and –37 (HNF4a-BS6), which were accidentally discovered while searching for putative SOX9-binding sites (**Figure 4.19**) on the *Slc6a19* promoter.

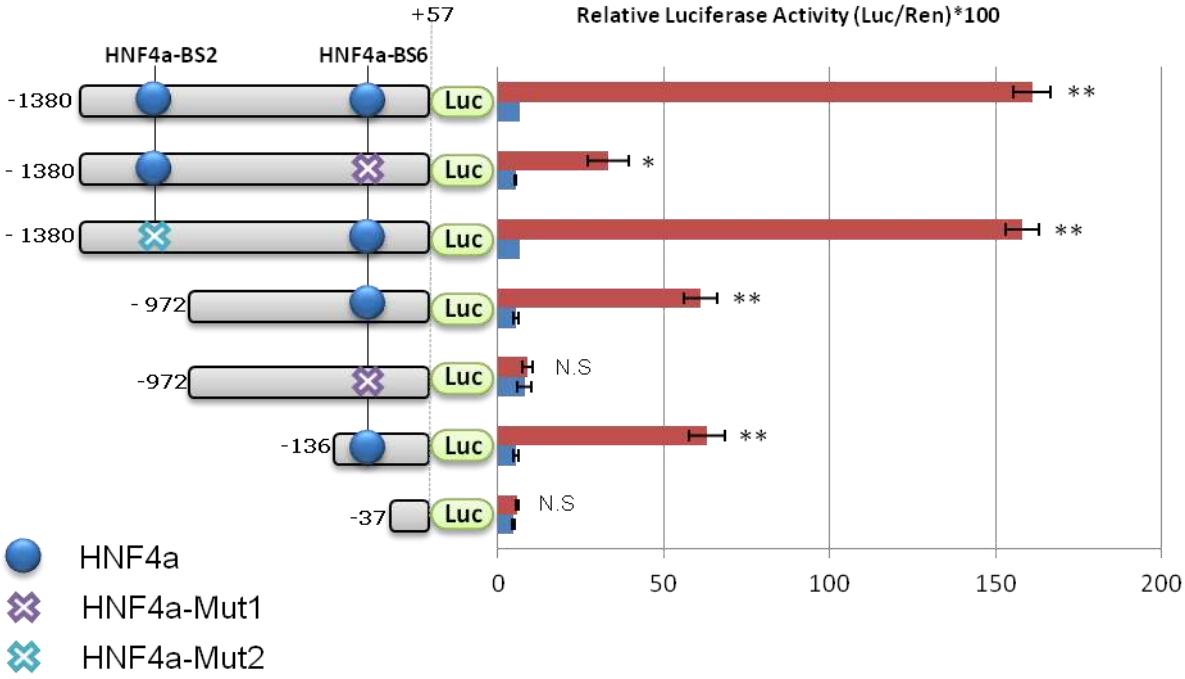

Figure 4.11: Determination of HNF4a-binding sites using mutated constructs

HEK293 cells were co-transfected with vectors expressing the *Firefly* luciferase downstream of the *Slc6a19* promoter constructs and with the *Renilla* luciferase as control. HNF4a expression vector (red bars) or empty pcDNA3.1 expression vector (blue bars) was co-expressed to activate transcription or serve as control, respectively. The following promoter constructs were used: pSlc6a19(–1380/+57), pSlc6a19(–1380/+57)Mut1, pSlc6a19(–1380/+57)Mut2, pSlc6a19(–1380/+57)Mut1,2, pSlc6a19(–972/+57), pSlc6a19(–972/+57)Mut1, pSlc6a19(–136/+57), or pSlc6a19(–37/+57). Twenty-four hours after transfection, luciferase activity was measured. Relative luciferase activity was determined by normalising the *Firefly* luciferase activity to the control *Renilla* luciferase activity. P values indicate the significance derived from three experiments, each using triplicate transfections. The data are means ± SD of triplicate experiments. Significant increases of promoter activity due to co-transfection of HNF4a are indicated by asterisks (* $p < 0.05$; ** $p < 0.01$). N.S designates non-significant results.

Mutation of the HNF4a-BS6 binding site on the shorter construct pSlc6a19(–972/+57), completely suppressed HNF4a-induced activation of the *Slc6a19* promoter. A very short promoter deleted upstream of position –37, did not induce luciferase activity. However, mutating the predicted HNF4a-binding site, HNF4a-BS2, on pSlc6a19(–1380/+57) did not reduce the reporter gene activity (**Figure 4.11**).

When we deleted the region from –1380 to –972, the luciferase activity was significantly reduced (**Figure 4.11**). Furthermore, reducing the distance between both HNF4a-binding sites increased reporter gene activity, suggesting that both sites were functional (**Figure 4.12**). These suggest the presence of another functional binding site for HNF4a between –1380 to –972.

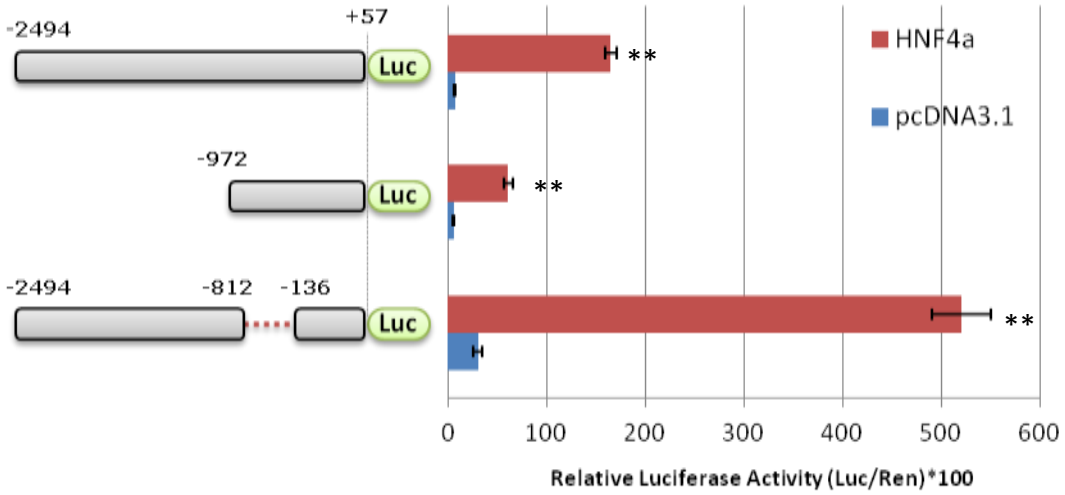

Figure 4.12: Reducing the distance between HNF4a-binding sites enhances *in vitro* luciferase expression driven by the *Slc6a19* promoter

HEK293 cells were co-transfected with vectors expressing the *Firefly* luciferase downstream of the *Slc6a19* promoter constructs and with the *Renilla* luciferase as control. HNF4a expression vector (red bars) or empty pcDNA3.1 expression vector (blue bars) was co-transfected to activate transcription or serve as control, respectively. The following promoter constructs were used: pSlc6a19(–2494/+57), pSlc6a19(–972/+57), or pSlc6a19(–2494/+57)[–812/–136]. Twenty-four hours after transfection, luciferase activity was measured. Relative luciferase activity was determined by normalising the *Firefly* luciferase activity to the control *Renilla* luciferase activity. The experiment was performed three times, each using triplicate transfections. The data are means ± SD of triplicate experiments. Significant increases of promoter activity due to co-transfection of HNF4a are indicated by asterisks (* $p < 0.05$; ** $p < 0.01$).

As a result, we predicted and mutated two further putative sites, namely HNF4a-BS4(–1105/–1108) and HNF4a-BS5(–1085/–1088) (**Figure 4.9**), and prepared more targeted deletion constructs to identify the second HNF4a-binding site. The deletion constructs showed a significant drop in reporter gene activity between –1226 to –1078. However, mutating HNF4a-BS4 and HNF4a-BS5 (HNF4a-Mut3 and HNF4-Mut4) did not reduce the luciferase activity (**Figure 4.13**).

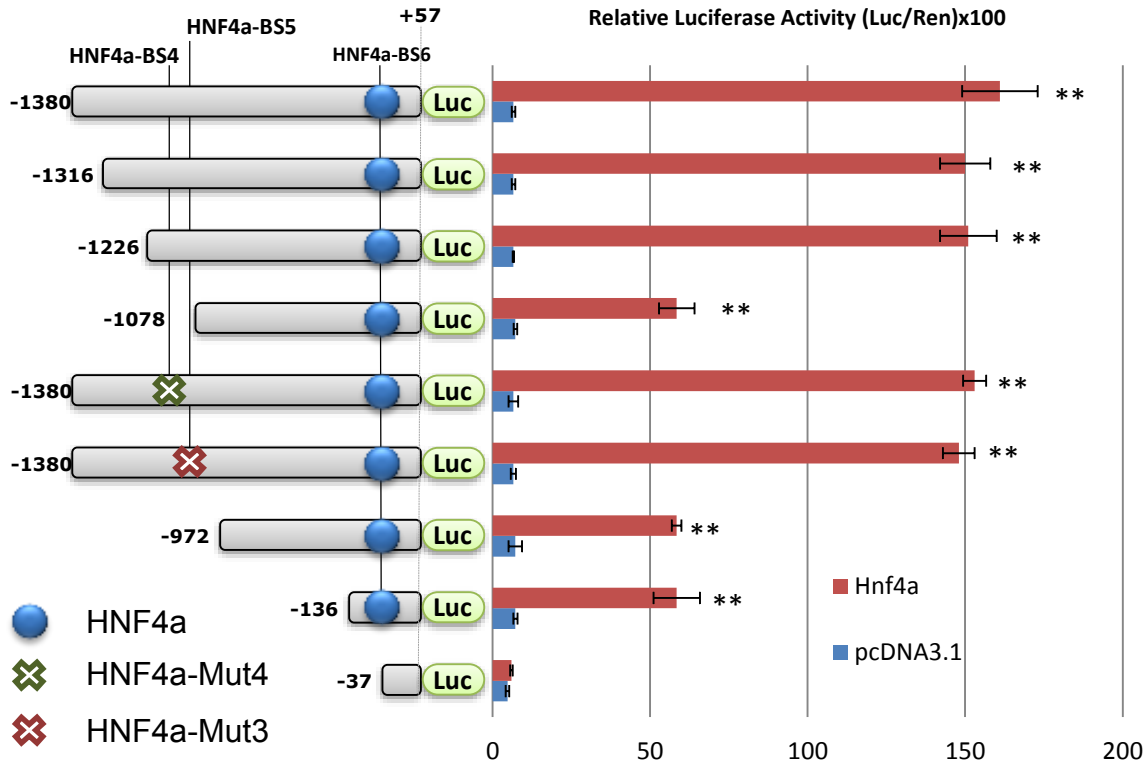

Figure 4.13: Detection of the second putative HNF4a-binding site using mutated constructs

HEK293 cells were co-transfected with vectors expressing the *Firefly* luciferase downstream of the *Slc6a19* promoter constructs and with the *Renilla* luciferase as control. HNF4a expression vector (red bars) or empty pcDNA3.1 expression vector (blue bars) was co-expressed to activate transcription or serve as control, respectively. The following promoter constructs were used: pSlc6a19(–1380/+57), pSlc6a19(–1316/+57), pSlc6a19(–1226/+57), pSlc6a19(–1078/+57), pSlc6a19(–1380/+57)Mut4, pSlc6a19(–1380/+57)Mut3, pSlc6a19(–972/+57), pSlc6a19(–136/+57), or pSlc6a19(–37/+57). Twenty-four hours after transfection, luciferase activity was measured. Relative luciferase activity was determined by normalising the *Firefly* luciferase activity to the control *Renilla* luciferase activity. Transfections were repeated at least three times using triplicate samples. The data are means ± SD of triplicate experiments. Significant increases of the promoter activity due to co-transfection of HNF4 are indicated by asterisks. (* $p < 0.05$; ** $p < 0.01$)

To verify whether HNF4a binds to the putative binding sites on the *Slc6a19* promoter in intact tissue, ChIP assays were performed. Cross-linked chromatin, isolated from scraped mouse intestinal mucosa, was used for ChIP assays. The intestinal enterocyte chromatin was immunoprecipitated using an antibody against HNF4a. Immunoprecipitated DNA was analysed by real-time PCR amplification generating amplicons of 100-250bp spanning position –1368 to +11 of the *Slc6a19* promoter, as shown in **Figure 4.14**. ChIP analysis of this DNA fragment showed that the two primer sets covering the region –353 to +11 showed the strongest signal for HNF4a-binding (**Figure 4.14**). This result confirmed the putative HNF4a-binding site at position –38 to –41, but failed to confirm any other strong binding site between –1226 and –1078.

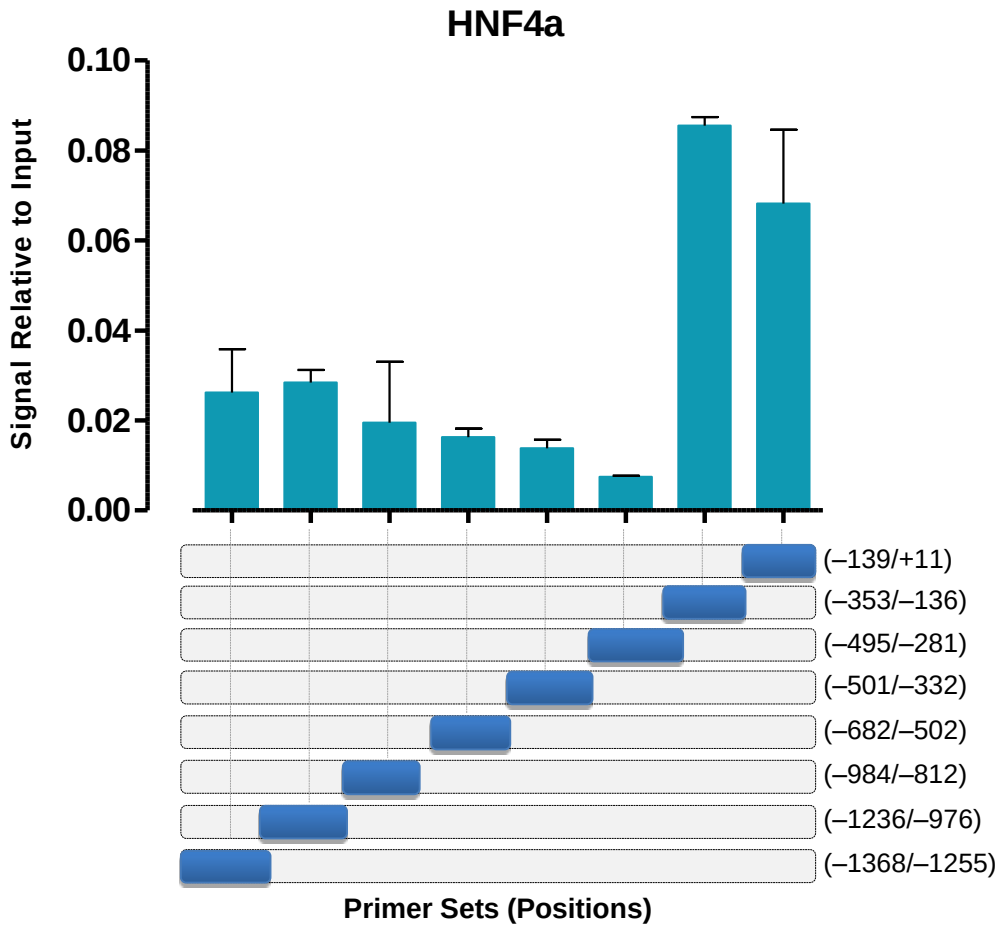

Figure 4.14: HNF4a directly binds to the *Slc6a19* promoter

ChIP assay was performed on cross-linked chromatin isolated from the mouse small intestine epithelium. Chromatin was immunoprecipitated using an antibody against HNF4a. After purification, the precipitated DNA was quantified by qPCR using primer sets specific for –139/+11, –353/–136, –495/–281, –501/–332, –682/–502, –984/–812, –1236/–976, or –1368/–1255 regions. The lower part of the graph shows the corresponding location of primer pairs used in the real-time PCR. The upper part of the graph presents that the ChIP signal relative to the input signal.

4.2.5 Synergistic effects of HNF1a and HNF4a co-transfection on the *Slc6a19* promoter activity

It has previously been reported that HNF1a and HNF4a can act synergistically to transcriptionally activate human α1-antitrypsin (*α1-AT*), UDP glucuronosyltransferase 1 family-polypeptide A9 (*UGT1A9*), and dihydrodiol dehydrogenase *(DD4*) (Eeckhoute et al., 2004, Ozeki et al., 2001, Hu and Perlmutter, 1999).

To determine whether HNF1a and HNF4a could also synergistically activate the *Slc6a19* promoter, both TFs were co-expressed in HEK293 cells (**Figure 4.15**). The experiment showed that co-expression of HNF1a and HNF4a did not increase the luciferase activity more than HNF4a-induced promoter activity alone.

Another study suggested synergistic action between HNF1a and Cdx2 at the lactase-phlorizin hydrolase (*LPH*) promoter (Mitchelmore et al., 2000). However, co-expression of HNF1a and Cdx2 using our *Slc6a19* reporter gene constructs did not significantly increase the luciferase activity compared to HNF1a-induced activity alone (**Figure 4.15**). CDX2 alone could not activate *Slc6a19* transcription (**Figure 4.3**).

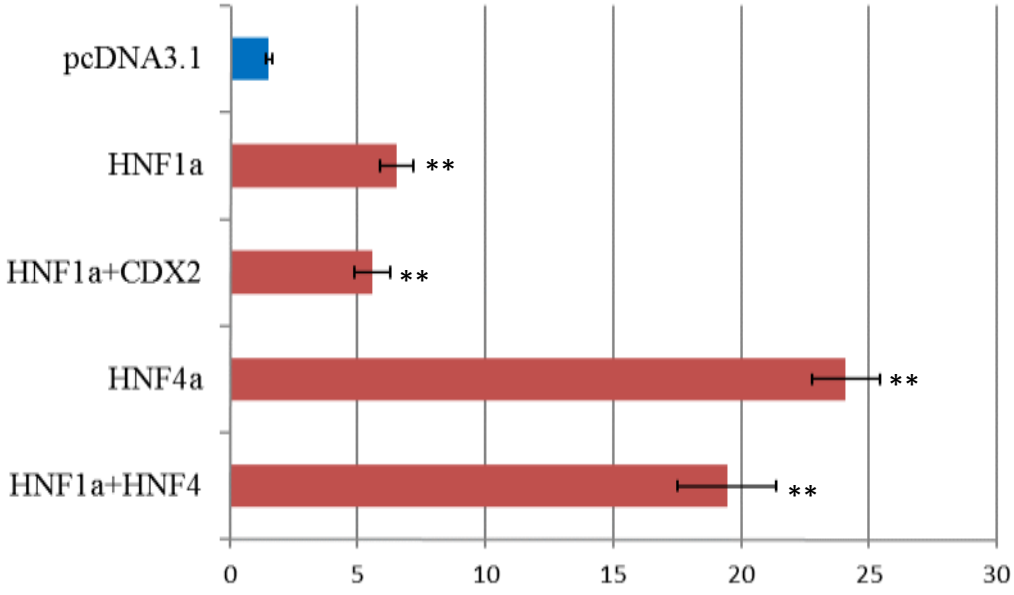

Figure 4.15: The combinatorial effect of CDX2 and HNF TFs on the *Slc6a19* promoter activity

HEK293 cells were co-transfected with vectors expressing the *Firefly* luciferase downstream of the promoter construct pSlc6a19(–2494/+57), together with various TFs and with the *Renilla* luciferase as control. The following combinations were used: HNF1a expression vector, HNF1a plus CDX2, HNF4a, HNF1a plus HNF4a, or empty pcDNA3.1 expression vector (blue bar). Twenty-four hours after transfection, the luciferase activity was measured. Relative luciferase activity was determined by normalising the *Firefly* luciferase activity to the control *Renilla* luciferase activity. Transfections were repeated at least three times using triplicate samples. The data are means ± SD of triplicate experiments.

4.2.6 SPDEF can activate *Slc6a19* transcription *in vitro*

According to the microarray data, SPDEF was highly expressed in the intestinal villus (**Figure 4.18**) and could therefore be a candidate TF to activate the *Slc6a19* promoter. Furthermore, the MatInspector program predicted that the *Slc6a19* promoter contains a putative SPDEF-binding site located between –27 bp to –7 bp (SPDEF-BS1) (**Figure 4.16**).

Luciferase assays, however, indicated that SPDEF-induced reporter gene activity dropped to background activity when deletions passed beyond position –201 (**Figure 4.17**). No further loss could be detected in the smallest construct pGL4(–136/+57), which contained the predicted SPDEF-binding region. The pGL4(–136/+57) construct also

could not be activated by co-expression of SPDEF, suggesting that the potential binding site was likely located upstream of the predicted site.

The consensus binding site for mouse SPDEF has previously been confirmed (Wei et al., 2010) to be the sequence CCGGAT. A similar site (CAGGAT) was identified in the *Slc6a19* promoter at position –183 to –180 (SPDEF-BS2) (**Figure 4.16**).

Figure 4.16: Predicted binding sites for the mouse SPDEF

Two putative SPDEF-binding sites are shown in red letters. Both sites were mutated to test their relevance.

Luciferase activity was measured to investigate the two putative SPDEF-binding sites. The assays showed a sevenfold and sixfold increase in activity of the pSlc6a19(–437/+57) and pSlc6a19(–201/+57) promoter constructs, respectively, when SPDEF was co-expressed (**Figure 4.17**). *Slc6a19* promoter activity was abolished by mutation of the second proposed SPDEF-BS2 binding site. Accordingly, a deletion upstream of position –136 bp abolished the effect of SPDEF on *Slc6a19* promoter activity. This experiment demonstrates that SPDEF, similar to HNF1a and HNF4a is sufficient to activate the *Slc6a19* promoter in the HEK293 cells.

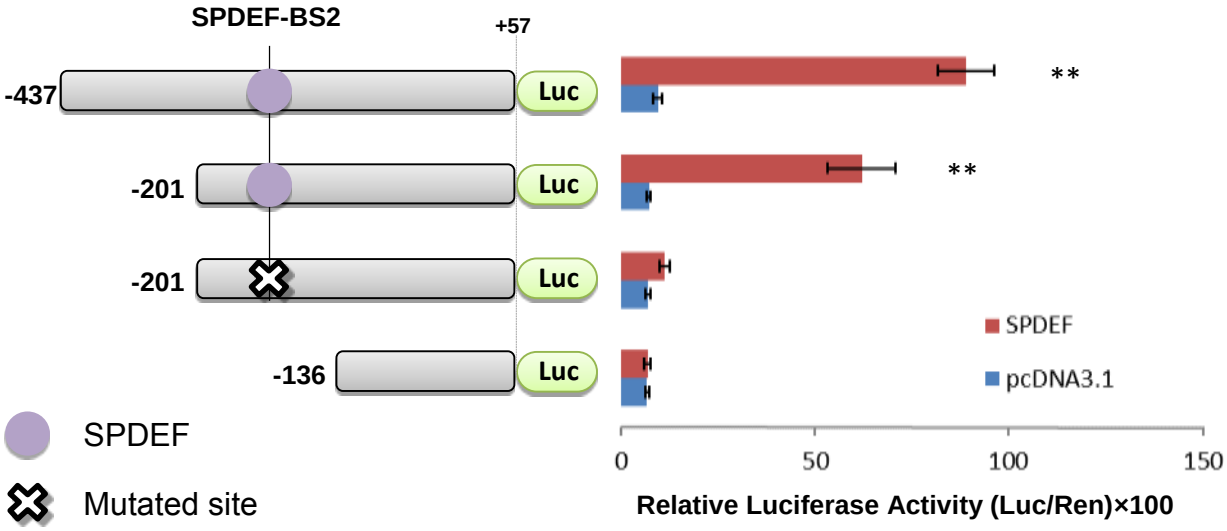

Figure 4.17: SPDEF induces *in vitro* luciferase activity driven by the *Slc6a19* promoter

HEK293 cells were co-transfected with vectors expressing the *Firefly* luciferase downstream of the *Slc6a19* promoter constructs and with the *Renilla* luciferase as control. SPDEF expression vector (red bars) or empty pcDNA3.1 expression vector (blue bars) was co-transfected to activate transcription or serve as control, respectively. The following promoter constructs were used: pSlc6a19(–437/+57), pSlc6a19(–201/+57), pSlc6a19(–201/+57)[mutated], or pSlc6a19(–136/+57). Twenty-four hours after transfection, the luciferase activity was measured. Relative luciferase activity was determined by normalising the *Firefly* luciferase activity to the control *Renilla* luciferase activity. P values indicate the significance derived from three experiments, each using triplicate transfections. The data are means ± SD of triplicate experiments. Significant increases of promoter activity due to co-transfection of SPDEF are indicated by asterisks (* $p < 0.05$; ** $p < 0.01$).

4.2.7 Identification of possible repressor(s) along the crypt–villus axis

The *in vitro* and *in vivo* experiments indicated that SPDEF, HNF1a and HNF4a strongly activated B^0AT1 transcription in the mouse intestine. qPCR was used to confirm the relative expression of TFs in the villus and the crypt as determined by microarray for some of the most prominent TFs (**Table 4.1**). Fractionation experiments followed by qPCR showed robust transcript levels of HNF1a and HNF4a along the crypt-villus axis (**Figure 4.18A**). HNF1a and HNF4a expression was high in the crypt region, but marked expression remained in villus cells.

All TF candidates tested thus far had higher levels of expression in crypts as ascertained by qPCR and microarray analysis (**Table 4.1**). Thus, *Slc6a19* mRNA expression in the villus cells could not be explained by a corresponding expression of SPDEF, HNF1a, or HNF4a.

Genome-wide analyses showed that 68 TFs had robust expression in the intestine and were expressed at significantly higher levels (ratio > 3) in the villus than in the crypt (**Table 8.6**). Of these, only STAT3 and CREB3L3 have putative binding sites on the *Slc6a19* promoter. However, co-transfection of STAT3 and CREB3L3 failed to activate reporter gene expression (**Figure 4.3**). Consequently, we hypothesized that other TF(s) might supress *Slc6a19* expression in the crypts.

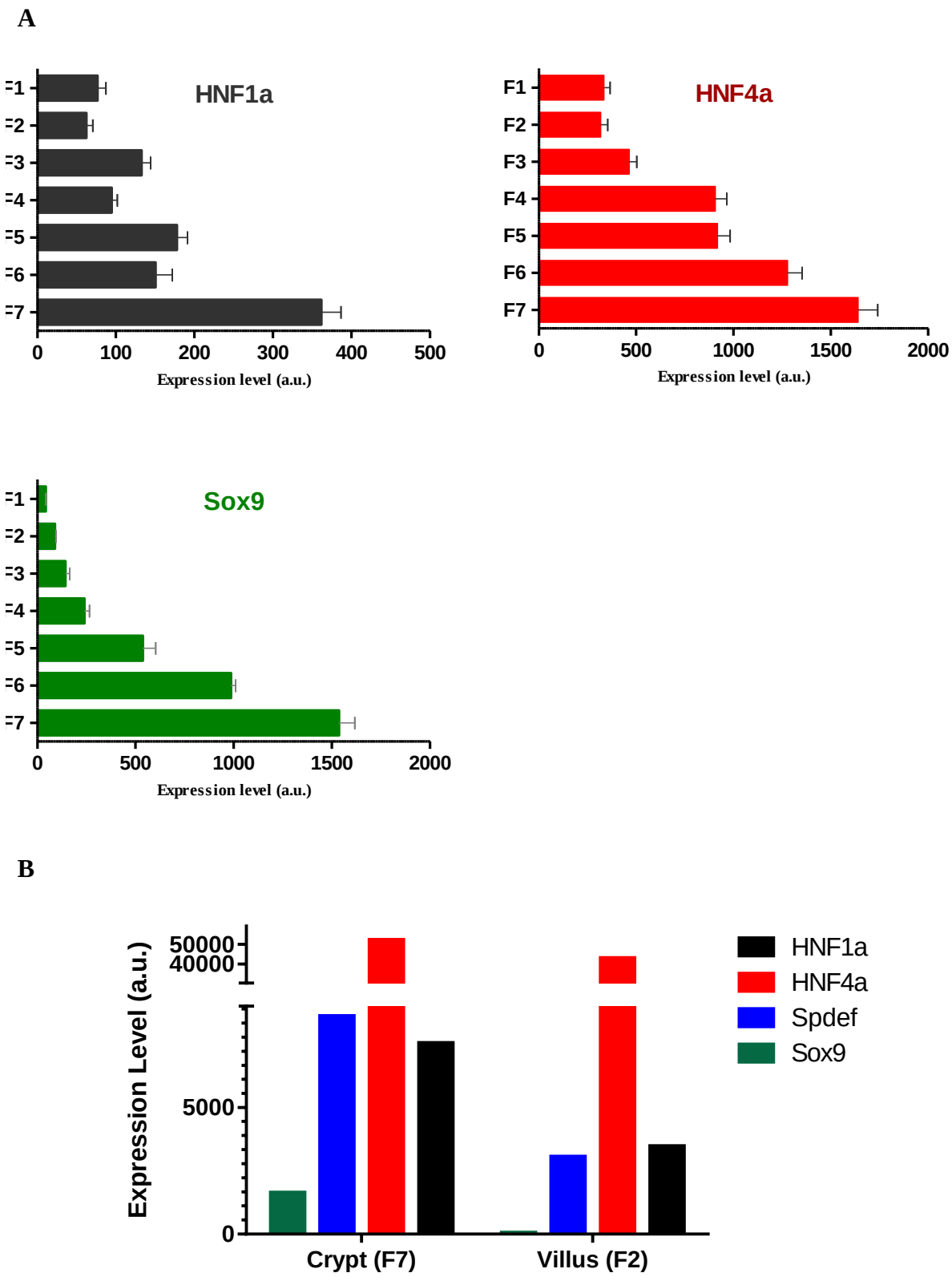

Figure 4.18: Expression profiles of putative TFs in the villus and crypt as determined by qPCR and microarray studies

(A) Expression levels of *Hnf1a*, *Hnf4a* and *Sox9* are shown in consecutive fractions derived from mouse small intestine (F1 villus tip – F7 crypts). **(B)** Microarray results showing expression levels in crypt and villus fractions.

4.2.8 Analysis of SOX9-binding on *Slc6a19* promoter

The TF Sox9 was particularly lowly expressed in the villus compared to crypt fractions (**Figure 4.18**.**A**). Microarray results confirmed expression patterns similar to those obtained by qPCR analyses (**Figure 4.18.B**). Moreover, it was markedly expressed in hepatic and pancreatic tissues (Mori-Akiyama et al., 2007, Kanai and Koopman, 1999), which do not express *Slc6a19* similarly to intestinal crypts.

The pGL4(–2494/+57) promoter construct contains two predicted SOX9-binding sites at positions between –37 and –34 (SOX9-BS1), and between –1150 and –1126 (SOX9-BS2) (**Figure 4.19**). To elucidate the effects of SOX9 on the regulation of *Slc6a19* promoter activity, SOX9 was co-expressed in HEK293 cells.

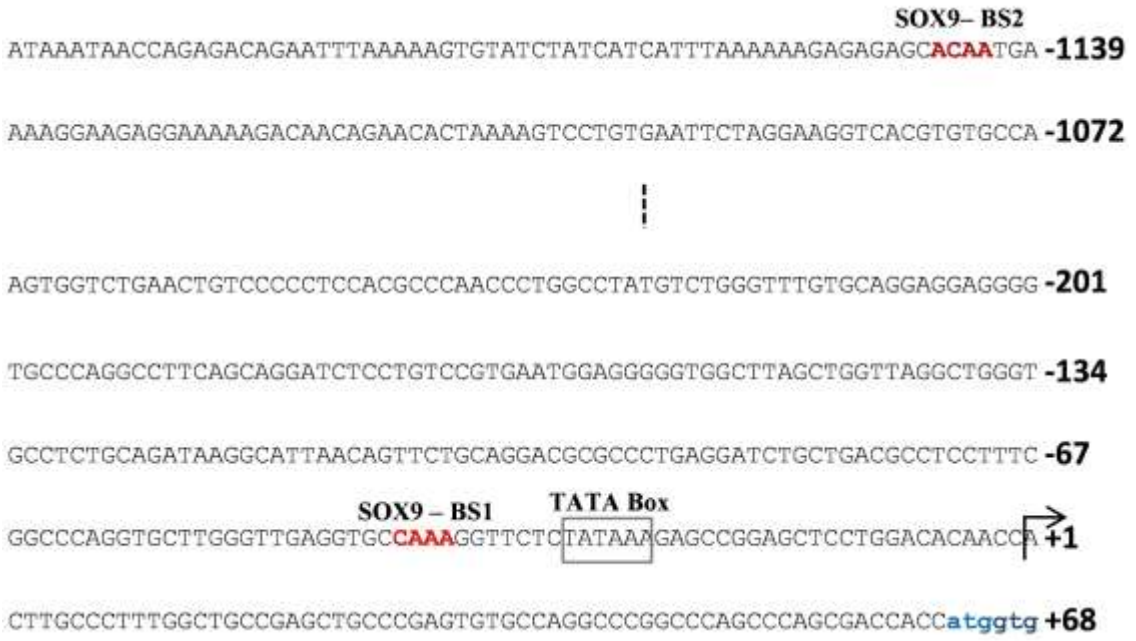

Figure 4.19: Predicted binding sites for SOX9 on the mouse *Slc6a19* promoter

The two predicted SOX9-binding sites on the *Slc6a19* proximal promoter region are indicated in red. The predicted TATA box and TSS (+1) are also shown.

Luciferase reporter assays showed that SOX9 did not activate *Slc6a19* transcription (**Figure 4.3**). However, when this TF was co-transfected with either HNF1a (**Figure 4.20**) or HNF4a (**Figure 4.21**), it strongly inhibited the promoter activity as long as the predicted SOX9-binding site BS1 was included in the tested construct.

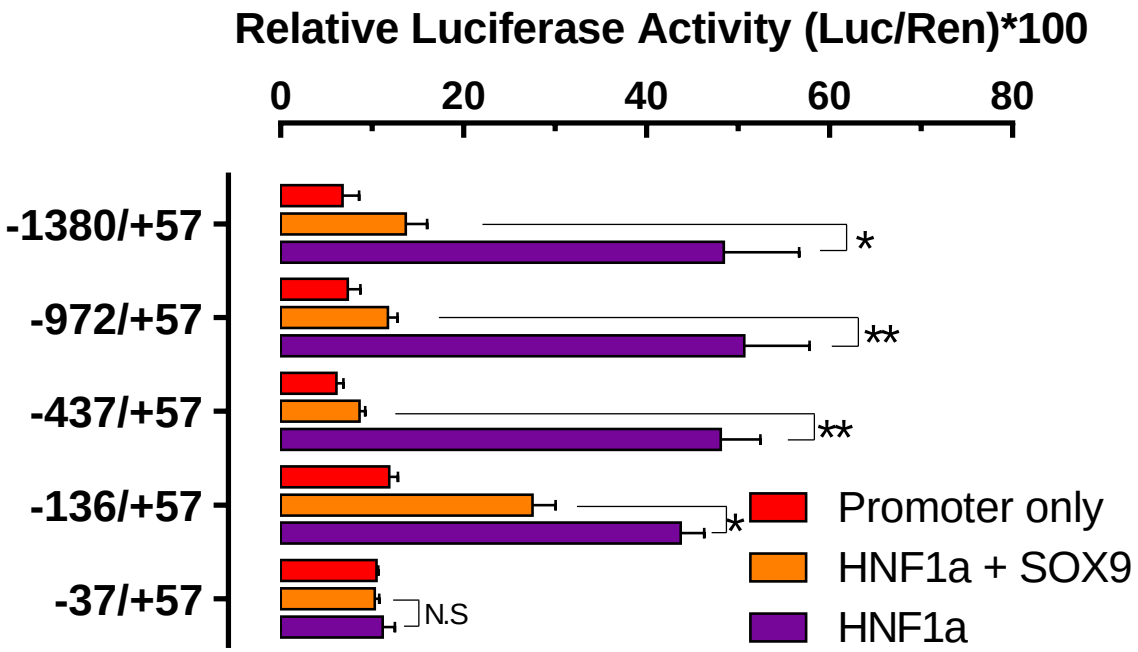

Figure 4.20: SOX9 inhibits *in vitro* luciferase activity induced by HNF1a

HEK293 cells were co-transfected with vectors expressing the *Firefly* luciferase downstream of the *Slc6a19* promoter constructs, with the *Renilla* luciferase as control. HNF1a expression vector (purple bars) or empty pcDNA3.1 expression vector (red bars) was co-expressed to activate transcription or serve as control, respectively. In a separate experiment, SOX9 was expressed together with HNF1a (orange bars). The following promoter constructs were used: pSlc6a19(–1380/+57), pSlc6a19(–972/+57), pSlc6a19(–437/+57), pSlc6a19(–136/+57), or pSlc6a19(–37/+57). Twenty-four hours after transfection, luciferase activity was measured. Relative luciferase activity was determined by normalising the *Firefly* luciferase activity to the control *Renilla* luciferase activity. P values indicate the significance derived from three experiments, each using triplicate transfections. The data are means ± SD of triplicate experiments. Significant changes in promoter activity due to co-transfection of SOX9 are indicated by asterisks (* $p < 0.05$; ** $p < 0.01$). N.S designates non-significant results.

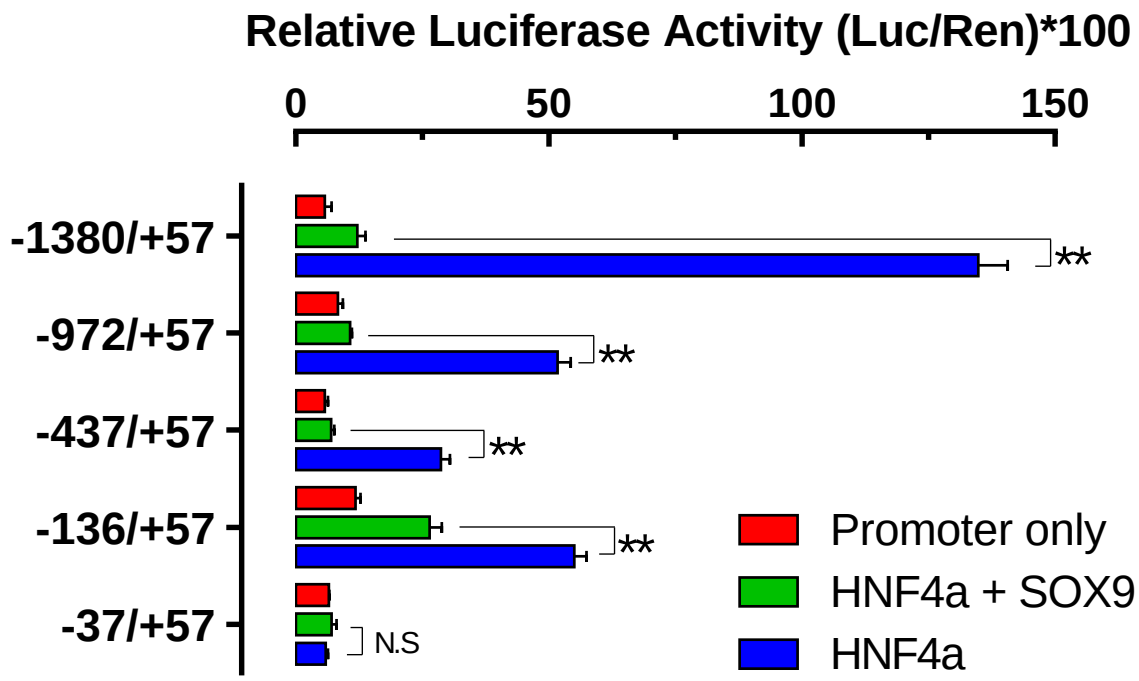

Figure 4.21: SOX9 inhibits luciferase expression activated by HNF4a *in vitro*

HEK293 cells were co-transfected with vectors expressing the *Firefly* luciferase downstream of the *Slc6a19* promoter constructs and with the *Renilla* luciferase as control. HNF4a expression vector (purple bars) or empty pcDNA3.1 expression vector (blue bars) was co-expressed to activate transcription or serve as control, respectively. In a separate experiment, SOX9 was co-expressed with HNF4a (green bars). The following promoter constructs were used: pSlc6a19(–1380/+57), pSlc6a19(–972/+57), pSlc6a19(–437/+57), pSlc6a19(–136/+57), or pSlc6a19(–37/+57). Twenty-four hours after transfection, luciferase activity was measured. Relative luciferase activity was calculated by normalising the *Firefly* luciferase activity relative to the control *Renilla* luciferase activity. Transfections were repeated at least three times using triplicate samples. The data are means ± SD of triplicate experiments. Significant changes of the promoter activity due to co-transfection of SOX9 are indicated by asterisks (* $p < 0.05$; ** $p < 0.01$). N.S designates non-significant results.

We were unable to analyse mutation of SOX9-binding site SOX9-BS1 (–37 to –34), because the proposed SOX9-BS1 binding site overlaps with the HNF4a-binding site (**Figure 4.22**); mutation of this site also abolishes activation by HNF4a. As shown in **Figure 4.20** and **Figure 4.21**, deletion of the SOX9-BS2 region (–1150 to –1126) did not abolish the inhibitory effect of SOX9 on *Slc6a19* promoter constructs –972/+57, –437/+57, and –136/+57, respectively.

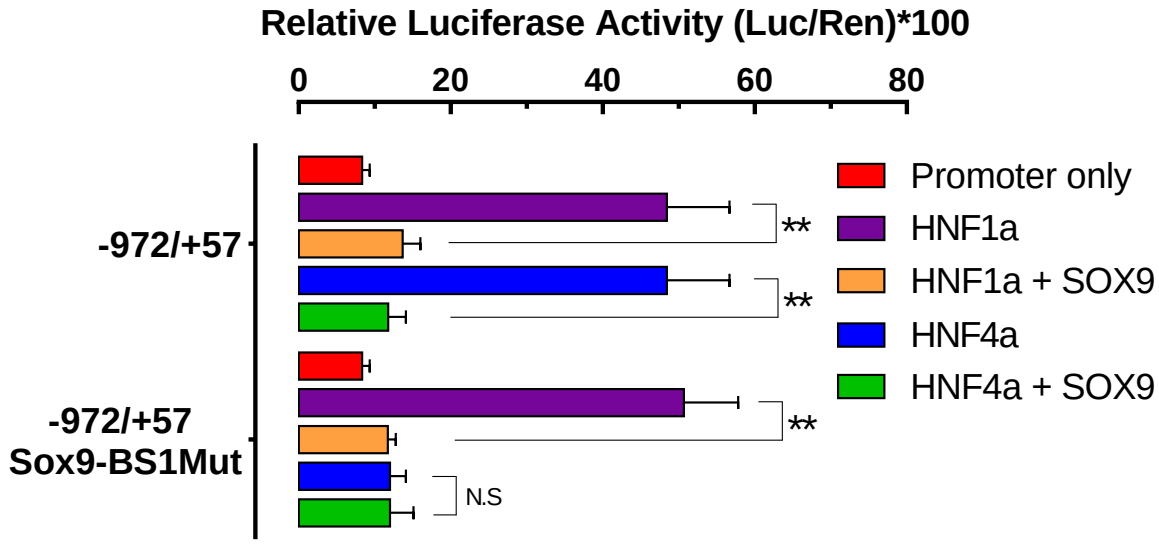

Figure 4.22: Investigation of the putative SOX9-binding site using wild-type and mutated pSlc6a19(–972/+57) constructs

HEK293 cells were co-transfected with *Renilla* luciferase as control and with vectors expressing the *Firefly* luciferase downstream of the promoter construct pSlc6a19(–972/+57) or the same construct with mutated SOX9-BS1. In addition different transcription factors were co-expressed. The following constructs were used: HNF1a expression vector (orange bars), HNF4a (green bars), HNF1a plus SOX9 (grey bars), or empty pcDNA3.1 expression vector (red bars). Twenty-four hours after transfection, the luciferase activity was measured. Relative luciferase activity was determined by normalising the *Firefly* luciferase activity to the control *Renilla* luciferase activity. Transfections were repeated at least three times using triplicate samples. The data are means ± SD of triplicate experiments. (* $p < 0.05$; ** $p < 0.01$).

To further validate the reporter gene results, SOX9-binding to the *Slc6a19* promoter was tested in isolated mouse intestinal cells by ChIP assay using cross-linked mouse intestinal chromatin. Chromatin fragments were immunoprecipitated using a polyclonal antibody against SOX9 and the *Slc6a19* promoter was detected by real-time PCR generating amplicons of 150-200 bp spanning the promoter region from position –1368 to +11.

These experiments (**Figure 4.23**) suggested that the SOX9 binding site was located between position –353 to –136 confirming findings by luciferase assays. The precise location, however, could not be determined.

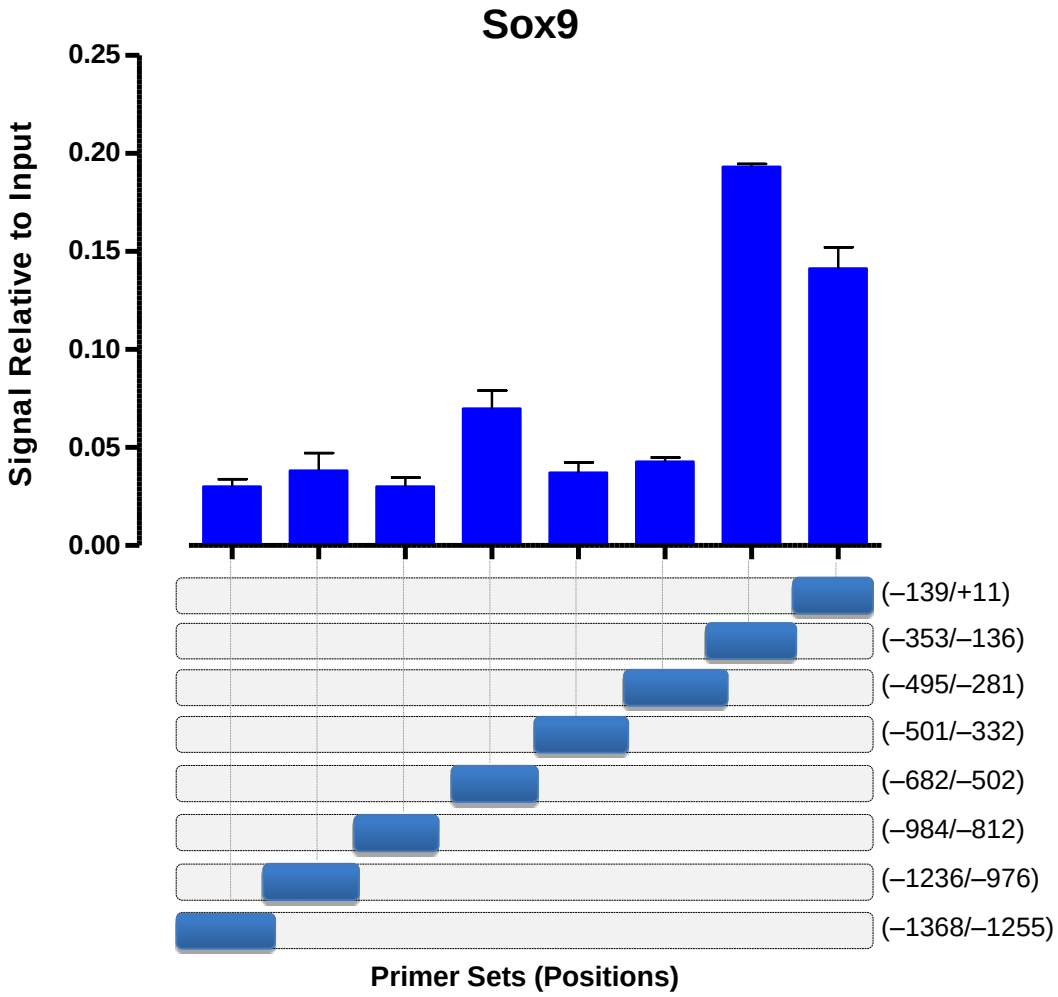

Figure 4.23: SOX9 directly binds to the *Slc6a19* promoter

ChIP assay was used to identify SOX9-binding sites on cross-linked chromatin isolated from mouse small intestinal epithelium. The chromatin was immunoprecipitated using an antibody against SOX9. After purification, the precipitated DNA was quantified by qPCR using primer sets specific for –139/+11, –353/–136, –495/–281, –501/–332, –682/–502, –984/–812, –1236/–976, or –1368/–1255. The lower part of the graph shows the location of primer pairs used in the real-time PCR. The upper part of the graph shows the ChIP signal relative to the input signal.

SOX9 has been shown to recognise an ACAA motif to regulate transcription (Harley et al., 1994) (**Figure 4.24.A**). Further inspection of the proximal promoter revealed possible binding sites at positions +10/+13 (SOX9-BS3) and –218/–215 (SOX9-BS4) (**Figure 4.24.B**).

A

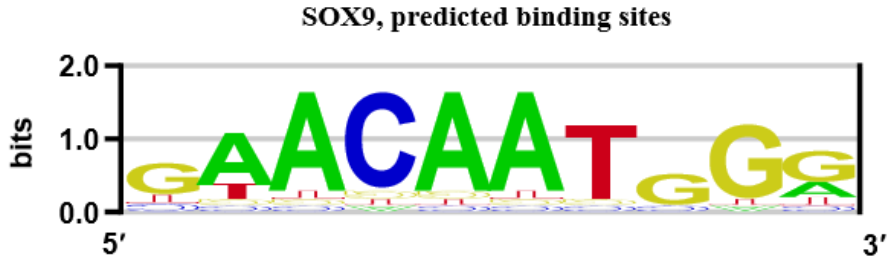

B

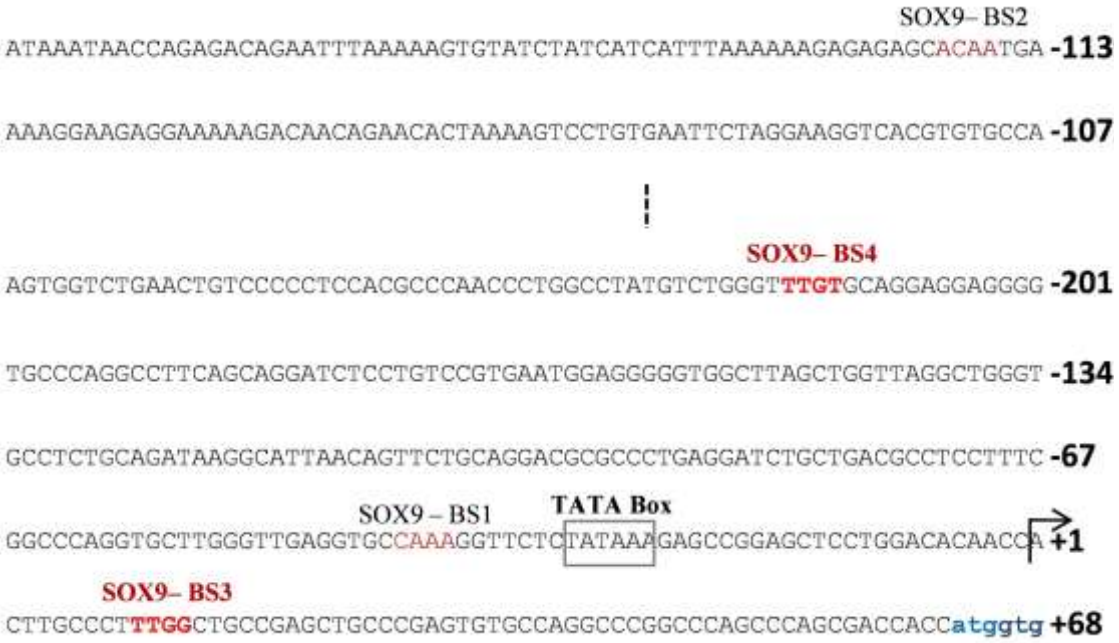

Figure 4.24: Predicted binding sites for SOX9

(A) Weblogo presentation of the SOX9 consensus sequence. **(B)** Location of predicted SOX9-binding on the *Slc6a19* promoter.

To check whether these binding sites could be targeted by SOX9, site-directed mutagenesis was performed. SOX9-BS3 mutation did not change the effect of SOX9 on luciferase activity. However, mutation of the SOX9-BS4 site increased the overall promoter activity and partially abrogated the effect of SOX9 regardless of whether transcription was driven by HNF1a or HNF4a (**Figure 4.25**).

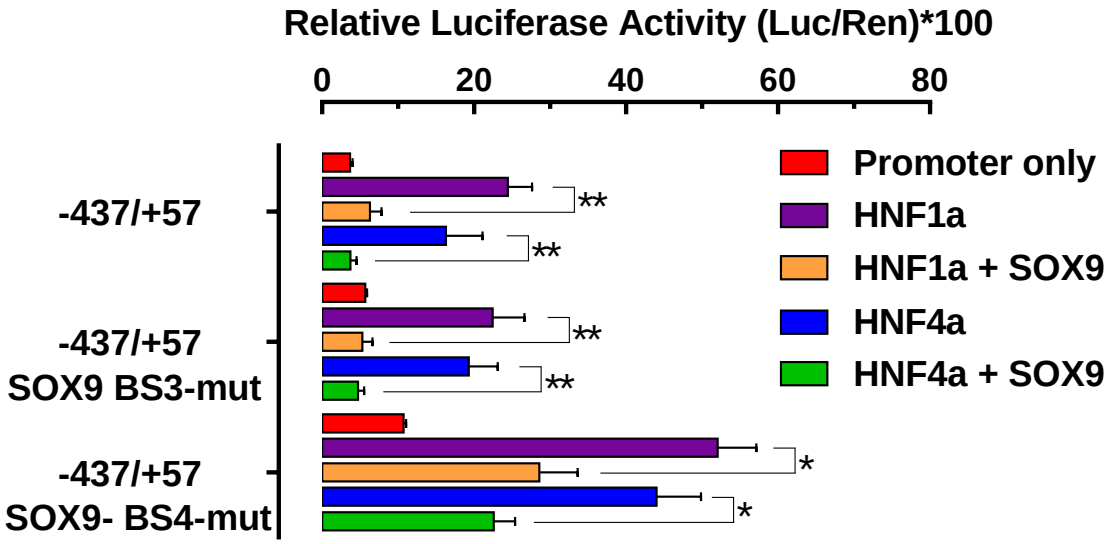

Figure 4.25: Investigation of the SOX9-binding sites using mutated constructs.

HEK293 cells were co-transfected with vectors expressing the *Firefly* luciferase downstream of the promoter constructs, together with various transcription factors and with the *Renilla* luciferase as control. The following constructs were used: pSlc6a19(–437/+57), SOX9-BS3 mutated pSlc6a19(–437/+57), SOX9-BS4 mutated pSlc6a19(–437/+57), together with HNF1a expression vector (orange bars), HNF1a plus SOX9 (grey bars), HNF4a (green bars), HNF4a plus SOX9 (red bars), or empty pcDNA3.1 expression vector (black bars). The *Renilla* luciferase was used as control vector. Twenty-four hours after transfection, the luciferase activity was measured. Relative luciferase activity was determined by normalising the *Firefly* luciferase activity to the control *Renilla* luciferase activity. Transfections were repeated at least three times using triplicate samples. The data are means ± SD of triplicate experiments. (* $p < 0.05$; ** $p < 0.01$).

Mutation of SOX9-BS4 did not completely abolish the inhibitory effect of SOX9, suggesting that this TF may affect transcription indirectly, for instance by binding to other TFs. To test whether the SOX9 effect required direct binding to the promoter region, the SOX9 DNA-binding domain was mutated. To this end, a well-known SOX9 mutation, H65Y, was chosen (McDowall et al., 1999), which affects its target sequence binding. The experiments indicated that the inhibitory effect of SOX9 was weakened but not completely abolished (**Figure 4.26**). This suggested that SOX9 may inhibit transcription through interaction with the promoter region and through protein-protein interaction with other TFs, such as HNF1a and HNF4a.

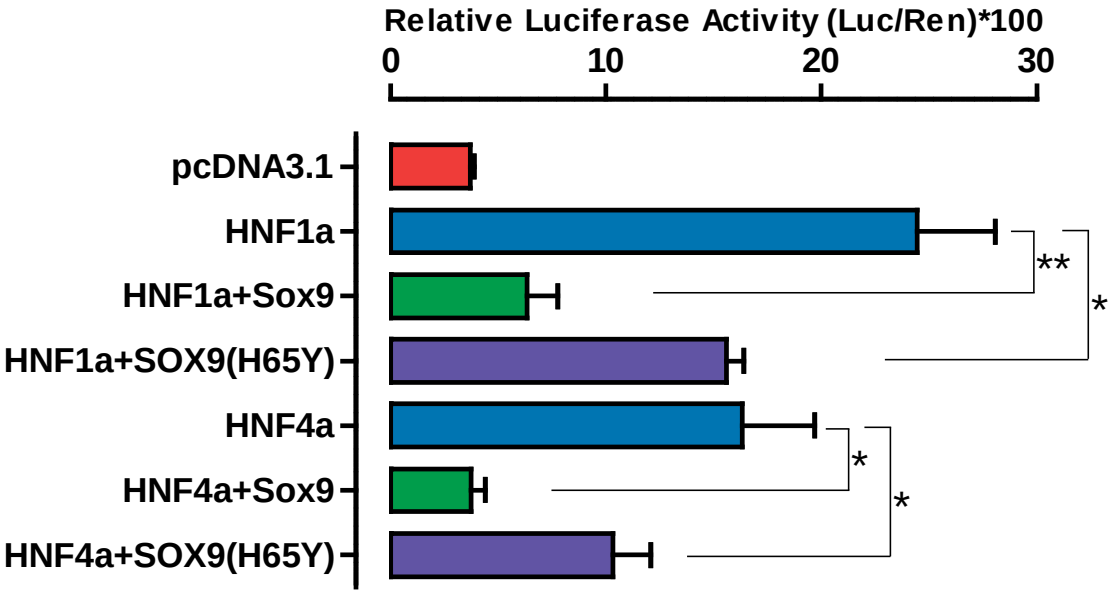

Figure 4.26: The effect of SOX9(H65Y) on the pSlc6a19(–437/+57)

HEK293 cells were co-transfected with vectors expressing the *Firefly* luciferase downstream of the promoter construct pSlc6a19(–437/+57), together with different TFs and with the *Renilla* luciferase as control. The following combinations were used: HNF4a expression vector, HNF4a plus SOX9, HNF4a plus SOX9(H65Y), HNF1a, HNF1a plus SOX9, HNF1a plus SOX9(H65Y), or empty pcDNA3.1 expression vector (red bar). Twenty-four hours after transfection, luciferase activity was measured. Relative luciferase activity was determined by normalising the *Firefly* luciferase activity to the control *Renilla* luciferase activity. P values indicate the significance derived from three experiments, each using triplicate transfections. The data are means ± SD of triplicate experiments. Significant changes of the promoter activity due to co-transfection of HNF1a and HNF4a are indicated by asterisks (* $p < 0.05$; ** $p < 0.01$).

To further investigate whether some of the SOX9 effects are independent of DNA-binding, SOX9(H65Y) was co-transfected with a promoter containing a mutated SOX9-binding site 4 which completely abolished the inhibitory effect of SOX9 (**Figure 4.27**). This result suggested that SOX9 can act both as a sequence-specific transcription factor and as an inhibitory cofactor. In summary SOX9 acts as powerful inhibitor of HNF4a and HNF1a-driven Slc6a19 expression.

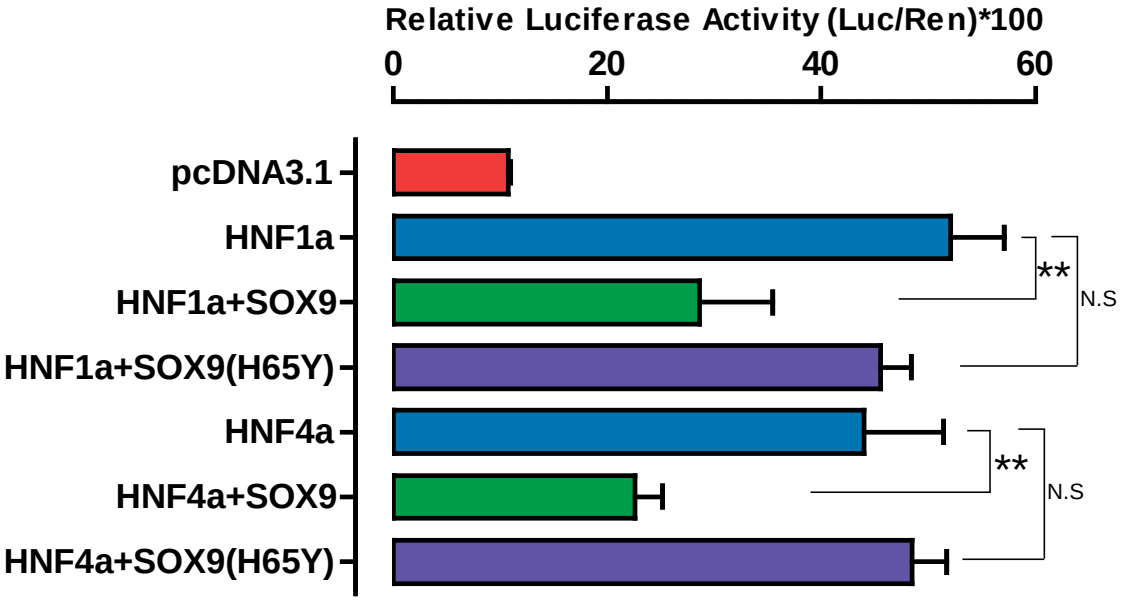

Figure 4.27: The combinatorial effects of SOX9(H65Y) and SOX9-binding-site mutation on pSlc6a19(–437/+57)

HEK293 cells were co-transfected with vectors expressing the *Firefly* luciferase downstream of promoter construct SOX9-BS4 mut/pSlc6a19(–437/+57), together with different TFs and with the *Renilla* luciferase as control. The combinations used were: HNF1a expression vector, HNF1a plus SOX9, HNF1a plus SOX9(H65Y), HNF4a, HNF4a plus SOX9, HNF4a plus SOX9(H65Y), or empty pcDNA3.1 expression vector (red bar). Twenty-four hours after transfection, luciferase activity was measured. Relative luciferase activity was determined by normalising the *Firefly* luciferase activity to the control *Renilla* luciferase activity. P values indicate statistical significance derived from three experiments, each using triplicate transfections. The data are means ± SD of triplicate experiments. Significant changes of promoter activity due to co-transfection of HNF4a and HNF1a are indicated by asterisks (* $p < 0.05$; ** $p < 0.01$).

4.2.9 Analysis of mouse *Collectrin* and *Ace2* promoters

To explain regulatory mechanisms driving ACE2 (*Ace2*) and TMEM27 (*Collectrin*) co-expression (see **Section 1.4.3**) with B^0AT1 in kidney and intestine, we analysed their promoter regions. To determine the length and position of the *Ace2* and *Collectrin* promoters and to determine highly conserved regions, bioinformatics was used to analyse promoter regions of the genes encoding *Collectrin* (NM_020626) and *Ace2* (NM_027286) upstream of their corresponding TSSs. As a result, a sequence 1450 kb upstream of the *Ace2* TSS (**Figure 4.28**.**A**) and another sequence 1800 bp upstream of the *Collectrin* TSS (**Figure 4.28**.**B**) were chosen.

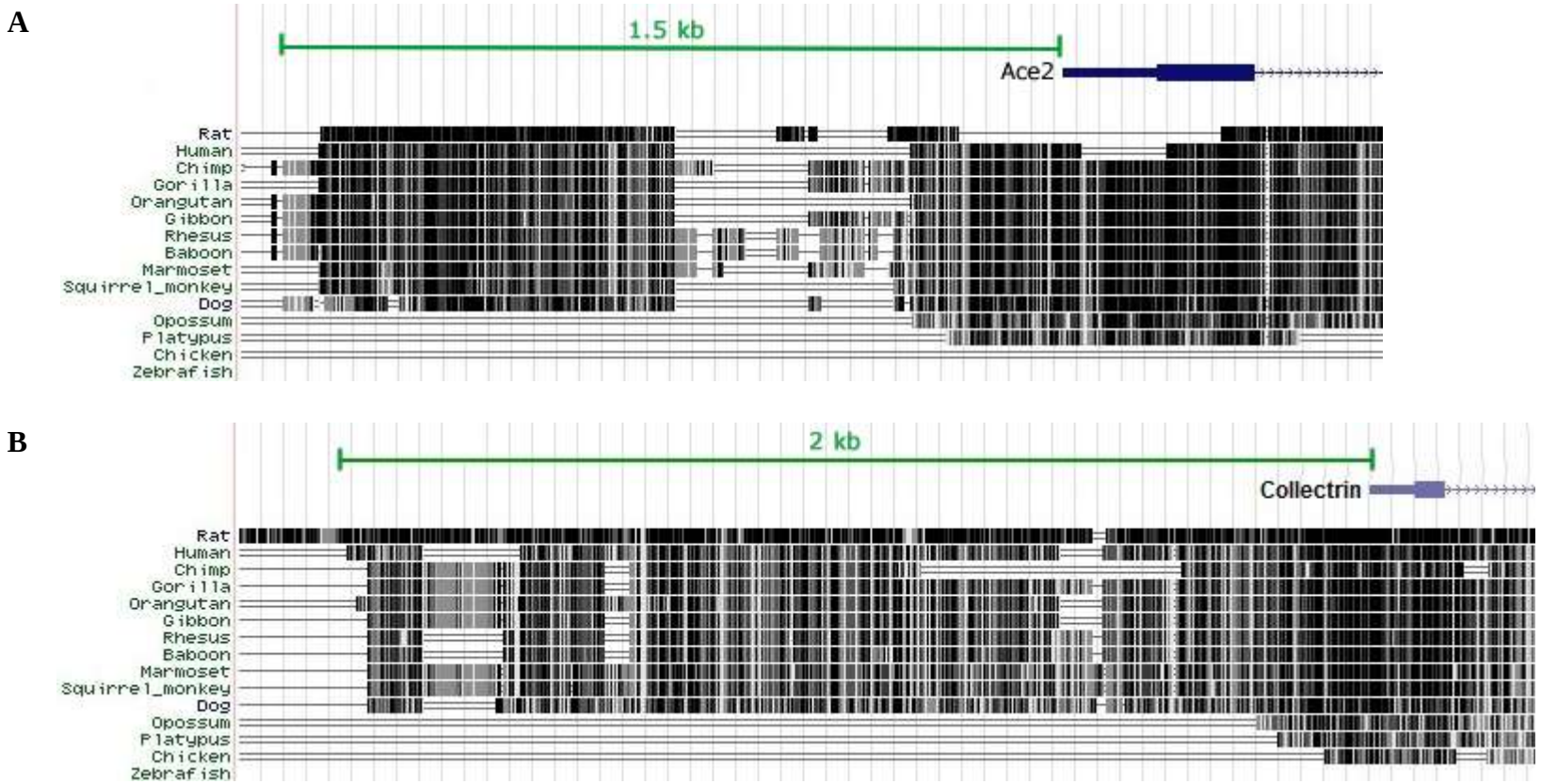

Figure 4.28: Sequence alignment of promoters of *Collectrin* and *Ace2* from different species

Alignments were generated using the UCSC Genome Browser. Black domains indicate conserved regions in different species. Regions 1.5 kb upstream of the *Ace2* TSS (**A**) and 2 kb upstream of the *Collectrin* TSS (**B**) were analysed.

The distributions of putative TF-binding sites on the *Collectrin* and *Ace2* promoters were examined by the MatInspector program. Possible binding sites for HNF1a, HNF1b and HNF4a, but not SOX9, were found on the *Collectrin* promoter (**Table 8.4**). The *Ace2* promoter had binding sites for HNF1a and HNF4a, but not HNF1b or SOX9 (**Table 8.5**).

To test whether the *Tmem27* and *Ace2* promoters were controlled by similar regulatory elements as the *Slc6a19* promoter, a region 2 kb upstream of the *Tmem27* TSS and another 1.5 kb upstream of the *Ace2* TSS were inserted separately into the pGL4.12 *firefly* luciferase reporter plasmid (see **Section 2.6.3**). Subsequently, HEK293 cells were co-transfected with reporter gene constructs and TFs previously identified to regulate the *Slc6a19* promoter (**Figure 4.29**).

Similar to *Slc6a19*, *Tmem27* and *Ace2* promoters were markedly transactivated by HNF1a and HNF1b transcription factors and these effects were suppressed by SOX9. However, HNF4a, did not activate Tmem27 and Ace2 promoters. While HNF1b did not affect the *Slc6a19* promoter. Despite these differences *Slc6a19* and *Ace2* are co-expressed in enterocytes (Kowalczuk et al., 2008), confirming the synergistic action of HNF1a and HNF4a in the intestinal epithelium (Shih et al., 2001).

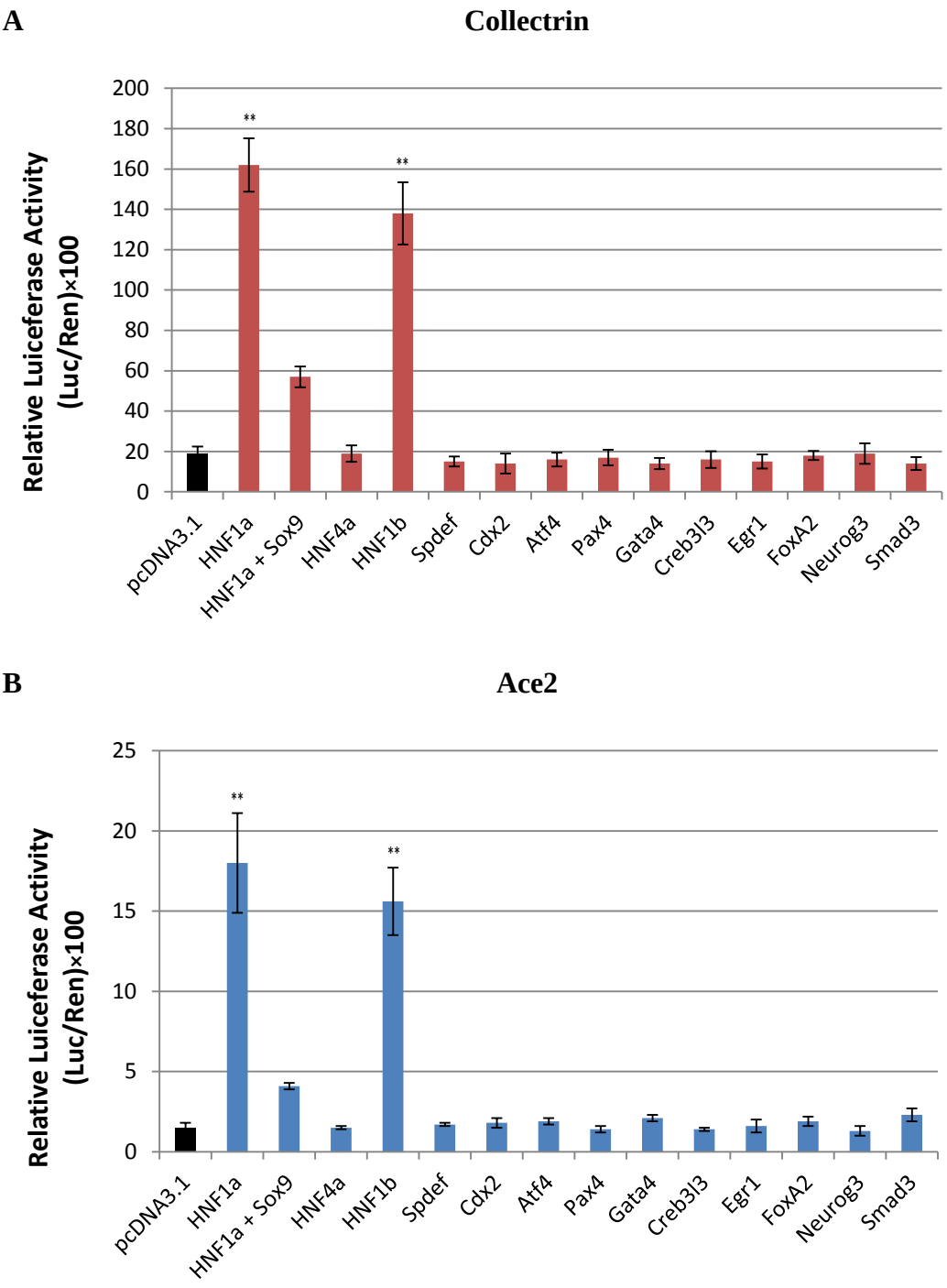

Figure 4.29 Effects of the different TFs on *Collectrin* and *Ace2* promoters

HEK293 cell were co-transfected with the *Firefly* luciferase inserted in (**A**) pCollectrin(–1903/+76) and (**B**) pAce2(–1509/+170) together with the *Renilla* luciferase vector as control. In addition, the following constructs were co-transfected separately: empty pcDNA3.1 (black bar), or pcDNA3.1 expressing HNF1a, HNF1a plus SOX9, HNF4a, HNF1b, SPDEF, CDX2, ATF4, PAX4, GATA4, CREB3L3, EGR1, FOXA2, NEUROG3, or SMAD3. Twenty-four hours after transfection, the luciferase activity was measured. Relative luciferase activity was determined by normalising the *Firefly* luciferase activity to the control *Renilla* luciferase activity. Transfections were repeated at least three times using triplicate samples. The data are means ± SD of triplicate experiments. (* $p < 0.05$; ** $p < 0.01$).

4.2.10 Effects of HNF1a mutation on *Ace 2 or Tmem27* promoter activities

One hundred and ninety-three different HNF1a mutations have been described in MODY patients (Ellard and Colclough, 2006). The HNF1a(R131W) mutation is the most common cause of type 3 MODY disorder. The R131W mutation is located in the DNA-binding domain of HNF1a; this mutation abrogates HNF1a-binding to its target sequence (Chi et al., 2002). When we co-transfected this HNF1a variant with *Ace2* and *Tmem27* promoters (**Figure 4.30**), transcriptional activation was largely abolished. While co-expression with the *Slc6a19* promoter reduced activation by about 50%.

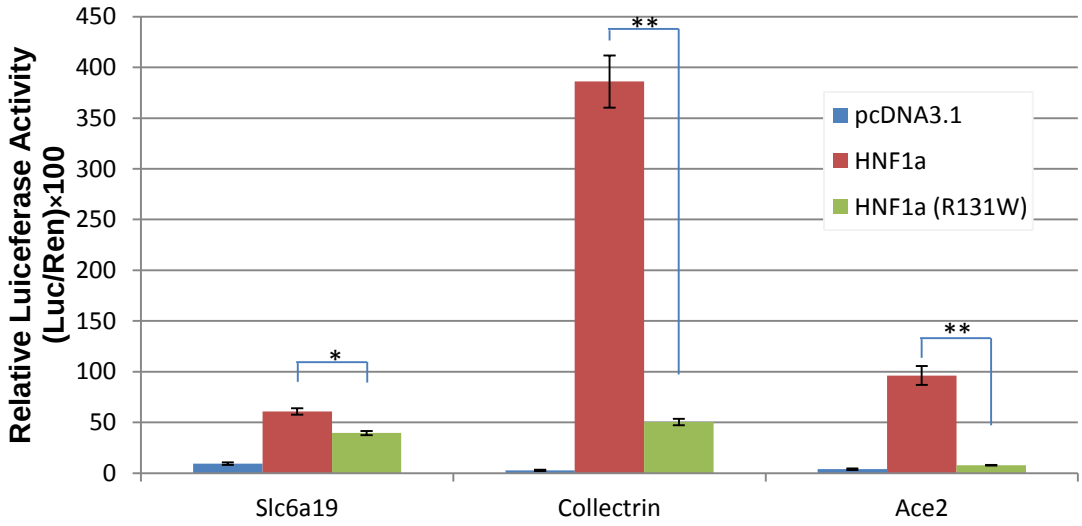

Figure 4.30: The effect of HNF1a(R131W) on *Slc6a19*, *Ace2* and *Tmem27* promoters.

HEK293 cells were co-transfected with the *Firefly* luciferase inserted in pSlc6a19(–1380/+57), pCollectrin(–1903/+76), or pAce2(–1509/+170) together with the Renilla luciferase vector as control. In addition, the following constructs were co-transfected: empty pcDNA3.1 (blue bars), and pcDNA3.1 expressing HNF1a (red bars) or HNF1a(R131W). Twenty-four hours after transfection, luciferase activity was measured. Relative luciferase activity was determined by normalising the *Firefly* luciferase activity to the control *Renilla* luciferase activity. P values indicate the significance derived from three experiments, each using triplicate transfections. The data are means ± SD of triplicate experiments. (* $p < 0.05$; ** $p < 0.01$).

4.3 Discussion

Previously, *Slc6a19* was shown to be highly expressed in intestinal enterocytes and epithelial cells of the kidney proximal tubule (Bröer et al., 2004). While the transport activity of B^0AT1 and its physiological roles in different organs have been described in some detail, the transcriptional regulation underlying its localised expression has not been investigated. In this chapter, I have examined the transcriptional regulation of the *Slc6a19* gene in detail.

4.3.1 Novel Hepatocyte Nuclear Factor response elements on the *Slc6a19* promoter

Hepatocyte Nuclear Factors are necessary for hepatocyte development. However, these TFs are not only expressed in the liver, but they are also expressed in the kidney and intestine. Accordingly, HNF1a and HNF4a have been shown to be important regulators of differentiation in intestinal epithelial cells (Pontoglio et al., 1996, Sladek et al., 1990).

Kikuchi et al. (2010) used bioinformatics and epigenetic analyses to investigate the regulation of amino acid transporters' genes in kidney (Kikuchi, Yagi et al. 2010). The bioinformatics analysis showed an HNF1a-binding site at position –111 to –114. The study also showed possible HNF1a-binding sites on all major amino acid transporter genes. To our knowledge, this was the first and only report suggesting HNF1a-binding motifs in the *Slc6a19* promoter region. In agreement with that study, our *in vitro* analysis confirmed that HNF1a binds to the *Slc6a19* promoter at this predicted murine promoter site. Additionally, our ChIP analysis using mouse intestinal chromatin verified that HNF1a binds the promoter region, *in vivo*. As shown in human patients with MODY disorder, HNF1a and HNF4a are also critical for glucose metabolism (Fajans et al., 2001). We replicated an HNF1a mutation, which causes MODY disorder, and co-transfected this mutated form of the TF with the *Slc6a19* promoter, but it did not completely abolish transcriptional activation.

To our knowledge, no other studies have investigated the regulatory function of HNF4a on the *Slc6a19* gene in the mammals. With similar methodology, an HNF4a-binding site was confirmed by *in vitro* and *in vivo* studies. This is the first study showing that HNF4a can regulate *Slc6a19* gene in the mammalian intestine. As discussed earlier (see **Section 1.3.2.3**), HNF1a-knockout mice suffer from renal Fanconi syndrome, which

is characterised by diabetes, glycosuria and aminoaciduria (Pontoglio et al., 1996). Recent clinical studies have shown that an R76W mutation in HNF4a causes Fanconi syndrome due to dysfunction of the renal tubules (Hamilton et al., 2013, Numakura et al., 2015). This new finding indicates that not only HNF1a, but also HNF4a, is necessary for proper functioning of the renal proximal tubules. In accordance with the above studies, our results suggest that HNF4a together with HNF1a controls *Slc6a19* expression along the renal proximal tubules.

Some studies have shown that a number of intestinal genes are regulated by combinatorial action of HNFs, GATA TFs and CDX2 (Boudreau et al., 2002, Coskun et al., 2010, Maher et al., 2006). In contrast, our luciferase experiments testing different combinations of these TFs did not show any synergistic regulatory effect on the *Slc6a19* promoter.

4.3.2 Negative effect of SOX9 on the *Slc6a19* activation

SOX9 is a well-known TF involved in transcriptional activation of genes (Bell et al., 1997, Bastide et al., 2007). Several studies have shown that SOX9 drives stem cell differentiation into mature enterocytes. Yet some genes can be negatively regulated by SOX9 in the crypt, including *Cdx2* and *Muc2* which are crucial for enterocyte maturation (Blache et al., 2004).

CDX2 positively regulates intestinal TFs such as *Cdx1*, *Hnf1a* and *Hnf4a*, which control gene expression in villus cells (Gao et al., 2009, Heath, 2010). Therefore, reduced SOX9 expression could allow CDX2 expression in the villus cells; thus, activating *Slc6a19* expression indirectly. However, we revealed that CDX2 expression in crypt cells is higher than in mature enterocytes; therefore, SOX9 is unlikely to indirectly activate *Slc6a19* expression via CDX2. Instead, while HNF1a and HNF4a activated the *Slc6a19* promoter, their action was directly inhibited by SOX9. SOX9 has direct and indirect effects on the expression of its target genes. It has been shown that SOX9 negatively regulates the B-catenin/Tcf4 pathway indirectly via cyclin D1 and c-Myc (Bastide, Darido et al. 2007). A recent study showed that genes involved in chondrocyte maturation are regulated by SOX9 either directly or indirectly (Ohba et al., 2015).

Our data further revealed a SPDEF consensus binding site on the *Slc6a19* promoter. Since SPDEF is expressed only in goblet and Paneth cells (Gregorieff et al.,

2009, Noah et al., 2010) it could cause expression of *Slc6a19* in these cells. However, SOX9 has a similar expression pattern, to SPDEF and is also expressed in Paneth cells (Mori-Akiyama et al., 2007). SOX9 down-regulation causes a significant decrease in the number of goblet cells (Bastide et al., 2007). Therefore, a possible activating effect of SPDEF could be supressed by SOX9 in Paneth and goblet cells. Further analysis should include *in vivo* studies to investigate SOX9 and SPDEF interaction, on the *Slc6a19* promoter of goblet and Paneth cells separately.

4.3.3 Ace2 and Collectrin

HNF1B was previously shown to transcriptionally regulate *Tmem27* expression in the pancreatic β-cell and in kidney (Zhang et al., 2007). HNF1b is a member of the same TF family as HNF1a and they share almost 90% homology at their corresponding DNA-binding domains (Tronche and Yaniv, 1992). HNF1B is expressed in epithelial cells along the whole nephron (Zhang et al., 2007). Our microarray results, however, did not reveal any significant expression of the *Hnf1b* mRNA in the crypt–villus fractions. In vitro luciferase assays confirmed that *Ace2* and *Tmem27* transcriptions were positively regulated by HNF1b co-transfection. However, no significant activation of the *Slc6a19* promoter by HNF1b was observed. These results indicating that despite co-expression of these trafficking proteins with B^0AT1, their transcriptions are controlled by different regulatory elements in the intestine and kidney.

Although Slc6a19 and Ace2 are in part trans-activated by different regulatory elements, B^0AT1 is co-expressed with the trafficking proteins in the intestine and kidney. These results may point to yet unknown TF(s), which help to coordinate the observed overlapping expression patterns”

4.3.4 Summary

The results from this study demonstrate a possible mechanism of the transcriptional regulation of the *Slc6a19* gene in the crypt–villus axis. *In vitro* and *in vivo* analyses revealed that HNF1a, HNF4a and SOX9 bind and orchestrate regulation of *Slc6a19* promoter in the mouse intestine.

Chapter 5 Methylation and histone modification of *Slc6a19* promoter in mouse intestine, liver and kidney

5.1 Introduction

In living cells, DNA is compacted as chromatin. The chromatin structure is an important regulator of the interaction of transcriptional factors with target regulatory DNA regions (Heintzman et al., 2007). Especially in differentiating cells, chromatin changes have been shown to play a central role in the regulation of transcription (Schübeler et al., 2004). Modifications on histone tails such as, methylation, acetylation and phosphorylation can affect transcriptional regulation (**Figure 5.1**).

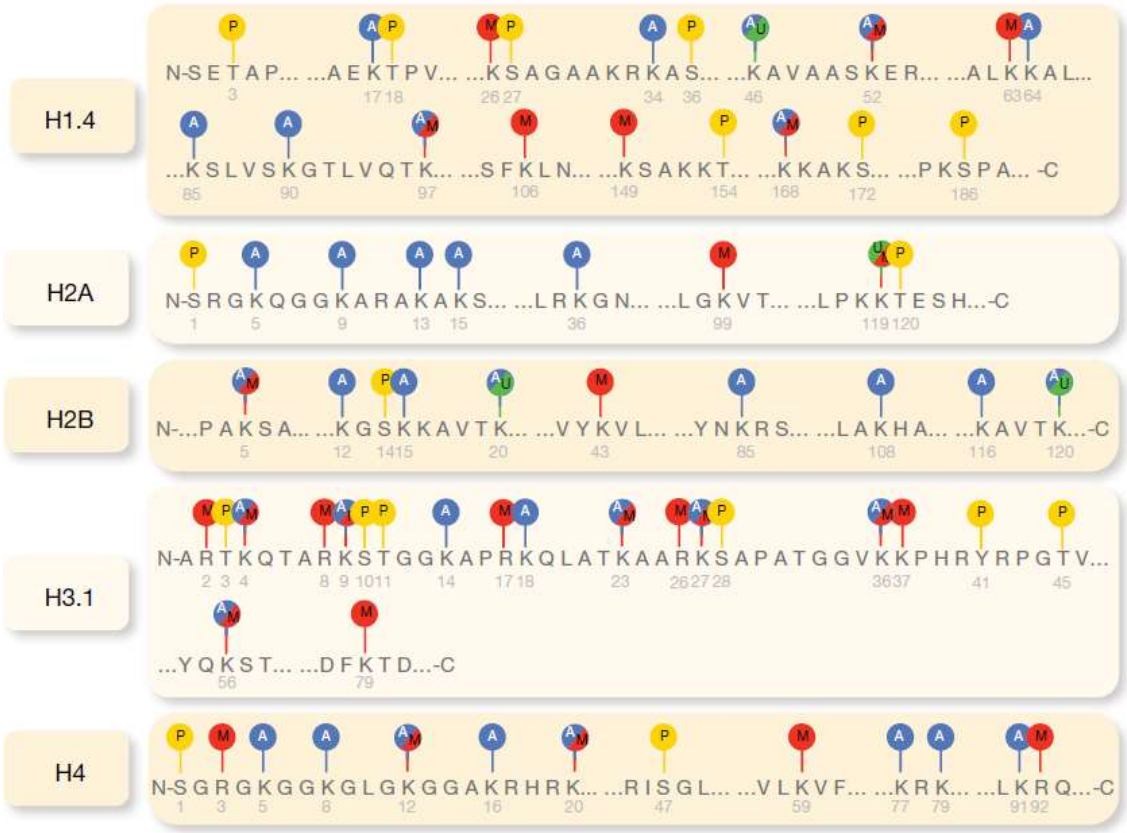

Figure 5.1 Possible positions of histone tail modification

Locations and types of well-known histone modifications are shown in the figure. Numbers under each amino acid residue represent location of a modification. A = acetylation, P = phosphorylation, U = ubiquitination, M = methylation. From (Portela and Esteller, 2010).

Acetylation of histone H3 tails is generally accompanied by transcriptional activation (Allfrey et al., 1964). For instance, acetylation of histone H3 tail at lysine 27 (H3K27ac) has been shown to correlate with transcription activation (Heintzman et al., 2007). However, methylation of H3 residues and its effect depend on the position. For example, methylation of the H3K36 histone tails (H3K36me3) leads to repression of transcription (Azuara et al., 2006). While, tri-methylation of the H3 histone tails at lysine 4 (H3K4me3) causes gene activation (Santos-Rosa et al., 2002).

DNA methylation and histone modification together play a critical role in the regulation of transcriptional activity. Recent studies suggest a close relationship between these two epigenetic modifications. As an example, DNA methylation can guide histone modifications, and vice versa histone modifications can affect the methylation status (Hayashi, Nagae et al. 2007). However, the mechanisms underlying these interactions are not well understood.

5.1.1 DNA methylation

DNA-methyltransferases (DNMT) are responsible for the transfer of the methyl group to cytosine nucleotides. Four major methyltransferases have been identified so far (DNMT1, DNMT3a, DNMT3b and DNMT3L) (Okano et al., 1999).

DNMT3a and DNMT3b are vital for embryonic development and *de novo* methylation in mammals (Chen et al., 2003). As a result, these enzymes need to access non-methylated CpG regions. Some histone modifications and specific DNA sequences can potentially initiate *de novo* methylation via recruitment of DNMT3a and DNMT3b (Klose and Bird, 2006).

DNMT3L lacks methyltransferase activity alone, but it has a stimulatory effect on the methylase activity of DNMT3a and DNMT3b (Suetake et al., 2004). DNMT3L is crucial for maternal imprinting at the gametogenesis stage (Bourc'his et al., 2001).

DNMT1 **(**maintenance methyltransferase**)** is the most common methyltransferases and the main enzyme for maintaining methylation during cell division (Richardson and Yung, 1999). DNMT1 has a high affinity for hemimethylated DNA strands during the S-phase of mitosis, thereby, transferring the methylation pattern to the newly synthesised DNA strand (**Figure 5.2**).

While methylation is well understood, demethylation remains to be fully described. During vertebrate development, DNA is globally demethylated during two stages of embryonic development. First, demethylation happens during germ cell development. Second, demethylation happens after fertilisation and implantation of an embryo. During the replication process, failing of DNMT1 function causes passive demethylation (Razin and Riggs, 1980). Active demethylation, by contrast, occurs during DNA repair processes by specific enzymes, such as Gadd45 (Barreto et al., 2007).

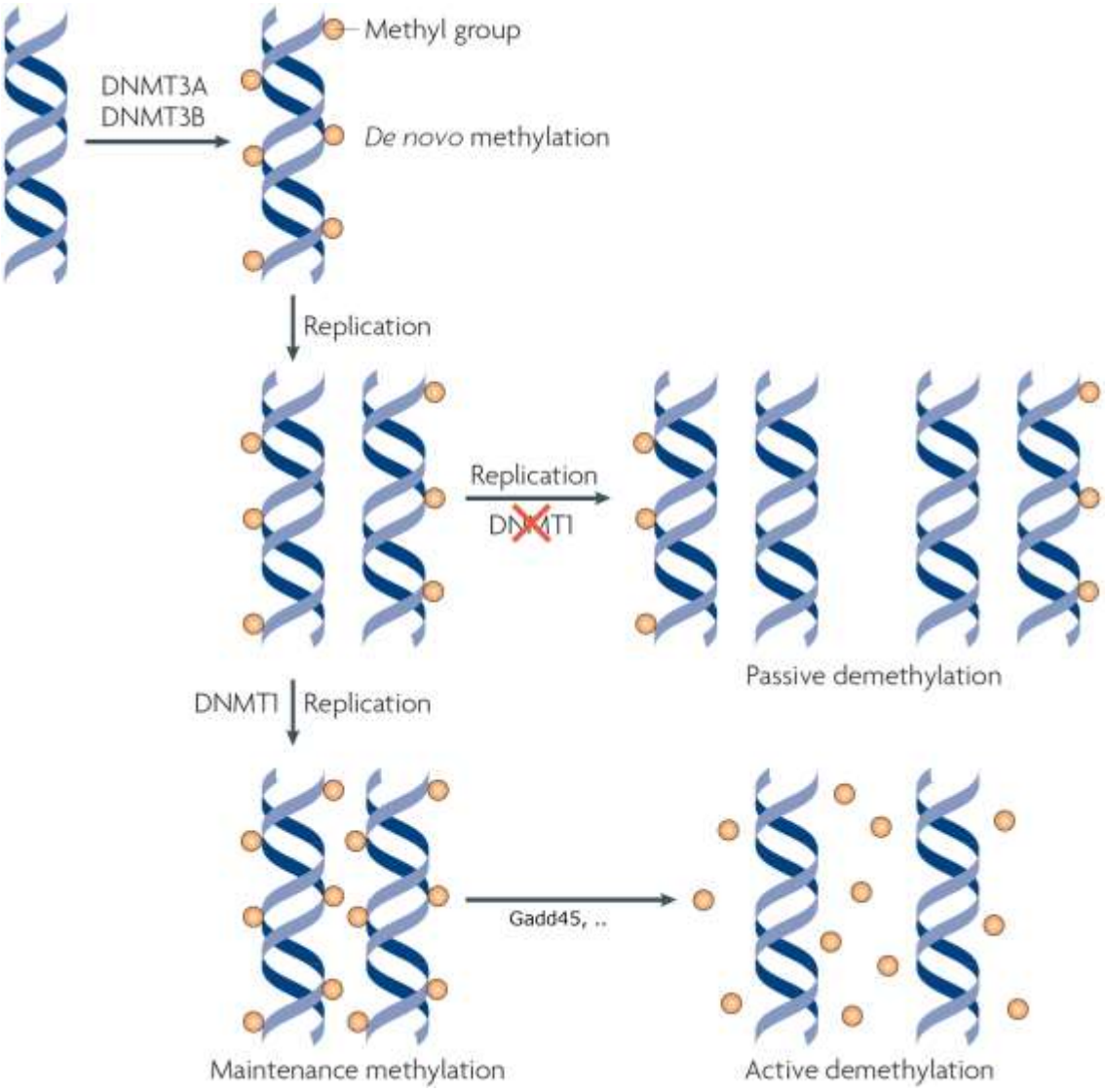

Figure 5.2. DNA methylation and demethylation

After global DNA demethylation, *de novo* methylation is re-established by DNMT3A and DNMT3B. Following cell division, this methylation pattern is preserved by DNMT1. Inhibition of DNMT1 during replication causes loss of methylation on the new DNA strand, this is called passive demethylation. Whereas, removal of methyl groups by enzymatic reaction is called active demethylation. From (Wu and Zhang, 2010).

5.1.2 DNase I hypersensitive sites

Deoxyribonuclease I (DNase I) is an endonuclease that catalyses cleavage of unprotected DNA. In the chromatin context, nucleosome-free DNA is more sensitive to fragmentation by DNase I; these regions are called DNase I hypersensitive sites. An average DNase I sensitive region is around 100 to 200 bp long and is a nucleosome-free DNA fragment (**Figure 5.3**). This region, most of the time, contains transcriptional

regulators. Accordingly, searching for DNase I hypersensitive sites on genomic material is crucial to determine regulatory elements of transcription.

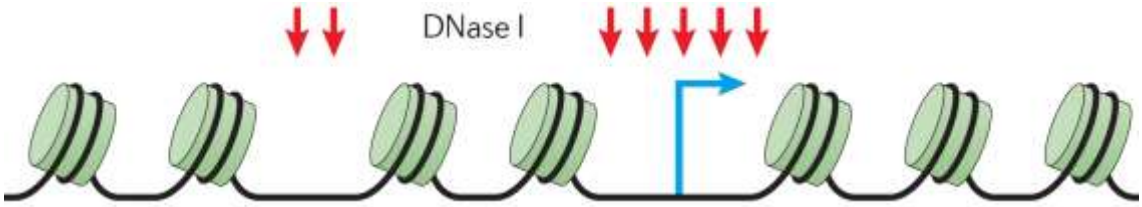

Figure 5.3 DNase I hypersensitive site in the chromatin context.

An example of a DNA fragment, showing DNase I hypersensitive sites (red arrows) around TSS (blue arrow) and promoter region, and protected areas of sequence. From (Bell et al., 2011).

5.2 Results

5.2.1 Analysis of H3K27ac and H3K4me3 histone modification associated with the 5' flanking region of *Slc6a19* promoter

To examine whether histone modifications are associated with the *Slc6a19* gene expression, ChIP assays were performed using two antibodies, one against acetylated histone H3 at residue K27 and the other against methylated histone H3 at residue K4.

H3K27ac is typically associated with gene activation (Heintzman et al., 2009). To verify whether H3K27ac is found in the vicinity of the *Slc6a19* promoter, ChIP was performed using cross-linked chromatin isolated from intestinal villus and crypt enterocytes using the fractionation protocol (see **Section 2.7.1.1**). The intestinal fractions and liver were immunoprecipitated using an antibody against H3K27ac. Immunoprecipitated DNA was analysed by real-time PCR generating amplicons of 150-200 bp spanning the *Slc6a19* promoter region from position –858 to +11. ChIP experiments demonstrated that acetylation of lysine 27 of histone H3 (H3K27ac) was significantly enriched in chromatin from villus tips compared to crypt and liver chromatin (**Figure 5.4**).

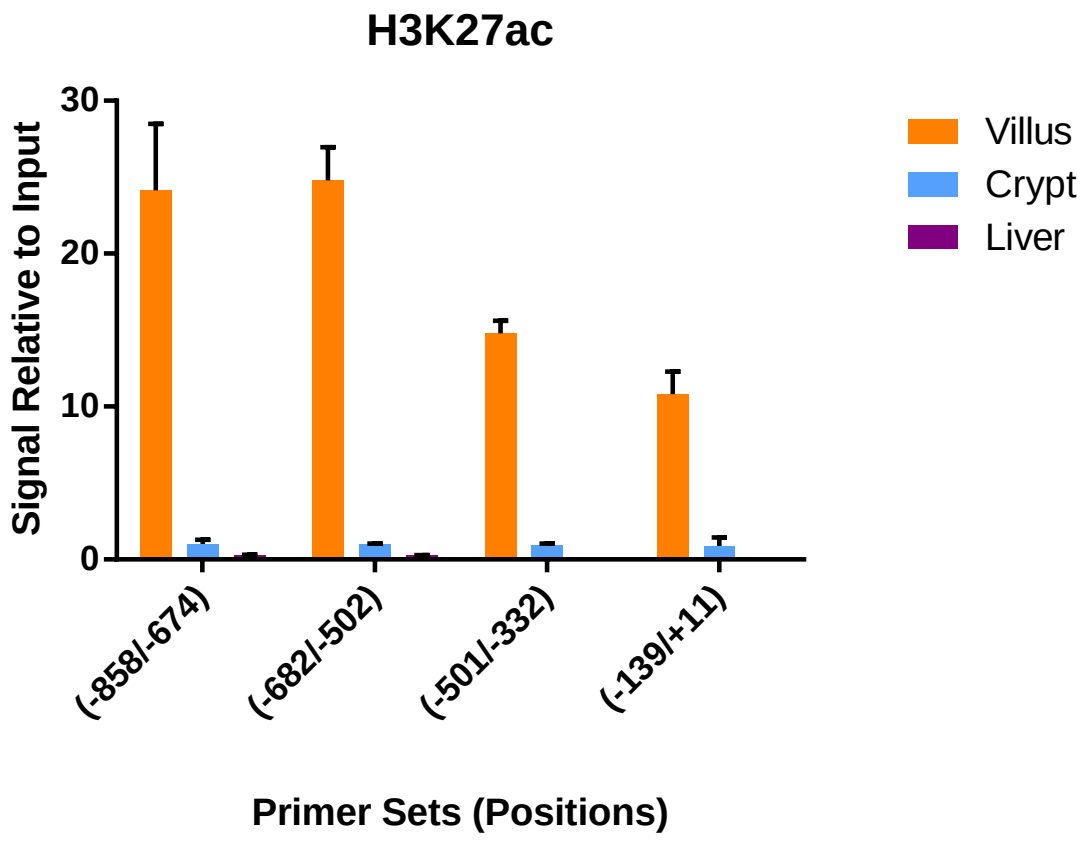

Figure 5.4 H3K27ac histone modification of the *Slc6a19* promoter region in liver and intestine

A H3K27ac-specific antibody was used in the ChIP assay. The genomic DNA was isolated from mouse villus and crypt cells, and from liver tissue. Data are given in percent signal relative to a real-time PCR reaction on input DNA. Primer pairs span the following promoter regions: –139/+11, –501/–332, –682/–502 and –858/–674. The data are means ± SD of triplicate experiments.

H3K4me3 is known to be associated with open chromatin regions (Santos-Rosa et al., 2002). ChIP assays were used to test whether H3K4me3 was bound to the promoter regions within living cells. The ChIP assay was performed using the chromatin isolated from intestinal fractionation, and from liver tissue. The enterocytes chromatin was immunoprecipitated using an H3K4me3 antibody. Real-time PCR was used to determine the localisation of the modified histones along the *Slc6a19* promoter. ChIP indicated that H3K4me3 was significantly enriched in the intestine and more than that in the liver (**Figure 5.5**).

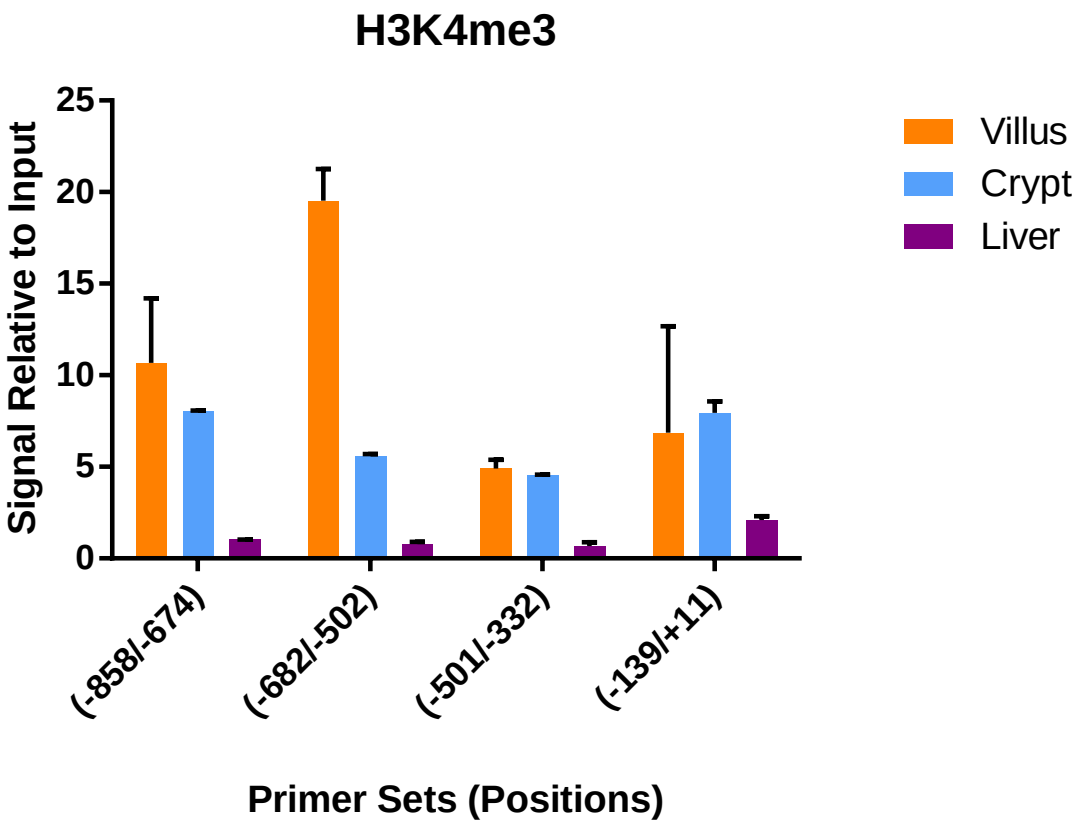

Figure 5.5 H3K4me3 histone modification of the *Slc6a19* promoter region in liver tissue and crypt–villus fractions

An H3K4me3-specific antibody was used in the ChIP assay. The Genomic DNA was isolated from mouse intestinal fractions and liver tissues. Data are given in percent signal relative to a real-time PCR reaction on input DNA. Primer pairs span the following promoter regions: –139/+11, –501/–332, –682/–502, –858/–674. The data are means ± SD of triplicate experiments.

5.2.2 Modifications of H3K4m3 and H3K36m3 in the N-terminus of histone H3

The ENCODE project (Rosenbloom et al., 2010) was completed by a worldwide consortium. The aim was to identify regulatory regions of the human genome in tissues and in more than 100 different cell lines. In addition to our ChIP experiments, the Encyclopedia of DNA Elements (ENCODE) database on the UCSC webpage (http://genome.ucsc.edu) was used to identify positioning of other histone modifications along the *Slc6a19* gene.

The ENCODE data indicated that the histone modification H3K4me3 was highly enriched over the promoter in kidney and small intestine, allowing binding of polymerase

II. Additionally, trimethylation of Lys36 in histone H3 (H3K36me3) was present over all exons confirming that the gene was actively transcribed. These two elements were absent in other tissues (**Figure 5.6**).

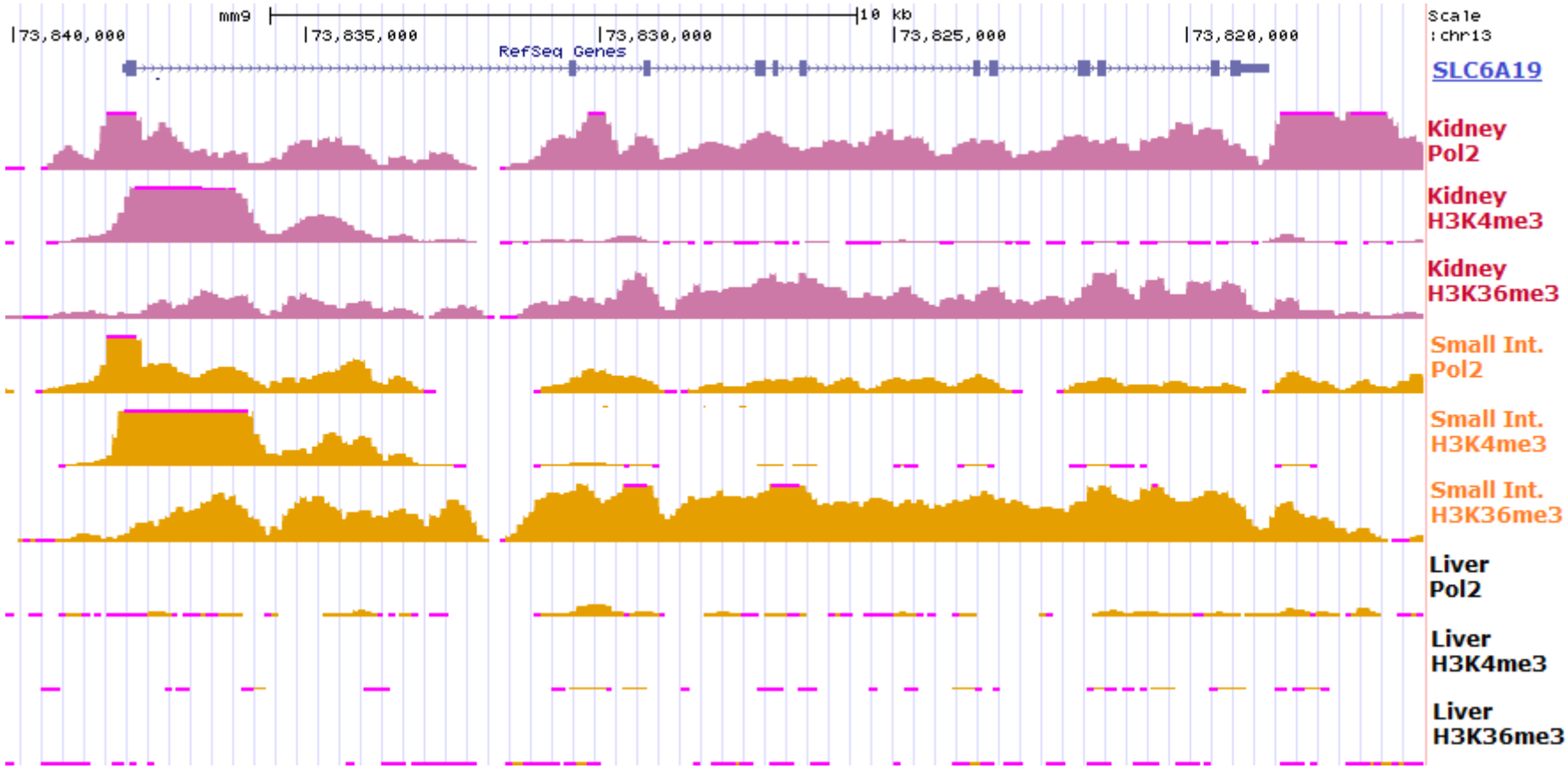

Figure 5.6. Histone modifications and polymerase II binding to the *Slc6a19* promoter

The ENCODE database was used to extract the distribution of histone modifications H3K4me3, H3K36me3, and RNA polymerase II binding along the mouse *Slc6a19* gene in different tissues. The *Slc6a19* gene shows active histone status and polymerase II binding in the small intestine and kidney but not in the liver.

5.2.3 DNase I hypersensitive sites on the *Slc6a19* promoter

To localise possible TF-binding sites on the *Slc6a19* gene, DNase I hypersensitive sites were identified using ENCODE data. Two sensitive regions were identified in the mouse *Slc6a19* promoter (**Figure 5.7**). The first hypersensitive fragment was located from +75 to –220, consistent with the core promoter region. The second hypersensitive region was located between position –1000 to –1200. The results suggested that the liver chromatin around the *Slc6a19* promoter region was more condensed than the kidney chromatin. This explains RNA polymerase may bind to DNA in the extended chromatin of kidney. ENCODE data does not supply any information about DNase I hypersensitive status of the small intestine in the mouse.

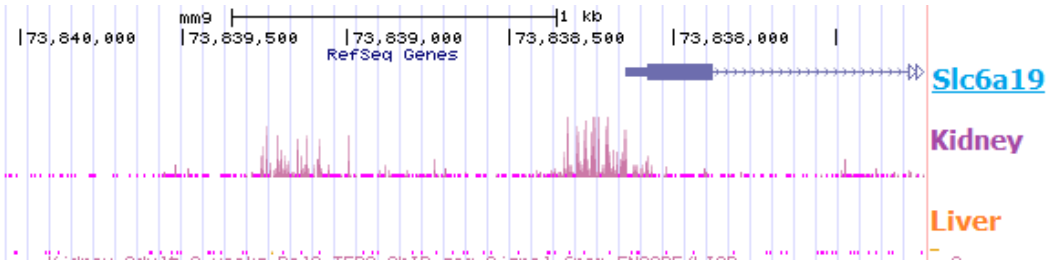

Figure 5.7 DNase I hypersensitive sites on the mouse the *Slc6a19* promoter

The histogram shows that two separate DNase I sensitive regions located around 1 kb upstream of the *Slc6a19* promoter in the kidney chromatin. In liver chromatin, no DNase I sensitive regions were identified in the same region.

5.2.4 DNA methylation profile of the *Slc6a19* promoter in mouse

In addition to showing the effects of histone modifications on the transcriptional activity, we also analysed the methylation status changes of the promoter in different tissues. Analysis of a region 1200 bp upstream of the *Slc6a19* TSS revealed 20 CpG dinucleotides (**Figure 5.8**). Ten CpGs were located between (–171 to +56), which covers binding sites for transcription factor SOX9, HNF1a, HNF4a and the TATA-binding protein. However, no CpG island was detected by UCSC Genome Browser (http://genome.ucsc.edu).

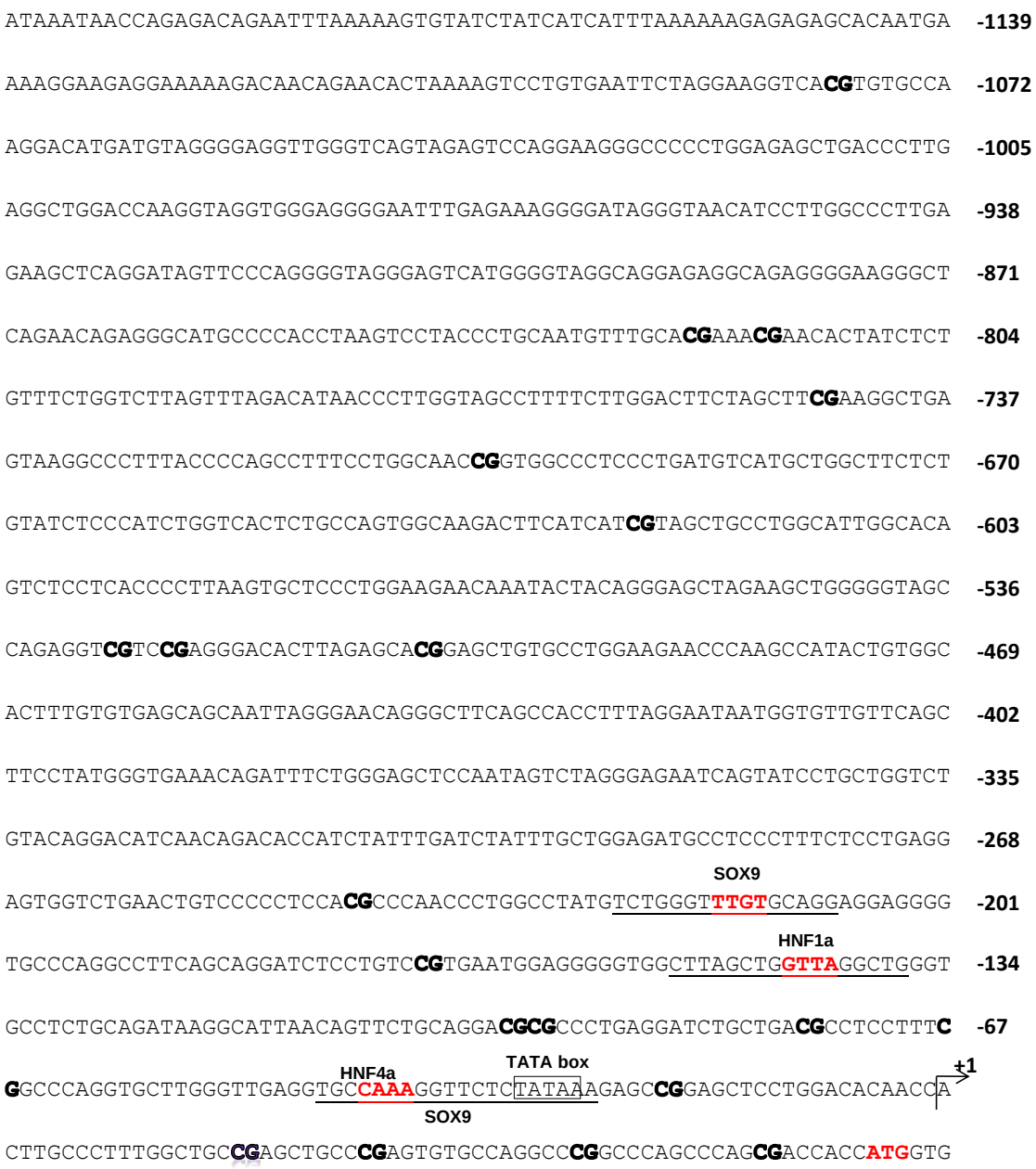

Figure 5.8. CpG dinucleotides positions in the mouse *Slc6a19* promoter

Locations of 20 CpG sites in the 1.2 kb upstream of the *Slc6a19* promoter was examined. The CpG dinucleotides (bold letters), putative TF-binding positions and TSS are indicated on the promoter.

To examine DNA methylation effects on the *Slc6a19* promoter, liver and kidney tissues were isolated from B6 mice as described in **Section 2.8.4**. Following DNA isolation, the methylation status of the target region was analysed using the bisulphite sequencing method. As shown in **Figure 5.9**, almost all CpG sites in the 5'-flanking sequence of the *Slc6a19* gene were methylated in both tissues.

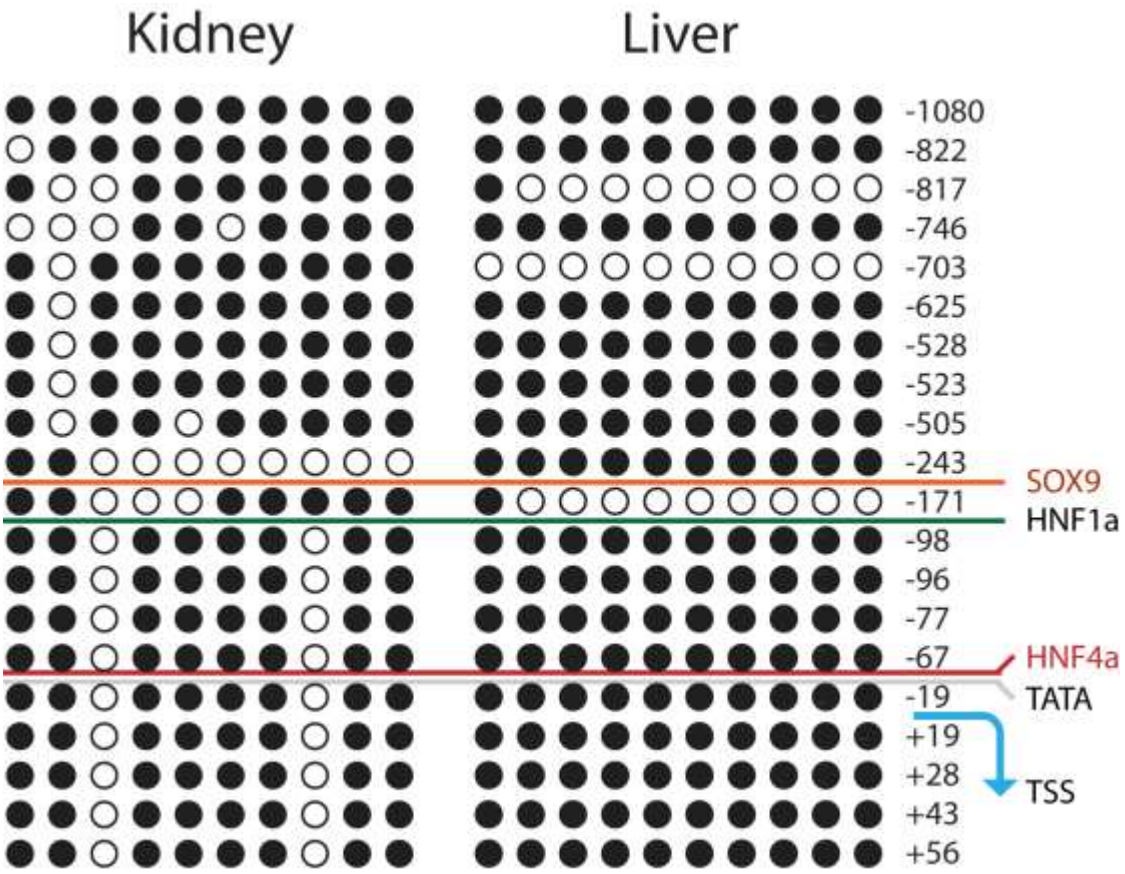

Figure 5.9 Methylation status of the *Slc6a19* promoter in the liver and kidney

Genomic material was isolated from the mouse kidney and liver. The methylation pattern of each tissue was analysed by bisulphite conversion and sequencing methods. Twenty different CpG locations (closed circle, methylated; open circle, unmethylated) and TF-binding sites (TATA, SOX9, HNF1a and HNF4a) are indicated.

To investigate the methylation status of the *Slc6a19* promoter during cell differentiation along the crypt–villus axis, the fractionation method was used. Only three of the fractions were analysed, namely F1 (villus), F4 (crypt/villus), and F5 (crypt) (**Figure 5.10**). Notably, DNA methylation around the core promoter region, spanning from +56 to –171, gradually decreased from crypt–villus cell fractions.

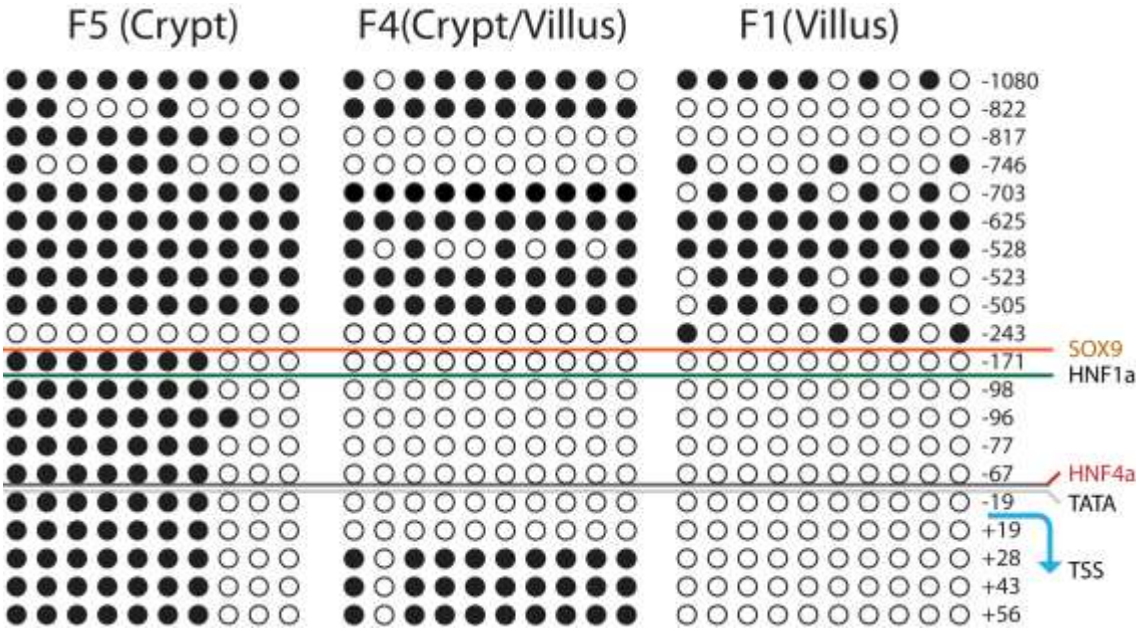

Figure 5.10 Methylation status of the *Slc6a19* promoter region in the intestine

Genomic material was isolated from three different intestinal cell fractions. The methylation pattern of each fraction was analysed by the bisulphite conversion method. CpG locations (closed circle, methylated; open circle, unmethylated) and TF-binding sites (TATA, SOX9, HNF1a and HNF4a) are indicated.

5.3 Discussion

Chromatin changes during transcription are controlled by histone modification and DNA methylation (Schubeler et al., 2004). Histone modifications are one of the major epigenetic mechanisms that alter gene expression. Generally, promoter regions of active genes have hyperacetylated histones and non-methylated CpG dinucleotides (Vaissière et al., 2008).

ChIP assays were performed to determine histone modification profiles of the *Slc6a19* promoter sequence. The results revealed that there was a significant difference in H3K27ac levels between crypt and villus. Acetylated histone H3K27 was highly enriched in the *Slc6a19* promoter in villus enterocytes. Similarly, the sucrase-isomaltase gene (SI) was shown to be regulated by histone acetylation in the crypt–villus axis (Suzuki et al., 2008). Acetylation of histone H3 (lysine 9 and 14) was found to be highly associated with active SI gene expression in the villus.

The general transcription factor TFIID can directly interact with H3K4me3 (van Ingen et al., 2008). Therefore, enrichment of H3K4me3 in a promoter region is crucial for initiating transcription. Studies in different species have showed that H3 acetylation occurs before H3K4 methylation (Rice and Allis, 2001). In contrast to this finding, our ChIP assay indicated that in crypts before histone acetylation started, H3K4me3 was highly enriched at the promoter. How histone modification affect one another is still debated (Maltby et al., 2012).

The ENCODE database results also supported expression of the *Slc6a19* gene in intestine and kidney. H3K4me3 levels were significantly higher in the intestine and kidney. Another modification H3K36me3, which is similarly found over active promoters, confirmed that the gene is actively transcribed in the intestine and kidney. However, molecular mechanisms underlying activation of genes by H3K27ac and H3K4me3 are still unclear.

In addition to histone modification, methylation of cytosine residues in genomic DNA is an important epigenetic factor that can contribute to gene silencing (Hayashi et al., 2007). Our findings indicated that DNA methylation was consistent with expression in the intestine, showing a highly methylated proximal promoter in the crypt, but complete demethylation in villus fractions. This result was contrary to a previous study (Kikuchi et al., 2010) showing differential methylation at position 1080 upstream of the TSS in intestinal cells. Our bisulphite sequencing data, by contrast, demonstrate differential methylation at the core promoter of the *Slc6a19* gene, which is <300 bp long and where binding of TFs and RNA polymerase II occurs.

Surprisingly, no significant difference was found between DNA methylation patterns in liver and kidney. The *Slc6a19* promoter was highly methylated in both tissues. One possible reason explaining the unexpected hypermethylation in the kidney is the fraction of *Slc6a19* expressed in the epithelial cells of the proximal tubules compared to other kidney cells. The methylation pattern of the *Slc6a19* core promoter region is likely to contribute to gene activation along the crypt–villus axis. The mechanism of DNA demethylation during enterocyte differentiation from crypt to villus remains to be determined. It could involve passive demethylation during cell mitosis in the crypt region or could be mediated by active demethylation.

5.4 Summary

In this chapter, I investigated whether histone modification and DNA methylation contribute to specific expression of the B^0AT1 protein in intestine and kidney. I defined histone marks and DNA methylation patterns of the *Slc6a19* promoter along the crypt–villus axis and in kidney cells. The results showed that coordination of histone acetylation–methylation activities with CpG dinucleotide methylation plays important roles in the differential expression of the gene.

Chapter 6 General discussion

The crypt–villus structure has interested many researchers because it is an ideal model for conveniently studying rapid differentiation of intestinal cells. As such, undifferentiated cells are located in the crypt which has been described as a perfect model for studying of stem cell niches (Clevers, 2013). After completing differentiation in the upper third of the crypt, cells gradually move up towards the villus tips. Explicit interplays between TFs and epigenetic regulatory mechanisms together control intestinal cells maintenance and differentiation. The *Slc6a19* is a perfect model for studying intestinal gene differentiation because it is only expressed in differentiated enterocytes in the crypt–villus axis.

6.1 Links between DNA methylation and transcription

Interactions between HNF1a and HNF4a have been well studied. The HNF1a promoter region includes conserved DNA-binding sites for HNF4a, and vice versa (Odom et al., 2004). Thus, HNF1a or HNF4a increase each other's transcription. These two TFs play important roles in the regulation of *Slc6a19* and some transporter genes. For example, HNF1a and HNF4a function as an important regulator controlling expression of many epithelial transporters (Kikuchi et al., 2010, Desvergne et al., 2006). In the kidney, HNF1a is expressed only in the proximal tubules (Pontoglio et al., 1996). This expression pattern mirrors that of the organic anion transporter 1 (OAT1) in mouse or human kidney. OAT1 is highly expressed in the renal proximal tubules. *Oat1* expression in renal proximal tubules is regulated by HNF1a and HNF4a (Maher et al., 2006). However, in extrarenal tissues, DNA methylation of the transporter promoter regions inhibits gene expression. Further, demethylated DNA in the promoter region of *Oat1* is crucial for kidney-specific expression (Kikuchi et al., 2007). Thus, HNF1a, HNF4a and DNA methylation act in concert to control organic anion transporters in a tissue-specific manner in the mouse or human kidney.

DNA methylation was long considered as a stable epigenetic mark. Inactivation of the X chromosome by DNA methylation during embryonic development was one of the first findings proving that DNA methylation was a dynamic epigenetic factor regulating gene expression (Mohandas et al., 1981). Moreover, genome-wide DNA

methylation studies have shown that DNA methylation is modified during the differentiation processes at relevant gene promoters (Ziller et al., 2013, Feldmann et al., 2013).

The DNA methylation status around the *Slc6a19* core promoter region decrease during differentiation. The methylated *Slc6a19* promoter in the crypt cells becomes fully demethylated after three to four cell divisions (Radtke and Clevers, 2005). Similarly, hormone-sensitive promoters and neuron-specific gene promoters have been found to undergo rapid demethylation (Ma et al., 2009b, Métivier et al., 2008). DNA demethylation could occur by two different mechanisms; first by lack of DNMT1 activity during mitosis, and second active demethylation by the DNA excision repair machinery (Ma et al., 2009a).We suggest that both mechanisms may be involved in the demethylation processes along the crypt–villus axis. Thus, DNMT1 is highly expressed in the crypt region while its expression decreases towards the villus. Ablation of DNMT1 in the intestine leads to expansion of crypts (Sheaffer et al., 2014). This finding indicates that DNA methylation is crucial in balancing cell proliferation and differentiation along crypt–villus axis.

Other reports have also demonstrated that many important intestinal TFs are controlled by epigenetic modifications. For example, DNA methylation analyses showed that the Lgr5 promoter was demethylated along the crypt–villus axis. Lgr5 is an intestinal stem cell marker. Lgr5 transcription is regulated by H3K4me3 modification, which are active in the crypts but repressed in the villi (Vincent et al., 2015). DNA methylation studies have also shown that complete DNA demethylation of SOX9 promoter occurs in the crypts, whereas it becomes gradually methylated in the villus cells except for goblet cells where SOX9 is highly expressed (Vincent et al., 2015). SOX9 expression has also been shown to be mainly regulated by the histone modification H3K4me2 in the cartilage tissues (Zhang et al., 2015).

CDX2 is one of the major transcription factors that controls cell differentiation in the intestine. Its expression is necessary for activation of other essential intestinal TFs such as, HNF4, HNF1a and CDX1. Epigenetic studies have revealed that CDX2 interplays between TFs and epigenetic modifications. CDX2 regulates histone modifications by triggering the formation of an active chromatin enhancer, H3K4me3 (Verzi et al., 2013). DNA Methylation status of the *Hnf1a* promoter in the liver, kidney and brain was investigated previously (Kikuchi et al., 2010). It was reported that except

in the brain, the *Hnf1a* promoter was hypomethylated in the liver and kidney where the gene was highly expressed. All these studies revealed that TFs which are essential regulators of transporter gens were also controlled by epigenetic factors.

6.2 The current model

Taken together, my studies propose a model (**Figure 6.1**) for the regulation of *Slc6a19* transcription along the crypt–villus axis. Hypermethylated CpG dinucleotides and deacetylated histone molecules cause condense chromatin state in the crypt and liver (**Figure 6.1**.**A**). DNA methylation affects expression of target genes by two mechanisms. First, methylated DNA directly interferes with TFs binding and prevents gene expression. Second, methylated cytosine residues can be recognised by methyl-CpG-binding domain (MBD) proteins which attracts chromatin remodelers to change nucleosome occupancy of TFs which in turn causes transcriptional inhibition (Salozhin et al., 2005). The inhibition mechanism of MBD proteins is not well understood. Studies showed that MBDs can interact with histone deactylases, which leads to a more condense chromatin status (Ballestar and Wolffe, 2001). Except position –243 other CpG residues were completely methylated in the core promoter region. Additionally, we located TF binding sites for HNF1a, HNF4a and SOX9 within a 250 bp region upstream of the TSS. We found eight differentially methylated CpG dinucleotides within the same region. DNA methylation at position –243 does coincide with the SOX9 binding site. This may allow direct SOX9 binding at the predicted position and lead to *Slc6a19* silencing in the crypts. Thus, SOX9-induced inhibition, hypermethylated DNA and deactylated histones around the core promoter region may lead to more condensed chromatin structures, which can inhibit the transcriptional machinery and silence the gene in the crypt and the liver.

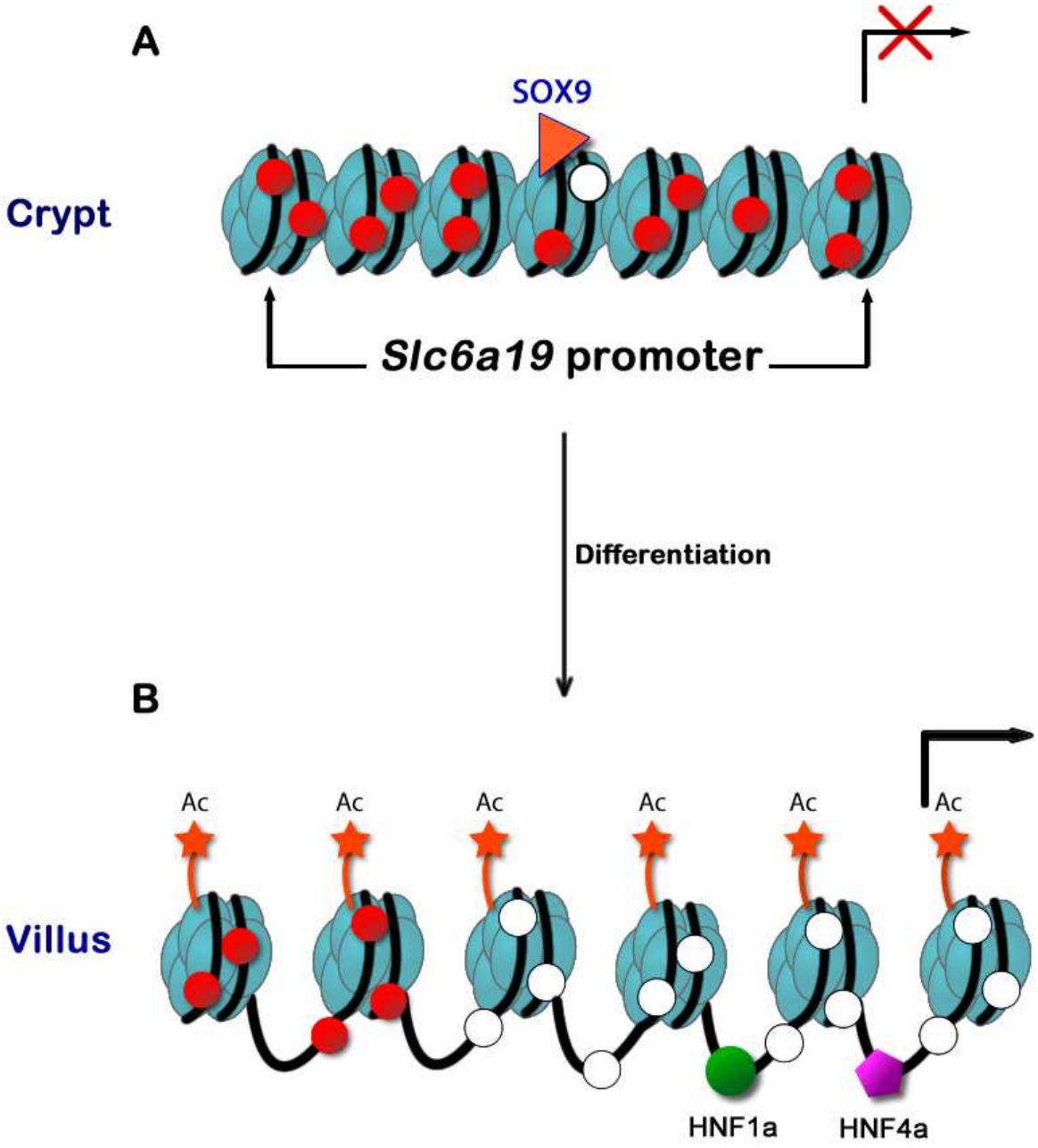

Figure 6.1 Working model for regulation of the *Slc6a19* along crypt–villus axis

The *Slc6a19* promoter region in the crypt and liver tissues showing condensed chromatin conformation (**A**), due to methylated CpG dinucleotides and deacetylated histone molecules. By contrast, demethylation of CpG dinucleotides and histone acetylation (on the *Slc6a19* promoter) allows binding of HNF1a and HNF4a TFs to activate gene expression in the villus (**B**). Differentially methylated CpG locations (red circle, methylated; white circle, unmethylated), acetylated histones and TFs (SOX9, HNF1a and HNF4a) are indicated.

During differentiation, demethylation of DNA and histone acetylation within the *Slc6a19* promoter lead open chromatin state in the villus (**Figure 6.1**.**B**). We speculated that an active DNA demethylation mechanism could involve in the *Slc6a19* activation.

Our study discovered that the marker H3K4me3 for active histones was already enriched within the hypermethylated promoter sequences. Methylation of CpG residues can change histone modifications and nucleosome distribution around the targeted promoter regions (Cedar and Bergman, 2009). Inhibitor of growth protein 1 (Ing1), which is a tumor suppressor gene and expressed in the intestine and epidermis (Pena et al., 2008), recognises and binds to H3K4me3 chromatin if this modification is enriched at methylated DNA regions. Binding of Ing1 to a methylated H3K4 recruits Gadd45a, which is a crucial player for active DNA demethylation, and triggers DNA excision repair mechanisms for DNA demethylation (Schäfer et al., 2013). Therefore, H3K4me3 histone modification may trigger active DNA demethylation during early differentiation phases. In addition to active demethylation, passive DNA demethylation may occur by lack of DNMT1 after mitosis. Furthermore, histones in the promoter receive acetylated H3K27 tails, thus increasing accessibility of the promoter region for transcriptional regulatory elements in the villus.

6.3 Limitations and future studies

There are some limitations to my study. We have conducted many fractionation experiments to use in ChIP, microarray and bisulphite sequencing assays. An alternative method could have been laser microdissection. However, instead of using laser microdissection, we had to use fractionation experiments to obtain sufficient amounts of DNA, and to keep fractionated samples consistent among different experiments. Furthermore, because of inherent limitations in the crypt–villus fractionation technique, our crypt fractions may not have included the cells from the very bottom of the crypt. Fractions may have also been contaminated with villus cells, but the crypt fractions were still highly enriched with undifferentiated cells originating from the crypt differentiation niches. The limitations of fractionation assays may have been compensated by studies using cell lines models of intestinal enterocytes. Caco-2, T84 and HT29 cells are resembling mature enterocytes and have been used as a cellular model of enterocytes for transport studies (Bolte et al., 1997). Ablating positive and negative regulating TF genes in these cell lines may help to support the TF effects.

Despite many attempts, we could not achieve a successful ChIP assay to immunoprecipitate TFs from fractionated intestinal cells likely due to insufficient binding of the antibodies used. This missing experiment would have further clarified the TFs'

roles in the crypt–villus cells' differentiation. Also, further investigations should focus on genome-wide DNA methylation and histone modification studies along the crypt–villus axis to shed light on the crosstalk between genetic and epigenetic changes during intestinal differentiation.

6.4 Summary

In my PhD project, I investigated the mechanism of *Slc6a19* transcriptional regulation by genetic and epigenetic mechanisms. The histone modification and DNA methylation status in the *Slc6a19* core promoter region might be key reasons for lack of gene transcription in the crypt and in the liver tissue. Also, this thesis proved that multiple modifications act in combination to regulate *Slc6a19* transcription dynamically along the crypt–villus axis.

In conclusion, this study contributes to our understanding of the transcriptional regulation of intestinal genes and intestinal cell differentiation. However, there is still intense debate on hierarchy of interactions between genetic and epigenetic factors driving histone modifications, regulating gene expression or repression. Although researchers have made remarkable contributions to the understanding of relationships between TFs and histone modifications, it is still unclear in which order epigenetic modifications change during intestinal cell differentiation.

Chapter 7 References

AKIYAMA, H., LYONS, J. P., MORI-AKIYAMA, Y., YANG, X., ZHANG, R., ZHANG, Z., DENG, J. M., TAKETO, M. M., NAKAMURA, T., BEHRINGER, R. R., MCCREA, P. D. & DE CROMBRUGGHE, B. 2004. Interactions between Sox9 and beta-catenin control chondrocyte differentiation. *Genes & development,* 18**,** 1072-87.

AKPINAR, P., KUWAJIMA, S., KRUTZFELDT, J. & STOFFEL, M. 2005. Tmem27: a cleaved and shed plasma membrane protein that stimulates pancreatic beta cell proliferation. *Cell metabolism,* 2**,** 385-97.

ALBERTS, B. 2004. *Essential cell biology,* New York, NY, Garland Science Pub.

ALLFREY, V. G., FAULKNER, R. & MIRSKY, A. E. 1964. Acetylation and Methylation of Histones and Their Possible Role in the Regulation of Rna Synthesis. *Proc Natl Acad Sci U S A,* 51**,** 786-94.

ANDERLE, P., SENGSTAG, T., MUTCH, D. M., RUMBO, M., PRAZ, V., MANSOURIAN, R., DELORENZI, M., WILLIAMSON, G. & ROBERTS, M. A. 2005. Changes in the transcriptional profile of transporters in the intestine along the anterior-posterior and crypt-villus axes. *BMC Genomics,* 6**,** 69.

ANDERSON, C. Z. F. Y. 2003. Wake KA Miyauchi S. Huang W. Thwaites DT Ganapathy V. Structure, function and immunolocalization of a proton-coupled amino acid transporter (hPAT1) in the human intestinal cell line Caco-2. *J Physiol,* 546**,** 349-361.

AZMANOV, D. N., KOWALCZUK, S., RODGERS, H., AURAY-BLAIS, C., GIGUERE, R., RASKO, J. E., BROER, S. & CAVANAUGH, J. A. 2008. Further evidence for allelic heterogeneity in Hartnup disorder. *Hum Mutat,* 29**,** 1217-21.

AZUARA, V., PERRY, P., SAUER, S., SPIVAKOV, M., JØRGENSEN, H. F., JOHN, R. M., GOUTI, M., CASANOVA, M., WARNES, G. & MERKENSCHLAGER, M. 2006. Chromatin signatures of pluripotent cell lines. *Nature cell biology,* 8**,** 532-538.

BALLESTAR, E. & WOLFFE, A. P. 2001. Methyl-CpG-binding proteins. *European Journal of Biochemistry,* 268**,** 1-6.

BARKER, N. & CLEVERS, H. 2007. Tracking down the stem cells of the intestine: strategies to identify adult stem cells. *Gastroenterology,* 133**,** 1755-60.

BARKER, N., VAN DE WETERING, M. & CLEVERS, H. 2008. The intestinal stem cell. *Genes Dev,* 22**,** 1856-64.

BARKER, N., VAN ES, J. H., KUIPERS, J., KUJALA, P., VAN DEN BORN, M., COZIJNSEN, M., HAEGEBARTH, A., KORVING, J., BEGTHEL, H., PETERS, P. J. & CLEVERS, H. 2007. Identification of stem cells in small intestine and colon by marker gene Lgr5. *Nature,* 449**,** 1003-7.

BARNARD, J. A., BEAUCHAMP, R. D., COFFEY, R. J. & MOSES, H. L. 1989. Regulation of intestinal epithelial cell growth by transforming growth factor type beta. *Proceedings of the National Academy of Sciences of the United States of America,* 86**,** 1578-82.

BARON, D. N., DENT, C. E., HARRIS, H., HART, E. W. & JEPSON, J. B. 1956. Hereditary pellagra-like skin rash with temporary cerebellar ataxia, constant renal amino-aciduria, and other bizarre biochemical features. *Lancet,* 271**,** 421-8.

BARRETO, G., SCHAFER, A., MARHOLD, J., STACH, D., SWAMINATHAN, S. K., HANDA, V., DODERLEIN, G., MALTRY, N., WU, W., LYKO, F. & NIEHRS, C. 2007. Gadd45a promotes epigenetic gene activation by repair-mediated DNA demethylation. *Nature,* 445**,** 671-5.

BASTIDE, P., DARIDO, C., PANNEQUIN, J., KIST, R., ROBINE, S., MARTY-DOUBLE, C., BIBEAU, F., SCHERER, G., JOUBERT, D., HOLLANDE, F., BLACHE, P. & JAY, P. 2007. Sox9 regulates cell proliferation and is required for Paneth cell differentiation in the intestinal epithelium. *The Journal of cell biology,* 178**,** 635-48.

BELL, D. M., LEUNG, K. K., WHEATLEY, S. C., NG, L. J., ZHOU, S., LING, K. W., SHAM, M. H., KOOPMAN, P., TAM, P. P. & CHEAH, K. S. 1997. SOX9 directly regulates the type-II collagen gene. *Nature genetics,* 16**,** 174-178.

BELL, O., TIWARI, V. K., THOMA, N. H. & SCHUBELER, D. 2011. Determinants and dynamics of genome accessibility. *Nat Rev Genet,* 12**,** 554-64.

BENOIT, Y. D., PARE, F., FRANCOEUR, C., JEAN, D., TREMBLAY, E., BOUDREAU, F., ESCAFFIT, F. & BEAULIEU, J. F. 2010. Cooperation between HNF-1alpha, Cdx2, and GATA-4 in initiating an enterocytic differentiation program in a normal human intestinal epithelial progenitor cell line. *Am J Physiol Gastrointest Liver Physiol,* 298**,** G504-17.

BERGER, S. L. 2002. Histone modifications in transcriptional regulation. *Current opinion in genetics & development,* 12**,** 142-8.

BERNARD, P., SIM, H., KNOWER, K., VILAIN, E. & HARLEY, V. 2008. Human SRY inhibits beta-catenin-mediated transcription. *The international journal of biochemistry & cell biology,* 40**,** 2889-900.

BESNARD, V., WERT, S. E., HULL, W. M. & WHITSETT, J. A. 2004. Immunohistochemical localization of Foxa1 and Foxa2 in mouse embryos and adult tissues. *Gene Expr Patterns,* 5**,** 193-208.

BLACHE, P., VAN DE WETERING, M., DULUC, I., DOMON, C., BERTA, P., FREUND, J. N., CLEVERS, H. & JAY, P. 2004. SOX9 is an intestine crypt transcription factor, is regulated by the Wnt pathway, and represses the CDX2 and MUC2 genes. *The Journal of cell biology,* 166**,** 37-47.

BLAU, J., XIAO, H., MCCRACKEN, S., O'HARE, P., GREENBLATT, J. & BENTLEY, D. 1996. Three functional classes of transcriptional activation domain. *Molecular and cellular biology,* 16**,** 2044-55.

BLUMENFELD, M., MAURY, M., CHOUARD, T., YANIV, M. & CONDAMINE, H. 1991. Hepatic nuclear factor 1 (HNF1) shows a wider distribution than products of its known target genes in developing mouse. *Development,* 113**,** 589-99.

BOHMER, C., BROER, A., MUNZINGER, M., KOWALCZUK, S., RASKO, J. E., LANG, F. & BROER, S. 2005. Characterization of mouse amino acid transporter B0AT1 (slc6a19). *Biochem J,* 389**,** 745-51.

BOLTE, G., BEUERMANN, K. & STERN, M. 1997. The cell lines Caco-2, T84, and Ht-29: models of enterocytic differentiation and function. *Journal of Pediatric Gastroenterology and Nutrition,* 24**,** 473.

BONZO, J. A., PATTERSON, A. D., KRAUSZ, K. W. & GONZALEZ, F. J. 2010. Metabolomics identifies novel Hnf1alpha-dependent physiological pathways in vivo. *Mol Endocrinol,* 24**,** 2343-55.

BOSSE, T., FIALKOVICH, J. J., PIASECKYJ, C. M., BEULING, E., BROEKMAN, H., GRAND, R. J., MONTGOMERY, R. K. & KRASINSKI, S. D. 2007. Gata4 and Hnf1alpha are partially required for the expression of specific intestinal genes during development. *Am J Physiol Gastrointest Liver Physiol,* 292**,** G1302-14.

BOUDREAU, F., RINGS, E. H., VAN WERING, H. M., KIM, R. K., SWAIN, G. P., KRASINSKI, S. D., MOFFETT, J., GRAND, R. J., SUH, E. R. & TRABER, P. G. 2002. Hepatocyte nuclear factor-1 alpha, GATA-4, and caudal related homeodomain protein Cdx2 interact functionally to modulate intestinal gene transcription. Implication for the developmental regulation of the sucrase-isomaltase gene. *The Journal of biological chemistry,* 277**,** 31909-17.

BOURC'HIS, D., XU, G.-L., LIN, C.-S., BOLLMAN, B. & BESTOR, T. H. 2001. Dnmt3L and the establishment of maternal genomic imprints. *Science,* 294**,** 2536-2539.

BOWLES, J., SCHEPERS, G. & KOOPMAN, P. 2000. Phylogeny of the SOX family of developmental transcription factors based on sequence and structural indicators. *Developmental biology,* 227**,** 239-55.

BRAISSANT, O., FOUFELLE, F., SCOTTO, C., DAUÇA, M. & WAHLI, W. 1996. Differential expression of peroxisome proliferator-activated receptors (PPARs): tissue distribution of PPAR-alpha,-beta, and-gamma in the adult rat. *Endocrinology,* 137**,** 354-366.

BROER, A., JUELICH, T., VANSLAMBROUCK, J. M., TIETZE, N., SOLOMON, P. S., HOLST, J., BAILEY, C. G., RASKO, J. E. & BROER, S. 2011. Impaired Nutrient Signaling and Body Weight Control in a Na+ Neutral Amino Acid Cotransporter (Slc6a19)-deficient Mouse. *The Journal of biological chemistry,* 286**,** 26638-51.

BRÖER, A., KLINGEL, K., KOWALCZUK, S., RASKO, J. E., CAVANAUGH, J. & BROER, S. 2004. Molecular cloning of mouse amino acid transport system B0, a neutral amino acid transporter related to Hartnup disorder. *The Journal of biological chemistry,* 279**,** 24467-76.

BROER, S. 2006. The SLC6 orphans are forming a family of amino acid transporters. *Neurochem Int,* 48**,** 559-67.

BROER, S. 2008. Apical transporters for neutral amino acids: physiology and pathophysiology. *Physiology (Bethesda),* 23**,** 95-103.

BROER, S. 2009. The role of the neutral amino acid transporter B0AT1 (SLC6A19) in Hartnup disorder and protein nutrition. *IUBMB Life,* 61**,** 591-9.

BROER, S. & PALACIN, M. 2011. The role of amino acid transporters in inherited and acquired diseases. *The Biochemical journal,* 436**,** 193-211.

BURRELL, L. M., JOHNSTON, C. I., TIKELLIS, C. & COOPER, M. E. 2004. ACE2, a new regulator of the renin-angiotensin system. *Trends in endocrinology and metabolism: TEM,* 15**,** 166-9.

CADIGAN, K. M. & NUSSE, R. 1997. Wnt signaling: a common theme in animal development. *Genes & development,* 11**,** 3286-305.

CAMARGO, S. M., SINGER, D., MAKRIDES, V., HUGGEL, K., POS, K. M., WAGNER, C. A., KUBA, K., DANILCZYK, U., SKOVBY, F., KLETA, R., PENNINGER, J. M. & VERREY, F. 2009. Tissue-specific amino acid transporter partners ACE2 and collectrin differentially interact with hartnup mutations. *Gastroenterology,* 136**,** 872-82.

CEDAR, H. & BERGMAN, Y. 2009. Linking DNA methylation and histone modification: patterns and paradigms. *Nature Reviews Genetics,* 10**,** 295-304.

CEREGHINI, S., RAYMONDJEAN, M., CARRANCA, A. G., HERBOMEL, P. & YANIV, M. 1987. Factors involved in control of tissue-specific expression of albumin gene. *Cell,* 50**,** 627-38.

CHAMPE, P. C., HARVEY, R. A. & FERRIER, D. R. 2005. *Biochemistry,* Lippincott Williams & Wilkins.

CHEN, T., UEDA, Y., DODGE, J. E., WANG, Z. & LI, E. 2003. Establishment and maintenance of genomic methylation patterns in mouse embryonic stem cells by Dnmt3a and Dnmt3b. *Molecular and cellular biology,* 23**,** 5594-5605.

CHEUNG, M. & BRISCOE, J. 2003. Neural crest development is regulated by the transcription factor Sox9. *Development,* 130**,** 5681-93.

CHI, Y.-I., FRANTZ, J. D., OH, B.-C., HANSEN, L., DHE-PAGANON, S. & SHOELSON, S. E. 2002. Diabetes mutations delineate an atypical POU domain in HNF-1α. *Molecular cell,* 10**,** 1129-1137.

CHILLARÓN, J., ROCA, R., VALENCIA, A., ZORZANO, A. & PALACÍN, M. 2001. Heteromeric amino acid transporters: biochemistry, genetics, and physiology. *American Journal of Physiology-Renal Physiology,* 281**,** F995-F1018.

CHOUARD, T., BLUMENFELD, M., BACH, I., VANDEKERCKHOVE, J., CEREGHINI, S. & YANIV, M. 1990. A distal dimerization domain is essential for DNA-binding by the atypical HNF1 homeodomain. *Nucleic acids research,* 18**,** 5853-5863.

CLATWORTHY, J. P. & SUBRAMANIAN, V. 2001. Stem cells and the regulation of proliferation, differentiation and patterning in the intestinal epithelium: emerging insights from gene expression patterns, transgenic and gene ablation studies. *Mechanisms of development,* 101**,** 3-9.

CLEVERS, H. 2006. Wnt/beta-catenin signaling in development and disease. *Cell,* 127**,** 469-80.

CLEVERS, H. 2013. The intestinal crypt, a prototype stem cell compartment. *Cell,* 154**,** 274-284.

COSENTINO, L., SHAVER-WALKER, P. & HEDDLE, J. A. 1996. The relationships among stem cells, crypts, and villi in the small intestine of mice as determined by mutation tagging. *Developmental dynamics,* 207**,** 420-428.

COSKUN, M., BOYD, M., OLSEN, J. & TROELSEN, J. T. 2010. Control of intestinal promoter activity of the cellular migratory regulator gene ELMO3 by CDX2 and SP1. *Journal of cellular biochemistry,* 109**,** 1118-28.

COSTA, R. H., KALINICHENKO, V. V., HOLTERMAN, A. X. L. & WANG, X. 2003. Transcription factors in liver development, differentiation, and regeneration. *Hepatology,* 38**,** 1331-1347.

CRACKOWER, M. A., SARAO, R., OUDIT, G. Y., YAGIL, C., KOZIERADZKI, I., SCANGA, S. E., OLIVEIRA-DOS-SANTOS, A. J., DA COSTA, J., ZHANG, L., PEI, Y., SCHOLEY, J., FERRARIO, C. M., MANOUKIAN, A. S., CHAPPELL, M. C., BACKX, P. H., YAGIL, Y. & PENNINGER, J. M. 2002. Angiotensin-converting enzyme 2 is an essential regulator of heart function. *Nature,* 417**,** 822-8.

CROSNIER, C., STAMATAKI, D. & LEWIS, J. 2006. Organizing cell renewal in the intestine: stem cells, signals and combinatorial control. *Nature Reviews Genetics,* 7**,** 349-359.

D'ANGELO, A., BLUTEAU, O., GARCIA-GONZALEZ, M. A., GRESH, L., DOYEN, A., GARBAY, S., ROBINE, S. & PONTOGLIO, M. 2010. Hepatocyte nuclear factor 1alpha and beta control terminal differentiation and cell fate commitment in the gut epithelium. *Development,* 137**,** 1573-82.

DANILCZYK, U., SARAO, R., REMY, C., BENABBAS, C., STANGE, G., RICHTER, A., ARYA, S., POSPISILIK, J. A., SINGER, D., CAMARGO, S. M., MAKRIDES, V., RAMADAN, T., VERREY, F., WAGNER, C. A. & PENNINGER, J. M. 2006. Essential role for collectrin in renal amino acid transport. *Nature,* 444**,** 1088-91.

DE LA CRUZ, X., LOIS, S., SANCHEZ-MOLINA, S. & MARTINEZ-BALBAS, M. A. 2005. Do protein motifs read the histone code? *BioEssays : news and reviews in molecular, cellular and developmental biology,* 27**,** 164-75.

DESVERGNE, B., MICHALIK, L. & WAHLI, W. 2006. Transcriptional regulation of metabolism. *Physiological reviews,* 86**,** 465-514.

DONG, C., WILHELM, D. & KOOPMAN, P. 2004. Sox genes and cancer. *Cytogenetic and genome research,* 105**,** 442-7.

DRAGO, S., EL ASMAR, R., DI PIERRO, M., GRAZIA CLEMENTE, M., SAPONE, A. T. A., THAKAR, M., IACONO, G., CARROCCIO, A., D'AGATE, C. & NOT, T. 2006. Gliadin, zonulin and gut permeability: Effects on celiac and non-celiac intestinal mucosa and intestinal cell lines. *Scandinavian journal of gastroenterology,* 41**,** 408-419.

DUNCAN, S. A., MANOVA, K., CHEN, W. S., HOODLESS, P., WEINSTEIN, D. C., BACHVAROVA, R. F. & DARNELL, J. E., JR. 1994. Expression of transcription factor HNF-4 in the extraembryonic endoderm, gut, and nephrogenic tissue of the developing mouse embryo: HNF-4 is a marker for primary endoderm in the implanting blastocyst. *Proceedings of the National Academy of Sciences of the United States of America,* 91**,** 7598-602.

EECKHOUTE, J., FORMSTECHER, P. & LAINE, B. 2004. Hepatocyte nuclear factor 4alpha enhances the hepatocyte nuclear factor 1alpha-mediated activation of transcription. *Nucleic acids research,* 32**,** 2586-93.

ELLARD, S. & COLCLOUGH, K. 2006. Mutations in the genes encoding the transcription factors hepatocyte nuclear factor 1 alpha (HNF1A) and 4 alpha (HNF4A) in maturity-onset diabetes of the young. *Hum Mutat,* 27**,** 854-69.

ERICKSON, R. H. & KIM, Y. S. 1990. Digestion and absorption of dietary protein. *Annual review of medicine,* 41**,** 133-139.

ESCAFFIT, F., PARÉ, F., GAUTHIER, R., RIVARD, N., BOUDREAU, F. & BEAULIEU, J.-F. 2006. Cdx2 modulates proliferation in normal human intestinal epithelial crypt cells. *Biochemical and biophysical research communications,* 342**,** 66-72.

FAIRWEATHER, S. J., BRÖER, A., SUBRAMANIAN, N., TUMER, E., CHENG, Q., SCHMOLL, D., O'MARA, M. L. & BRÖER, S. 2015. Molecular basis for the interaction of the mammalian amino acid transporters B0AT1 and B0AT3 with their ancillary protein collectrin. *Journal of Biological Chemistry,* 290**,** 24308-24325.

FAJANS, S. S., BELL, G. I. & POLONSKY, K. S. 2001. Molecular mechanisms and clinical pathophysiology of maturity-onset diabetes of the young. *New England Journal of Medicine,* 345**,** 971-980.

FELDMANN, A., IVANEK, R., MURR, R., GAIDATZIS, D., BURGER, L. & SCHÜBELER, D. 2013. Transcription factor occupancy can mediate active turnover of DNA methylation at regulatory regions.

FELIUBADALÓ, L., FONT, M., PURROY, J., ROUSAUD, F., ESTIVILL, X., NUNES, V., GOLOMB, E., CENTOLA, M., AKSENTIJEVICH, I. & KREISS, Y. 1999. Non-type I cystinuria caused by mutations in SLC7A9, encoding a subunit (bo,+ AT) of rBAT. *Nature genetics,* 23**,** 52-57.

FERGUSON, A. 1977. Intraepithelial lymphocytes of the small intestine. *Gut,* 18**,** 921-937.

FISCHLE, W., WANG, Y. & ALLIS, C. D. 2003. Histone and chromatin cross-talk. *Current Opinion in Cell Biology,* 15**,** 172-183.

FURUYAMA, K., KAWAGUCHI, Y., AKIYAMA, H., HORIGUCHI, M., KODAMA, S., KUHARA, T., HOSOKAWA, S., ELBAHRAWY, A., SOEDA, T., KOIZUMI, M., MASUI, T., KAWAGUCHI, M., TAKAORI, K., DOI, R., NISHI, E., KAKINOKI, R., DENG, J. M., BEHRINGER, R. R., NAKAMURA, T. & UEMOTO, S. 2011. Continuous cell supply from a Sox9-expressing progenitor zone in adult liver, exocrine pancreas and intestine. *Nature genetics,* 43**,** 34-41.

GAO, N., WHITE, P. & KAESTNER, K. H. 2009. Establishment of intestinal identity and epithelial-mesenchymal signaling by Cdx2. *Dev Cell,* 16**,** 588-99.

GARRISON, W. D., BATTLE, M. A., YANG, C., KAESTNER, K. H., SLADEK, F. M. & DUNCAN, S. A. 2006. Hepatocyte nuclear factor 4alpha is essential for embryonic development of the mouse colon. *Gastroenterology,* 130**,** 1207-20.

GEORGE, M. D., WEHKAMP, J., KAYS, R. J., LEUTENEGGER, C. M., SABIR, S., GRISHINA, I., DANDEKAR, S. & BEVINS, C. L. 2008. In vivo gene expression profiling of human intestinal epithelial cells: analysis by laser microdissection of formalin fixed tissues. *BMC Genomics,* 9**,** 209.

GERBE, F., VAN ES, J. H., MAKRINI, L., BRULIN, B., MELLITZER, G., ROBINE, S., ROMAGNOLO, B., SHROYER, N. F., BOURGAUX, J. F., PIGNODEL, C., CLEVERS, H. & JAY, P. 2011. Distinct ATOH1 and Neurog3 requirements define tuft cells as a new secretory cell type in the intestinal epithelium. *J Cell Biol,* 192**,** 767-80.

GREGORIEFF, A., STANGE, D. E., KUJALA, P., BEGTHEL, H., VAN DEN BORN, M., KORVING, J., PETERS, P. J. & CLEVERS, H. 2009. The ets-domain transcription factor Spdef promotes maturation of goblet and paneth cells in the intestinal epithelium. *Gastroenterology,* 137**,** 1333-45 e1-3.

HAMILTON, A. J., BINGHAM, C., MCDONALD, T. J., COOK, P. R., CASWELL, R. C., WEEDON, M. N., ORAM, R. A., SHIELDS, B. M., SHEPHERD, M. & INWARD, C. D. 2013. The HNF4A R76W mutation causes atypical dominant Fanconi syndrome in addition to a β cell phenotype. *Journal of medical genetics***,** jmedgenet-2013-102066.

HARLEY, V. R., LOVELL-BADGE, R. & GOODFELLOW, P. N. 1994. Definition of a consensus DNA binding site for SRY. *Nucleic Acids Res,* 22**,** 1500-1.

HAYASHI, H., NAGAE, G., TSUTSUMI, S., KANESHIRO, K., KOZAKI, T., KANEDA, A., SUGISAKI, H. & ABURATANI, H. 2007. High-resolution mapping of DNA methylation in human genome using oligonucleotide tiling array. *Human genetics,* 120**,** 701-711.

HEATH, J. K. 2010. Transcriptional networks and signaling pathways that govern vertebrate intestinal development. *Curr Top Dev Biol,* 90**,** 159-92.

HEINTZMAN, N. D., HON, G. C., HAWKINS, R. D., KHERADPOUR, P., STARK, A., HARP, L. F., YE, Z., LEE, L. K., STUART, R. K. & CHING, C. W. 2009. Histone modifications at human enhancers reflect global cell-type-specific gene expression. *Nature,* 459**,** 108-112.

HEINTZMAN, N. D., STUART, R. K., HON, G., FU, Y., CHING, C. W., HAWKINS, R. D., BARRERA, L. O., VAN CALCAR, S., QU, C. & CHING, K. A. 2007. Distinct and predictive chromatin signatures of transcriptional promoters and enhancers in the human genome. *Nature genetics,* 39**,** 311-318.

HOLLIDAY, R. 1996. DNA methylation in eukaryotes: 20 years on. *Cold Spring Harbor Monograph Archive,* 32**,** 5-27.

HU, C. & PERLMUTTER, D. H. 1999. Regulation of α1-antitrypsin gene expression in human intestinal epithelial cell line Caco-2 by HNF-1α and HNF-4. *American Journal of Physiology-Gastrointestinal and Liver Physiology,* 276**,** G1181-G1194.

HUET, C., SAHUQUILLO-MERINO, C., COUDRIER, E. & LOUVARD, D. 1987. Absorptive and mucus-secreting subclones isolated from a multipotent intestinal cell line (HT-29) provide new models for cell polarity and terminal differentiation. *The Journal of cell biology,* 105**,** 345-357.

KANAI, Y. & HEDIGER, M. A. 2003. The glutamate and neutral amino acid transporter family: physiological and pharmacological implications. *European journal of pharmacology,* 479**,** 237-247.

KANAI, Y. & KOOPMAN, P. 1999. Structural and functional characterization of the mouse Sox9 promoter: implications for campomelic dysplasia. *Human molecular genetics,* 8**,** 691-6.

KANEHISA, M. & GOTO, S. 2000. KEGG: kyoto encyclopedia of genes and genomes. *Nucleic acids research,* 28**,** 27-30.

KIEFER, J. C. 2007. Back to basics: Sox genes. *Developmental dynamics : an official publication of the American Association of Anatomists,* 236**,** 2356-66.

KIKUCHI, R., KUSUHARA, H., HATTORI, N., KIM, I., SHIOTA, K., GONZALEZ, F. J. & SUGIYAMA, Y. 2007. Regulation of tissue-specific expression of the human and mouse urate transporter 1 gene by hepatocyte nuclear factor 1 α/β and DNA methylation. *Molecular pharmacology,* 72**,** 1619-1625.

KIKUCHI, R., YAGI, S., KUSUHARA, H., IMAI, S., SUGIYAMA, Y. & SHIOTA, K. 2010. Genome-wide analysis of epigenetic signatures for kidney-specific transporters. *Kidney Int,* 78**,** 569-77.

KISHIMOTO, T. 1993. Signal transduction through homo-or heterodimers of gp130. *Stem cells (Dayton, Ohio),* 12**,** 37-44; discussion 44-5.

KLETA, R., ROMEO, E., RISTIC, Z., OHURA, T., STUART, C., ARCOS-BURGOS, M., DAVE, M. H., WAGNER, C. A., CAMARGO, S. R., INOUE, S., MATSUURA, N., HELIP-WOOLEY, A., BOCKENHAUER, D., WARTH, R., BERNARDINI, I., VISSER, G., EGGERMANN, T., LEE, P., CHAIROUNGDUA, A., JUTABHA, P., BABU, E., NILWARANGKOON, S., ANZAI, N., KANAI, Y., VERREY, F., GAHL, W. A. & KOIZUMI, A. 2004. Mutations in SLC6A19, encoding B0AT1, cause Hartnup disorder. *Nat Genet,* 36**,** 999-1002.

KLOSE, R. J. & BIRD, A. P. 2006. Genomic DNA methylation: the mark and its mediators. *Trends in biochemical sciences,* 31**,** 89-97.

KORINEK, V., BARKER, N., MOERER, P., VAN DONSELAAR, E., HULS, G., PETERS, P. J. & CLEVERS, H. 1998. Depletion of epithelial stem-cell compartments in the small intestine of mice lacking Tcf-4. *Nature genetics,* 19**,** 379-83.

KORMISH, J. D., SINNER, D. & ZORN, A. M. 2010. Interactions between SOX factors and Wnt/beta-catenin signaling in development and disease. *Developmental dynamics : an official publication of the American Association of Anatomists,* 239**,** 56-68.

KORNBERG, R. D. & LORCH, Y. 1999. Twenty-five years of the nucleosome, fundamental particle of the eukaryote chromosome. *Cell,* 98**,** 285-294.

KOUZARIDES, T. 2007. Chromatin modifications and their function. *Cell,* 128**,** 693-705.

KOWALCZUK, S., BRÖER, A., MUNZINGER, M., TIETZE, N., KLINGEL, K. & BRÖER, S. 2005. Molecular cloning of the mouse IMINO system: an Na+-and Cl−-dependent proline transporter. *Biochemical Journal,* 386**,** 417-422.

KOWALCZUK, S., BROER, A., TIETZE, N., VANSLAMBROUCK, J. M., RASKO, J. E. & BROER, S. 2008. A protein complex in the brush-border membrane explains a Hartnup disorder allele. *FASEB J,* 22**,** 2880-7.

LATCHMAN, D. S. 2008. *Eukaryotic transcription factors,* Amsterdam ; Boston, Elsevier/Academic Press.

LEE, Y. H., SAUER, B. & GONZALEZ, F. J. 1998. Laron dwarfism and non-insulin-dependent diabetes mellitus in the Hnf-1alpha knockout mouse. *Molecular and cellular biology,* 18**,** 3059-68.

LEWIN, B. 2004. *Genes VIII,* Upper Saddle River, NJ, Pearson Prentice Hall.

LEWIS, J. 2007. *Molecular biology of the cell,* New York

London, Garland Science ;

Taylor & Francis [distributor].

LODISH, H. F. 2003. *Molecular cell biology,* New York, W.H. Freeman and Company.

LOGAN, C. Y. & NUSSE, R. 2004. The Wnt signaling pathway in development and disease. *Annual review of cell and developmental biology,* 20**,** 781-810.

LORENTZ, O., DULUC, I., DE ARCANGELIS, A., SIMON-ASSMANN, P., KEDINGER, M. & FREUND, J.-N. 1997. Key role of the Cdx2 homeobox gene in extracellular matrix–mediated intestinal cell differentiation. *The Journal of cell biology,* 139**,** 1553-1565.

LUSSIER, C. R., BRIAL, F., ROY, S. A., LANGLOIS, M. J., VERDU, E. F., RIVARD, N., PERREAULT, N. & BOUDREAU, F. 2010. Loss of hepatocyte-nuclear-factor-1alpha impacts on adult mouse intestinal epithelial cell growth and cell lineages differentiation. *PLoS One,* 5**,** e12378.

MA, D. K., GUO, J. U., MING, G.-L. & SONG, H. 2009a. DNA excision repair proteins and Gadd45 as molecular players for active DNA demethylation. *Cell Cycle,* 8**,** 1526-1531.

MA, D. K., JANG, M.-H., GUO, J. U., KITABATAKE, Y., CHANG, M.-L., POW-ANPONGKUL, N., FLAVELL, R. A., LU, B., MING, G.-L. & SONG, H. 2009b. Neuronal activity–induced Gadd45b promotes epigenetic DNA demethylation and adult neurogenesis. *Science,* 323**,** 1074-1077.

MAENZ, D. D. & PATIENCE, J. F. 1992. L-threonine transport in pig jejunal brush border membrane vesicles. Functional characterization of the unique system B in the intestinal epithelium. *The Journal of biological chemistry,* 267**,** 22079-86.

MAHER, J. M., SLITT, A. L., CALLAGHAN, T. N., CHENG, X., CHEUNG, C., GONZALEZ, F. J. & KLAASSEN, C. D. 2006. Alterations in transporter expression in liver, kidney, and duodenum after targeted disruption of the transcription factor HNF1alpha. *Biochemical pharmacology,* 72**,** 512-22.

MALAKAUSKAS, S. M., QUAN, H., FIELDS, T. A., MCCALL, S. J., YU, M. J., KOURANY, W. M., FREY, C. W. & LE, T. H. 2007. Aminoaciduria and altered renal expression of luminal amino acid transporters in mice lacking novel gene collectrin. *Am J Physiol Renal Physiol,* 292**,** F533-44.

MALIK, S. & KARATHANASIS, S. K. 1996. TFIIB-directed transcriptional activation by the orphan nuclear receptor hepatocyte nuclear factor 4. *Molecular and cellular biology,* 16**,** 1824-31.

MALTBY, V. E., MARTIN, B. J., BRIND'AMOUR, J., CHRUSCICKI, A. T., MCBURNEY, K. L., SCHULZE, J. M., JOHNSON, I. J., HILLS, M., HENTRICH, T. & KOBOR, M. S. 2012. Histone H3K4 demethylation is negatively regulated by histone H3 acetylation in Saccharomyces cerevisiae. *Proceedings of the National Academy of Sciences,* 109**,** 18505-18510.

MARIADASON, J. M., NICHOLAS, C., L'ITALIEN, K. E., ZHUANG, M., SMARTT, H. J. M., HEERDT, B. G., YANG, W., CORNER, G. A., WILSON, A. J., KLAMPFER, L., ARANGO, D. & AUGENLICHT, L. H. 2005. Gene expression profiling of intestinal epithelial cell maturation along the crypt-villus axis. *Gastroenterology,* 128**,** 1081-1088.

MCDOWALL, S., ARGENTARO, A., RANGANATHAN, S., WELLER, P., MERTIN, S., MANSOUR, S., TOLMIE, J. & HARLEY, V. 1999. Functional and structural studies of wild type SOX9 and mutations causing campomelic dysplasia. *The Journal of biological chemistry,* 274**,** 24023-30.

MÉTIVIER, R., GALLAIS, R., TIFFOCHE, C., LE PÉRON, C., JURKOWSKA, R. Z., CARMOUCHE, R. P., IBBERSON, D., BARATH, P., DEMAY, F. & REID, G. 2008. Cyclical DNA methylation of a transcriptionally active promoter. *Nature,* 452**,** 45-50.

MITCHELMORE, C., TROELSEN, J. T., SPODSBERG, N., SJOSTROM, H. & NOREN, O. 2000. Interaction between the homeodomain proteins Cdx2 and HNF1alpha mediates expression of the lactase-phlorizin hydrolase gene. *The Biochemical journal,* 346 Pt 2**,** 529-35.

MOHANDAS, T., SPARKES, R. & SHAPIRO, L. 1981. Reactivation of an inactive human X chromosome: evidence for X inactivation by DNA methylation. *Science,* 211**,** 393-396.

MOOSEKER, M. S. 1985. Organization, chemistry, and assembly of the cytoskeletal apparatus of the intestinal brush border. *Annual review of cell biology,* 1**,** 209-241.

MORAIS DA SILVA, S., HACKER, A., HARLEY, V., GOODFELLOW, P., SWAIN, A. & LOVELL-BADGE, R. 1996. Sox9 expression during gonadal development implies a conserved role for the gene in testis differentiation in mammals and birds. *Nature genetics,* 14**,** 62-8.

MORI-AKIYAMA, Y., VAN DEN BORN, M., VAN ES, J. H., HAMILTON, S. R., ADAMS, H. P., ZHANG, J., CLEVERS, H. & DE CROMBRUGGHE, B. 2007. SOX9 is required for the differentiation of paneth cells in the intestinal epithelium. *Gastroenterology,* 133**,** 539-46.

MORIN, P. J., SPARKS, A. B., KORINEK, V., BARKER, N., CLEVERS, H., VOGELSTEIN, B. & KINZLER, K. W. 1997. Activation of beta-catenin-Tcf signaling in colon cancer by mutations in beta-catenin or APC. *Science,* 275**,** 1787-90.

MUNCK, B. G. 1980. Lysine transport across the small intestine. Stimulating and inhibitory effects of neutral amino acids. *The Journal of membrane biology,* 53**,** 45-53.

NAN, X., NG, H.-H., JOHNSON, C. A., LAHERTY, C. D., TURNER, B. M., EISENMAN, R. N. & BIRD, A. 1998. Transcriptional repression by the methyl-CpG-binding protein MeCP2 involves a histone deacetylase complex. *Nature,* 393**,** 386-389.

NOAH, T. K., KAZANJIAN, A., WHITSETT, J. & SHROYER, N. F. 2010. SAM pointed domain ETS factor (SPDEF) regulates terminal differentiation and maturation of intestinal goblet cells. *Exp Cell Res,* 316**,** 452-65.

NOZAKI, J., DAKEISHI, M., OHURA, T., INOUE, K., MANABE, M., WADA, Y. & KOIZUMI, A. 2001. Homozygosity mapping to chromosome 5p15 of a gene responsible for Hartnup disorder. *Biochemical and biophysical research communications,* 284**,** 255-60.

NUMAKURA, C., HASHIMOTO, Y., DAITSU, T., HAYASAKA, K., MITSUI, T. & YORIFUJI, T. 2015. Two patients with HNF4A-related congenital hyperinsulinism and renal tubular dysfunction: A clinical variation which includes transient hepatic dysfunction. *Diabetes research and clinical practice*.

NUSSBAUM, R., MCINNES, R. R. & WILLARD, H. F. 2007. *Thompson & Thompson genetics in medicine*, Elsevier Health Sciences.

ODOM, D. T., ZIZLSPERGER, N., GORDON, D. B., BELL, G. W., RINALDI, N. J., MURRAY, H. L., VOLKERT, T. L., SCHREIBER, J., ROLFE, P. A., GIFFORD, D. K., FRAENKEL, E., BELL, G. I. & YOUNG, R. A. 2004. Control of pancreas and liver gene expression by HNF transcription factors. *Science,* 303**,** 1378-81.

OHBA, S., HE, X., HOJO, H. & MCMAHON, A. P. 2015. Distinct Transcriptional Programs Underlie Sox9 Regulation of the Mammalian Chondrocyte. *Cell reports,* 12**,** 229-243.

OKANO, M., BELL, D. W., HABER, D. A. & LI, E. 1999. DNA methyltransferases Dnmt3a and Dnmt3b are essential for de novo methylation and mammalian development. *Cell,* 99**,** 247-257.

OLSEN, L., HANSEN, M., EKSTRØM, C. T., TROELSEN, J. T. & OLSEN, J. 2004. CVD: the intestinal crypt/villus in situ hybridization database. *Bioinformatics,* 20**,** 1327-1328.

OXENDER, D. L. & CHRISTENSEN, H. N. 1963. Distinct Mediating Systems for the Transport of Neutral Amino Acids by the Ehrlich Cell. *The Journal of biological chemistry,* 238**,** 3686-99.

OZEKI, T., TAKAHASHI, Y., KUME, T., NAKAYAMA, K., YOKOI, T., NUNOYA, K., HARA, A. & KAMATAKI, T. 2001. Co-operative regulation of the transcription of human dihydrodiol dehydrogenase (DD) 4/aldo–keto reductase (AKR) 1C4 gene by hepatocyte nuclear factor (HNF)-4α/γ and HNF-1α. *Biochem. J,* 355**,** 537-544.

PENA, P., HOM, R., HUNG, T., LIN, H., KUO, A., WONG, R., SUBACH, O., CHAMPAGNE, K., ZHAO, R. & VERKHUSHA, V. 2008. Histone H3K4me3 binding is required for the DNA repair and apoptotic activities of ING1 tumor suppressor. *Journal of molecular biology,* 380**,** 303-312.

PONTOGLIO, M., BARRA, J., HADCHOUEL, M., DOYEN, A., KRESS, C., BACH, J. P., BABINET, C. & YANIV, M. 1996. Hepatocyte nuclear factor 1 inactivation results in hepatic dysfunction, phenylketonuria, and renal Fanconi syndrome. *Cell,* 84**,** 575-85.

PORTELA, A. & ESTELLER, M. 2010. Epigenetic modifications and human disease. *Nature biotechnology,* 28**,** 1057-1068.

QUANDT, K., FRECH, K., KARAS, H., WINGENDER, E. & WERNER, T. 1995. Matlnd and Matlnspector: new fast and versatile tools for detection of consensus matches in nucleotide sequence data. *Nucleic acids research,* 23**,** 4878-4884.

QUARONI, A. & BEAULIEU, J. F. 1997. Cell dynamics and differentiation of conditionally immortalized human intestinal epithelial cells. *Gastroenterology,* 113**,** 1198-1213.

QUARONI, A. & MAY, R. J. 1979. Establishment and characterizaton of intestinal epithelial cell cultures. *Methods in cell biology,* 21**,** 403-427.

RADTKE, F. & CLEVERS, H. 2005. Self-renewal and cancer of the gut: two sides of a coin. *Science,* 307**,** 1904-1909.

RAZIN, A. & RIGGS, A. D. 1980. DNA methylation and gene function. *Science,* 210**,** 604-610.

RICE, J. C. & ALLIS, C. D. 2001. Histone methylation versus histone acetylation: new insights into epigenetic regulation. *Current opinion in cell biology,* 13**,** 263-273.

RICHARDS, E. J. & ELGIN, S. C. 2002. Epigenetic codes for heterochromatin formation and silencing: rounding up the usual suspects. *Cell,* 108**,** 489-500.

RICHARDSON, B. & YUNG, R. 1999. Role of DNA methylation in the regulation of cell function. *Journal of Laboratory and Clinical Medicine,* 134**,** 333-340.

ROBERTSON, K. D. 2002. DNA methylation and chromatin-unraveling the tangled web. *Oncogene,* 21**,** 5361-5379.

ROMEO, E., DAVE, M. H., BACIC, D., RISTIC, Z., CAMARGO, S. M., LOFFING, J., WAGNER, C. A. & VERREY, F. 2006. Luminal kidney and intestine SLC6 amino acid transporters of B0AT-cluster and their tissue distribution in Mus musculus. *Am J Physiol Renal Physiol,* 290**,** F376-83.

ROSENBLOOM, K. R., DRESZER, T. R., PHEASANT, M., BARBER, G. P., MEYER, L. R., POHL, A., RANEY, B. J., WANG, T., HINRICHS, A. S. & ZWEIG, A. S. 2010. ENCODE whole-genome data in the UCSC Genome Browser. *Nucleic acids research,* 38**,** D620-D625.

RUSSELL, P. J. 2002. *iGenetics,* San Francisco, Benjamin Cummings.

RYFFEL, G. U. 2001. Mutations in the human genes encoding the transcription factors of the hepatocyte nuclear factor (HNF)1 and HNF4 families: functional and pathological consequences. *Journal of molecular endocrinology,* 27**,** 11-29.

SALOZHIN, S., PROKHORCHUK, E. & GEORGIEV, G. 2005. Methylation of DNA—one of the major epigenetic markers. *Biochemistry (Moscow),* 70**,** 525-532.

SANCHO, E., BATLLE, E. & CLEVERS, H. 2004. Signaling pathways in intestinal development and cancer. *Annual review of cell and developmental biology,* 20**,** 695-723.

SANSOM, O. J., REED, K. R., HAYES, A. J., IRELAND, H., BRINKMANN, H., NEWTON, I. P., BATLLE, E., SIMON-ASSMANN, P., CLEVERS, H., NATHKE, I. S., CLARKE, A. R. & WINTON, D. J. 2004. Loss of Apc in vivo immediately perturbs Wnt signaling, differentiation, and migration. *Genes & Development,* 18**,** 1385-90.

SANTOS-ROSA, H., SCHNEIDER, R., BANNISTER, A. J., SHERRIFF, J., BERNSTEIN, B. E., EMRE, N. T., SCHREIBER, S. L., MELLOR, J. & KOUZARIDES, T. 2002. Active genes are tri-methylated at K4 of histone H3. *Nature,* 419**,** 407-411.

SATO, T., VRIES, R. G., SNIPPERT, H. J., VAN DE WETERING, M., BARKER, N., STANGE, D. E., VAN ES, J. H., ABO, A., KUJALA, P., PETERS, P. J. & CLEVERS, H. 2009. Single Lgr5 stem cells build crypt-villus structures in vitro without a mesenchymal niche. *Nature,* 459**,** 262-5.

SAUVAGET, D., CHAUFFETON, V., CITADELLE, D., CHATELET, F. P., CYWINER-GOLENZER, C., CHAMBAZ, J., PINCON-RAYMOND, M., CARDOT, P., LE BEYEC, J. & RIBEIRO, A. 2002. Restriction of apolipoprotein A-IV gene expression to the intestine villus depends on a hormone-responsive element and parallels differential expression of the hepatic nuclear factor 4alpha and gamma isoforms. *The Journal of biological chemistry,* 277**,** 34540-8.

SCHÄFER, A., KARAULANOV, E., STAPF, U., DÖDERLEIN, G. & NIEHRS, C. 2013. Ing1 functions in DNA demethylation by directing Gadd45a to H3K4me3. *Genes & development,* 27**,** 261-273.

SCHÜBELER, D., MACALPINE, D. M., SCALZO, D., WIRBELAUER, C., KOOPERBERG, C., VAN LEEUWEN, F., GOTTSCHLING, D. E., O'NEILL, L. P., TURNER, B. M. & DELROW, J. 2004. The histone modification pattern of active genes revealed through genome-wide chromatin analysis of a higher eukaryote. *Genes & development,* 18**,** 1263-1271.

SCHUBELER, D., MACALPINE, D. M., SCALZO, D., WIRBELAUER, C., KOOPERBERG, C., VAN LEEUWEN, F., GOTTSCHLING, D. E., O'NEILL, L. P., TURNER, B. M., DELROW, J., BELL, S. P. & GROUDINE, M. 2004. The histone modification pattern of active genes revealed through genome-wide chromatin analysis of a higher eukaryote. *Genes Dev,* 18**,** 1263-71.

SCOVILLE, D. H., SATO, T., HE, X. C. & LI, L. 2008. Current view: intestinal stem cells and signaling. *Gastroenterology,* 134**,** 849-64.

SEOW, H. F., BROER, S., BROER, A., BAILEY, C. G., POTTER, S. J., CAVANAUGH, J. A. & RASKO, J. E. 2004. Hartnup disorder is caused by mutations in the gene encoding the neutral amino acid transporter SLC6A19. *Nat Genet,* 36**,** 1003-7.

SERFAS, M. S. & TYNER, A. L. 1993. HNF-1 alpha and HNF-1 beta expression in mouse intestinal crypts. *The American journal of physiology,* 265**,** G506-13.

SHEAFFER, K. L., KIM, R., AOKI, R., ELLIOTT, E. N., SCHUG, J., BURGER, L., SCHÜBELER, D. & KAESTNER, K. H. 2014. DNA methylation is required for the control of stem cell differentiation in the small intestine. *Genes & development,* 28**,** 652-664.

SHIAU, Y.-F. 1987. Lipid digestion and absorption. *Physiology of the gastrointestinal tract,* 2**,** 1527-1556.

SHIH, D. Q., SCREENAN, S., MUNOZ, K. N., PHILIPSON, L., PONTOGLIO, M., YANIV, M., POLONSKY, K. S. & STOFFEL, M. 2001. Loss of HNF-1alpha function in mice leads to abnormal expression of genes involved in pancreatic islet development and metabolism. *Diabetes,* 50**,** 2472-80.

SILK, D. B., GRIMBLE, G. K. & REES, R. G. 1985. Protein digestion and amino acid and peptide absorption. *Proc Nutr Soc,* 44**,** 63-72.

SLADEK, F. M., ZHONG, W. M., LAI, E. & DARNELL, J. E. 1990. Liver-enriched transcription factor HNF-4 is a novel member of the steroid hormone receptor superfamily. *Genes & Development,* 4**,** 2353-2365.

SOKOL, S. Y. 2007. *Wnt signaling in embryonic development,* Amsterdam ; London, Elsevier.

STAPPENBECK, T. S., MILLS, J. C. & GORDON, J. I. 2003. Molecular features of adult mouse small intestinal epithelial progenitors. *Proceedings of the National Academy of Sciences,* 100**,** 1004-1009.

STEGMANN, A., HANSEN, M., WANG, Y., LARSEN, J. B., LUND, L. R., RITIE, L., NICHOLSON, J. K., QUISTORFF, B., SIMON-ASSMANN, P., TROELSEN, J. T. & OLSEN, J. 2006. Metabolome, transcriptome, and bioinformatic cis-element analyses point to HNF-4 as a central regulator of gene expression during enterocyte differentiation. *Physiol Genomics,* 27**,** 141-55.

STEVENS, B. R., ROSS, H. J. & WRIGHT, E. M. 1982. Multiple transport pathways for neutral amino acids in rabbit jejunal brush border vesicles. *The Journal of membrane biology,* 66**,** 213-25.

STEVENS, B. R. & WRIGHT, E. M. 1985. Substrate specificity of the intestinal brush-border proline/sodium (IMINO) transporter. *The Journal of membrane biology,* 87**,** 27-34.

STEVENS, B. R. & WRIGHT, E. M. 1987. Kinetics of the intestinal brush border proline (Imino) carrier. *The Journal of biological chemistry,* 262**,** 6546-51.

STRACHAN, T. & READ, A. P. 2004. *Human molecular genetics 3,* London ; New York, Garland Press.

STROBER, W. 2001. Trypan blue exclusion test of cell viability. *Current protocols in immunology***,** A. 3B. 1-A. 3B. 2.

SUETAKE, I., SHINOZAKI, F., MIYAGAWA, J., TAKESHIMA, H. & TAJIMA, S. 2004. DNMT3L stimulates the DNA methylation activity of Dnmt3a and Dnmt3b through a direct interaction. *Journal of Biological Chemistry,* 279**,** 27816-27823.

SUZUKI, T., MOCHIZUKI, K. & GODA, T. 2008. Histone H3 modifications and Cdx-2 binding to the sucrase-isomaltase (SI) gene is involved in induction of the gene in the transition from the crypt to villus in the small intestine of rats. *Biochem Biophys Res Commun,* 369**,** 788-93.

TARAVIRAS, S., MONAGHAN, A. P., SCHUTZ, G. & KELSEY, G. 1994. Characterization of the mouse HNF-4 gene and its expression during mouse embryogenesis. *Mechanisms of development,* 48**,** 67-79.

TATE, P. H. & BIRD, A. P. 1993. Effects of DNA methylation on DNA-binding proteins and gene expression. *Current opinion in genetics & development,* 3**,** 226-231.

TERADA, T., SHIMADA, Y., PAN, X., KISHIMOTO, K., SAKURAI, T., DOI, R., ONODERA, H., KATSURA, T., IMAMURA, M. & INUI, K. 2005. Expression profiles of various transporters for oligopeptides, amino acids and organic ions along the human digestive tract. *Biochem Pharmacol,* 70**,** 1756-63.

TJIAN, R. & MANIATIS, T. 1994. Transcriptional activation: a complex puzzle with few easy pieces. *Cell,* 77**,** 5-8.

TRABER, P. G. 1990. Regulation of sucrase-isomaltase gene expression along the crypt-villus axis of rat small intestine. *Biochemical and biophysical research communications,* 173**,** 765-73.

TRABER, P. G., GUMUCIO, D. L. & WANG, W. 1991. Isolation of intestinal epithelial cells for the study of differential gene expression along the crypt-villus axis. *Am J Physiol,* 260**,** G895-903.

TROMPETTE, A., BLANCHARD, C., ZOGHBI, S., BARA, J., CLAUSTRE, J., JOURDAN, G., CHAYVIALLE, J. A. & PLAISANCIÉ, P. 2004. The DHE cell line as a model for studying rat gastro-intestinal mucin expression: effects of dexamethasone. *European journal of cell biology,* 83**,** 347-358.

TRONCHE, F., RINGEISEN, F., BLUMENFELD, M., YANIV, M. & PONTOGLIO, M. 1997. Analysis of the distribution of binding sites for a tissue-specific transcription factor in the vertebrate genome. *Journal of molecular biology,* 266**,** 231-45.

TRONCHE, F. & YANIV, M. 1992. HNF1, a homeoprotein member of the hepatic transcription regulatory network. *BioEssays : news and reviews in molecular, cellular and developmental biology,* 14**,** 579-587.

TURNER, B. M. 2002. Cellular memory and the histone code. *Cell,* 111**,** 285-291.

VAISSIÈRE, T., SAWAN, C. & HERCEG, Z. 2008. Epigenetic interplay between histone modifications and DNA methylation in gene silencing. *Mutation Research/Reviews in Mutation Research,* 659**,** 40-48.

VAN BEERS, E. H., AL, R. H., RINGS, E., EINERHAND, A., DEKKER, J. & BULLER, H. A. 1995. Lactase and sucrase-isomaltase gene expression during Caco-2 cell differentiation. *Biochem. J,* 308**,** 769-775.

VAN BEEST, M., DOOIJES, D., VAN DE WETERING, M., KJAERULFF, S., BONVIN, A., NIELSEN, O. & CLEVERS, H. 2000. Sequence-specific high mobility group box factors recognize 10-12-base pair minor groove motifs. *The Journal of biological chemistry,* 275**,** 27266-73.

VAN DE WETERING, M., SANCHO, E., VERWEIJ, C., DE LAU, W., OVING, I., HURLSTONE, A., VAN DER HORN, K., BATLLE, E., COUDREUSE, D., HARAMIS, A. P., TJON-PON-FONG, M., MOERER, P., VAN DEN BORN, M., SOETE, G., PALS, S., EILERS, M., MEDEMA, R. &

CLEVERS, H. 2002. The beta-catenin/TCF-4 complex imposes a crypt progenitor phenotype on colorectal cancer cells. *Cell,* 111**,** 241-50.

VAN DER FLIER, L. G. & CLEVERS, H. 2009. Stem cells, self-renewal, and differentiation in the intestinal epithelium. *Annual review of physiology,* 71**,** 241-60.

VAN ES, J. H., JAY, P., GREGORIEFF, A., VAN GIJN, M. E., JONKHEER, S., HATZIS, P., THIELE, A., VAN DEN BORN, M., BEGTHEL, H., BRABLETZ, T., TAKETO, M. M. & CLEVERS, H. 2005. Wnt signalling induces maturation of Paneth cells in intestinal crypts. *Nature cell biology,* 7**,** 381-6.

VAN INGEN, H., VAN SCHAIK, F. M., WIENK, H., BALLERING, J., REHMANN, H., DECHESNE, A. C., KRUIJZER, J. A., LISKAMP, R. M., TIMMERS, H. T. M. & BOELENS, R. 2008. Structural insight into the recognition of the H3K4me3 mark by the TFIID subunit TAF3. *Structure,* 16**,** 1245-1256.

VERZI, M. P., SHIN, H., SAN ROMAN, A. K., LIU, X. S. & SHIVDASANI, R. A. 2013. Intestinal master transcription factor CDX2 controls chromatin access for partner transcription factor binding. *Molecular and cellular biology,* 33**,** 281-292.

VINCENT, A., KAZMIERCZAK, C., DUCHENE, B., JONCKHEERE, N., LETEURTRE, E. & VAN SEUNINGEN, I. 2015. Cryosectioning the intestinal crypt-villus axis: an ex vivo method to study the dynamics of epigenetic modifications from stem cells to differentiated cells. *Stem Cell Res,* 14**,** 105-13.

WALLERMAN, O., MOTALLEBIPOUR, M., ENROTH, S., PATRA, K., BYSANI, M. S. R., KOMOROWSKI, J. & WADELIUS, C. 2009. Molecular interactions between HNF4a, FOXA2 and GABP identified at regulatory DNA elements through ChIP-sequencing. *Nucleic acids research,* 37**,** 7498-7508.

WANG, J., CORTINA, G., WU, S. V., TRAN, R., CHO, J. H., TSAI, M. J., BAILEY, T. J., JAMRICH, M., AMENT, M. E., TREEM, W. R., HILL, I. D., VARGAS, J. H., GERSHMAN, G., FARMER, D. G., REYEN, L. & MARTIN, M. G. 2006. Mutant neurogenin-3 in congenital malabsorptive diarrhea. *N Engl J Med,* 355**,** 270-80.

WATSON, J. D. 2003. *Molecular biology of the gene,* San Francisco, Pearson/Benjamin Cummings.

WEAVER, R. F. 2012. *Molecular Biology,* New York, McGraw-Hill.

WEI, G.-H., BADIS, G., BERGER, M. F., KIVIOJA, T., PALIN, K., ENGE, M., BONKE, M., JOLMA, A., VARJOSALO, M. & GEHRKE, A. R. 2010. Genome-wide analysis of ETS-family DNA-binding in vitro and in vivo. *The EMBO journal,* 29**,** 2147-2160.

WOLPERT, L. 2007. *Principles of development,* Oxford ; New York, Oxford University Press.

WU, S. C. & ZHANG, Y. 2010. Active DNA demethylation: many roads lead to Rome. *Nat Rev Mol Cell Biol,* 11**,** 607-20.

YAMAGATA, K., FURUTA, H., ODA, N., KAISAKI, P. J., MENZEL, S., COX, N. J., FAJANS, S. S., SIGNORINI, S., STOFFEL, M. & BELL, G. I. 1996a. Mutations in the hepatocyte nuclear factor-4alpha gene in maturity-onset diabetes of the young (MODY1). *Nature,* 384**,** 458-60.

YAMAGATA, K., ODA, N., KAISAKI, P. J., MENZEL, S., FURUTA, H., VAXILLAIRE, M., SOUTHAM, L., COX, R. D., LATHROP, G. M., BORIRAJ, V. V., CHEN, X., COX, N. J., ODA, Y., YANO, H., LE BEAU, M. M., YAMADA, S., NISHIGORI, H., TAKEDA, J., FAJANS, S. S., HATTERSLEY, A. T., IWASAKI, N., HANSEN, T., PEDERSEN, O., POLONSKY, K. S., BELL, G. I. & ET AL. 1996b. Mutations in the hepatocyte nuclear factor-1alpha gene in maturity-onset diabetes of the young (MODY3). *Nature,* 384**,** 455-8.

YAMASHITA, A., SINGH, S. K., KAWATE, T., JIN, Y. & GOUAUX, E. 2005. Crystal structure of a bacterial homologue of Na+/Cl--dependent neurotransmitter transporters. *Nature,* 437**,** 215-23.

YE, D. Z. & KAESTNER, K. H. 2009. Foxa1 and Foxa2 control the differentiation of goblet and enteroendocrine L- and D-cells in mice. *Gastroenterology,* 137**,** 2052-62.

YOUNG, J. A. & FREEDMAN, B. S. 1971. Renal tubular transport of amino acids. *Clin Chem,* 17**,** 245-66.

ZHANG, H., WADA, J., HIDA, K., TSUCHIYAMA, Y., HIRAGUSHI, K., SHIKATA, K., WANG, H., LIN, S., KANWAR, Y. S. & MAKINO, H. 2001. Collectrin, a collecting duct-specific transmembrane glycoprotein, is a novel homolog of ACE2 and is developmentally regulated in embryonic kidneys. *The Journal of biological chemistry,* 276**,** 17132-9.

ZHANG, M., HUA, Q., MILLER, A., BARNTHOUSE, N. & WANG, J. 2015. Developmental switch in SOX9 expression in articular cartilage is regulated by epigenetic histone methylation. *Osteoarthritis and Cartilage,* 23**,** A195-A196.

ZHANG, Y., WADA, J., YASUHARA, A., ISEDA, I., EGUCHI, J., FUKUI, K., YANG, Q., YAMAGATA, K., HIESBERGER, T., IGARASHI, P., ZHANG, H., WANG, H., AKAGI, S., KANWAR, Y. S. & MAKINO, H. 2007. The role for HNF-1beta-targeted collectrin in maintenance of primary cilia and cell polarity in collecting duct cells. *PLoS One,* 2**,** e414.

ZHAO, Q., EBERSPAECHER, H., LEFEBVRE, V. & DE CROMBRUGGHE, B. 1997. Parallel expression of Sox9 and Col2a1 in cells undergoing chondrogenesis. *Developmental dynamics : an official publication of the American Association of Anatomists,* 209**,** 377-86.

ZHONG, Z., WEN, Z. & DARNELL, J. 1994. Stat3: a STAT family member activated by tyrosine phosphorylation in response to epidermal growth factor and interleukin-6. *Science,* 264**,** 95-98.

ZILLER, M. J., GU, H., MÜLLER, F., DONAGHEY, J., TSAI, L. T.-Y., KOHLBACHER, O., DE JAGER, P. L., ROSEN, E. D., BENNETT, D. A. & BERNSTEIN, B. E. 2013. Charting a dynamic DNA methylation landscape of the human genome. *Nature,* 500**,** 477-481.

Chapter 8 Appendix

8.1 Plasmids

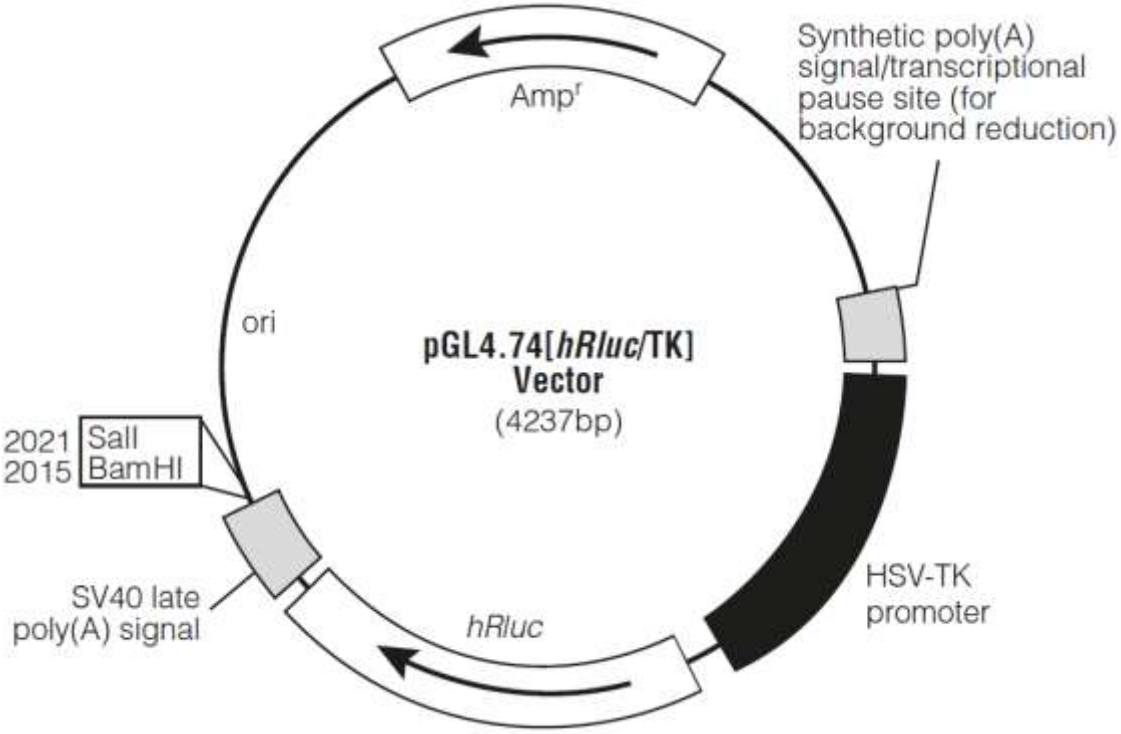

Figure 8.1: A plasmid map of the pGL4, the basic luciferase reporter vector, detailing key constructs and restriction enzyme sites

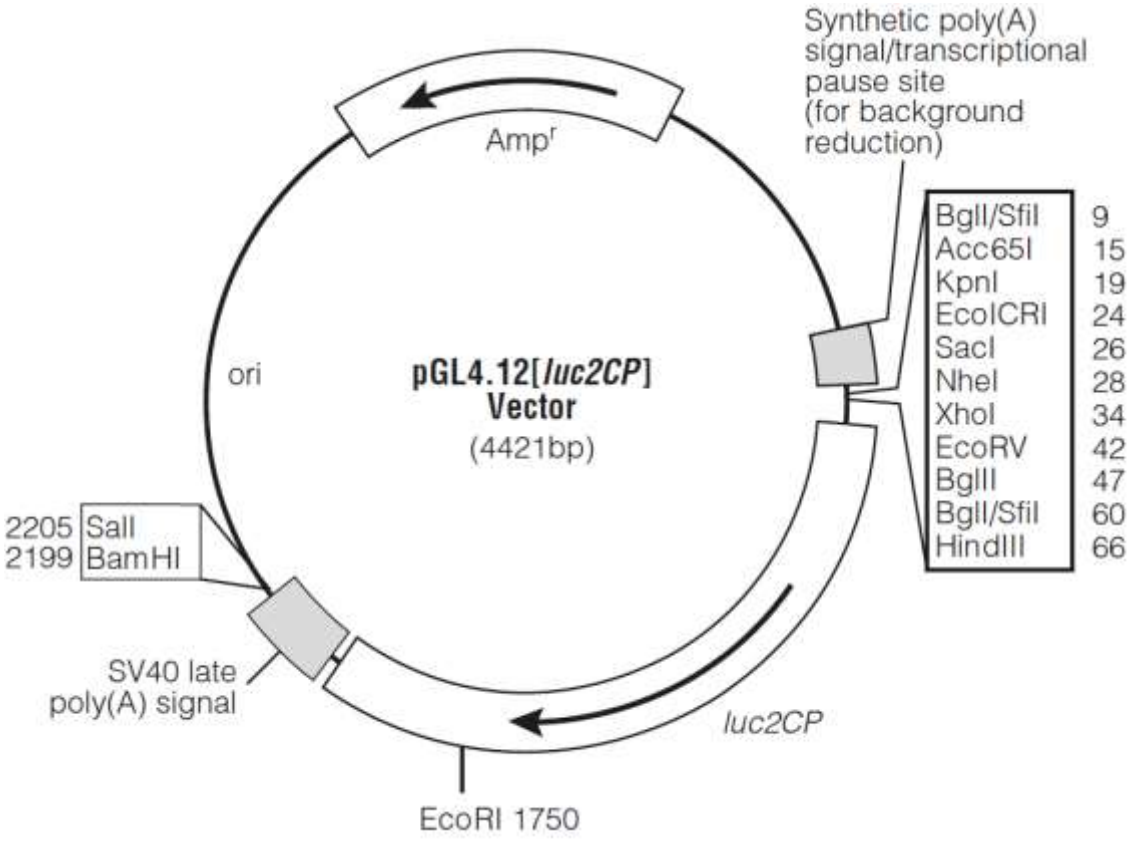

Figure 8.2: A plasmid map of the pGL4, the basic luciferase reporter vector, detailing key constructs and restriction enzyme sites

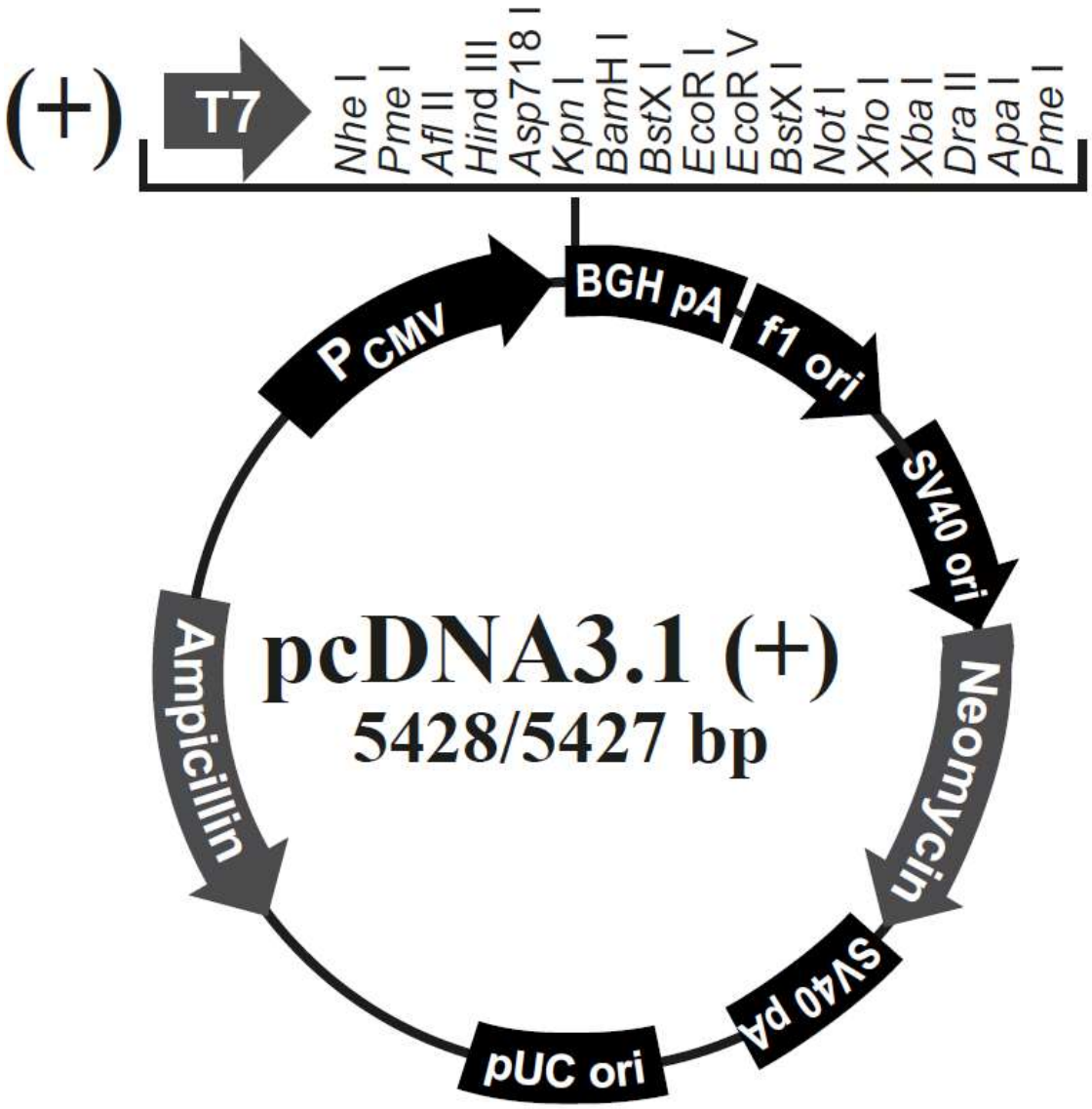

Figure 8.3: A plasmid map of the pcDNA3.1

8.2 Thermal cycler conditions

Table 8.1: Cycling conditions for the *PfuUltra* enzyme

Process	Temperature (°C)	Time (min:sec)	Number of repeats
Denaturation	95	5:00	–
Denaturation	95	0:30	30
Annealing	50–58 (depending on T_m of primers)	0:30	
Extension	72	6:00	
Extension (Final)	72	10:00	–

Table 8.2: Cycling condition for the Phusion® high-fidelity enzyme

Process	Temperature (°C)	Time (min:sec)	Number of repeats
Denaturation	98	0:30	–
Denaturation	98	0:10	30
Annealing	50–58 (depending on T_m of primers)	0:30	
Extension	72	2:00	
Extension (Final)	72	5:00	–

Table 8.3: Cycling condition for ChIP PCR

Process	Temperature (°C)	Time (min:sec)	Number of repeats
Denaturation	94	5:00	–
Denaturation	94	0:30	35–40
Annealing	50–58 (depending on T_m of primers)	0:30	
Extension	72	1:00	
Extension (Final)	72	5:00	–

8.3 Gene ontology terms enriched in the villus (significant changes in expression of genes between crypt and villus)

Biological Process/ Organic Substance Transport

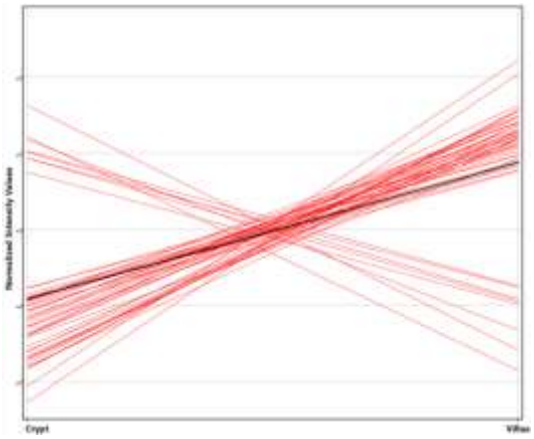

Adjusted p value : 9.146E-5
p value : 8.728E-8
Total genes in GO class : 392
Genes in input list in GO class : 44

Biological Process/Na^+ Transport

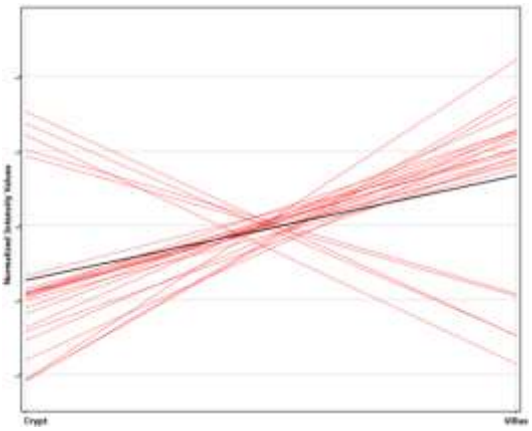

Adjusted p value : 2.626E-4
p value : 2.94E-7
Total genes in GO class : 145
Genes in input list in GO class : 23

Biological Process/ Organic Acid Transport

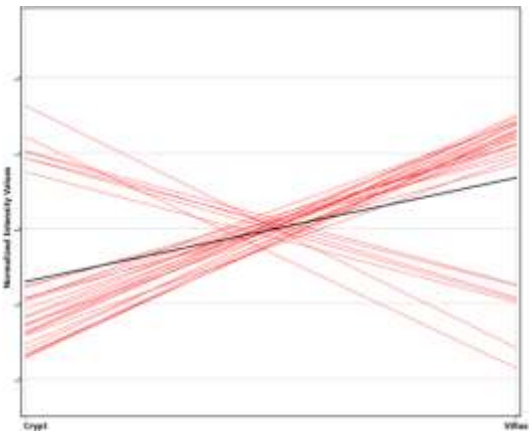

Adjusted p value : 0.003
p value : 4.44E-6
Total genes in GO class : 181
Genes in input list in GO class : 24

Biological Process/ Nitrogen Compound Tr.

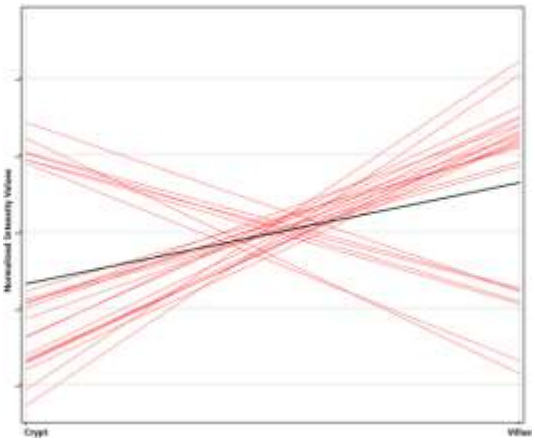

Adjusted p value : 0.003
p value : 5.341E-6
Total genes in GO class : 147
Genes in input list in GO class : 21

Biological Process/ Lipoprotein Transport

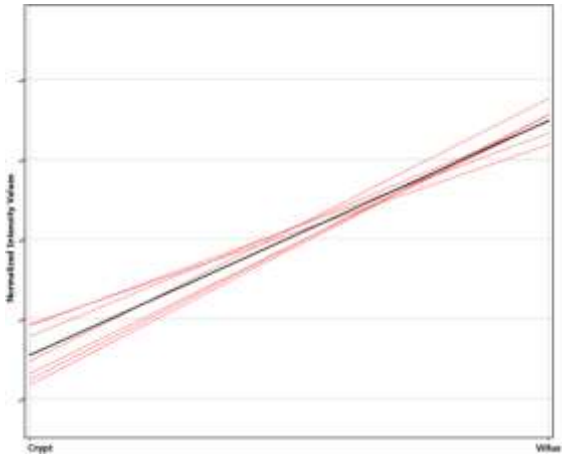

Adjusted p value : 0.049
p value : 1.358E-4
Total genes in GO class : 12
Genes in input list in GO class : 5

Cellular Component/ Brush Border

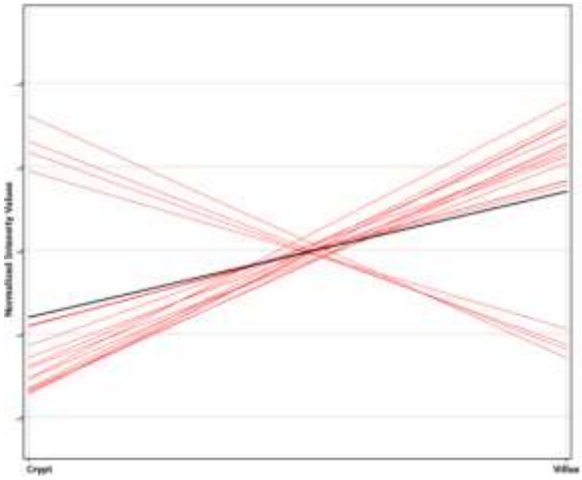

Adjusted p value : 0.002
p value : 4.03E-6
Total genes in GO class : 61
Genes in input list in GO class : 13

Biological Process/Carboxylic Acid Transport

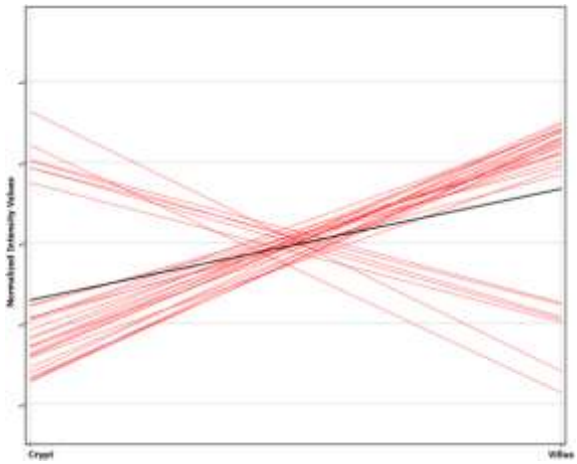

Adjusted p value : 0.002
p value : 3.65E-6
Total genes in GO class : 179
Genes in input list in GO class : 24

Molecular Function/ Symporter Activity

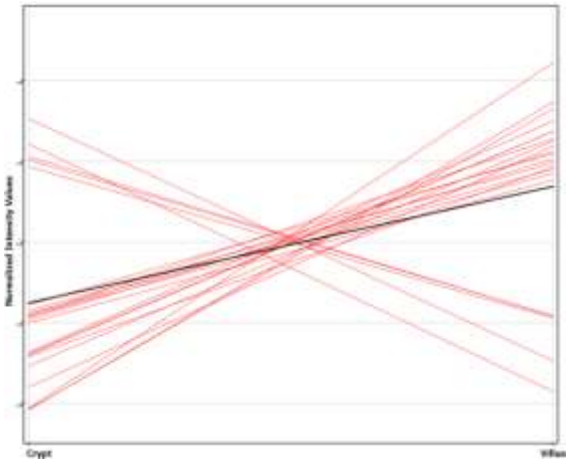

Adjusted p value : 2.883E-4
p value : 3.281E-7
Total genes in GO class : 114
Genes in input list in GO class : 20

Molecular Function/ Cofactor Transporter Activity

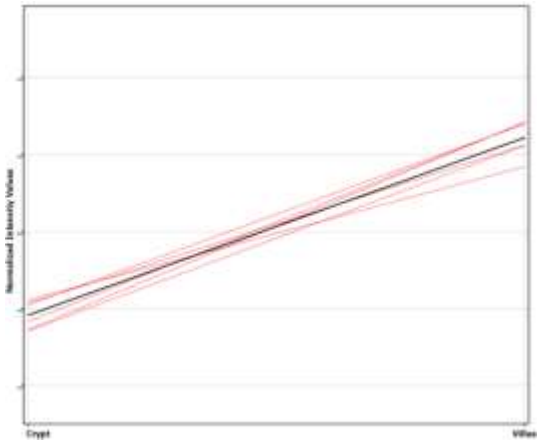

Adjusted p value : 0.035
p value : 8.24E-5
Total genes in GO class : 11
Genes in input list in GO class : 5

Molecular Function/ Carboxylic Acid Transmembrane Transporter Activity

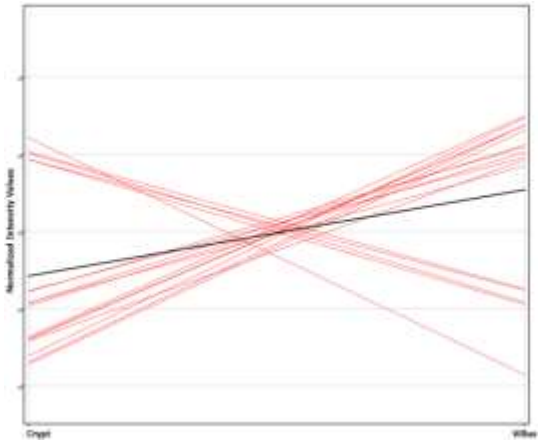

Adjusted p value : 0.049
p value : 1.363E-4
Total genes in GO class : 95
Genes in input list in GO class : 14

Molecular Function/ Solute: Sodium Symporter Activity

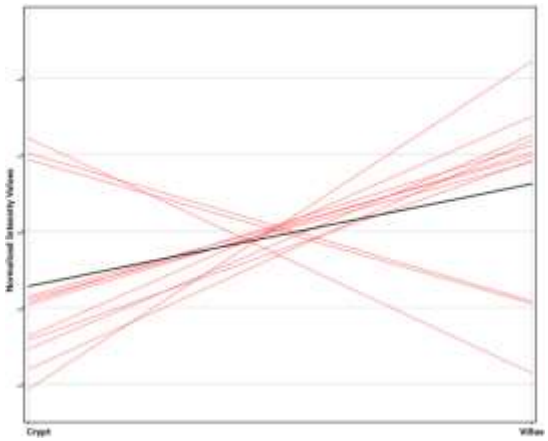

Adjusted p value : 8.926E-4
p value : 1.229E-6
Total genes in GO class : 47
Genes in input list in GO class : 12

8.4 Gene ontology terms enriched in the crypt (significant changes of genes between crypt and villus)

Biological Process/ M phase of mitotic cell cycle

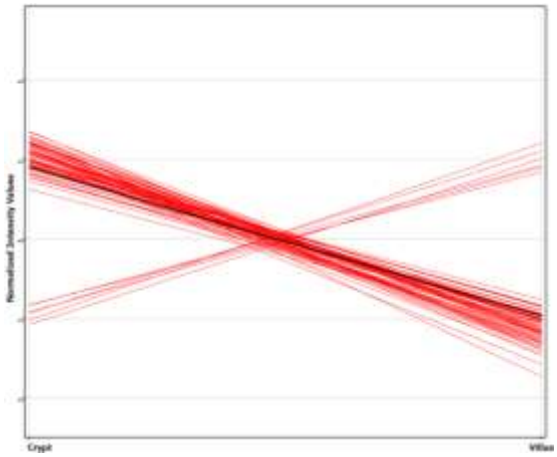

Adjusted p value : 3.434E-28
p value : 9.526E-33
Total genes in GO class : 216
Genes in input list in GO class : 63

Biological Process/ Cell cycle

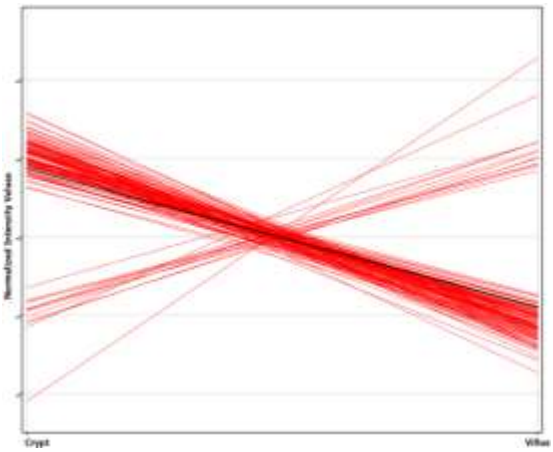

Adjusted p value : 4.478E-24
p value : 5.753E-28
Total genes in GO class : 787
Genes in input list in GO class : 115

Biological Process/ DNA Replication

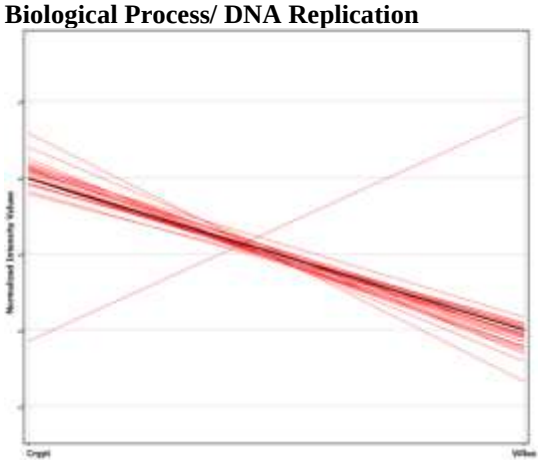

Adjusted p value : 4.658E-5
p value : 4.36E-8
Total genes in GO class : 152
Genes in input list in GO class : 25

Biological Process/ DNA Repair

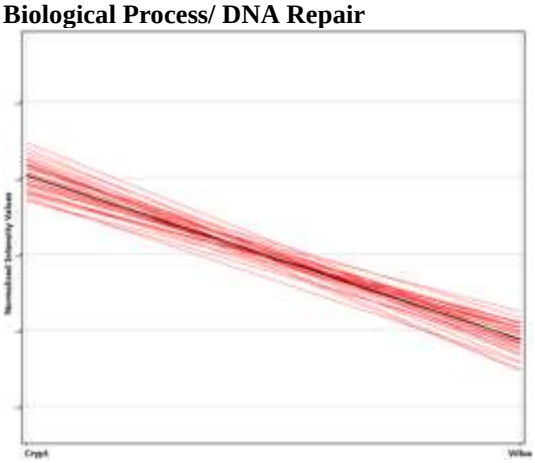

Adjusted p value : 0.002
p value : 2.801E-6
Total genes in GO class : 291
Genes in input list in GO class : 33

Molecular Function/ Microtubule Motor Activity

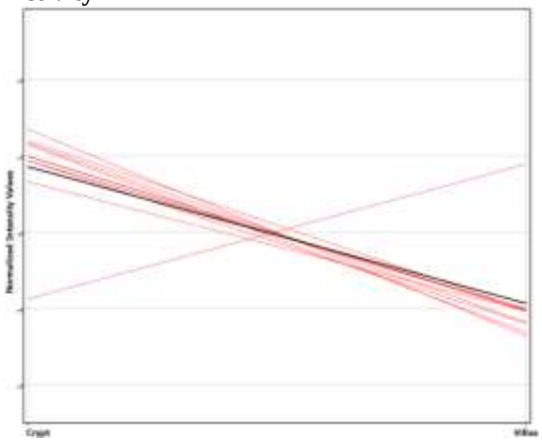

Adjusted p value : 0.013
p value : 2.881E-5
Total genes in GO class : 44
Genes in input list in GO class : 10

Cellular Component/ Microtubule Cytoskeleton

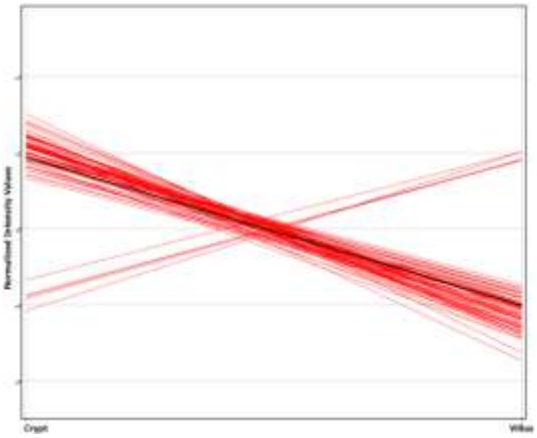

Adjusted p value : 2.157E-7
p value : 1.188E-10
Total genes in GO class : 627
Genes in input list in GO class : 68

Cellular Component/ Nuclear Part

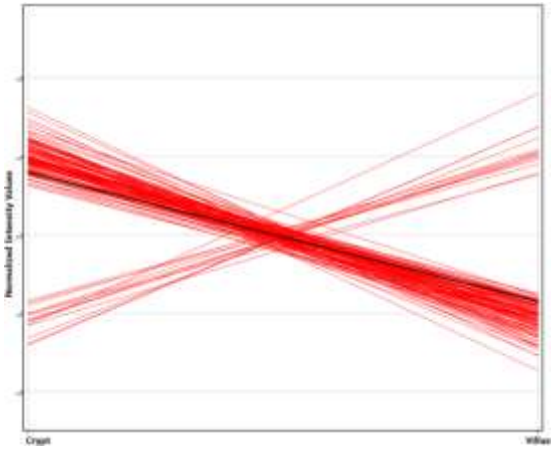

Adjusted p value : 0.007
p value : 1.405E-5
Total genes in GO class : 1745
Genes in input list in GO class : 120

Cellular Component/ Chromosome

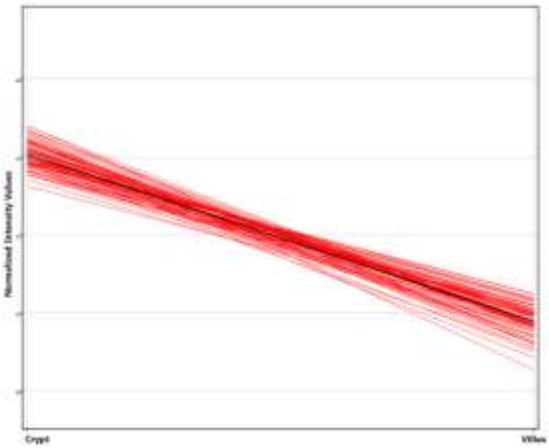

Adjusted p value : 2.443E-11
p value : 7.62E-15
Total genes in GO class : 498
Genes in input list in GO class : 67

Biological Process/ Chromosome Segregation

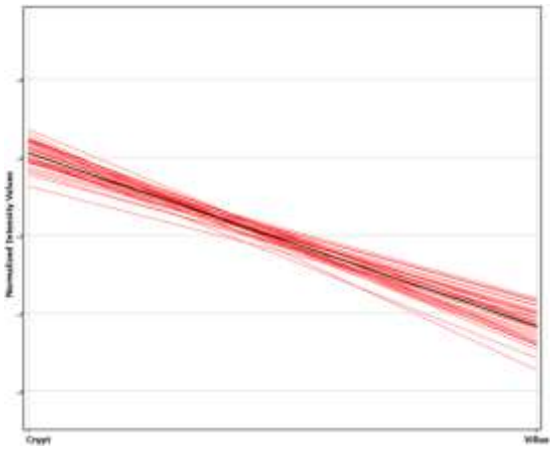

Adjusted p value : 1.805E-12
p value : 5.3E-16
Total genes in GO class : 105
Genes in input list in GO class : 30

Table 8.4: Predicted TF-binding sites in the *Collectrin* promoter.

A matrix number of 1.00 indicates an exact match with the binding site consensus sequence. Position and the core binding site of the TFs are indicated.

TFs	Position	Strand	Matrix	Sequence
HNF1b	–706/–690	–	0.866	taacaATTTatcaagcg
	–711/–695	+	0.797	gataaATTGttactgat
HNF1a	–56/–40	+	0.948	tccaaattattaATTGc
	–58/–42	–	0.910	ccgcaattaataATTTg
	–77/–61	–	0.849	gcataATTGggttgact
	–84/–68	–	0.836	gatacctgcataATTGg
	–235/–219	–	0.889	atcgaATTGgtttgttg
	–299/–283	+	0.858	gtccgATTGgttagact
	–401/–385	–	0.931	taacaATTGgttggttg
	–406/–390	+	0.882	aaccaATTGttaagggt
	–408/–392	–	0.865	caacccttaacaATTGg
	–431/–415	–	0.857	ctcaaATTGgatcggta
	–659/–643	–	0.928	gttgaATTGatttactg
HNF4a	–284/–260	+	0.839	aaccgtattagAAACacgggaaagt

Table 8.5: Predicted TF-binding sites in the *Ace2* promoter.

A matrix number of 1.00 indicates an exact match of the binding site consensus sequence. Position and the core binding site of the TFs are indicated.

TFs	Position	Strand	Matrix	Sequence
HNF1a	–189/–173	–	0.919	cagtaATTGctcaagt
	–196/–180	–	0.802	gaaaaagcagtaATTGc
	–213/–197	–	0.853	agacaATTGtagaataa
	–218/–202	+	0.894	ctacaATTGtctgccca
	–462/–446	+	0.860	ttaaaATTGctttggag
	–770/–754	+	0.829	aatttatttttaATTTt
	–814/–798	+	0.824	tagctgtctttgATTGg
	–1222/–1206	+	0.845	agcttATTGatagaatt
HNF4a	–234/–210	–	0.778	cgctttattctTAAAcctgggcagac
	–681/–657	+	0.920	atgactgcttgAAACtttaccaaag
	–1377/–1353	–	0.770	tggccaaatcAAAAcctggacatt

Table 8.6: List of TFs which were significantly expressed along crypt–villus axis ($p < 0.05$**)**

TFs expressed in the villus (Fold change >3)

1. Etv2
2. Pou2f2
3. Hoxb13
4. Prrx2
5. Hsf5
6. Vax1
7. Prrx1
8. Gcm2
9. Mafb
10. Epas1
11. Stat3
12. Creb3l2
13. Creb3l3
14. Tbx3
15. Stat4
16. Tcf7l2
17. Max
18. Fosl2
19. Mta3
20. Nlrc5
21. Nfatc2
22. Crebl2
23. Foxo6
24. Elk3
25. Trp63
26. Pax3
27. Spib
28. Zfp423
29. Lhx6
30. Barx2
31. Crebl2
32. Ikzf1
33. Tcf7l2
34. Pura
35. Maf
36. Epas1
37. Dlx3
38. Pura
39. Maf
40. Cebpe
41. Hmbox1
42. Msx2
43. Obfc1
44. Foxi1
45. Edf1
46. Bach1
47. Erf
48. Fosl2
49. Fli1
50. Hnf4g
51. Prdm1
52. Klf4
53. Edf1
54. Pax8
55. Foxo3
56. Pbx1
57. Lhx9
58. Uncx
59. Esr2
60. Srebf1
61. Elk3
62. Tef
63. Bcl6
64. Alx4
65. Pif1
66. Sox13
67. Ets1
68. Nkx6-1

TFs expressed in the crypt (Fold change >3)

1. Ascl2
2. Atf7
3. Esrrg
4. Uhrf1
5. Myc
6. Nr2e3
7. Top2a
8. Nr5a2
9. Esrrg
10. Nkx3-2
11. Sox9
12. Tcfap4
13. Foxm1
14. Ehf
15. Zfp711
16. Pitx1
17. Ncl
18. Klf2
19. Nr4a1
20. Ncl
21. Sox4
22. Ehf
23. Egr1
24. E2f1
25. Dnmt1
26. Msx3
27. Msh2
28. Foxp3
29. Mcm2
30. Tgif1
31. Hes1
32. Irx3
33. Six5
34. Hdac2
35. Mlh3
36. Nr5a2
37. Sox4
38. Zc3h8
39. Bcl11b
40. Bcl11b
41. Orc2
42. Hoxb7
43. Pbx1
44. Dnmt3b
45. Sox4
46. Pbx1
47. Fosb
48. Lass4
49. Terf1
50. Hsf1
51. Meis1
52. Trim28
53. Lonp1
54. Thrb
55. Nme1
56. Nme1
57. Nfyb
58. Rfc1
59. Nkx2-2
60. Foxa2
61. Etv6
62. Terf2
63. Foxk1
64. Hnrnpk
65. Osr2
66. Hnrnpd
67. Srf
68. Trp53bp1
69. Tsn
70. Ybx1
71. Hnrnpab
72. Foxa2
73. Hnrnpk

TFs evenly expressed in the crypt–villus axis (Fold change <3)

1. Elf2
2. Nfyb
3. E2f5
4. Mta3
5. Elf3
6. Zfp105
7. Isl1
8. Hnrnpk
9. Fos
10. Pura
11. Zfp238
12. Nr2c1
13. Crebzf
14. Creb5
15. Zhx3
16. Bptf
17. Tcf3
18. Usf2
19. Hnrnpa2b1
20. Hnrnpab
21. Vax2
22. Med1
23. Ctcf
24. Obfc1
25. Atf5
26. Ppara
27. Cebpb
28. Crebzf
29. Cdx2
30. Pbx2
31. Ppara
32. Creb3l4
33. Lrwd1
34. Drap1
35. Foxp1
36. Pole4
37. Pole3
38. Thap1
39. Erf
40. Pbx3
41. Xbp1
42. Cdx1
43. Cebpa
44. Pot1a
45. Atf1
46. Cebpd
47. Pax4
48. Tcf3
49. Tgif2
50. Nr5a1
51. Spdef
52. Ybx1
53. Med1
54. Elk3
55. Crebzf
56. Nfyb
57. Srf
58. Obfc1
59. Gatad1
60. Mecp2
61. Junb
62. Foxd4
63. Hnrnpa2b1
64. Lhx1
65. Mbd2
66. Lass6
67. Nfyc
68. Adnp2
69. Ncor2
70. Sp1
71. Hopx
72. Nr4a2
73. Creb1
74. Dnmt3b
75. Chrac1
76. Msh3
77. Med1
78. Nr1d1
79. Foxp1
80. Trim24
81. Stat5b
82. Foxa1
83. Lass5
84. Ets2
85. Batf3
86. Nfkb1
87. Zfp191
88. Arx
89. Atf3
90. Rxrb
91. Cxxc1
92. Safb
93. Mta3
94. Foxa3
95. Orc4
96. Nme1
97. Isx
98. Foxp4
99. Smg6
100. Mta1
101. Gata4
102. Nfkb1
103. Thap1
104. Xrcc5
105. Lbx2
106. Pbx3
107. Nr2f2
108. Dr1
109. Thrb
110. Orc4
111. Usf2
112. Pou2f1
113. Nfe2l2
114. Nfyc
115. Stat5b
116. Foxp4
117. Mta2
118. Srebf2
119. Atf6b
120. Meis3
121. Foxp1
122. Hnf1a
123. Thra
124. Etv5
125. Ybx1
126. Nfil3
127. Zhx1
128. Terf2
129. Vsx1
130. Hnf1b
131. Creb3l1
132. Rest
133. Foxk2
134. Pitx2
135. Tsnax
136. Stat5a
137. Zfp191
138. Jund
139. Prdm16
140. Hopx
141. Dnmt3a
142. Nr1h4
143. Tinf2
144. Zfp110
145. Terf2
146. Rbpj
147. Fosl1
148. Atf1
149. Nr4a2
150. Homez
151. Vdr
152. Trim24
153. Ncor1
154. Nr2c1
155. Mbd2
156. Hoxb3
157. Cebpg
158. Batf
159. Pparg
160. Batf2
161. Nr1h2
162. Purb
163. Ep300
164. Foxl2
165. Ahr
166. Gzf1
167. Alx3
168. Crem
169. Cux1
170. Stat6
171. Nr1h3
172. Meis2
173. Irx4
174. Neurod1
175. Ncor2
176. Hhex
177. Crem
178. Dbp
179. Sox1
180. Rela
181. Barhl1
182. Foxj3
183. Nfe2l1
184. Lonp2
185. Msx1
186. Nr3c1
187. Fev
188. Rxra
189. Atoh1
190. Mafg
191. Jdp2
192. Zglp1

193. Tinf2
194. Cux1
195. Thra
196. Mef2d
197. Ppard
198. Sox1
199. Nr1h3
200. Dnmt3b
201. Onecut2
202. Ppara
203. Elf1
204. Ddit3
205. Zfp148
206. Atf2
207. Nr2c2
208. Maff
209. Rarg
210. Jun
211. Etv3
212. Foxl2
213. Foxs1
214. Arnt
215. Rorc
216. Foxf1a
217. Pou2f1
218. Nanog
219. Elf1
220. Mef2a
221. Lass2
222. Usf1
223. Pitx3
224. Mef2d
225. Kdm6b
226. Mafg
227. Meis3
228. Nr3c1
229. Nr1i2
230. Pou3f1
231. Lbx1
232. Foxn3
233. Tshz1
234. Nfatc2
235. Mef2a
236. Ncor1
237. Tcf4
238. Hnf4a
239. Arnt
240. Hoxa4
241. Nr2c2
242. Lmx1a
243. Rara
244. Stat6
245. Ncor1
246. Evx2
247. Zhx3
248. Ppard
249. Notch1
250. Dbp
251. Creb3
252. Atf2
253. Pdx1
254. Tcf7l2
255. Pou5f2
256. Trp73
257. Zfp281
258. Gatad1
259. Rara
260. Foxo1
261. Nr1d2
262. Esrra
263. Etv1
264. Gata6
265. Pura
266. Mafg
267. Rxra
268. Mafk
269. Tlr9
270. Ets1
271. Irf1
272. Epas1
273. Nkx2-2
274. Foxo1
275. Pura
276. Srebf2
277. Mafg
278. Pole3
279. Mafa
280. Hsf2
281. Atf2
282. Dlx6
283. Rxrg
284. Zgpat
285. Nr2f6
286. Mef2d
287. Nr1d2